DOCTORAL THESIS

Measurement Based Approach for Residential Customer Stochastic Current Harmonic Modelling

Muhammad Naveed Iqbal

Measurement Based Approach for Residential Customer Stochastic Current Harmonic Modelling

MUHAMMAD NAVEED IQBAL

TAL
TECH
PRESS

TALLINN UNIVERSITY OF TECHNOLOGY
School of Engineering
Department of Electrical Power Engineering and Mechatronics

The dissertation was accepted for the defence of the degree of Doctor of Philosophy on 3 August 2021

Supervisor: Professor Lauri Kütt,
Department of Electrical Power Engineering and Mechatronics, School of Engineering,
Tallinn University of Technology,
Tallinn, Estonia

Opponents: Associate Professor, João Martins, Ph.D.,
Department of Electrical Engineering,
Faculty of Sciences and Technology,
Universidade Nova de Lisboa,
Lisbon, Portugal

Professor Saulius Gudžius, Ph.D.,
Faculty of Electrical and Electronics Engineering,
Kaunas University of Technology,
Kaunas, Lithuania

Defence of the thesis: 2 September 2021, Tallinn

Declaration:
Hereby I declare that this doctoral thesis, my original investigation and achievement, submitted for the doctoral degree at Tallinn University of Technology, has not been submitted for any academic degree elsewhere.

Muhammad Naveed Iqbal

_____
signature

Mõõtmispõhine lähenemine olmetarbijate vooluharmoonikute juhusliku esinemise modelleerimiseks

MUHAMMAD NAVEED IQBAL

Contents

List of publications

The present Ph.D. thesis is based on the following publications:

I M. N. Iqbal, L. Kütt, B. Asad, N. Shabbir, and I. Rasheed, "Time-dependent variations in current harmonic emission by LED lamps in the low-voltage network," Electrical Engineering, vol. 103, p. 1525–1539, 2021

II M. N. Iqbal, L. Kütt, B. Asad, T. Vaimann, A. Rassõlkin, and G. L. Demidova, "Time dependency of current harmonics for switch-mode power supplies," Applied Sciences, vol. 10, p. 7806, Nov 2020

III M. N. Iqbal, L. Kütt, M. Lehtonen, R. J. Millar, V. Püvi, A. Rassõlkin, and G. L. Demidova, "Travel activity based stochastic modelling of load and charging state of electric vehicles," Sustainability, vol. 13, p. 1550, Feb 2021

IV M. N. Iqbal, L. Kütt, K. Daniel, M. Jarkovoi, B. Asad, and N. Shabbir, "Bivariate stochastic model of current harmonic analysis in the low voltage distribution grid," Proceedings of the Estonian Academy of Sciences, vol. 70, no. 2, p. 190, 2021

V M.N. Iqbal; L. Kütt; K. Daniel; B. Asad; P.S. Ghahfarokhi, "Estimation of harmonic emission of electric vehicles and their impact on low voltage residential network," Sustainability, vol. 13, p. 8551, July 2021

VI M. N. Iqbal and L. Kütt, "End-user electricity consumption modelling for power quality analysis in residential building," in 2018 19th International Scientific Conference on Electric Power Engineering (EPE), IEEE, May 2018

VII M. N. Iqbal, L. Kütt, and A. Rosin, "Complexities associated with modeling of residential electricity consumption," in 2018 IEEE 59th International Scientific Conference on Power and Electrical Engineering of Riga Technical University (RTUCON), IEEE, Nov 2018

VIII M. N. Iqbal, M. Jarkovoi, L. Kütt, and N. Shabbir, "Impact of LED thermal stability to household lighting harmonic load current modeling," in 2019 Electric Power Quality and Supply Reliability Conference (PQ) and 2019 Symposium on Electrical Engineering and Mechatronics (SEEM), IEEE, June 2019

IX M. Jarkovoi, M. N. Iqbal, and L. Kütt, "Analysis of harmonic current stability and summation of LED lamps," in 2019 Electric Power Quality and Supply Reliability Conference and 2019 Symposium on Electrical Engineering and Mechatronics, PQ and SEEM2019, IEEE, June 2019

X M. Jarkovoi, L. Kütt, and M. N. Iqbal, "Probabilistic bivariate modeling of harmonic current," in 2020 19th International Conference on Harmonics and Quality of Power (ICHQP), IEEE, July 2020

XI M. N. Iqbal, L. Kütt, , B. Asad, N. Shabbir, "Impact of cable impedance on the harmonic emission of LED lamps," in 21st International Scientific Conference on Electric Power Engineering (EPE), Oct. 2020

XII M. N. Iqbal, L. Kutt, N. Shabbir, and B. Asad, "Comparison of current harmonic emission by different lighting technologies," in 2020 IEEE 61th International Scientific Conference on Power and Electrical Engineering of Riga Technical University (RTUCON), IEEE, Nov 2020

Author's contributions to the publications

   I M.N. Iqbal was the main author and wrote the manuscript.

  II M.N. Iqbal was the main author, analysed the results, and wrote the manuscript.

 III M.N. Iqbal was the main author, prepared the test bench, conducted experiment, performed simulation, and wrote the manuscript.

 IV M.N. Iqbal was the main author, conducted experiment, performed analysis, and wrote the manuscript.

  V M.N. Iqbal was the main author, performed simulation, and wrote the manuscript.

 VI M.N. Iqbal was the main author, conducted the experiment, analyse results, and wrote the manuscript.

VII M.N. Iqbal was the main author, performed measurement, simulation, and wrote the manuscript.

VIII M.N. Iqbal was the main author, conducted experiment, performed analysis, and wrote the manuscript.

 IX M.N. Iqbal was the second author, prepared the test bench and analysed the results.

  X M.N. Iqbal was the third author, prepared the test bench, proposed the algorithm and analysed the results.

 XI M.N. Iqbal was the main author, performed the measurements, simulation, and wrote the manuscript.

XII M.N. Iqbal was the main author, performed the analysis, simulation, and wrote the manuscript.

Abbreviations

ABM	Activity based model
AC	Alternating current
BEV	Battery electric vehicle
CFL	Compact fluorescent lamp
CRT	Cathode ray tube
DAQ	Data acquisition
DC	Direct current
DFT	Discrete Fourier transform
DU	Device usage
DUOATS	Direct use of observed activity-travel schedules
EBH	Empirical bivariate histogram
ECDF	Empirical cumulative distribution function
EMC	Electromagnetic compatibility
EV	Electric vehicle
FFT	Fast Fourier transform
FL	Fluorescent lamp
HL	Halogen lamp
HTS	Household travel survey
IEC	International electrotechnical commission
IEEE	Institute of electrical and electronics engineers
IL	Incandescent lamp
ITU	International telecommunication union
JNB	Joint normal distribution
KCL	Kirchhoff's current law
KDE	Kernel density estimation
LED	Light emitting diode
LV	Low voltage
NC	Norton couple
NTS	National traffic survey
PANDA	equipment harmonic database
PCC	Point of common coupling
PDF	Probability density function
PFC	Power factor correction
PHEV	Plug-in hybrid electric vehicle
PQ	Power quality
PV	Photo-voltaic
SB	Shopping and business
SHE	Stochastic harmonic estimation
SMPS	Switch mode power supply
SOC	State of charge
THD	Total harmonic distortion
TUS	Time use survey
VL	Vacation and leisure
WS	Work and school

Symbols

a_0	DC component in the Fourier series
Ah_{80}	80% value of the magnitude or phase
Ah_f	Final value of the magnitude or phase
a_n	Fourier series's coefficient
Ah_o	Initial value of the magnitude or phase
b_n	Fourier series's coefficient
c_n	Complex component
$C(x,y)$	Number of samples in a bin at (x,y)
Cor	Calibration correction
d_A	Difference between Ah_f and Ah_o
D_{oc}	Occupancy duration
d_{ns}	Duration of noise event
d_{sw}	Duration of switching event
E	Energy
f_h	Frequency of harmonic h
f_s	Sampling frequency
γ	Difference between Ah_{80} and Ah_o
h	Harmonic number
$\mathbf{I}$	Indicator function
Ih_n	Current of h_n harmonic
I_{pri}	Primary instrument current
I_{ref}	Reference instrument current
K	Kernel
$Linc$	Linearization error
LS	Long term stability
λ	Variance of Poisson distribution
μ	Mean
N	Number of data points or intervals
ω	Angular frequency
Ω_{ik}	Indicator of data point i belong to the cluster k
O_f	Occupancy function
p	Probability
P	Power
P_b	Background power
P_H	Power during high energy consumption cycle of a device
P_{IL}	Power of the interactive loads
P_l	Power during low energy consumption cycle of a device
p_m	Probability of the mth sample
P_{NIL}	Power of the non-interactive loads
P_{sd}	Standby power of a device
$P_T(t)$	Total power at time t
Res	Resolution effect of ADC
$Stab$	Stability
T_m	Time duration of the mth interval
T_{oc}	Occupancy time
t_s	Sampling interval
τ	time constant

u_c	Calibration uncertainty
u_d	Device uncertainty
u'_d	Method uncertainty
V_{coef}	Voltage coefficient of programmable power supply
V_h	Voltage magnitude of the harmonic h
V_{out}	Voltage output of programmable power supply
V_{range}	Voltage range of programmable power supply
W_x	Dimension of the bin
ψ	Phase angle
Y	Admittance
Zh_n	Impedance at harmonic frequency h_n
ϑ	Phase

1 Introduction

The electric power system has continuously been evolving since the first power station's establishment at the end of the 19th century. The transformers, developed in 1885, revolutionised the alternating current (AC) transmission and distribution system capable of carrying electricity from generating stations. Initially, electric machines and appliances were designed from the perspective of cost-effectiveness, and their efficiency was not a prime concern for the manufacturers. However, as the demand grows with a more competitive market, performance and efficiency parameters start playing their role. Today, the power system is an interconnection of generation, transmission, and distribution subsystems and responsible for maintaining the quality and reliability of the power supply.

Power quality refers to the supply voltage and similarly current quality. According to the Institute of Electrical and Electronics Engineers (IEEE) standard 1159, electromagnetic phenomena that describe voltage and current in a power system at a specific time and location is defined as power quality [1]. Electromagnetic disturbances referring to the deviation of any parameter outside the expected range would reduce power quality and could lead to problems in the power system that could prevent normal operation of end-user equipment. Most often, supply voltage quality is considered as most critical due to its impact reaching towards more load endpoints and directing their operation. One critical attribute of supply voltage and current is related to maintaining their waveform near sinusoidal with rated values at instantaneous and steady-state conditions.

The distortion of current and voltage waveforms started emerging in the power system back in the early 20th century [2]. The initial problems included telephone interference, electric motor overheating, and power system over voltages due to harmonic distortions [3]. The power quality term started to appear in the literature in the 1970s when electronic-based circuits started to emerge in the electrical loads [4]. These circuits contain diodes, thyristors, transistors, and other nonlinear and switching devices.

The International Electrotechnical Commission (IEC) defines power quality in terms of electromagnetic compatibility (EMC). The IEC 61000-1-1 standard states that an electrical system's ability to function satisfactorily in its electromagnetic environment without adding any electromagnetic disturbance to anything within the environment defines its electromagnetic compatibility [5]. The electromagnetic disturbances can deteriorate the operation of electrical equipment or system up to a level of misoperation or malfunction. Therefore a power quality problem can be defined as any problem caused by supply voltage or current deviations that could result in the inferior performance of the end-user equipment or even failure [6].

AC grid-fed electrical equipment is designed to operate with the standard voltage waveform, a sinusoidal shape at rated magnitude and frequency. Therefore, electrical devices can malfunction as a result of significant deviations in the voltage waveform. One of the common reasons, though, which can lead to voltage waveform distortion, is current flow through the network source and line impedance. As electronic devices draw a non-linear current rather different from a standard sinusoidal waveform, this distorted current waveform affects the wave shape of the voltage on the network impedance components. Such an effect causes voltage waveform deterioration and power quality problems. The inrush and short circuit current is also a reason for these waveform distortions.

Power quality problems are classified based on the specific property of the problem. The IEC 61000-2-5 defines three categories, as shown in Table 1.1. These electromagnetic disturbances degrade the quality of current and voltage waveforms in the power system. The power quality should be high, and all characteristics maintained within operational boundaries to ensure the network's reliability. In a broader sense, the electric power sys-

tem in addition to good power quality would have to provide compliance to electromagnetic compatibility aspects to all the network elements.

Table 1.1 – Phenomena responsible for electromagnetic disturbances [5]

Phenomena		Types
Low frequency	Conducted	Harmonics, interharmonics
		Signaling voltage
		Voltage fluctuations
		Voltage dips
		Voltage imbalance
		Power frequency variations
		Induced low-frequency voltages
		DC components in AC networks
	Radiated	Magnetic fields
		Electric fields
High frequency	Conducted	
	Radiated	
Electrostatic discharge		
Nuclear electromagnetic pulse		

The low-frequency phenomena described in Table 1.1 are momentary disturbances that propagate through the power system for a few nanoseconds to 3 seconds except harmonics. The harmonics refer to the sinusoidal currents or voltages with frequencies that are an integral multiple of the power system frequency. In ideal terms, the power system is expected to provide distortion-free sinusoidal current and voltages. The harmonics disturbance typically penetrates the power system near the end-user vicinity in high frequencies and lasts until mitigated by altering the source impedance; therefore, considered steady-state electromagnetic disturbances. They interact with the network impedance and alter the current and voltage waveform. As a result, all the users connected to the network are affected by these harmonic disturbances. The complex waveform generated across harmonic sources is a mix of the fundamental frequency and higher frequency harmonic components. The distorted voltage waveform can be expressed as Eq. (1.1).

$$V(t) = V_f \sin(\omega t + \vartheta_1) + V_{2f} \sin(\omega t + \vartheta_2) + \ldots V_{nf} \sin(\omega t + \vartheta_n) \qquad (1.1)$$

In the past, researchers mainly focused on harmonic distortions in industrial and commercial electrical networks; however, the recent advances in power electronics have enabled manufacturers to make energy-efficient appliances. These electronic domestic appliances are significantly affecting the power quality of the residential networks. Furthermore, the zero-energy buildings with photo-voltaic (PV) distribution generation and electric vehicles (EV) are prone to deteriorate the residential distribution grid's power quality by adding additional current harmonics. IEC standard 61000-3-2 provides harmonic limits for maximum current harmonic emission from individual equipment, while 61000-2-2 provides maximum voltage harmonics and total harmonic distortion limits at the point of common coupling (PCC).

Lower order harmonics (less than 2 kHz) are given more attention towards voltage distortions in the grid. The main reason is that current harmonic emission from the nonlinear loads lies in these frequency ranges that correspond to the most voltage deviations. The lower order harmonics are recurrent and will propagate in the system; however, there

are some known countermeasures. As the share of power electronic-based equipment increases, the harmonic filters could become necessary to ensure harmonic current emission limits by the devices.

The high-frequency harmonics in the range of 2 - 150 kHz are referred to as supraharmonics. The term high frequency is used for signals in the range of 3 to 30 MHz by the international telecommunication union (ITU); hence the term supraharmonics is adopted for high-frequency harmonics. This additional term is defined because the distortion caused by supraharmonics shows a broadband characteristic compared to the narrow-band properties of low-frequency harmonic distortions [7]. The propagation of supraharmonics is different in the sense that they tend to flow between connected devices and cannot be aggregated like low order harmonics. Studies have shown that by increasing the number of nonlinear devices, the current spectrum's magnitude decreases between 40-50 kHz at the point of delivery but increases for individual devices [8, 9]. Therefore, supraharmonics are more difficult to quantify numerically. However, because of the undesirable repercussions such as malfunction and lifetime reduction of the devices, the upper limits on superharmonic emission in the network are essential [10]. The traditional harmonic analysis approach might not provide the best accuracy for supraharmonics [8, 11]. Supraharmonics are not primarily researched in this thesis, and the scope of this thesis is only limited to lower order harmonics only.

1.1 Motivation

The modern power system dynamics are changing swiftly because of the evolution in energy generation and consumption trends. The increase in the number of distributed generation units such as PV and proliferation of power electronic based loads will contribute towards high harmonic emission in the residential grids. Although the magnitude of the harmonic distortion of individual devices load current waveforms may be minimal, their collective impact could be significant to impose limits for the network power delivery capacity, for example keeping in mind the operation of the transformers. Traditional loads such as incandescent lamps are gradually replaced by compact fluorescent lamps (CFL), and now a transition towards a more efficient light-emitting diode (LED) lamp is underway. Electric motor-based appliances efficiency is improved by adopting invert-based drives that can support various working modes. The harmonic emission profile of each working mode can be different.

Furthermore, harmonic current cancellation and variation because of thermal stability, and cable impedance make the voltage's levels estimation task even more complex. On the other hand, an accurate assessment of harmonic emission for present and future loads is critical for the network operators to improve the capacity and planning for additional investments. The effectiveness of quantifying and designing harmonic mitigation measures also relies on the accuracy of these estimations.

The harmonic current and voltage estimation accuracy can only be improved by considering the variation and uncertainties associated with load and network. The network parameters are dynamic, and the load connected to it is changing continuously throughout the day. Because of modern nonlinear device's stochastic nature of utilisation, it is not easy to model their usage and operational behaviour. Many studies are available related to power flow modelling, but the nonlinear load modelling and stochastic current harmonic estimations are relatively contemporary. The classical residential load models are developed to predict energy consumption patterns; therefore, unable to estimate current harmonic emissions mainly because of their low time resolution. Usage patterns for the majority of the household devices depend on occupant behaviour. Several social and

economic factors influence the behaviour of a person and their living style. The residential building's architecture, climate conditions, and the type of electrical appliances are major contributors that can affect energy consumption.

In order to develop a harmonic estimation model that can represent an authentic picture of the residential network, respective uncertainties have to be taken into account that has been generally neglected or not considered in the previous models available in the literature. The random harmonic estimations can support to study of the impact of regulatory policy changes and network planning decisions.

1.2 Thesis objective

This thesis aims to develop a probabilistic current harmonic estimation model capable of including different uncertainties related to network and load for the low voltage distribution network. In contrast to previous approaches to evaluating harmonic emission impact based on the measurement of network or loads, the prime focus of the thesis will be to estimate current harmonics with actual load variation and dynamic network conditions. The main research targets are as follows:

1. Statistical modelling of the loads to generate usage patterns of different household loads with a high temporal resolution.

2. Research and analysis of recent harmonic estimation models and factors that can affect the harmonic emission of loads in the network.

3. Development of a measurement approach capable of power quality measurements at different voltage waveform.

4. Evaluation of the accuracy of the measurement system using signal processing techniques.

5. Analysis of the variations in current harmonic emission due to thermal stability by nonlinear loads.

6. Estimation of the effect of cable impedance on the current harmonics.

7. Analysis of current harmonics emission profile of nonlinear loads operating in different working modes.

8. Classification of loads based on circuit topologies and comparison of their harmonic emission profile.

9. Development of probabilistic harmonic estimation algorithm that can address both magnitude and phase variations.

10. Estimation of the harmonic emission difference under technology evolution of end-user loads in the residential buildings.

11. Analysis of the impact of future loads on harmonics in the low voltage networks.

1.3 Hypothesis

The primary hypothesis of the thesis are as follows:

- The increase in the penetration of nonlinear loads will increase the current harmonic emission levels in the low voltage network that will compromise the network's capacity and reliability.

- The stochastic approach is suitable for harmonic estimation as it can include necessary uncertainties and variations related to network and load operation.

1.4 Scientific novelties

The scientific novelties of the thesis are described as follows:

1. Probabilistic load usage models are developed based on the bottom-up approach using device-level measurement data. Different surveys are also used for improving user behaviours to enhance the capability of the model to provide realistic results. The model is unique with its simplified approach and provides high-resolution variations to support harmonic emission estimations.

2. A new method is presented to evaluate the accuracy of power quality measurement system.

3. Accuracy and uncertainties such as time-dependent variations and the impact of network impedance on the current harmonic emissions are evaluated.

4. A bivariate harmonic modelling approach is used to include the effect of both magnitude and phase variations in the current harmonic estimations.

5. The network uncertainties are included in the model by taking into account the effect of grid-side voltage variations on the harmonic emission profile of different household devices.

6. The model can also be used to analyse harmonic cancellation as the phase angles are included in the current harmonic's probabilistic estimation.

7. The model provides an accurate and simplified approach in comparison to the traditional harmonic estimation model based on standard probability density functions.

1.5 Practical novelties

The practical novelties of the thesis are as follows:

1. The current harmonic emission estimation is based on the real-time variability of load usage in residential buildings; therefore, it provides a realistic impact of electronic loads in the LV residential network.

2. The effect of voltage waveform distortions on the harmonic emission provides a range of probable values of current harmonics in the LV network.

3. The additional impact on the harmonic emission for high electric vehicle penetration in the low voltage network is estimated.

4. The influence of the electronic circuit topology on current harmonic emission is estimated.

5. The impact on power consumption and harmonic emission by technological advancements, such as replacing incandescent lamps and compact fluorescent lamps with LED lights, is provided.

1.6 Thesis outline

- Chapter 2 provides an introduction to the harmonic distortions. The sources of harmonics and their effect on the power system are described. A literature review of existing techniques of current harmonic modelling is discussed.

- Chapter 3 presents the methodology used to construct the harmonic estimation model for the low voltage residential network.

- Chapter 4 focuses on stochastic modelling of residential electrical appliance usage patterns. It also provides the method to evaluate the electrical vehicle load profiles.

- Chapter 5 investigates the inaccuracies and uncertainties that may effect the outcome of harmonic estimation model. It also address the method to evaluate measurement system accuracy.

- Chapter 6 provides different results by using the harmonic estimation models. The impact of technological advancements, circuit topologies, electrical vehicles and nonlinear devices in the low voltage network is discussed.

2 Literature review

2.1 Current harmonics and waveform distortions

The waveform distortions are steady-state deviations from the ideal sinusoidal signal and are considered as one of the most critical electromagnetic disturbances in the power system. These distortions include both current and voltage waveform distortions. The voltage distortions affect the end-user equipment, and the current distortions generated by the end-user equipment affect the network voltage.

These periodic distortions can be decomposed into the sum of a fundamental component of the frequency and harmonics. The harmonics refer to the sinusoidal waveform that is an integral multiple of the fundamental component's frequency. Ideally, the power utility should provide only sinusoidal voltages and currents that do not have any distortion component. The current harmonics are generated when a load draws a nonlinear current that is not changing proportionally to the voltage in the power system, which in turn affects the voltage across the load.

J.B.J. Fourier proposed in 1822 that any signal that is continuous and periodic over time interval T can be represented as an aggregation of a DC component, a fundamental frequency component, and higher frequency components as given by Eq. (2.1).

$$y(t) = a_0 + \sum_{n=1}^{\infty} [a_n \cos(n\omega t) + b_n \sin(n\omega t)] \tag{2.1}$$

Here ω is the fundamental frequency of the function $y(t)$ in radians. The a_0 is the dc component while a_n and b_n are the Fourier series's coefficient and can be calculated by Eqs. (2.2), (2.3) and (2.4).

$$a_0 = \frac{1}{2\pi} \int_{-\pi}^{\pi} x(\omega t) d(\omega t) \tag{2.2}$$

$$a_n = \frac{1}{\pi} \int_{-\pi}^{\pi} x(\omega t) \cos(n\omega t) d(\omega t) \tag{2.3}$$

$$b_n = \frac{1}{\pi} \int_{-\pi}^{\pi} x(\omega t) \sin(n\omega t) d(\omega t) \tag{2.4}$$

Eq. (2.1) can also be written as a series of phase shifted sine terms as follows.

$$y(t) = a_0 + \sum_{n=1}^{\infty} [d_n \sin(n\omega t + \psi_n)] \tag{2.5}$$

where,

$$d_n = \sqrt{a_n^2 + b_n^2} \tag{2.6}$$

and,

$$\psi_n = \tan^{-1} \left[\frac{b_n}{a_n} \right] \tag{2.7}$$

Eq. (2.1) can also be written in terms of magnitude A_n and phase ϑ_n as indicated by Eq. (2.8)

$$y_n = a_0 + \sum_{n=1}^{\infty} [A_n \cos(n\omega t) + \vartheta_n] \tag{2.8}$$

By using trigonometric identity $\cos(\alpha + \beta) = \cos\alpha\cos\beta - \sin\alpha\sin\beta$, Eq. (2.8) can be written as follows.

$$y_n = a_0 + \sum_{n=1}^{\infty} [A_n \cos(n\omega t) cos(\vartheta_n)] - \sum_{n=1}^{\infty} [A_n \sin(n\omega t) sin(\vartheta_n)] \qquad (2.9)$$

Therefore, in the vector form, the nth harmonic can be represented by Eq. (2.10)

$$A_n \angle \vartheta_n = a_n + jb_n \qquad (2.10)$$

The magnitude A_n and phase ϑ_n can be calculated by using Eq. (2.11) and (2.12) respectively.

$$A_n = \sqrt{a_n^2 + b_n^2} \qquad (2.11)$$

$$\vartheta_n = \tan^{-1}\left[\frac{b_n}{a_n}\right] \qquad (2.12)$$

Eq. (2.1) can also be written in complex from and is shown by Eq. (2.13).

$$y(t) = \sum_{n=1}^{\infty} c_n e^{jn\omega t} \qquad (2.13)$$

where,

$$c_n = \frac{a_n - jb_n}{2} \quad \text{for } n > 0 \qquad (2.14)$$

The c_n can also be calculated using Eq.(2.15).

$$c_n = \frac{1}{\pi} \int_{-\pi}^{\pi} x(\omega t) e^{jn\omega t} d(\omega t) \qquad (2.15)$$

Eq. (2.13) can be integrated over an infinite period, and as a result, values between harmonic frequencies will tend towards zero value. The component c_n will now be a continuous function and the resultant relation is known as Fourier transform as shown by Eq. (2.16).

$$Y_f = \int_{-\infty}^{\infty} y(t) e^{-jn\omega T} d(\omega t) \qquad (2.16)$$

Y_f is a complex function and called the spectral density of $y(t)$.

$$Y_f = Re(Y_f) + jImg(Y_f) \qquad (2.17)$$

The amplitude and phase spectrum can be obtained by Eq. (2.18) and Eq. (2.19) respectively.

$$Y_f = \sqrt{Re(Y_f)^2 + jImg(Y_f)^2} \qquad (2.18)$$

$$\vartheta_f = \tan^{-1}\left[\frac{ImgY_f}{ReY_f}\right] \qquad (2.19)$$

As in digital signal processing, the data is recorded by sampling in the time domain. For the frequency domain analysis of discrete data, the Fourier transform can be represented as summation of discrete signals as shown in Eq. (2.20).

$$Y_n = \sum_{-\infty}^{\infty} \left[x(nt_s) e^{-j2\pi f nt_s} \right] \qquad (2.20)$$
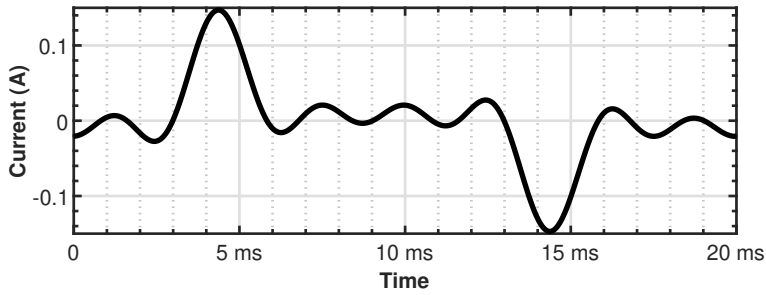
Figure 2.1 – Nonlinear current draw by a LED lamp

here $t_s = 1/f_s$ is sampling interval and f_s is the sampling frequency. In MATLAB and other computational softwares, Fourier transform of a discrete signal is calculated by using discrete Fourier transform (DFT). The frequency domain results are also discrete for DFT and can be calculated by using Eq. (2.21).

$$Y_{f_k} = \frac{1}{N} \sum_{n=0}^{N-1} \left[x(t_n) e^{-j2\pi kn/N} \right] \tag{2.21}$$

where N is the number of samples in time and frequency domain.

Using the Fourier transform, the distorted voltage can be decomposed into harmonics with frequencies that are integral multiple of fundamental component. Fig. 2.1 shows the nonlinear current draw by a typical LED lamp while Fig. 2.2 shows the decomposed
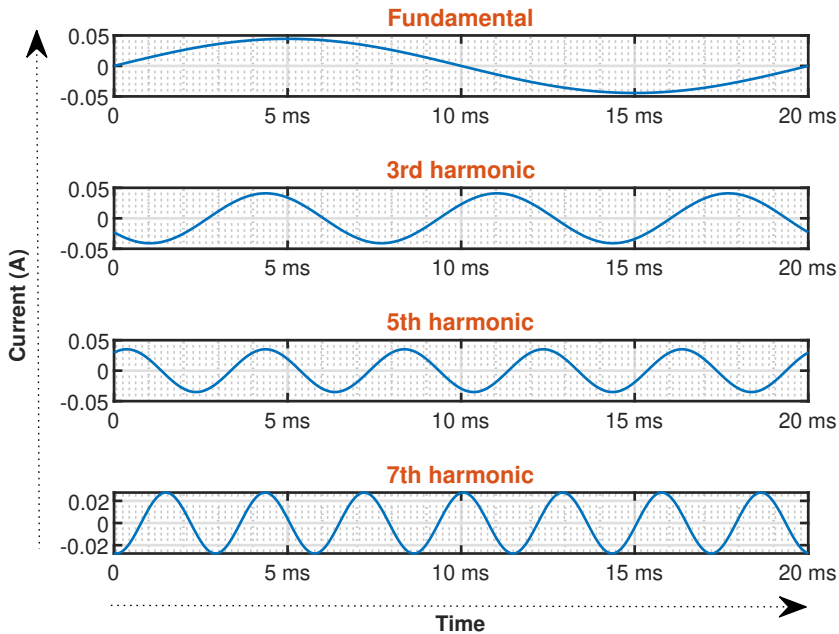

Figure 2.2 – Harmonic components of the current draw by a LED lamp

harmonic components.

Another important term that quantifies a signal's overall distortion is known as total harmonic distortion (THD). It provides the ratio of the aggregated magnitude of each harmonic component to the fundamental component's magnitude. The THD of a signal Y can be calculated as using Eq. (2.22).

$$THD_Y = \frac{\sqrt{\sum_{n=2}^{\infty}(Y_n^2)}}{Y_1} \tag{2.22}$$

2.2 Sources of current harmonics

The harmonic sources are electromagnetic or semiconductor electrical devices that draw nonsinusoidal currents and are commonly known as nonlinear loads. The electromagnetic nonlinear devices include stationary and rotating electrical machines such as transformers, motors, and generators. The harmonic emission from these devices depends on the design and material properties used in the construction. The harmonic content added by electromagnetic devices is often less compared to semiconductor-based power supply units [12]. The electronic loads contain switching devices and can generate a significant amount of harmonic content in the power system; therefore, considered as major sources of harmonics. Electronic devices' share is increasing rapidly every year as they are now an integral part of the power supplies. All modern appliances include switch-mode power supplies (SMPs) to improve efficiency and power management. A typical SMPS contains a rectifier, and its harmonic emission depends on the filter and power factor correction circuit topologies. The energy-efficient lamps such as CFL and LEDs contain power electronic based driver circuit and contribute towards harmonic emission.

With the impending building regulation in the EU to move towards buildings with nearly zero energy consumption using on-site renewable electricity generation, the current harmonic emission of customer endpoints will potentially be escalated further because of the large three-phase power supply inverter units (photo-voltaic and battery storage). The penetration of electric vehicles will also increase with time and draw current from the grid by nonsinusoidal waveforms as they charge their batteries during a stay at home through power electronic circuits. Thus current harmonic estimation in a distribution network is a complex set of problems defined not only by the present state of loads but also includes future perspectives of potential load device profiles.

2.3 Harmonics effect of power system

Presence of small nonsinusoidal components cannot be basically avoided, as a waveform, in any case, would include some nonsinusoidal noise. However, in an AC power supply system, distortions from either voltage or current sinusoidal waveform can raise several concerns.

The high-frequency harmonic components interact with the power system components such as capacitors and transformers to produce additional losses and heat in them. Some of the common problems caused by the harmonics are:

1. The high-frequency harmonics can cause excessive currents in capacitors leading to overload up to a point where capacitors in the power factor correction units can be destroyed. Capacitor current is linearly dependent on the harmonic voltage component; thus, higher-order voltage harmonics impose more heating stress than the main component.

2. Capacitors inherently define resonant frequency as a result of their interaction with the power system inductance. High voltage distortion can occur if the current harmonic's frequency matches the supply system's resonant frequency [4].

3. Transformers are heated because of the additional losses caused by the harmonics and results in reduced efficiency and life span. Furthermore, the insulation can be degraded because of the additional stress.

4. The voltage harmonics can also saturate the transformer core and the unsymmetrical properties of the harmonics also contributes to this cause [13, 14].

5. The harmonic voltages produce harmonic flux in the motor that does not contribute to motor torque. The motor's efficiency is decreased under the influence of voltage harmonics, and additional heat, noise, and vibration are produced [4, 15].

6. The transmission line losses increase, and their capacity is reduced because of the increase in skin and proximity effects. Harmonic currents can cause a voltage drop across the impedance of the system and increase the dielectric stress of the cables [16].

7. The measurement instrument can show errors as they are calibrated on sinusoidal current and voltages [17].

8. The protection equipment in the power system can malfunction because of the harmonics. The relay operation can be disturbed. The circuit breakers tripping points may also shift due to extra heating in the solenoids caused by the harmonics [13].

9. The harmonics also affects the operation of household appliances. The computer, televisions, and lighting are affected by voltage harmonics [17].

In order to limit the adheres effects that could lead to damage or danger, the power supply waveforms are rather limited in the harmonic content permitted. For example, total harmonic distortion for voltage waveform needs to be under 8% for residential areas, in order for the power supply to be considered reliable [18].

2.4 Relevant standards

Both IEEE and IEC have provided the guidelines for the limits, mitigation, and measurements of harmonics in their standards. The summary and description of different standards related to harmonics are listed below.

1. **EN 50160**: Provides the low, medium and high voltage supply characteristics such as variations, harmonics, transients, flickers, dips and, swells in the public networks [18].

2. **IEEE 519-2014**: Provides the recommendations to control harmonic in the electric power system, including details of the harmonic measurement procedure and recommended harmonic limits [1].

3. **IEC 61000 1-4**: Discusses sources, effect, and mitigation of the power frequency conduction for the range of up to 2 kHz [19].

4. **IEC 61000 2-1**: Provides information about different disturbances, including harmonics [20].

5. **IEC 61000 2-2**: Defines the compatibility levels of conducted voltage disturbances in the range of up to 150 kHz in the public access power supply networks [21].

6. **IEC 61000 2-4**: Defines the compatibility levels of conducted voltage disturbances for industrial sites [22].

7. **IEC 61000 2-5**: Defines description and classification of electromagnetic environments, including power supply networks and the phenomena associated with disturbances [23].

8. **IEC 61000 3-2**: Provides harmonic current emission limits for equipment with a current rating of less than 16 A [24].

9. **IEC 61000 3-4**: Guidelines for voltage distortion and fluctuation for the equipment with current rating of 16 A or less [25].

10. **IEC 61000 3-12**: Provides harmonic current emission limits for the equipment connected to a low voltage network with a current rating of 16 A to 75 A [26].

11. **IEC 61000 4-7**: Provides harmonic current emission limits for the equipment connected to the low voltage network with rated current greater than 16 A [27].

12. **IEC 61000 4-13**: Covers the measurement and testing procedure for for the verification of the device's immunity to voltage harmonics [28].

13. **IEC 61000 4-30**: Defines the measurement methodology of power quality parameters and interpretation of the measurement results in the AC supply system [29].

2.5 Review of harmonic estimation models

The impact of harmonic voltage's levels on the distribution network can be studied by using harmonic estimation models. An important task for the network operator is to maintain voltage level emissions within limits in the network; therefore, a realistic estimation of current harmonics emission is critical. A detailed harmonic analysis could provide insight into the power system behaviour under voltage and current distortions.

Several models are available in the literature to estimate the current harmonics in the power system. These models can be categorized into numerical and probabilistic models [IV].

2.5.1 Numerical models

The numerical models are based on the electrical parameters of the loads. The loads can be classified based on the circuit topologies, and current, voltage and impedance values are used to formulate the harmonic estimation model in frequency or time domain.

Frequency domain models   The frequency-domain models are easier to compute and consider the frequency domain attributes of the electrical equipment. The simplest frequency domain model is the current source model based on the magnitude and phase measurement of each current harmonic under consideration. Any nonlinear load can be represented by the sum of constant current sources for each harmonic frequency [30]. Each current harmonic source is independent of the input voltage. This model cannot analyse the effect of the voltage distortions on current harmonics [31]. As the voltage waveform in a distribution network changes continuously depending on the type and

amount of connected load, current source models are not effective for harmonic analysis.

The Norton models address this problem by considering the admittance matrix. The model parameters are estimated by switching the operating condition of the power system as shown in Fig. 2.3. The current and voltage harmonics will be changed ($I_{1,n}$ to $I_{2,n}$ and $V_{1,n}$ to $V_{2,n}$) and are used to estimate the model parameters from Eqs. (2.23) and (2.24).
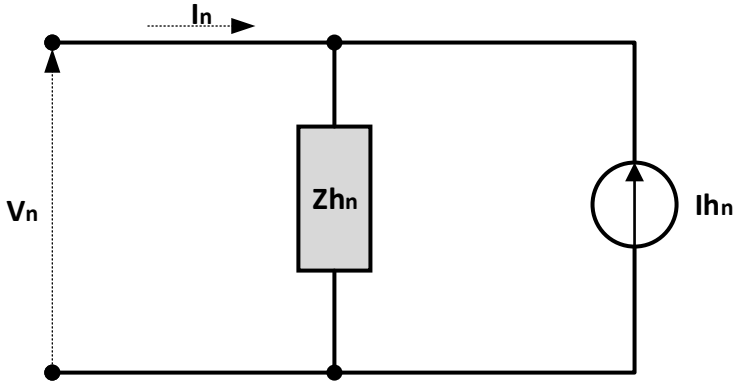

Figure 2.3 – Norton equivalent model

$$Zh_n = \frac{V_{2,n} - V_{1,n}}{I_{2,n} - I_{1,n}} \tag{2.23}$$

$$Ih_n = \frac{V_{1,n}}{Zh_n} - I_{1,n} \tag{2.24}$$

Although this approach provides some advantages over the current source model, it cannot consider the cross dependency of harmonics. The harmonic currents only depend on the corresponding voltage harmonics and not on the voltage waveform itself. This shortcoming was improved by using a crossed frequency admittance matrix in the Norton coupled (NC) model. The estimated harmonic currents using this model will not only depend on voltage harmonics of the same frequency but on the other frequencies as well. Eq. (2.25) and (2.26) represents the mathematical form of the NC model.

$$\vec{I} = \vec{Y} \times \vec{V} \tag{2.25}$$

$$
\begin{bmatrix} \vec{I}_{1m} \\ \vec{I}_{2m} \\ \vec{I}_{3m} \\ \cdots \\ \vec{I}_{nm} \end{bmatrix} =
\begin{bmatrix}
\vec{Y}_{11} & \vec{Y}_{12} & \vec{Y}_{13} & \cdots & \vec{Y}_{1m} \\
\vec{Y}_{21} & \vec{Y}_{22} & \vec{Y}_{23} & \cdots & \vec{Y}_{2m} \\
\vec{Y}_{31} & \vec{Y}_{32} & \vec{Y}_{33} & \cdots & \vec{Y}_{3m} \\
\vdots & \vdots & \vdots & \cdots & \vdots \\
\vec{Y}_{n1} & \vec{Y}_{n2} & \vec{Y}_{n3} & \cdots & \vec{Y}_{nm}
\end{bmatrix} \cdot
\begin{bmatrix} \vec{V}_{1m} \\ \vec{V}_{2m} \\ \vec{V}_{3m} \\ \cdots \\ \vec{V}_{nm} \end{bmatrix} \tag{2.26}
$$

The verification and comparison of frequency-domain models are presented in [32, 33].

Time-domain models The time-domain models are based on the load's actual circuits and give a rather complete information about the harmonic emission profile. However, it is challenging to model every load connected to the grid using its circuit schematics. The time-domain harmonic analysis approach is applied to nonlinear loads categorised based on their circuit topologies in [31]. Most electronic devices contain switch mode power supplies; therefore, equivalent time-domain models of SMPS are made. The current harmonic estimation was provided on simulated and measured waveforms. A similar model is used for computer loads connected to a single transformer [34]. The results show harmonic cancellation and voltage waveform distortion at the transformer. The mathematical models of low power compact fluorescent lamps were made to study harmonic penetration in [35]. The voltage and current waveforms were recorded and analysed using circuit simulation software. Although able to present an accurate harmonic analysis approach, the time-domain models have limited application as it is challenging to model every load connected to the grid using its circuit schematic.

2.5.2 Stochastic models

Distinctive load models In the distinctive load modelling approach, the load connected to the network is categorised based on their electrical properties, and the probability distribution of each group is defined to estimate the overall harmonic emission. For example, the network load can be divided into linear or nonlinear devices. These devices can be additionally split up based on circuit topology and power quality characteristics. A similar probabilistic harmonic analysis model was proposed in 1987 [36]. The model categorised nonlinear loads into four categories based on the switching state and operating mode. The harmonic aggregation analysis was performed using the Monte-Carlo approach with probability density functions (PDF) of harmonic magnitude and phase angles. Based on the appliance measurement data and their usage patterns, a harmonic analysis approach is used to study the harmonic impacts of the household appliance in the low voltage distribution grid [37]. The results obtained from the harmonic model is then compared with the real-time measurements of the network. A similar bottom-up probabilistic harmonic estimation modeling approach is presented in [38]. The model generates household appliance's usage patterns based on occupant behavior, and the appliance's equivalent circuits are used to analyse the harmonic emission. The simulation results of harmonic loads are compared with the actual grid measurement results to extract correlated data. In another study, a probabilistic model to analyse waveform distortions was presented under the influence of high penetration of electric vehicles (EV). The authors highlight this approach's importance as uncertainties associated with the EV charging patterns can be easily accounted [39]. The single and three-phase nonlinear loads are divided into groups based on their current THD in [40]. The participation of these load groups were obtained based on energy usage patterns at different times of the day. The author selects the customer database parameters by assuming that the data of any particular device type belongs to a normal distribution. The voltage distortion in the low voltage network was evaluated based on this probabilistic method.

Measurement based models In the measurement-based models, current harmonics emission is analysed from the probability distributions of harmonic current measurement data. The measurements could be taken at the electrical appliance level in a bottom-up approach, and aggregated harmonic analysis could give the harmonic estimation at the point of common coupling. In the top-down approach, measurements are taken at the distribution transformer. In both cases, extensive measurement data is usually compared

with an appropriate probability distribution. The voltage distortion in the distribution network was estimated by using Monte Carlo simulation of aggregated harmonic currents in [41]. The measurement data assume to fit a normal distribution. The harmonic currents are measured for the residential and commercial loads at the point of common coupling in [42]. The measurements are divided into low, medium, and high demand subgroups and compared with normal distribution and uniform distributions.

2.6 Stochastic modelling methodologies

Two different approaches can be used to construct a probabilistic model based on the type and amount of data [X]. The first approach could be termed as a parametric model where a finite set of data parameters can be compared with predefined distributions. In the second non-parametric approach, the model is based on distributions calculated from the data itself [43].

Parametric approach The parametric models mostly employ normal distribution defined by mean and variance. The probability density function of a normal distribution is indicated by Eq. (2.27).

$$p_x = \frac{1}{\sqrt{2\pi\sigma^2}} \times e^{-\frac{(x-\mu)^2}{2\sigma^2}} \tag{2.27}$$

Here σ is the standard deviation, and μ is the mean value of x.

In the early harmonic models, normal distribution was used to describe both magnitude and phase angles as independent variables. However, this assumption is not accurate for harmonic analysis. Therefore, a joint or bivariate probabilistic approach is more effective where the estimated variable depends on the probability density function of two variables. In [30], the load current for residential buildings is estimated using beta bivariate distributions. In [31, 32], joint normal distribution (JNB) is used for the forecasting of harmonic emissions. The parameters of the normal joint distribution, σ (standard deviation) and μ (mean value) are calculated by using Eqs. (2.28) and (2.29) using the complex components of the current i_x and i_y.

$$\mu_{xy} = \begin{bmatrix} i_x \\ i_y \end{bmatrix} \tag{2.28}$$

$$\sum xy = \begin{bmatrix} \sigma^2 i_x & \sigma(i_x, i_y) \\ \sigma(i_x, i_y) & \sigma^2 i_y \end{bmatrix} \tag{2.29}$$

Fig. 2.4a shows the 15th harmonic current when normal distribution fitting parameters are applied in a complex plane for a display monitor. The individual probability density of the real and imaginary parts of the current harmonics is shown by red and blue lines, respectively. The green circle enclosed the part of the distribution responsible for 95 percentile of the estimated values. Although the joint probability distribution provides better results than the individual normal distribution for x and y values; however, it can be effective only when both components are linearly dependent. The nonlinear devices with multiple operating modes result in different harmonic currents. The resultant distribution fit of these devices could be very different from the normal distribution. Fig. 2.4b shows the 9th harmonic current spread of a personal computer (PC) stress test in a complex plane where three different clusters are clearly visible. The normal joint distribution cannot represent this data efficiently. This problem can be addressed by clustering the data

and apply JNB to respective clusters. This approach is known as a multivariate normal mixture and provides a more flexible distribution fit [44]. The distribution mixture approach is used in [45] to study power quality impact in low voltage distribution. The PDF of the current harmonics are calculated by finite normal distribution components with their associated weights. The drawback of this approach is that the model requires predefined cluster information.
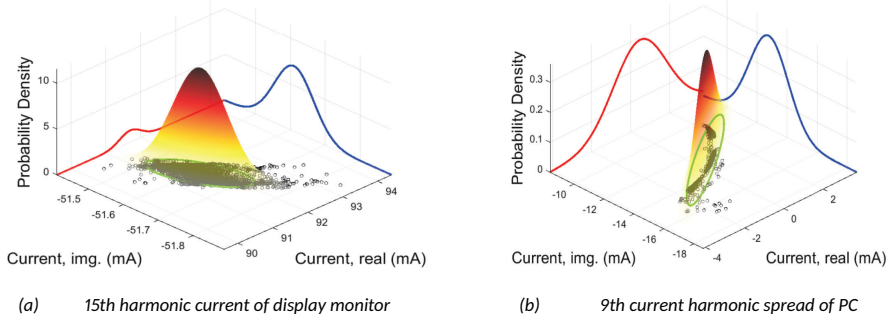

(a)   15th harmonic current of display monitor   (b)   9th current harmonic spread of PC

Figure 2.4 – Joint probability distribution applied to harmonic currents drawn by monitor and PC [X]

Non-parametric models   A non-parametric adaptive kernel density estimation (KDE) with a plug-in bandwidth selection approach is presented in [46]. The KDE algorithm designates probability distribution for every data point using a kernel function and bandwidth, also known as the smoothing parameter, indicated in Eq. (2.30).

$$p_h = \frac{1}{N} \sum_{n=1}^{N} K_b(h - h_n) = \frac{1}{N_b} \sum_{n=1}^{N} K \frac{(h - h_n)}{b} \tag{2.30}$$

Here, p_h provides the PDF of h for N observations. K is the kernel and b is the bandwidth. The sum of kernels provides the total probability density of a variable. The optimal bandwidth selection is critical in a KDE model. A large bandwidth will smooth the probability density curve but results in fewer data points in each kernel. As a result, information about data variation will be lost. The optimal methods for finding bandwidth are presented in [47].

The KDE algorithm, along with the Monte-Carlo simulation, is used to estimate harmonic load flow in [43] and [48]. However, harmonic current magnitude and phase angles are estimated independently, which will provide inaccurate phasors data results. A joint distribution from the KDE algorithm can generate better results where multidimensional vectors represent the parameters. In Fig. 2.5a, the KDE is applied to the 5th harmonic current measured during the PC stress test. This method requires intensive calculations, and high computational power is needed for even a small scale harmonic analysis.

Empirical bivariate histogram (EBH) distribution is another approach that divides data into predefined bins. The EBH distribution data is normalized by using Eq. (2.31) to create a probability density mesh.

$$p_{x,y} = \frac{C(x,y)}{N \cdot W_x \cdot W_y} \tag{2.31}$$

Here $p_{x,y}$ is the probability density of a bin at (x,y), $C(x,y)$ are the number of samples in the bin and W_x, W_y defines the area of the bin. N defines the total number of data
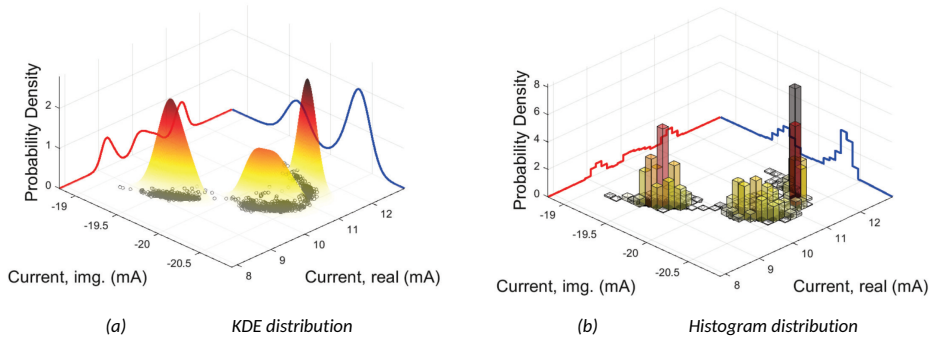
Figure 2.5 – KDE and histogram distribution applied to the 5th harmonic current of a PC [X]

points. Fig. 2.5b shows the histogram distribution applied to the 5th harmonic current of a PC under stress test. The advantage of EBH over KDE distribution is that it requires less computational power, however, both EBH and KDE distribution generate unused data space in the PDF when clusters are present in the data. Data sampling for these techniques is quite challenging.

3 Methodology

Household current harmonic emission estimation and modeling could be affected by several factors, including network configurations, load variations, and measurement uncertainties [49]. The modern electronic equipment has various operating modes, and their current harmonic spread is irregular with clustered data. The probabilistic approach of modelling current harmonics has the advantage of tackling any sporadic variations. Various stochastic models to estimate the current harmonics described in the previous chapter have several limitations in terms of accuracy or computational complexity. Most often, predefined probability distribution functions, such as normal distribution or joint-normal distribution, are compared with the current harmonic measurement data. This approach is not appropriate for the majority of the measurement data as they show different distribution spreads with clusters. The KDE and histogram distribution algorithms require bandwidth selection and become inefficient for clustered data. Load variations also have a significant impact on the current harmonics emission but mostly ignored in the existing models. Most appliances also have dynamic harmonic emission profiles because of a various operating modes. Therefore, the harmonic estimation methodology must be capable of addressing different uncertainties to reflect a realistic outcome.

3.1 Proposed stochastic harmonic estimation model

A stochastic harmonic estimation (SHE) model is proposed in this thesis to evaluate the impact of current harmonics emission in the low voltage residential network. The measurement data of end-user appliances is modelled with an empirical bivariate probability distribution approached. The bivariate analysis provides the impact of both magnitude and phase variation on harmonic estimations. The stochastic load usage patterns are generated based on the device level measurements and survey data.

The model consists of three parts; device usage model (DU), measurement database, and bivariate harmonic current (BHC) model. The model will simulate the required number of houses for a given number of days to estimate harmonic currents magnitude and phase angles generated by each household appliance and electric vehicle [IV].

The household appliances and EVs are measured by using a controllable power supply on different voltage waveforms. In the BHC model, the current harmonic magnitude data is used to generate the empirical cumulative distribution function (ECDF) for all harmonics under consideration. The ECDF will group the data into bins along with their probabilities based on the predefined resolution. Each magnitude group is then mapped with the phase groups generated by a separate ECDF for the harmonic phase data. A Monte Carlo simulation is used, and all houses are populated with the appliance stock. During each iteration, the DU model generates the usage pattern of each appliance or EV by comparing uniform random numbers with the respective distribution functions. All end-user devices are simulated individually, and the total harmonic emission of an individual household is aggregated after each iteration. The aggregation of the current harmonics is performed in a complex plane by vector addition; therefore, the model provides the real and complex (X and Y) harmonic components for all devices. The algorithm of the model is described with a flow chart, as shown in Fig. 3.1. The dotted lines separate the model's input simulation parameters, including the number of houses and days. The DU and BHC models are shown by red and green dotted boxes.
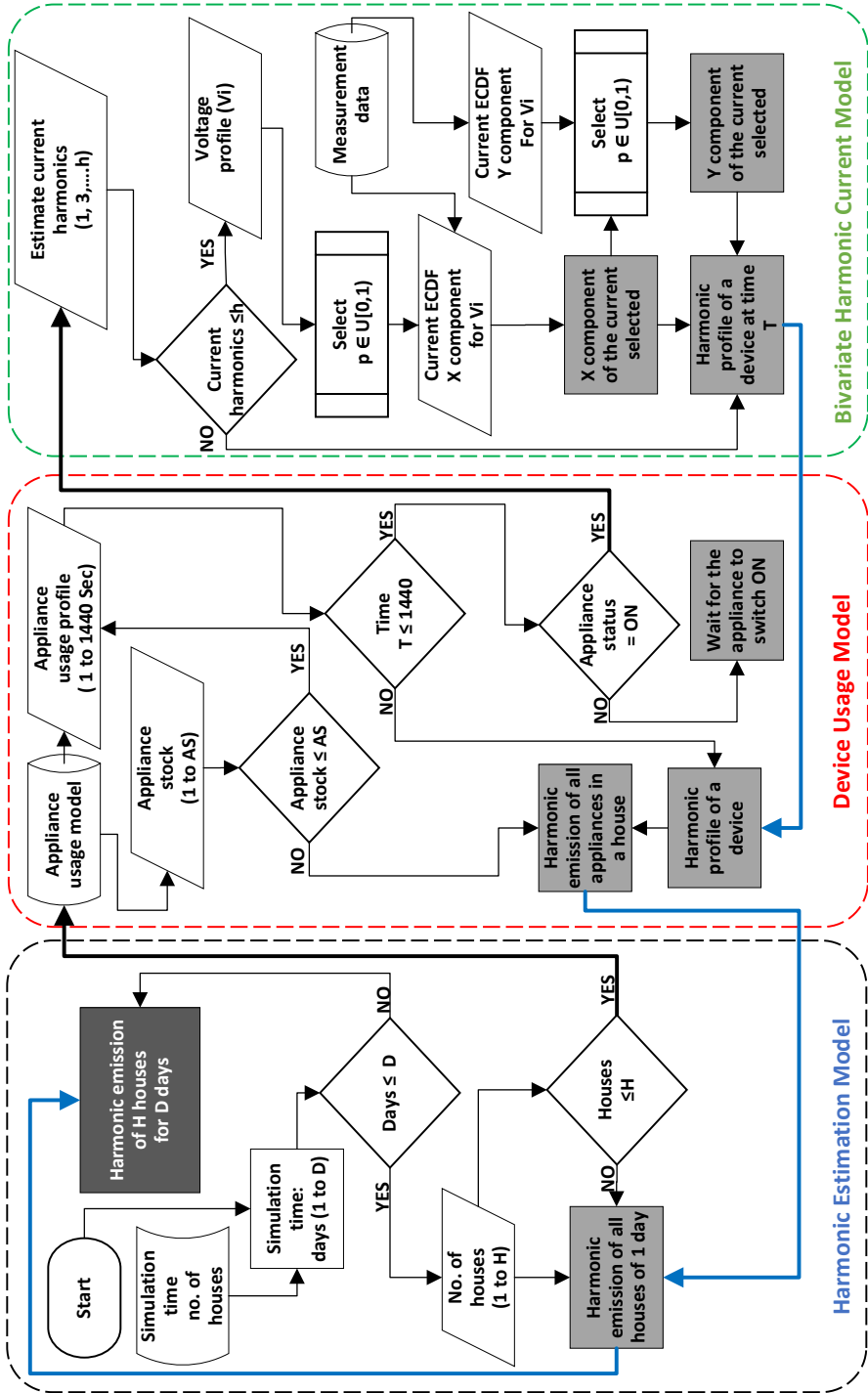
Figure 3.1 – Flow chart of the proposed model [IV]

3.1.1 Measurement database

The measurement database will include current harmonic measurements of different domestic loads. It will consist of measurements of appliances with different operating modes at various voltage waveforms. Sinusoidal, peak top, flat top, and real-time grid voltage waveforms are used as an input. For the real-case grid voltage waveforms, a low voltage residential network is measured at 5-minute intervals for a day to record the voltage harmonic magnitude and phase angles.

A test bench has been developed for the measurements of loads with support of up to 16 loads at a time. The sockets are connected to a controllable supplied bus-bar through relays. A control box controls the relays and consists of a DC power supply and transistor switches. A National Instruments data acquisition module (DAQ) is used to provide the digital inputs to the control box and analogue reference signal to the controllable power supply. Two different controllable power supplies, 4 kVA Chroma 61505 and 1.7 kVA Omicron C356 are used to generate desired voltage waveform. Power supplies are controlled via reference signal V_R provided by the DAQ.

$$V_R = \frac{V_{out}}{V_{range}} \times V_{coef} \tag{3.1}$$

Here, V_{coef} is 7.072, and V_{range} is 300 V. A MATLAB program is used to generate this reference voltage and digital signals for the control box through the DAQ module. Amplitude and phase angles for each odd harmonic are used to synthesise the programmable power supply's reference signal. Eq. (3.2) is used to calculate the V_{out} from the given amplitude and phase angle of the fundamental and odd harmonics up to the 19th harmonic.

$$V_{out} = \sum_{n=1}^{N} \sqrt{2} \times A_n \sin(2\pi f_n t_s + \alpha_m) \tag{3.2}$$

Here, A_n is the RMS value of harmonic magnitude and f_n is its frequency. The α_n is the
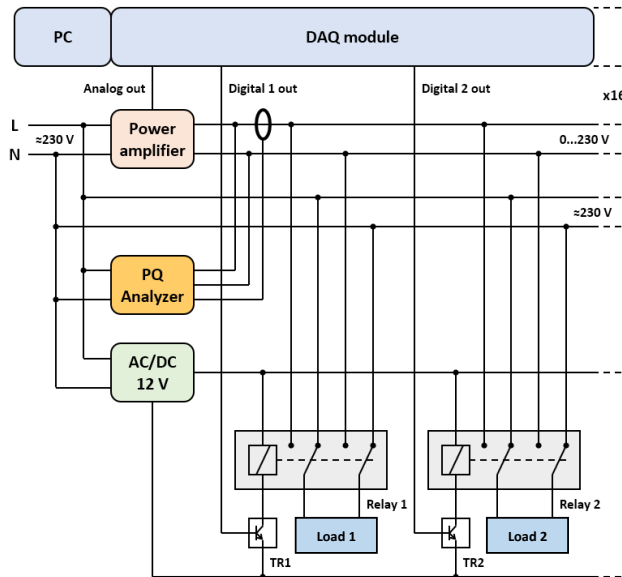

Figure 3.2 – Measurement setup [IV]

phase difference between the harmonic and the fundamental component. t_s is the sampling interval for which the calculation has to be made. It is calculated from the sampling frequency f_s as shown in Eq. (3.3).

$$t_s = \frac{1}{f_s} \tag{3.3}$$

The sampling frequency can be calculated by the time duration T_m of the waveform to be generated and the number of samples in that interval N as shown by Eq.(3.4).

$$f_s = \frac{N}{T_m} \tag{3.4}$$

This setup has enabled us to generate a pure sinusoidal voltage with a sampling frequency of 100 kHz. For power quality measurements, A-Eberle PQ-BOX 200 is used to record harmonic magnitude and phase angles with 41 kHz sampling frequency. The PQ-BOX 200 is capable of recording power quality data with a 1-second resolution. The 1-second data is based on the average values calculated at 200-ms according to IEC 61000-4-30 standard. Fig. 3.2 shows the block diagram of our measurement setup.

3.1.2 Bivariate harmonic current model

The bivariate harmonic current modelling approach is suitable for harmonic analysis of loads with the dynamic profile of harmonic emission and also capable of addressing different uncertainties responsible for current harmonics variations. The current harmonics of individual appliances will be modeled using ECDF. In the first step, the ECDF for the real part of the current in the complex domain is calculated. Each group of this ECDF is further mapped with the complex part of variable's data group, and the ECDF of each bivariate data group is calculated. The resolution of the ECDF determines the accuracy of the harmonic estimation model. ECDFs for both real and imaginary components are calculated using Eq. (3.5).

$$p_m(X \leq x) = \frac{1}{m} \sum_{k=1}^{m} \mathbf{I}[x_k \leq x] \tag{3.5}$$

Here p_m is the cumulative probability function of m groups. The $\mathbf{I}$ is called indicator function and has two possible values as shown by Eq. (3.6).

$$\mathbf{I}[x_k \leq x] = \begin{cases} 1 & for\ x_k \leq x \\ 0 & for\ x_k > x \end{cases} \tag{3.6}$$

Fig. 3.3 shows the how ECDFs of real and imaginary components of the current harmonics can be used to create distributions in the complex plane. The red line shows the ECDF of the real component of the harmonics and each blue line indicates the ECDF of the imaginary components at each group of the real component ECDF.

3.1.3 Device usage model

An efficient current harmonic estimation model should take into account the load variation in the distribution grid. Harmonic injection in a network at a given time depends on the type and amount of load connected to the grid on that particular instant. However, the load prediction is a complex task as it is difficult to estimate when the consumer will use a particular appliance. The occupant behavior of using electrical appliances is challenging to model as it depends on many factors. Occupants interact with the electrical and nonelectric systems installed in the building, thus, altering the energy usage patterns [50].
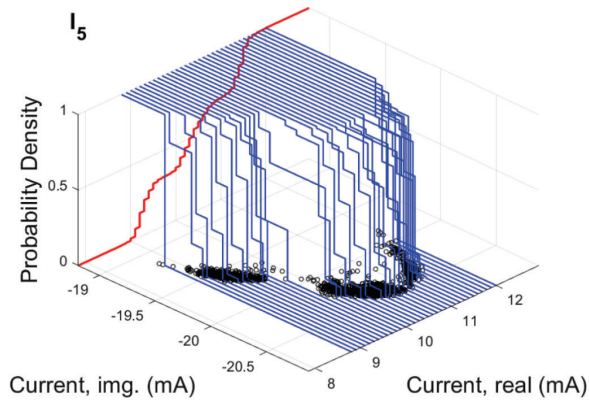
Figure 3.3 – Empirical bivariate distribution applied to the 5th harmonic of the PC under stress test [X]

The International Energy Agency (IEA) also regards occupant actions as the primary cause of controlling the environmental parameters to maintain a comfortable living atmosphere [51]. These occupant actions are responsible for 71% variation in the building's energy consumption [52]. However, various factors influence the resident's behavior, including their age, income, social status, and cultural background [53]. The building structure, insulation quality, climate conditions also play their role. Therefore, universal occupancy modeling is near to impossible.

The electricity consumption models can be broadly classified into three categories: top-down models, bottom-up models, and hybrid models [VI]. The top-down modeling approach is based on data collected on the macro-level. It may include an electricity billing database, national census, or survey data. The researchers have frequently used the Time Use Survey (TUS) data collected in Europe, Britain, and America for their energy consumption models. These surveys collect data from the targeted groups based on different parameters. The models based on similar data have many drawbacks and lack the capability to provide a detailed analysis of the physical behavior of the building systems.

The bottom-up models are based on physical measurements at the device or building level. Nevertheless, these models provide accurate information regarding energy consumption in a building but are complicated to construct due to the involvement of several variables. These variables include occupancy, occupant behavior, climate conditions, building structure, and an extensive database of appliance's measurements. As it is difficult to consider each variable in detail, a compromise is required to make a specific model for a particular research problem. Another approach is to combine the benefits of both bottom-up and top-down approaches to improve efficiency. These models are termed as hybrid models [54].

A residential electricity consumption model to estimate current harmonic emissions from the building is required. Therefore, a high-resolution bottom-up model is required to provide usage patterns of domestic appliances that can be compared with the power quality measurements. Fig. 3.4 shows the abstract diagram of the device usage model for residential buildings. For this purpose, a residential building in Estonia is measured at the device level for one month. The data is used to construct a probabilistic model to estimate the switching behavior of the appliances. The model consist of active occupancy profiles, appliance stock in the households, and the electricity consumption measurements
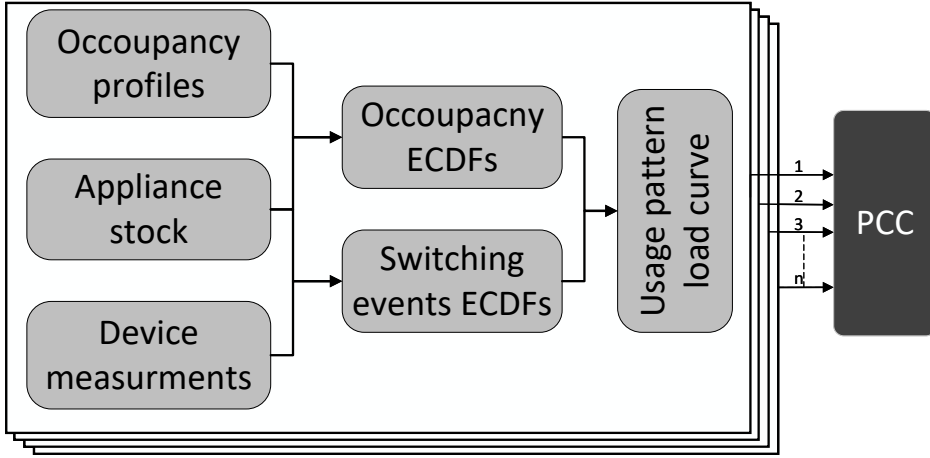
as shown in Fig. 3.4.

Figure 3.4 – Abstract diagram of the harmonic estimation model [IV]

Active occupancy profiles are created based on the electricity consumption of the appliance that comes under the direct influence of the occupant's activities. Usage of lighting, media, kitchen, cleaning, and laundry appliances directly depends on the occupant's behavior. Electricity consumption meter data has been used for occupancy modelling in many studies [55, 56, 57, 58]. A similar approach is used here to create a two state active occupancy profile. ECDFs are created for both weekdays and weekends occupancy status based on the electricity consumption data. A survey related to the occupant's daily activities is also used to improve these occupancy profiles.

Every household has a different set of appliances depending on the family size, geographical location and socioeconomic status. Appliances are also available from different manufacturers with various specification. Manufacturers introduce new models every year with improved functionality and energy ratings. The appliance ownership information can be extracted from several surveys conducted on national level in different countries. A domestic energy model is created on the bases of common appliance provided by national ownership statistics for United Kingdom (UK) in [59]. Similar surveys are also conducted in Europe, and USA.

The device usage model will provides the information when a particular appliance is switched ON in the house. The ECDFs are used to generate switching and duration interval of each appliance in the house. The total electricity consumption of a single housing unit can be determined from the Eq. (3.7).

$$E = \sum_{day=1}^{D} \left[\sum_{ap=1}^{n} [P_w \times d_w] + [P_{sd} \times d_{sd}] \right] \tag{3.7}$$

Here P_w shows the active power of the appliance ap in its working mode and P_{sd} is its active power consumption in the standby mode. d_w and d_{sd} are the time duration of the appliance operating in active or standby mode during a day.
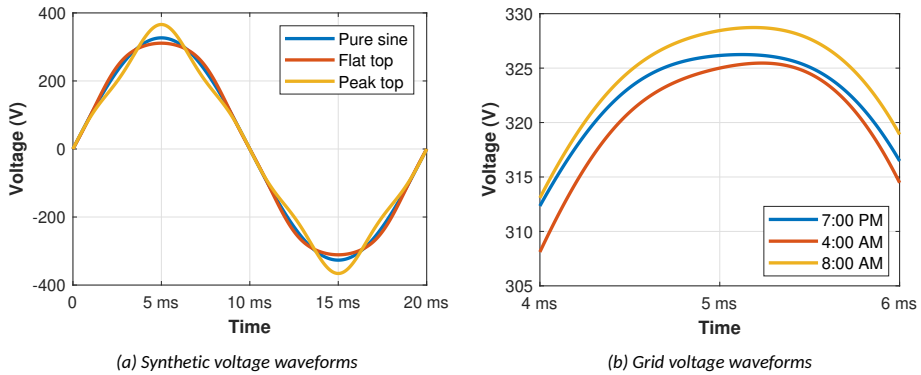
| (a) Synthetic voltage waveforms | (b) Grid voltage waveforms |

Figure 3.5 – Voltage waveforms used for current harmonics measurements [IV]

3.2 Measurement database

The measurement database contains the current harmonic measurements of different household appliances operating at different working modes on various voltage waveforms. We have used sinusoidal, peak top, flat top, and real-time grid voltage waveforms as an input to measure current harmonics.

For the real-time grid voltage waveforms, a low voltage residential network is measured at 5-minute intervals for a day to record the voltage harmonic magnitude and phase angles. Fig. 3.5 shows the voltage waveform used to measure the current harmonic emission from the household appliances using the measurement test bench.

The harmonic current estimation model is based on the power quality measurement data of the appliance portfolio. The device usage patterns are compared with each household appliance's harmonic current profiles. The model can be used to evaluate total harmonic emission of multiple house as shown by Fig. 3.6.
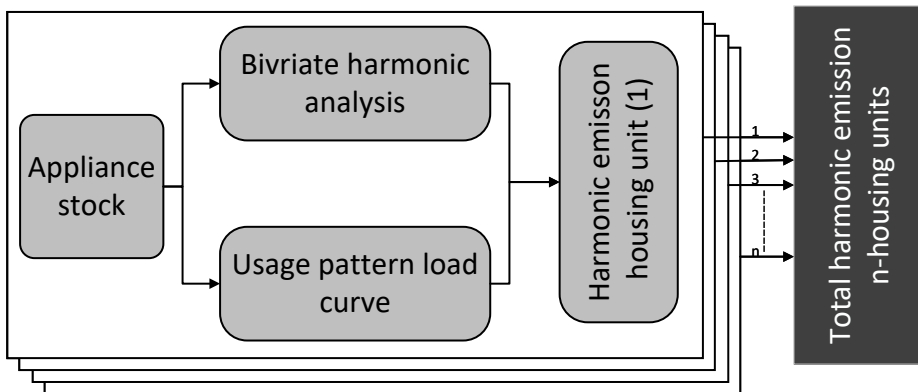

Figure 3.6 – Harmonic current estimation of multiple households [IV]

35

4 Device usage modelling

The harmonic emission in the low voltage residential grid is stochastic in nature because of the random states of the load. A load can be in an ON or OFF state at a particular instance during a day. Furthermore, modern loads, such as washing machines and dishwashers, also have different operating modes. The occupant behaviour and preference also affect the amount of load connected to the network. Therefore, a bottom-up stochastic modelling approach is required to estimate usage patterns that could provide information about various domestic load's state and operating modes.

With every passing year, more efficient versions of appliances will be available. It is, therefore, essential to make the device usage model compatible with future advancements. A feasible approach is to make a model that will estimate only the usage pattern of all electrical appliances in a house instead of their output power at any given time. This approach would require a detailed analysis of the working of the appliance and how the dwellers are using them. Appliance ownership surveys are regularly conducted in different counties and provide the ownership share of major appliances in households. Researchers frequently use this data to construct their energy models. An energy model developed for households in the United Kingdom (UK) has selected the most common residential building appliances based on national ownership statistics in the UK [60].

Household appliances can be grouped into cold appliances, standby appliances, active appliances, and continuous appliances [61]. Table 4.1 shows some of the standard appliances found in the residential buildings. All these appliances are used and work in a different way when compared with each other. Hence, a different approach is required to model each of them.

Table 4.1 – Categories of household appliances [VII]

Type	Appliances
Cold appliances	Refrigerators, freezers and heating or cooling systems
Standby appliances	Entertainment units: TV units, sound systems, gaming consoles, computers
Active appliances	Laundry appliances: irons, cloth washers and dryers Kitchen appliances: cookers, dishwashers, blenders, mixers Cleaning appliances: vacuum cleaners
Transport	Electric vehicles, electric scooters

4.1 Occupancy model

Occupant activities are the primary reasons for the high variation in residential electricity demand. Occupant behaviour affects the electricity demand in the residential building actively and passively. For example, when the building is occupied, demand variations for lighting, heating, and cooling are the passive effects that alter electricity consumption. The impact of active occupancy includes the occupant's interaction with the thermostat setting, usage of the electrical appliance, window blinds settings, and windows or door opening to improve indoor environment quality.

Demand sharing is an important aspect to consider during occupancy modelling. The increase in occupancy level in the residential buildings does not increase the electricity demand in the same proportion. The reason behind it is the sharing of appliances such as lighting and heating among occupants. The occupancy data is difficult to record because of privacy concerns, and therefore reliable data-sets are not available. An alternative ap-

proach is to use electricity demand data to determine the occupancy parameters. The electricity consumption data of appliances that come under the direct influence of occupants can reflect the occupancy status of a building with reasonable accuracy [58, 62]. The two-state or binary occupancy models based on electricity consumption data is presented in [63]. The model can detect occupancy states in residential and commercial buildings using non-intrusive learning algorithms on aggregated electricity consumption data. A more straightforward approach is to use smart meter data installed at the device level to record appliance electricity consumption. Several studies have proposed occupancy models based on the electricity consumption data-set obtained through smart meters [64, 56, 65, 66].

A similar approach is used and the device-level electricity consumption data is converted into two-state occupancy profiles. The electrical appliances are categorized as interactive and noninteractive loads. The interactive loads include entertainment units, lighting, dishwashers, washing machines and other plug-in appliances, while refrigerator and heating are considered as noninteractive loads. The electricity consumption data of noninteractive load is regarded as the background load with a relatively consistent range and can be calculated by the following relation.

$$P_b(t) = \sum_{NIL=1}^{n} P_{IL} + \sum_{sd=1}^{m} P_{sd} \qquad (4.1)$$

Here P_b is the background load equal to the sum of power consumption P_{NIL} of n non-interactive devices and standby power P_{sd} of m interactive device operating at time t. During any time in a day, the instantaneous power consumption $P_T(t)$ of a residential unit includes the individual electricity consumption of both Interactive and noninteractive appliances.

$$P_T(t) = \sum_{IL=1}^{N} P_{IL} + \sum_{NIL=1}^{M} P_{NIL} \qquad (4.2)$$

P_{IL} and P_{NIL} are the power consumption of any individual interactive and noninteractive loads, respectively. A residential building has active occupants if the instantaneous power consumption of the residential building is greater than the maximum value of the background load consumption, as shown by Eq. (4.3).

$$O_f(t) = \begin{cases} 1 & \text{when } P_T(t) > P_b(max) \\ 0 & \text{when } P_T(t) \leq P_b(max) \end{cases} \qquad (4.3)$$

Fig. 4.1 shows the electricity consumption of a household on a weekday. The top graph shows the load of background appliances, and the middle graph shows the load of interactive devices. The red line shows the binary state occupancy curve. The high value of occupancy indicates the presence of active occupants in the house. The occupancy detection algorithm extracts the binary occupancy profiles from the measurement of household electricity consumption data. The data is divided into morning, evening and day time occupancy cycles. For each cycle, the initial and final time interval of the occupancy cycle is stored. The data will provide start time T_{oc} and the duration D_{oc} of each occupancy cycle. Empirical distributions are used to construct a stochastic occupancy model.

Empirical distributions is a probability distribution based on observed data. They can be visually represented as empirical histograms. For a given data-set $X_1, X_2, ... X_n$, the empirical distribution function $p_n(x)$ places mass $1/n$ in the n points. If $y_1 < y_2 < y_3$ are the order of the observed random sample and no observation is equal to each other, then
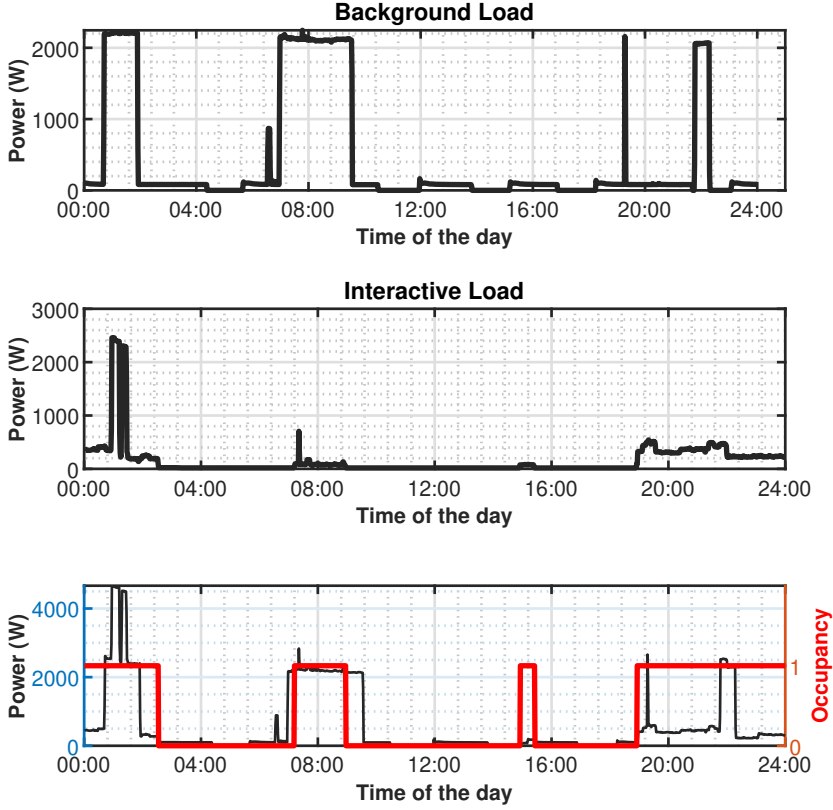
Figure 4.1 – Occupancy curve from the load profiles

$p_n(x)$ can be defined as:

$$p_n(x) = \begin{cases} 0 & \text{for } x < y_1 \\ k/n & \text{for } y_k < x < y_{k+1} \\ 1 & \text{when } x \geq y_k \end{cases} \qquad (4.4)$$

Here $k = 1, 2, ..., (n-1)$ and mathematically it can be defined as:

$$p_n(x) = \frac{1}{n} \sum_{k=1}^{n} \mathbf{I}\{X_k \leq x\} \qquad (4.5)$$

where $\mathbf{I}$ is the indicator function

$$\mathbf{I}[X_k \leq x] = \begin{cases} 1 & for\ X_k \leq x \\ 0 & for\ X_k > x \end{cases} \qquad (4.6)$$

The empirical distribution and histogram of the start time T_{oc} for the evening occupancy cycle is shown in Fig. 4.2. Similarly, the empirical distributions for the occupancy cycle duration D_{oc} is determined. The occupancy is determined for each day using a Monte Carlo simulation by generating a random number $x_U[0\ 1]$ from a uniform distribution in
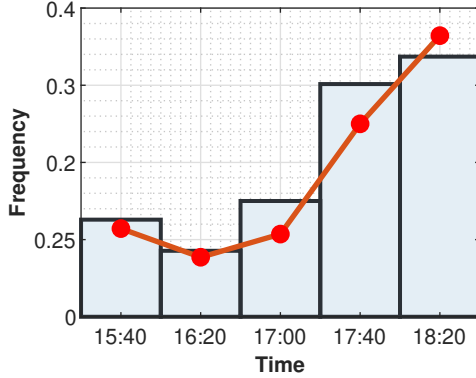
38

Figure 4.2 – Empirical distribution of occupancy

each iteration. T_{oc} and D_{oc} are estimated by comparing the random number with the respective ECDFs using the following equation.

$$y = y_1 \left(1 - \frac{x_U - x_1}{x_2 - x_1} \right) + y_2 \left(1 - \frac{x_2 - x_U}{x_2 - x_1} \right) \tag{4.7}$$

Where x_1 and x_2 are the probabilities for y_1 and y_2.

4.2 Lighting load

Lighting consumes a significant portion of the total end-user electricity consumption in the residential sector. It is highly variable because of its dependence on the solar cycle, irradiance factor, building design, and dweller's preference for lighting needs. Building indoor environment, aesthetics, number and size of the windows also play a vital role in the amount of lighting used. Therefore, the lighting load of different apartments in the same building can be very different from each other. An efficient lighting model must also be capable of tackling daily and annual variations in the lighting demand with the seasonal and solar cycle variation.

A residential building can have several lamps, depending on the floor size. The power rating and light output of each lamp could be different. The selection of a lamp by the customer is influenced by the price tag, power ratings, lumens, and light quality. However, they are not aware of the lamp characteristics, power quality information, and design technology.

A lighting switching-based strategy is proposed in this thesis that can provide a high-resolution model based on a residential building's measurement data. Usage patterns of light switches are modelled instead of lighting power demand. This model can simulate the lighting usage of each lamp at a high time resolution of 1-minute.

For the lighting load, a single sub-meter provided the aggregated power consumption of all the lights in the building. The aggregated consumption data of lighting load is decomposed to find individual lamp's usage profiles using clustering. The clusters are compared with the active power of unique lamps in the building to find each lamp's usage patterns. The total consumption is further divided into three intervals: morning, day and evening cycles. The measurement data shows an identical usage pattern during these intervals. The consumption patterns during weekdays and weekends were also different.

The usage pattern of each lamp is divided into switching and noise events. A switching

event occurs when the lamp is used for more than 10 minutes. Usage interval of less than 10 minutes is accounted for a noise event. The switching and noise events during the morning, day, and evening intervals are calculated for all the lamps.

A Markov chain model is used to determine the type of event. The Markov chain is a stochastic approach that describe a sequence of possible event where the probability of the future event depends only on the present state. For the $s_0, s_1, s_2, ..., s_n$ possible states of a random variable, the nth state can be calculated using Eq (4.8).

$$p(X_n = s_n \mid X_{n-1} = s_{n-1}) = p(X_n = s_n \mid X_0 = s_0, \ X_1 = s_1, ..., X_n = s_n) \qquad (4.8)$$

Since there are only two states of a light event; therefore, for every time step $t = 1, 2, .., N$, the event must have any of the two states as shown in Fig. 4.3.
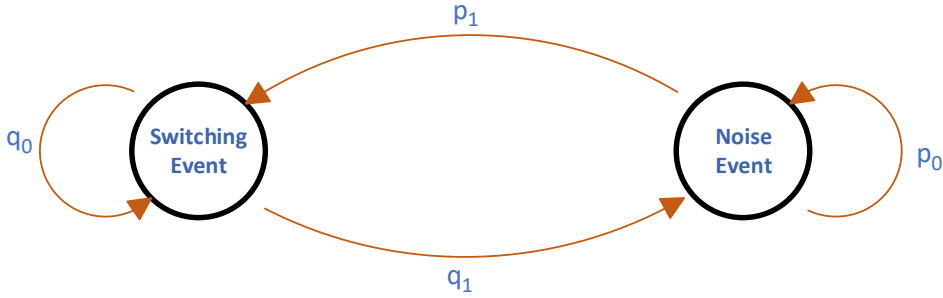

Figure 4.3 – Transition probability of lighting events

After each event at time step t to $t+1$ the transition probability p_t will determine the next event going from state i to j. The transition probability is defined by the Eq. (4.9)

$$p_t(ij) = \begin{bmatrix} p_0 & q_1 \\ p_1 & q_0 \end{bmatrix} \qquad (4.9)$$

The transition probabilities will vary and selected from the precalculated groups based on the measurement data. As the lighting usage depends on the active occupancy in a building, the occupancy model is used to determine the morning, day and evening lighting interval's start time and duration.

The empirical distribution functions for the number of switching events, noise events and their duration during each lighting interval for all days is calculated using Eq. (4.6) and Eq. (4.7). The duration of each switching event d_{sw} and noise events d_{ns} can be used to find the total lighting demand of each house for a day with 1-second resolution, as shown by Eq. (4.10).

$$P_T = \sum_{sw=1}^{n} (d_{sw} \times P_{sw}) + \sum_{ns=1}^{n} (d_{ns} \times P_{ns}) \qquad (4.10)$$

The lighting power consumed during each switching and noise events P_{sw} and P_{ns} can be calculated by Eq. (4.11) and Eq. (4.12).

$$P_{sw} = \sum_{s=1}^{n} \sum_{L=1}^{m} P_L \times T_s \qquad (4.11)$$

$$P_{ns} = \sum_{N=1}^{n} \sum_{L=1}^{m} P_L \times T_N \qquad (4.12)$$

The T_s and T_N are the time duration for each individual switching and noise event, respectively. A Monte-Carlo approach is used by selecting random lamps based on the light output needed in each room. The light output is calculated by the type of lamps used in the building measured for the data collection. During each run, lamps were selected randomly form uniform distribution. Fig. 4.4 shows the mean, and 90th percentile values of power consumption of LED lamp usage in 60 houses.
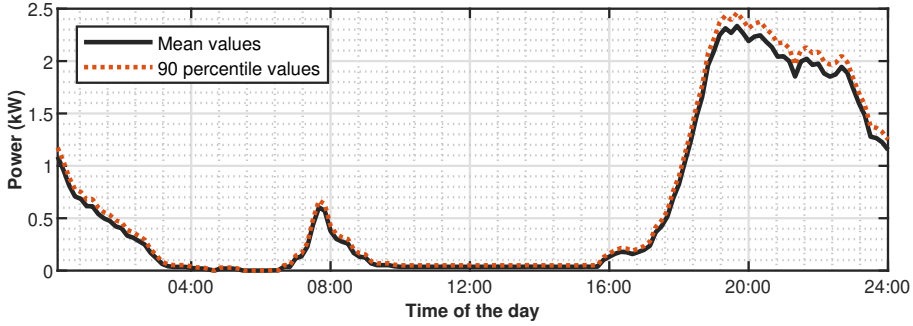

Figure 4.4 – Lighting power consumption of 60 houses (only LED lights)

4.3 Cold appliances

The cold appliance includes freezers, refrigerators and heating equipment. These appliances are controlled by thermostat settings and operate continuously in a cyclic manner. The energy consumption of cold appliances is relatively constant over a daily basis and, therefore, easier to model. The influencing factor on energy consumption of these appliances is user preference and ambient temperature. The electric operation of the cold appliance is categorized into high power P_{hi} and low power P_{low} cycles. The variation in both cycle's time duration depends on the influencing factors and can vary in a predefined range based on the measurement data. For example, in the case of refrigerators or freezers, the length of operating cycles depends on the thermal efficiency of the storage compartment, the amount of food storage, and the frequency of opening the door [60]. When the residential building is actively occupied, human interaction alters the duration of operating cycles of cold appliances. The high power and low power cycle duration's are separately calculated for both occupancy states. The total power consumption of a cold appliance can be calculated by using the following equation.

$$P_{cold} = \sum_{O_f=0}^{1} \left(\sum_{n=1}^{N} (d_n \times P_{hi}) + \sum_{m=1}^{M} (d_m \times P_{low}) \right) \tag{4.13}$$

The duration d_n and d_m are obtained from their ECDF's calculated during both occupancy states using Eq. (4.5) and Eq. (4.7).

4.4 Standby appliances

Standby appliances include entertainment devices such as television sets, speakers, gaming consoles and IT equipment, including computers, printers, etc. These devices have a low power standby mode that helps the user to start the device immediately by pressing a button. The power consumption in the standby mode is almost negligible in compari-

son to the active mode. However, patterns of both modes are required to simulate the behaviour of standby appliances.

The active mode duration depends on occupancy and occupant's behaviour. For example, it is more likely that entertainment devices will be used during the evening period on weekdays. Similarly, computer or laptops usage also depends on occupant behaviour. This usage pattern of each standby appliance varies and, therefore, should be simulated individually. The Eq. (4.14) represents the power consumption of a standby appliance for a day.

$$P_T = P_H + P_{sd} \tag{4.14}$$

Where P_H and P_{sd} are the power consumption during device usage and in standby mode and can be calculated using Eq. (4.15) and Eq. (4.16), respectively.

$$P_H = |\sum_{n=1}^{N} (d_H \times P_h)| \quad \text{for } O_f = 1 \tag{4.15}$$

$$P_{sd} = |\sum_{m=1}^{M} (d_{sd} \times P_s)| \quad \text{for } O_f = 0 \tag{4.16}$$

Here d_H and d_{sd} are the duration of device usage and standby cycles and calculated by their ECDF's using Eq. (4.5) and Eq. (4.7).

4.5 Active appliances

All other household appliances that do not fall into the above mention categories are termed active appliances. These appliances are difficult to model as their usage patterns depend on the individual user preferences and behaviour. These appliances are further categorised based on their relation to the type of occupant activities. Time-series power consumption data is used to determine each appliance's ON and OFF time in the house. The operating duration of a device is calculated based on t_{ON} and t_{OFF}.

$$D_t = t_{OFF} - t_{ON} \tag{4.17}$$

The data of the time values at which a particular device is turned ON during the measurement data of 1 month is clustered to determine the ON-time groups. The clustering is based on dividing N data points into k clusters in which each data point belongs to the cluster with the minimum distance from its centroid. The centroid of each cluster depends on the mean value of the data points assigned to that cluster.

A set of m data points $t^{(1)},...,t^{(m)}$ grouped into a few cohesive clusters. The vectors for each data point $t^{(u)} \in \mathbb{R}^n$ are given without labels. The algorithm will predict k centroids and a label $c^{(u)}$ for each data point. The k-means clustering algorithm is a two step algrothim. In the first step, the centroids are selected randomly $\mu_1, \mu_2, ..., \mu_k \in \mathbb{R}^n$ and then minimize the objective function indicated by Eq. (4.18).

$$J = \sum_{u=1}^{m} \sum_{k=1}^{K} \zeta_{uk} \ ||t^u - \mu_k||^2 \tag{4.18}$$

where,

$$\zeta_{uk} = \begin{cases} 1 & \text{if } t^u \in k\text{th cluster} \\ 0 & otherwise \end{cases} \tag{4.19}$$

During each iterating, first J is minimized with respect to ζ_{uk} and the centroids are considered as constant. In the second step, the J is minimized with respect to μ_k. The centroids are updated after assigning values to the clusters in each step. Therefore, the $(m-1)$th step is:

$$\frac{\partial J}{\partial \zeta_{uk}} = \sum_{u=1}^{m} \sum_{k=1}^{K} \zeta_{uk} \ \|t^u - \mu_k\|^2 \implies \zeta_{uk} = \begin{cases} 1 & \text{if } k = argmin_j \|t^u - \mu_j\|^2 \\ 0 & otherwise \end{cases} \tag{4.20}$$

The t^u is assigned to a cluster based on the least squared distance from its centroid. The mth step is:

$$\frac{\partial J}{\partial \mu_k} = 2 \sum_{u=1}^{m} \zeta_{uk} \ (t^u - \mu_k) = 0 \implies \mu_k = \frac{\sum_{u=1}^{m} \zeta_{uk} \, t^u}{\sum_{u=1}^{m} \zeta_{uk}} \tag{4.21}$$

The probabilities are assigned to each ON-time group to determine from the clustering. If there are N data points, then the probability assigned to each cluster P_k is based on the number of data points n_k belong to that cluster.

$$P_k = \frac{n_k}{N} \tag{4.22}$$

The data point in the clusters are used to construct the empirical distribution using Eq. (4.5) and Eq. (4.7).

4.5.1 Laundry appliances

The washing machines and dryers have high variation in their usage, and their usage patterns are modelled over weekly rather than on a daily basis. The usage of laundry appliances depends on the occupant decision to use them. Modern washing machines have various operating modes for different washing cycles. A typical washing cycle includes water heating, spinning, washing and rinse sub-cycles. The power consumption and harmonic emission of each cycle are also different and therefore challenging to model. The usage patterns are modelled without taking into account various operating modes. The power consumption and harmonic emission variation for different operating modes will be performed in the harmonic estimation model.

The device-level electricity consumption data indicates that usage of laundry appliances is more frequent on weekends. However, usage frequency could vary from zero to multiple values. The usage times are clustered into groups using Eq. (4.18) and probabilities are assigned to each group. The usage time is selected from the group based on the Markov chain model. The power consumption of the washing machine can be calculated using the following relation.

$$P_{Laundry} = |\sum_{n=1}^{N} \sum_{t=1}^{d_n} (P_t)| \quad \text{for } O_f = 1 \tag{4.23}$$

Here d_n is the duration of each washing cycle.

4.5.2 Kitchen appliances

The kitchen appliances include dishwashers, stoves, blenders and mixers. The usage patterns of dishwashers and stoves are more consistent as they follow the eating schedule of the occupants, while the usage patterns of remaining kitchen appliances are more random during active occupancy. The duration of usage of kitchen appliances is mostly variable

except for dishwashers. The dishwasher can be operated in various modes, and duration of each mode can be different. However, it is more likely that occupants are habitual to select a single operating mode most of the time, while other operating modes are selected rarely. Few kitchen appliances have more frequent usage during the morning period, such as coffee makers and toasters.

The eating schedule is simulated during the evening time based on the occupancy profiles. The cooking time is selected based on a random selection between short, medium and long time values required for the recipe. The start times are selected from a normal distribution applied to a particular house's probable eating schedule.

$$p(T_n) = |\frac{1}{\sigma\sqrt{2\pi}} e^{-\frac{1}{2}\left(\frac{T_n - \mu}{\sigma}\right)^2}| \quad \text{for } O_f = 1 \tag{4.24}$$

Where μ is the mean cooking time and σ is the variance. The cooking duration is selected using the same method. The kitchen appliances are selected based on the assumed probability of usage. The duration of usage for each appliance is also selected from the probability matrix assigned to each device. The appliances like food processor and blender has low usage time while the electrical cooker has high usage time.

During the morning time, the breakfast schedule is estimated using Eq. (4.24). The usage of coffee machine and toaster are assigned based on the device usage probability matrix.

### 4.5.3 Cleaning and other plug-in appliances

The usage of a cleaning appliance such as a vacuum cleaner is random when the building has active occupancy. The probability of using cleaning appliances by the occupant is more during weekdays evening period and on weekends. The usage time is also variable every time. In addition to vacuum cleaners, other plug-in appliances used by the occupants during 30 days of measurements are modelled together as power outlets for plug-in devices is measured using a single meter. The devices are separated later by matching the power consumption of individual plug-in appliances with the measurement data.

The device usage times are clustered using Eq. (4.18). The probabilities are assigned to each cluster based on the number of elements in each cluster. The ECDFs are calculated for the device usage duration and the usage times for each cluster using Eq. (4.5) and Eq. (4.7).

Fig. 4.5a and Fig. 4.5b shows the device usage patterns on a weekday and weekend. While simulating several houses, appliance are added based on the appliance stock data obtained by Estonian household survey.

4.6 Electric vehicles

The transport sector is a significant contributor to GHG emissions. Road transportation has the largest share and accounts for almost 75% of the total emission from the transport sector. Passenger vehicles are the primary contributors, with a CO2 emissions share of more than 45%. With the transport sector primarily relying on fossil fuels for energy sources, policymakers are encouraged to shift towards alternative technologies to reduce emissions and improve energy efficiency practices. The electrification of the transport sector provides a sustainable alternative to achieve these targets. Electric vehicles (EVs) provide high conversion efficiency with the potential to use renewable sources to deliver the energy needed. However, the increasing penetration of EVs also presents new challenges for the existing power system infrastructure [III].
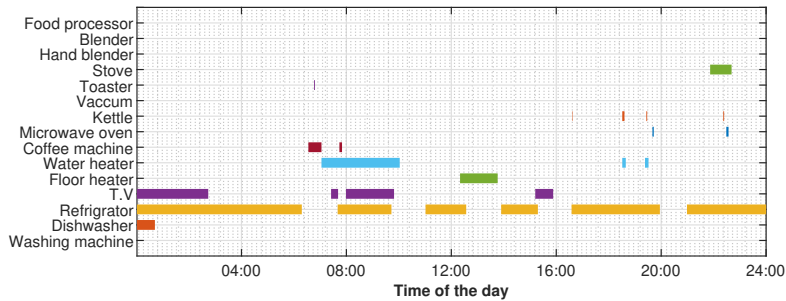
(a) Weekday device usage patterns
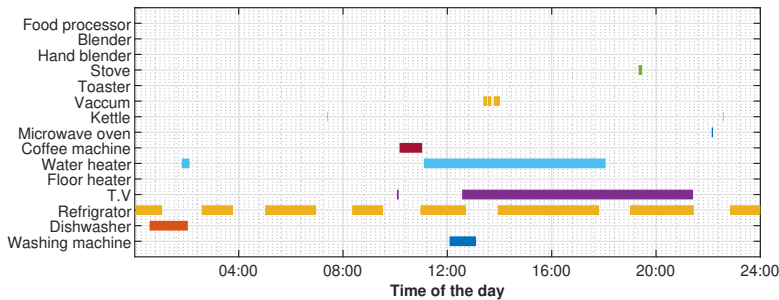
(b) Weekend device usage patterns

Figure 4.5 – Device usage patterns generated by the DU model

The growth in the share of EVs is increasing rapidly during the last decade, and the global stock of EVs is now more than thirty million vehicles [67, 68]. This number is expected to increase rampantly in the coming years because of the favourable policies. The payback price of an EV is also likely to decrease to five years in comparison to combustion engine vehicles [69].

High EV penetration can impact the performance of the electrical distribution network. The additional battery charging load may overload the distribution transformers and cables. The EV battery chargers are power electronic based circuits and inject current harmonics in the distribution network. The increase in harmonic content may affect the network component's performance and the loads connected to that network[70, 71]. The major impact of the EV battery charging will be on the low voltage residential networks. It is expected that the majority of EV users will prefer slow overnight home charging because of its convenience [69]. The lack of availability of the EV charging infrastructure also contributes to this regard. Nearly 90% of the EV charging is performed using the home-based charger because of its cost-effectiveness [72]. The public charging infrastructure contributes to only 4% of EV charging, and the ratio of EVs to public chargers is also decreased during the last few years [73, 74].

It is crucial to assess the impact of EV charging on the power system network, especially at the low voltage distribution side. The high charging demand during peak hours may bottleneck the transmission and distribution network performance even with sufficient electric power generation capacity in the system [75]. Therefore representative mathematical models are required to estimate the impact of high EV penetration in the distribution network. These models could provide valuable input for the optimal planning and up-gradation of the distribution networks.

The researchers have employed several approaches to formulate the EV usage models to evaluate the technical and economic aspects of the mass adoption of EVs [76]. These models often are able to output the charging demand profiles of EVs. One approach utilises the existing transport data provided by various travel surveys to estimate the EV usage impact on charging energy demand. The main drawback of this approach is that the traditional vehicle's dynamics are somewhat different compared to the EVs, such as driving range and charging time. An alternative approach is to conduct studies based on the behaviour of individual EV consumers; however, that may require significant resources. On the other hand, a hybrid approach may provide better results by using data from both travel surveys and EV measurement databases.

This section provides a mathematical model to estimate the EV load based on the daily travel activities of the individuals. The model is based on the data related to the travel patterns of the individual car owners from a travel survey and the EV charging power quality measurement portfolio. It provides charging profiles and state of charge (SOC) of EVs using a Monte-Carlo simulation. Individual trips are modelled based on the travel behaviour of commuters that generates the trip requirements. The model provides EV load profiles by considering the randomness and variance in the distance, travel time and commute modes. The measurement-based charging characteristics provides the capability to estimate harmonic emission, network overloading and unbalancing under various charging schemes.

4.6.1 Overview of the existing models

Various methodologies are available in the literature to model EV usage patterns and charging profiles in the spatial or temporal dimension. Existing EV usage mathematical models, primarily rely on travel surveys, parking data, and vehicle ownership statistics, provide both qualitative and quantitative attributes of EV integration [77]. These models provide valuable information for policymakers to assess the impact of EV growth on the environment, energy markets and economy.

EV user behaviour is influenced by the socioeconomic status of the users, regional traffic conditions, energy pricing, policy decisions and climate conditions. The travel patterns are stochastic in nature as the variables such as travel distance and travel time are highly variable and depend on the nature of the trip. The four-state approach has been widely discussed in the literature for transport modelling problems [78]. Trips are generated based on the daily activities of commuters in each region in the first step. The nature of the trip is decided based on the point of origin and ending point. The origin point of the trips are called production end, and the ending points are labelled as attractions. Trips can be modelled on a regional or individual level, while the origin and final ending points are mostly home. The second step of the four-state approach is to define trip origin and destination. Generally, trips are originated from one zone of a city and will end at a nearby zone, while few trips have attracted to the zones at a moderate distance. The probability of the trips ending at far-off zones is usually low. Travel modes are selected in the third step and define the type of vehicles and number of travellers. The routes are predicted in the final step.

The disadvantage of the four-state model is that it does not consider traveller activities that may affect the trip parameters. In reality, households include multiple residents from various age groups, and their daily activities are responsible for generating trip demands. The most common trips are home to work, home to shopping, and leisure or holiday activities. The commuter's daily activities only affect the trip generation part of the four-state approach, while the other states have little or no influence. This approach is used to eval-

uate the traffic flow, economic impacts of EV or electricity demand forecasting [79].

A better EV usage modelling approach should take account of the daily activities of the commuters. These activities can provide a framework to create a model capable of generating EV travel patterns based on user preferences and behaviours. These activity-based EV load models can provide more realistic data about the battery charging trends of EV users. This modelling approach is divided into two categories; direct use of observed activity-travel schedules (DUOATS) and activity-based models (ABM) [76, 78].

In the DUOATS model, travel statistics for the existing vehicles are used to model the EV usage patterns. Travel surveys conducted in various countries are available and provide valuable data related to the travel patterns of individuals. Web-based surveys are also used to generate energy usage profiles of EVs [80]. The survey participant provided their travel log, including the number of trips, commute time, and travelled distance. US Household Travel Survey (HTS) is also used to develop a Monte Carlo based EV model to estimate the additional electricity demand for the battery chargers [81]. Outgoing and incoming trip timings are converted into charging demand. Another EV model used a probabilistic approach to generate charging profiles using empirical distribution functions for the data extracted from the HTS survey [82]. Swiss mobility survey is also used to estimate the EV charging impacts on the distribution grids in Switzerland [83]. Similarly, multivariate probabilistic approach is used to determine the impact of large scale EV charging based on travel survey statistics in New Zealand. DUOATS models provide reliable outcomes but are primarily based on travel surveys conducted for conventional car owners; therefore, they do not consider variables related to EV usage, such as driving range and battery charging characteristics.

The ABM models are based on a set of activities influencing the travel behaviour of the people. It models the trips using individual's activity patterns that can be affected by the traveller's personal preferences rather than the nature of the trips. Various socioeconomic factors influence the travel behaviour of individuals. The travel schedules are generated within the model in the ABM approach, while the DUOATS approach relies on external travel schedules. Several models are available in the literature that uses the activity-based approach to estimate the influence of EV mass adoption. The household activity model is used to generate the load profiles of plug-in hybrid electric vehicles under uncontrolled charging scenarios, in [84]. The model provides the charging load of PHEV and also estimates the electricity consumption of other domestic appliances. The impact of vehicle-to-grid (V2G) from the EVs on the distribution grid is also estimated by using an activity-based modelling approach [85]. The travel logs and occupant household activities that may influence their travel decision are used to develop a four-stage ABM model that can simulate the electricity demand required for battery charging of EV load in Belgium [86, 87]. In another study, data from the travel survey is used to define probability density functions of trips by considering the parameters such as incoming time, outgoing time and distance covered in a trip to make EV usage patterns [88, 89, 90]. The generated travel patterns are compared with the EV charging data such as SOC and charging profiles.

The travel demand based on household activities can also be simulated using transport simulation software. The impact of PHEV penetration on the distribution grid is evaluated using a transport simulator TRANSIMS in [91]. MAT-Sim is another multi-agent transport simulation that can handle large scale traffic flow. The impact of EV penetration in Switzerland is analysed based on travel activities in [92]. The model is only suitable to study the effects of PHEV and lacks to handle critical variables such as the driving range factor.

Table 4.2 – Daily indicators for domestic travel [93]

Domestic travel indicator	Average value per day
Number of domestic trips per person	2.89
Travel expense per person	41.4 (euros)
Total journey time per person	65.5 (minutes)
The average distance of a trip	14.3 (km)
Average travel time per km	22.7 (minutes)

4.6.2 Methodology

The overview of the existing EV models in the previous section confirms the effectiveness of the ABM modelling approach because its flexibility and bottom-up structure can handle domestic activity-based travel behaviour. EV home charging is expected to have a significant impact on the low voltage residential grids. As the majority of the EV owners are expected to charge their vehicles at home in the evening, as it will be convenient and cost-effective, the electricity demand in the residential is likely to increase during the peak hours. The EV model aims to simplify the load estimation limited to the residential grids.

The input data for the model is selected from the national traffic survey (NTS), and EV user travel patterns are categorised based on the most common travel activities. The probability distribution function is defined for the incoming and outgoing trips. Trip chaining is employed to estimate the travelled distance and the timing of the incoming and outgoing trips. Battery charging decision depends on the SOC evaluated at the end of each trip. The charging will occur when the SOC drops below a certain threshold or vehicles do not have sufficient battery resources to make the next trip.

The NTS is carried out in Finland every six years and collects yearly travel data for all days and seasons from 30,000 people [93]. It provides information about the mobility patterns of Finnish people, such as the activities responsible for trip generations, transportation modes, and travel preferences of different population groups. The survey participants are requested to provide background information about their gender, age, type of residence, family members, driving licence information, income, employment status and vehicle ownership. Additional questions include the information about the location of their home, workplace, school, other preferred destinations and their ideal means of travel. Table 4.2 provides the daily indicators for domestic trips.

4.6.3 Travel activities

The trips are categorised based on the daily domestic activities responsible for generating trip needs. Most popular trips are associated with educational and work-related activities. The other everyday activities responsible for trip demand includes shopping, holiday trip and, leisure activities. Table 4.3 describes the number of trips and distance travelled for most frequent daily activities. The travel activities during the weekdays are quite similar, and the most common trips are for educational and work-related activities. The trips related to other activities also follow similar patterns during the weekdays. The visits have a low occurrence in the first five days of the week, while the number of work and school trips also drops significantly over the weekend. On the other hand, the trip demand for leisure and visit related activities increases over the weekends. The frequency of shopping trips is almost identical for all days of the week except Sunday. Similarly, business trips also have a high frequency on weekdays. This data from the NTS survey provides a good base to formulate the EV model on the assumption that the activities responsible for travel demand would remain the same for EV users.

Table 4.3 – Weekly travel information for different trips [93]

Day	Work	School	Business	Shopping	Visits	Leisure	All
Number of trips							
Monday	0.64	0.27	0.13	1.02	0.04	0.69	2.79
Tuesday	0.62	0.26	0.14	1.14	0.03	0.71	2.9
Wednesday	0.65	0.29	0.16	1.12	0.03	0.75	3.01
Thursday	0.65	0.27	0.13	1.09	0.03	0.64	2.8
Friday	0.54	0.25	0.11	1.11	0.04	0.68	2.72
Saturday	0.13	0.01	0.03	1.03	0.05	0.88	2.13
Sunday	0.12	0	0.02	0.58	0.06	0.81	1.59
Average	**0.48**	**0.19**	**0.11**	**1.01**	**0.04**	**0.74**	**2.56**
Distance traveled for each trip (km)							
Monday	15.8	7.74	34.04	6.87	40.48	11.18	116.11
Tuesday	16.73	6.04	33.94	6.6	49.11	11.94	124.36
Wednesday	14.92	6.29	36.77	6.87	38.56	9.6	113
Thursday	17.53	7.82	37.55	6.34	57.17	11.84	138.25
Friday	15.28	7.54	58.2	8.3	80.08	19.12	188.52
Saturday	16.55	25.16	53.21	7.99	48.22	19.48	170.59
Sunday	13.13	69.81	95.58	9.03	65.46	16.56	269.56
Average	**15.98**	**7.27**	**41.39**	**7.3**	**55.14**	**14.43**	**141.52**

4.6.4 Departure times

Three activities are defined from the activity-based travel data summarised in Table 4.3. The first category is termed "Work and school" (WS) and is the most frequent trip during the weekdays. These trips have very low variation in the travelled distance, outgoing and incoming timings. The second category is defined as "Shopping and business" (SB). These trips are also quite frequent during the weekdays; however, variations in the trip timings and travelled distance are high compared to the WS trips. The daily frequency of these trips also varies. The last category is labelled as "Leisure and vacation" (LV). These trips have high dispersion as the trip timing and length have high variations.

NTS survey also provides the average length of the trips for various travel activities. Table 4.3 presents the data related to distance travelled during different trips. For the trips related to educational activities, it is assumed that commuters are doing university or vocational studies; therefore, longer trip distances are linked with these activities in contrast to travelling to the local school. Business trips are also supposed to have similar characteristics to work-related trips, such as visiting a specialised commercial facility. Shopping trips with a long travel distance have low probability and are mostly expected to end at a shorter length. The same assumption is valid for the LV trips. However, these trips have a low probability of occurrence in comparison to the SB trips. Fig. 4.6a shows the outgoing time for each travel activity on a weekday. For the EV model, outgoing time data is converted into WS, SB, and LV activities, as shown in Fig. 4.6b.

Fig. 4.6b does not show any differentiation between Individual time distributions for incoming and outgoing trips for various trip activities. However, such parameters are critical for accurate EV load modelling. Furthermore, the time resolution of the data provided by the NTS survey is relatively low, and data interpolation is applied to improve time resolution.
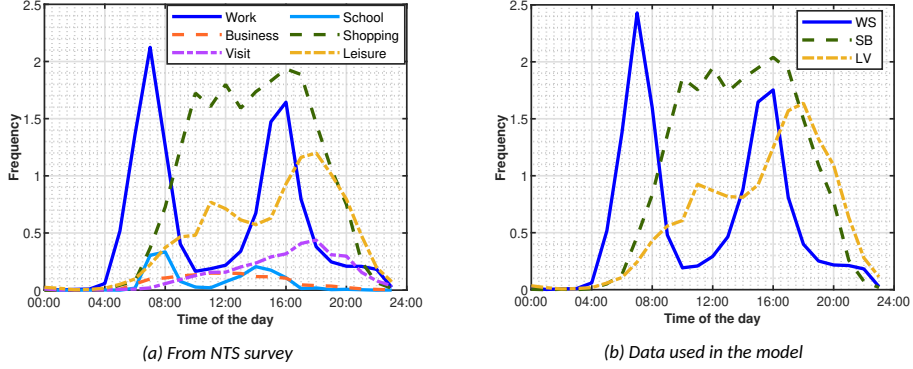
(a) From NTS survey   (b) Data used in the model

Figure 4.6 – Departure time frequency per hour [III]

4.6.5 Incoming trip estimation

Battery charging of electric vehicles will occur when the vehicles reached home, and the SOC level drops below a certain threshold. The probability distributions for the incoming trips is therefore critical for the EV load modelling. Multiple peaks can be observed from the time distribution of trips for different travel-related activities as shown in Fig. 4.6b. The morning and evening peak of trip starting time can be assumed as outgoing and incoming time distributions for the WS trip category. This assumption is supported by the low probability of nighttime work-related trips. The spread of the evening peak is relatively large in comparison to the morning peak. T-location-scale distribution can be applied to morning and evening peaks to define the probability density functions of incoming and outgoing trip times. Fig. 4.7 shows the morning and evening peak probability distributions defined for incoming and outgoing trips. Eq. (4.25) represents the PDF of the t-location-scale distribution.

$$p(x, v, \sigma, \mu) = \frac{\Gamma^{\frac{(v+1)}{2}}}{\sigma\sqrt{v\pi} \times \Gamma(\frac{v}{2})} \times \left[\frac{v(\frac{x-\mu}{\sigma})^2}{v} \right]^{-(\frac{v+1}{2})} \tag{4.25}$$

Here σ and μ determine the scale and location of the distribution while v defines its shape. The t-location-scale distribution approaches a normal distribution as v tends to positive infinity; however, the smaller values of v results in heavier tail.

LV trip timing distribution in Figure 4.6b also shows two peaks. The magnitude of the evening peak is significantly higher than the morning peak and indicates the leisure activities of the commutes during the evening after work or school related activities. The mean time spends by the commuters at the leisure activities is assumed to be 180 minutes. The time duration of leisure activities is estimated by the Poisson distribution, and its PDF can be calculated using the following relation.

$$p(x|\lambda) = \frac{\lambda^x}{x!} e^{-\lambda} \tag{4.26}$$

Here λ indicates the variance of the Poisson distribution while e represents the Euler's number. Distance travelled during different travel activities is another critical parameter for EV load modelling. The NTS survey also provides the average trip distance for various travel activities at different times during the day. Figure 4.8a represents the average distance for various travel activities extracted from the NTS survey. Based on this data, the probability distributions of the distance travelled for WS, SB, and VH travel activities are
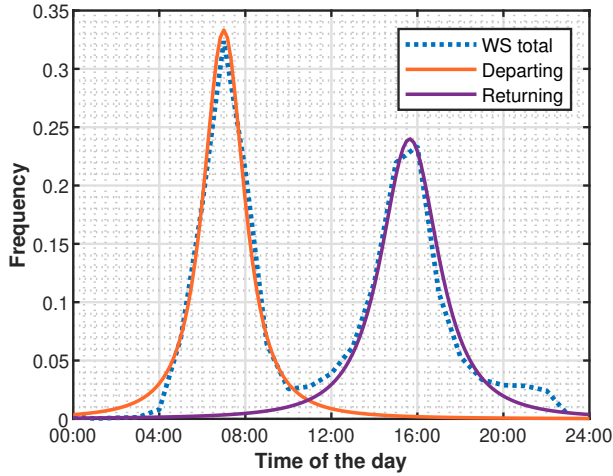
Figure 4.7 – Probability plots of outgoing and incoming trip for WS travel activity [III]

defined. Fig. 4.8b shows the distance travelled for the travel activities used in the EV load model. Poisson and log-normal distributions provide a close fit to the data related to the travelled distance. Eq. (4.27) represents the PDF of a log-normal distribution's probability density function. μ and σ shows the value of the mean, and variance, respectively.

$$p(x,\sigma,\mu) = \frac{1}{x\sigma\sqrt{2\pi}}exp(-\frac{(ln(x)-\mu)^2}{2\sigma^2}) \qquad (4.27)$$

(a) NTS survey data

(b) Data used in the model
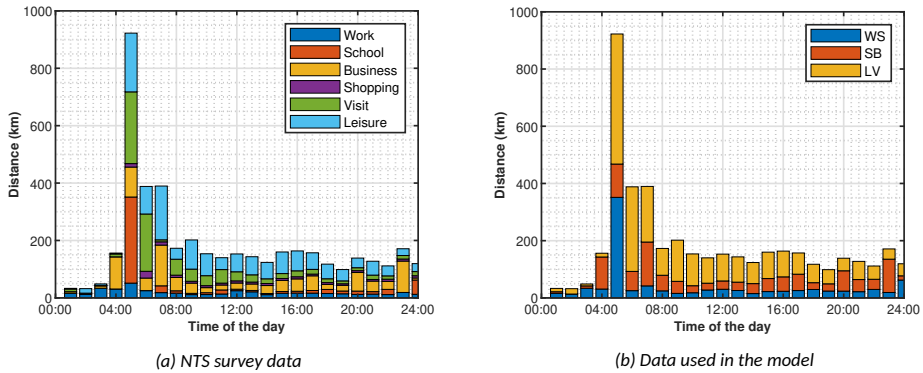
Figure 4.8 – Trip distance frequency per hour for different travel activities [III]

4.6.6 Electric vehicle characteristics

EV modelling also depends on the various characteristics of electric vehicles, such as battery capacity and driving range. It is crucial to select an appropriate mix of different EVs available in the market. Several EV models are available in the market offered by various auto manufacturers; however, the number of EV users is still low compared to traditional combustion engine-based cars. EV's power quality measurement data is also not readily

Number	Type	Battery capacity (kWh)	Driving range (km)	THDI %
EV 1	BEV	22	170	4.8
EV 2	BEV	16.8	100	7.2
EV 3	BEV	31	160	2.8
EV 4	BEV	40	220	11.7
EV 5	BEV	14.5	171	8.4
EV 6	PHEV	11.2	50	3.1
EV 7	BEV	18.7	165	2.4
EV 8	PHEV	9.4	36	2.5
EV 9	BEV	17.6	145	4.4
EV 10	BEV	58	335	7.1
EV 11	PHEV	8.8	26	2.4

Table 4.4 – Summary of the measured EVs [III]

available, and it's not feasible to measure every EV available. A careful selection of vehicles is crucial to model the charging profiles of EVs accurately. The remaining travel-related parameters are expected to follow similar trends in the future.

Eleven different EVs are selected, including BEV and PHEV, and an equal share is assumed in the EV load model. These vehicles are selected based on their share in the current EV market. Table 4.4 shows different characteristics of the selected EVs used in the model.

EV charging characteristics play a crucial role in the charging profiles. A typical battery charger draws current that could be constant, ramp-up or ramp down depending on the battery SOC. Fig. 4.9 shows the charging current drawn by the EVs at different SOC levels of their batteries.
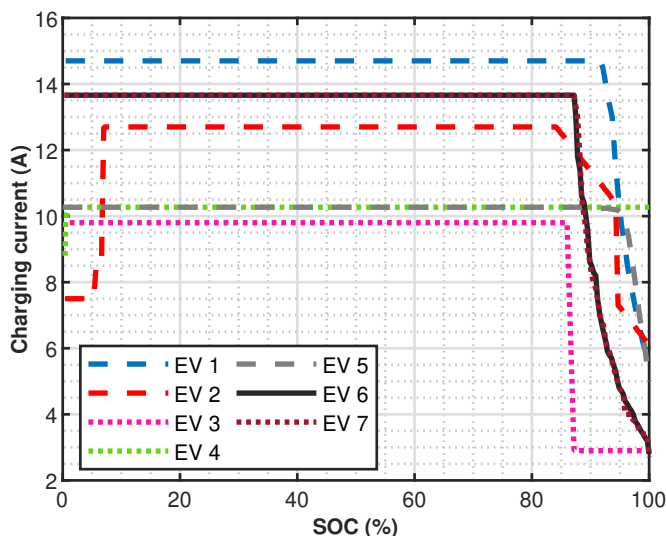

Figure 4.9 – Charging current levels during charging span of 0 % - 100 % of the full charge [III]

The energy consumption during the trips is assumed to be 180 Wh/km and is based on data provided by the EV manufacturers. The assumption is expected to be valid for

future models as well because of the high energy conversion values of the current EVs. The climate conditions and terrain variations may significantly impact battery energy consumption values but are not considered. The battery evaluation is performed after the end of each trip, and the SOC level is estimated as the vehicle arrives home. The level of SOC is analysed before generating the parameters for the next trip. The EV will go for battery charging if the battery does not have enough resources to make the next trip.

4.6.7 Daily routine estimation

The NTS survey categorised the commuters based on gender and age groups. This data is used to estimate the number of people using private cars for their daily trips related to WS travel activities. The remaining people are assumed to be on vacation, retired or engaged in other travel activities. Random seed numbers are assigned to each vehicle owner to estimate its daily travel activities. Initially, the more consistent routine parameters are assigned and are used as an input for the EV model to generate daily trip activities. A vehicle schedule is created using the daily trip parameters. After the routine travel activity estimation, the other activities are estimated based on their daily probabilities. Vehicle daily activities are evaluated using ten different states. The first state is defined as the home state, while each travel activity (WS, SB, VL) has three states; outgoing state, at the activity, and incoming state.

The battery utilisation is calculated during the incoming and outgoing state of a trip. The incoming state always ends at home, and SOC will drop depending on the battery utilisation during the trip. The battery utilisation depends on the distance travelled during the outgoing and incoming state of the trip. During the home state, the SOC level will determine whether the EV required charging or have sufficient resources to make the next trip. If the next trip is scheduled for the next day and SOC is below the threshold, the vehicle will be charged until the battery is full. Monte-Carlo simulation is used to simulate the EV charging profiles for any given number of EVs. Following steps are performed during each iteration.

- Step 1: Estimate the probability of the routine travel activity (WS).

- Step 2: Determine the probabilities of the other travel activities (SB or VL) after the routine activity is complete.

- Step 3: Calculate the distance travelled for all travel activities during the outgoing and incoming state.

- Step 4: Duration for all WS, SB, and VL activities .

- Step 5: Battery utilisation and the SOC after each trip.

- Step 6: SOC threshold when EV owner always charges the vehicle.

- Step 7: Probability of the owner to charge after incoming state.

Fig. 4.10 shows the algorithm of the EV load model. For each day, travel activities responsible for trip generation are estimated. The trip parameters are determined for each travel activity, including outgoing time, distance, battery utilisation, duration, and the incoming time based on their probability distribution functions. The battery evaluation is performed to calculate SOC after each trip. Any given number of EVs can be simulated to generate their charging profiles for the required number of days.
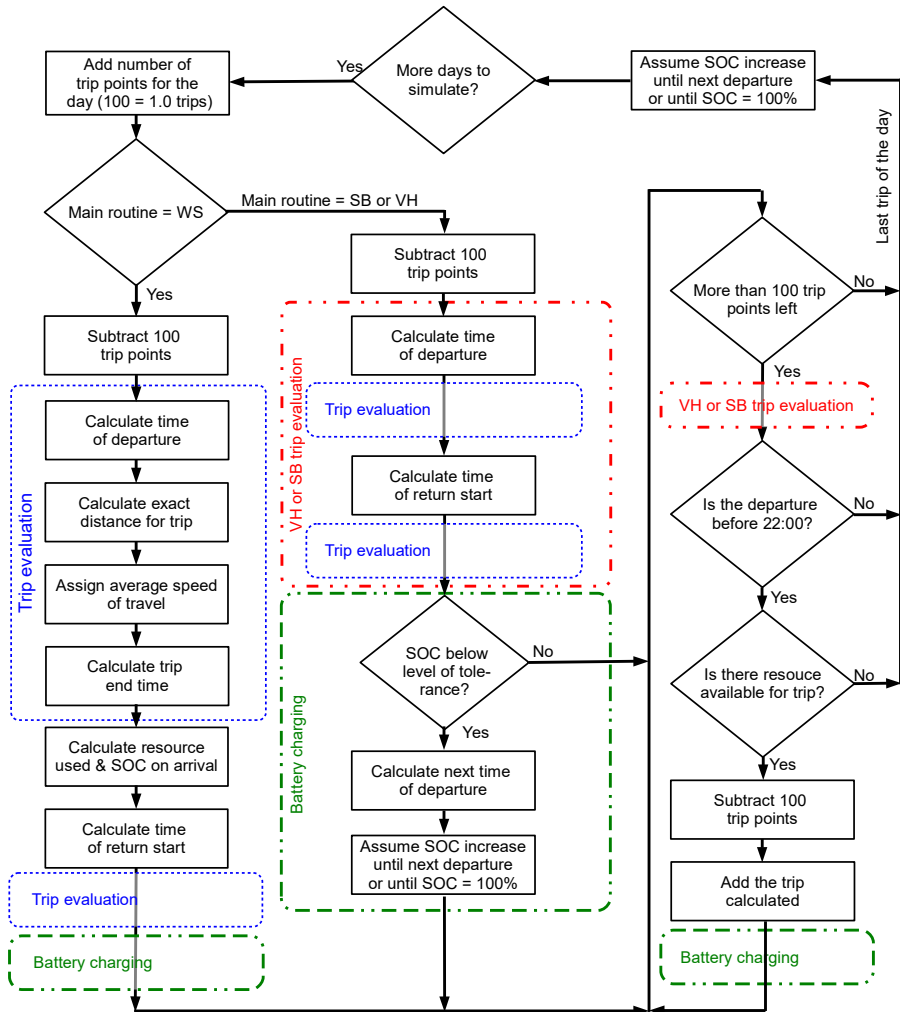
Figure 4.10 – Algorithm of the EV charging profile model [III]

4.6.8 Results

The EV load model is capable of simulating charging profiles and load for any number of EVs. To evaluate its performance, 50 EVs are simulated over 100 days to estimate their charging load. The model estimated the daily schedule of each vehicle and SOC after each trip. The measurement data of eleven electric vehicles is used to estimate the charging currents. The current values are assigned based on the SOC level of the vehicle. The total EV load will be the aggregation of charging currents of all vehicles charging at a given time.

The model can provide EV load under various charging schemes. Aggregated charging load based on two different charging schemes, unmanaged charging and managed charging, is presented in this section. In the first scenario, the load of 50 vehicles is estimated using the unmanaged charging scheme, where the EV owners can charge their vehicles at any time during the day. Fig. 4.11a shows the mean and 90th percentile values of the charging current of 50 EVs over 100 days. The black and red lines show the mean and 90th percentile values of the number of vehicles charging at different times during the

day. The EV load starts increasing from mid-day and reaches its peak value between 17:30 to 18:30. Most EV owners start charging their vehicles as soon as they arrive from their routine travel activity. The mean and 90th percentile values of the maximum number of EVs charging at any time during a day are 34 and 42, respectively. After 18:00, the EV load starts decreasing gradually and becomes half of peak charging demand level around 24:00. The mean and 90th percentile values of the number of EVs charging is reduced to less than 10 after 03:00, while the load curve reaches its minimum value between 06:00 and 08:00.

(a) Unmanaged charging　　　　　　　　(b) Managed charging
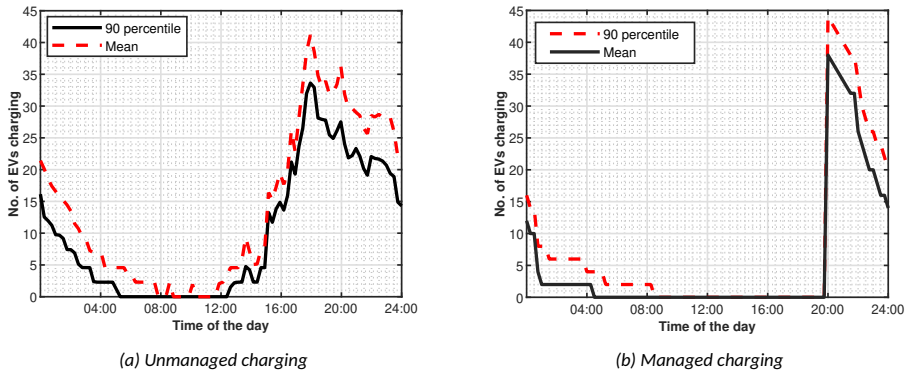
Figure 4.11 – Electrical vehicle load curves estimated by the model [III]

The EVs are forced to charge during the off-peak time to reduce the peak load in the managed charging scheme. Figure 4.11b shows the mean load curve of 50 vehicles charging over 100 days. The EV charging now starts at 20:00, and the load curve increases to its maximum mean and 90th percentile values of 38 and 44, respectively. The load curves decrease abruptly from 22:00 on-wards, and the mean and 90th percentile values of the number of vehicles charging are reduced to 14 and 22 EVs, respectively.

The EV load model provides reliable load curves under various charging scenarios. Additional charging load for any given number of EVs can be estimated for a distribution network. The model can provide data for the network operators to optimise their network planning for the future EV load. It can also be used to estimate current harmonic emissions by using power quality measurement data.

The RMS charging current of 50 EVs is estimated here using the EV load model and power quality measurement data. The EVs are measured on sinusoidal voltage using the measurement test bench described in section 3.1.1. The charging currents are assigned to the EVs based on their SOC level, and aggregated values of the total RMS current of EVs are calculated for the unmanaged charging scenarios. The mean and 90th percentile values of the RMS current drawn by 50 vehicles of a 100 days is shown in Fig. 4.12a. The peak RMS current could exceed 180 A during the evening. As a result, an additional 42 kW power is required to tackle the EV load of 50 vehicles in a distribution grid, as shown in Fig. 4.12b.

The EV load model provides a simplistic approach to estimate charging or harmonic currents while flexible enough to tackle any amount and type of EVs. The power consumption results follow similar trends of the EV load estimated in other studies [94, 88, 89, 90]. However, the proposed EV load model offers improved flexibility and a simple approach with fewer variables. The results also confirm the NTS travel survey data's applicability
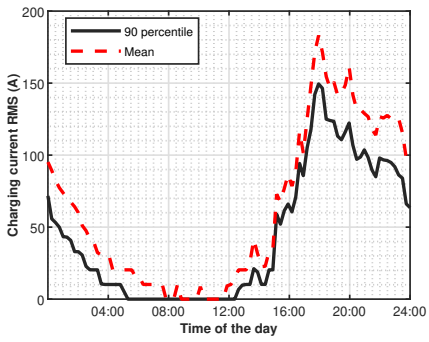
(a) EVs charging current
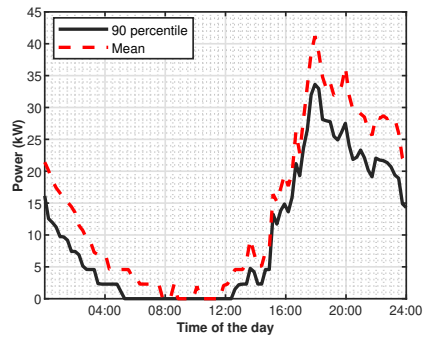
(b) EVs power consumption

Figure 4.12 – Unmanaged charging scenario results [III]

compared to the other travel surveys used in various studies to model EV charging pro-
files.

5 Accuracy and uncertainties

The stochastic modelling of harmonics can be affected by various uncertainties and in-accuracies related to the load and network behaviour. The composition of the load connected to the network is continuously changing all the time. Several linear and nonlinear loads with various circuit topologies are used by the end-users. It will result in a dynamic harmonic emission profile of each house connected to the LV network. Harmonic current injecting at the point PCC is also affected by the harmonic cancellation. The supply voltage harmonics and network impedance further affect the current harmonics.

The probabilistic harmonic estimation models used different assumptions and random variables; therefore, a certain level of inconsistency is present in the outcome. As the models are based on measurement datasets, therefore, inaccuracies in the measurement process are also reflected in the harmonic estimation results. The chapter discusses the impact of different uncertainties related to the load and network.
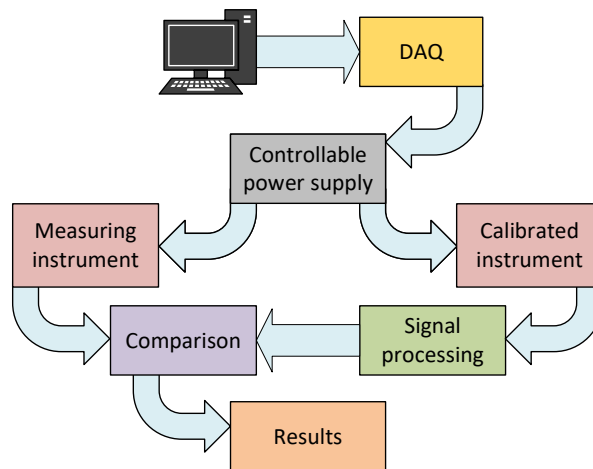

Figure 5.1 – Schematic of the measurement accuracy evaluation method

5.1 Measurement accuracy

The stochastic harmonic estimation models rely on individual device's power quality measurements at various distorted voltages. These measurements are performed using controllable power supplies and power quality analysers under a controlled environment. The precision of the measurement systems is vital as it will affect the harmonic estimation model's result. The laboratory instruments are used for various research and academic tasks, and therefore measurement setup reliability is crucial. The reliability of the measurement results depends on how often the system involved in the measurement procedure is calibrated. The calibration measurement of the measurement systems is a costly procedure performed by accredited organisations.

A two-step method is proposed using signal processing and metrology techniques to evaluate the accuracy of the measurement setup. The detail of different components of the measurement system is already discussed in section 3.1.1, and it consists of a power quality analyser, PQ-Box 200, and auxiliary equipment, including a controllable power supply and data acquisition module. The system's accuracy includes the uncertainties added by the auxiliary equipment while generating desired distorted signals and inaccu-

racies of the power quality analyser.

In the first step, the performance of the primary power quality analyser is compared with a reference calibrated measurement device in a certified metrology laboratory. Multiple current waveforms are generated using the calibrator CP11B. The output of the CP11B was applied to the primary winding of the current transformer I509. The current values were measured at the secondary winding of the current transformer by means of the sampling watt-meter SWM3458. The watt-meter consists of two synchronised multi-meters, Agilent 3458A, current shunts and the software PowerLF (v1.2). The same measurements are also performed using the primary power quality analyser simultaneously, as shown in Fig. 5.1. The difference between the individual harmonics RMS and phase angles is listed in Table 5.1 and 5.2. The bold values indicate the maximum difference for the current magnitude or phase angles recorded between the measurements from the reference instrument and the primary instrument.

In the second step, the accuracy of the system setup is evaluated. As illustrated in Fig. 5.1, a similar setup is used, but the calibrated reference instrument in this scenario is a Keysight 34465A. It is capable of recording current and voltage waveform at a sampling frequency of 50118 Hz. A 12-ohm shunt is used for the current harmonic's measurement. Discrete Fourier transform (DFT) is performed over a 1-second recorded waveform to extract current or voltage harmonics. The RMS values of harmonics are compared to find the difference between the primary and reference instrument measurements. Table 5.3

Table 5.1 – RMS difference (%) between reference and primary instruments

Harmonics	Signal 1	Signal 2	Signal 3	Signal 4	Signal 5
Order no.	Current (%)				
1	0.05	-0.01	0.17	0.15	**0.26**
3	**-0.36**	-0.24	-0.32	-0.33	-0.32
5	**-0.37**	-0.29	-0.36	-0.36	-0.35
7	-0.38	**-0.39**	-0.37	-0.38	-0.37
9	**-0.41**	-0.40	-0.40	-0.41	-0.40
11	-0.47	-0.33	-0.46	**-0.47**	-0.45
13	-0.55	-0.38	-0.53	**-0.55**	-0.53
15	-0.64	-0.51	-0.63	**-0.65**	-0.63
17	-0.74	-0.55	-0.74	**-0.74**	-0.73
19	-0.83	-0.58	-0.82	**-0.84**	-0.82

Table 5.2 – Phase difference (absolute) between the reference and primary instruments

Harmonics	Signal 3	Signal 4	Signal 5
Order no.	Degrees		
3	0.30	0.20	**0.41**
5	0.37	0.20	**0.54**
7	0.47	0.22	**0.71**
9	0.58	0.26	**0.88**
11	0.70	0.30	**1.06**
13	0.81	0.35	**1.24**
15	0.93	0.40	**1.42**
17	1.05	0.44	**1.61**
19	1.17	0.49	**1.80**

shows the difference in the measurements performed by the primary instrument by using the same set of input data used in the previous experiment. The correction difference indicates the variation between the data set entered in MATLAB to generate reference signal and the measurement results. This correction difference is also adjusted by using the calibration difference from Table 5.1.

Table 5.3 – Correction difference for the primary instrument

DATASET	Lab measurements differences		Correction
Harmonic components (%)	Primary instrument (%)	Reference instrument (%)	(%)
0.0448	-0.5459	-0.0108	-0.6045
0.0368	0.1357	0.0566	0.5008
0.0281	0.2401	0.1564	0.6214
0.0198	0.3533	0.2551	0.7478
0.0135	0.4298	0.4250	0.8556
0.0099	0.7339	0.6368	1.2094
0.0081	0.8972	0.8999	1.4545
0.0072	1.1666	1.2018	1.8192
0.0065	1.5424	1.5553	2.2942
0.0057	1.9114	1.9545	2.7498

The correction difference reflects the uncertainties and noise added by the auxiliary equipment as the inaccuracy of the primary instrument is already considered. To evaluate the accuracy margins, additional calculations are performed using the measurements results obtained from the reference instrument, Keysight 34465A. The recorded signals were obtained using the digitisation option, and DFT is performed. Any uncertainty or noise added by the system will also propagate into the frequency domain and must be taken into account. For this purpose, a simulation is performed in MATLAB by generating the same synthetic signals after adding additional noise. The noise is calculated by using calibration parameters of the Keysight 34465A and are shown in Table 5.4.

Table 5.4 – Noise parameters

Components	Uncertainty k=1 (A)	Sensitivity Coefficient	Contribution to Uncertainty (A)
Minimum RMS measurement (I_{rms})	0.001443376	1	0.001443376
Calibration correction (Cor)	0.00265	1	0.00265
Linearization error ($Linc$)	0.00025913	1	0.00025913
Resolution effect of ADC (Res)	0.031558351	1	0.031558351
Long term stability (LS)	0.004618802	1	0.004618802
Stability ($Stab$)	0.043272403	1	0.043272403

The noise can be calculated using Eq. (5.1).

$$u_{Ith} = \sqrt{I_{rms}^2 + Cor^2 + Linc^2 + Res^2 + LS^2 + Stab^2} \tag{5.1}$$

A Monte-Carlo simulation is performed in MATLAB with fifty thousand iterations to determine the effect of the noise element in the frequency domain. During each iteration, each input signal is calculated by adding random noise using the following relation.

Harmonics	RMS	Calibration Uncertainty u_c	Device Uncertainty u_d	Method Uncertainty u_d'	Average Difference u_a
	Current (A)	Current (μA)			
H1	0.014174	97.82	15.41	20.78	86.70
H3	0.006201	97.79	3.39	10.68	32.66
H5	0.002688	97.45	0.68	1.44	38.04
H7	0.001278	97.38	1.09	0.87	36.01
H9	0.001008	98.30	0.17	3.46	46.54
H11	0.000831	97.71	0.12	1.15	61.55
H13	0.000774	97.34	0.29	1.73	77.68
H15	0.000415	97.89	0.17	0.87	54.69
H17	0.000252	97.82	3.84	0.58	39.22
H19	0.000244	97.59	0.07	0.87	47.48

$$I = \left[\sqrt{2} \times i_n \times \sin(2\pi f_n t + \theta_n) + (\mathbf{r} \times u_{Ith}) - \frac{u_{Ith}}{2}\right] \tag{5.2}$$

Here, $\mathbf{r} \in [0,1]$ is a uniform random number, and i_n and θ_n are the magnitude and phase angle of each harmonic. DFT is performed, and the calibration uncertainty is determined by using standard deviation using Eq. (5.3).

$$u_c = \sqrt{\frac{1}{M} \sum_{m=1}^{M} |I_m - \mu|^2} \tag{5.3}$$

Where M is the number of observations and U is the mean of the current harmonic. The measurement setup is used to measure the same signals by the primary and the reference instrument. The current harmonics are generated individually and measured three times to include any possible variations. The uncertainty of measurement and reference instrument is determined using equation Eq. (5.4).

$$u_d = \frac{|I_{MAX} - I_{MAX}|}{2\sqrt{3}} \tag{5.4}$$

An additional parameter, average deviation, is also used to calculate the accuracy margin of the measurement system. The average deviation between the measurement results obtained from primary and reference instrument is calculated by Eq. (5.5).

$$u_a = \frac{|\overline{I_{pri}} - \overline{I_{ref}}|}{2\sqrt{3}} \tag{5.5}$$

Here, $\overline{I_{pri}}$ and $\overline{I_{ref}}$ are the average values of current measured by the primary and the reference instrument. Different uncertainties estimated for the current minimum levels measured or generated by the measurement system is listed in Table 5.5.

The total accuracy margin for the measurement system for is calculated using the following relation.

$$u_{k=1} = \sqrt{u_c^2 + u_d^2 + u_d'^2 + u_a^2} \tag{5.6}$$

The accuracy margins for the current minimum levels measured and generated by the measurement system are listed in Table 5.6. $k = 1$ and $k = 2$, respectively, show the 66 and

Table 5.6 – Accuracy margins of the measurement system

	H1	H3	H5	H7	H9	H11	H13	H15	H17	H19
	Current (μA)									
k = 1	133	104	105	104	109	115	125	112	105	109
k = 2	266	207	209	208	218	231	249	224	211	217

95 confidence interval accuracy. However, measurements uncertainties observed during experiments are relatively low.

5.2 Probabilistic accuracy

Several probabilistic approaches can be used for current harmonic estimation models based on various power system variables and uncertainties. The probability distribution choice to classify the input data has implications for the model's computational complexity and accuracy [95].

The impact of statistical methodologies on various research problems related to the electric power system is widely addressed in the literature [96, 97]. The probability distribution for the input data is selected based on the goodness of fit and ease of usage. The normal distribution is extensively used because of its simple computation and application. The other standard distributions are beta, Wei-bull, log-normal and exponential distributions. However, in harmonics and load modelling, associated random variables can be interdependent in many cases. The inter-dependency of these random variables can be positive or negative. For example, harmonics magnitude and phase angles are highly interdependent. In load modelling, inter-dependency on several variables has to be considered while modelling the usage pattern of end-user appliances. Empirical distribution functions are more suitable for harmonic and load modelling because of their flexibility and accuracy. However, the computational time and complexity will be increased but can easily be handled with simulation software and modern-day computational power.

The empirical distribution can describe any data with finite points. For n independent random numbers $(X_1, X_2, ...X_N)$, the empirical distribution function $p_N : \mathbb{R} \to [0,1]$ is a step function with a step size of $1/N$ with values less than or equal to X.

$$p_N(X) = \frac{finite\ points\ in\ a\ sample\ data \leq X}{N} \qquad (5.7)$$

$$p_N(X) = \frac{1}{N} \sum_{n=1}^{N} \mathbf{I}(X_n \leq X) \qquad (5.8)$$

Where $\mathbf{I}(X_n \leq X)$ is an indicator function and will be equal to 1 if $(X_n \leq X)$ only and zero otherwise.

The selection of distribution fit for stochastic models is highly critical as it will directly affect the model's outcome. A wrong choice may result in inaccurate estimation. A comparison between empirical distribution and distribution selection based on goodness of fit has been made to estimate the impact of probabilistic distribution selection for the data. The selected data contains lighting usage duration in the evening interval between 5 PM to 12 AM. Distributions are applied to compare the effectiveness of empirical distribution against the distributions selected based on goodness of fit.

Fig. 5.2 shows the histogram of the data. A distribution is selected using the MATLAB distribution fit function. The red curve shows the best fit distribution for the data. The
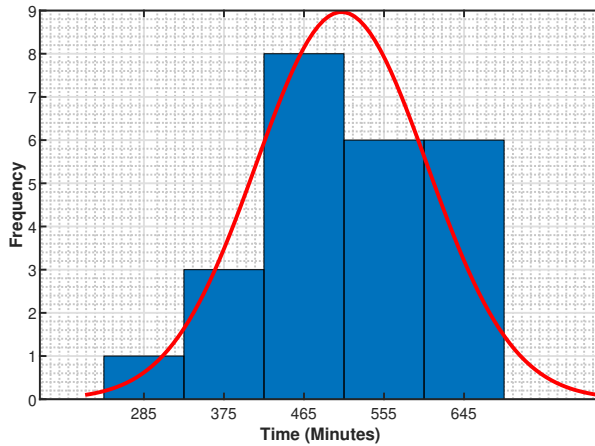
Figure 5.2 – Selected data-set with best fit probability distribution

PDF of the selected distribution is used to generate a thousand random samples. The histogram of this simulated data is shown in Fig. 5.3. The top graph shows the histogram of the original data, and the middle graph shows the histogram of the simulated data using the PDF of best-fit distribution. A clear difference can be observed, which indicates that this selection will generate inaccurate data samples in a stochastic model.
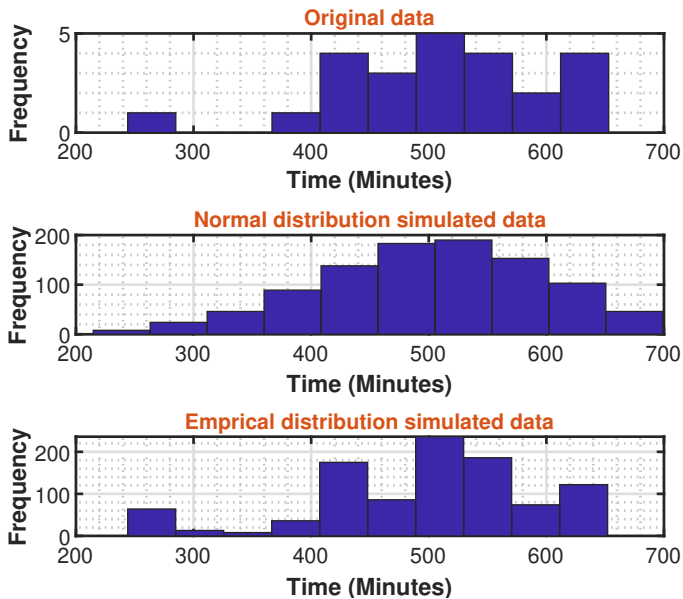

Figure 5.3 – Comparison of simulated data using different distributions

The empirical distribution is applied to the lighting usage duration data, and a thousand random samples are generated. The histogram of the simulated data using empirical distribution function is shown in the bottom graph of Fig. 5.3. The comparison with the original data shows a close resemblance in contrast to the best-fit distribution simulated results. As the harmonic emission data can be highly variable with clusters, empirical dis-

tribution is preferred over other distribution functions in this thesis.

5.3 Harmonic aggregation accuracy

In a distribution network, several loads are connected at PCC. According to Kirchhoff's current law (KCL), the sum of currents entering or leaving a node is equal to zero. Therefore, it is possible to add harmonics components of all currents drawn by various loads to determine the resulting current at PCC. The harmonic currents at the same frequency may have a different phase angle and magnitudes. Therefore, the aggregation may increase or decrease the resultant harmonic current, and this effect is known as harmonic cancellation [IX].

The effect of harmonic cancellation for household loads has been studied in [98, 99, 100, 101]. The cancellation depends on the load types and configurations. Although harmonic summation and cancellation are inevitable in the real-time scenario, however, in mathematical simulations, the cancellation may generate different results because of the inaccuracies and limitations of the measurement device and its results. Therefore, a comparison of real-time measurement data and mathematical aggregation of harmonic currents can provide the range of uncertainties for the harmonic aggregation model.

(a) Low-order harmonic current magnitude

(b) High-order harmonic current magnitude.
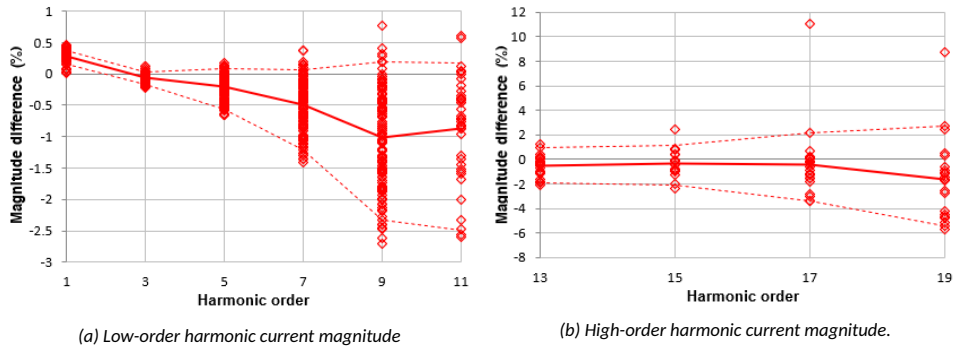
Figure 5.4 – Magnitude error harmonic current [IX]

(a) Low-order harmonic current

(b) High-order harmonic current
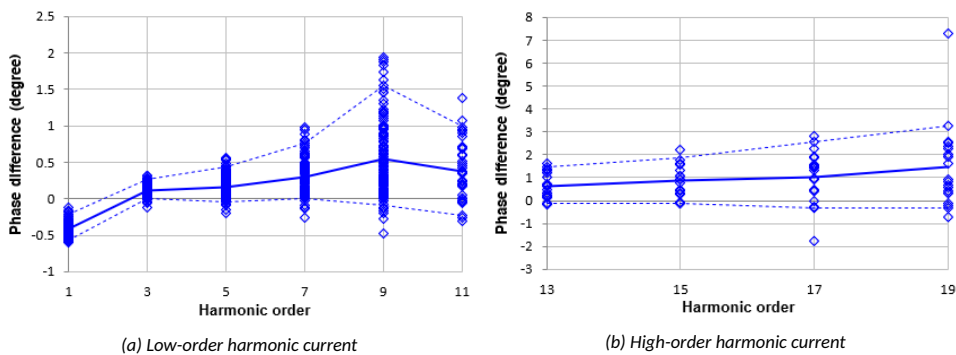
Figure 5.5 – Phase error of harmonic current [IX]

An experiment has been performed to assess the accuracy of mathematical aggregation of harmonics using LED lamps. Sixteen LED lamps have been selected with power

ratings of 7 – 13 W. Two different controllable power supplies are used in this experiment. The first measurement was performed using Chroma 61505 power supply. 230 V sinusoidal voltage has been generated by using the setup described in section 3.1.1. The power supply and LED lamps were warmed up for an hour to eliminate any variation due to thermal instability. The magnitude and phase angles of current harmonics were measured using A-Eberle PQ-box 200.

All sixteen lamps were measured individually and in various combinations. A total of 137 combinations were used to switch ON different LED lamps at the same. The switching was performed using the digital signals for relays generated by the DAQ box. During each combination, magnitude and phase angles were recorded for a 1-minute duration at a resolution of 1-second.

The results of the mathematical aggregation of all combinations are compared with the actual measurement data. The magnitude difference is presented in percentage, while the phase difference is shown in degree. Fig. 5.4 shows the magnitude difference between mathematical aggregation and measurement results. The difference for the low order harmonic is between 0.5 to -2.5% for 95th percentile values, while the difference for higher-order harmonics is between -6 to 2.5%. A few exceptions show a magnitude difference of 10% for the 17th and 19th harmonic.

For 95th percentile values, the phase angles show a difference of -0.5 to 2 degrees for the low order harmonics, as shown in Fig. 5.5. The mean difference is only between -0.25 to 0.5 degrees. The mean and 95th percentile values difference between the phase angles reach almost 2 and 4 degrees for higher-order harmonics, respectively.

The second experiment is performed using Ormicron 356 power supply which provides less output variation in comparison to Chroma 61505. The Omicron has a low power rating
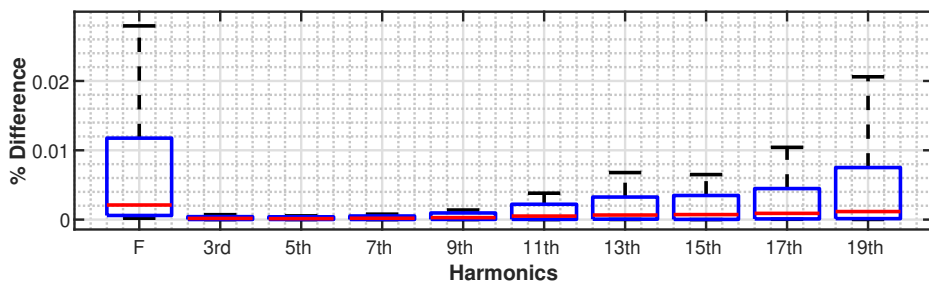

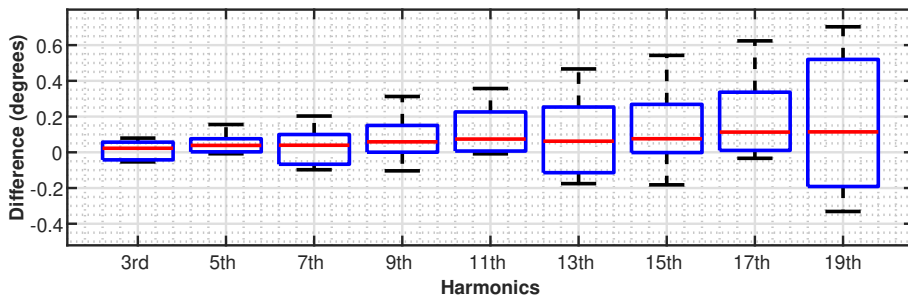Figure 5.6 – Magnitude difference between measured and aggregated values

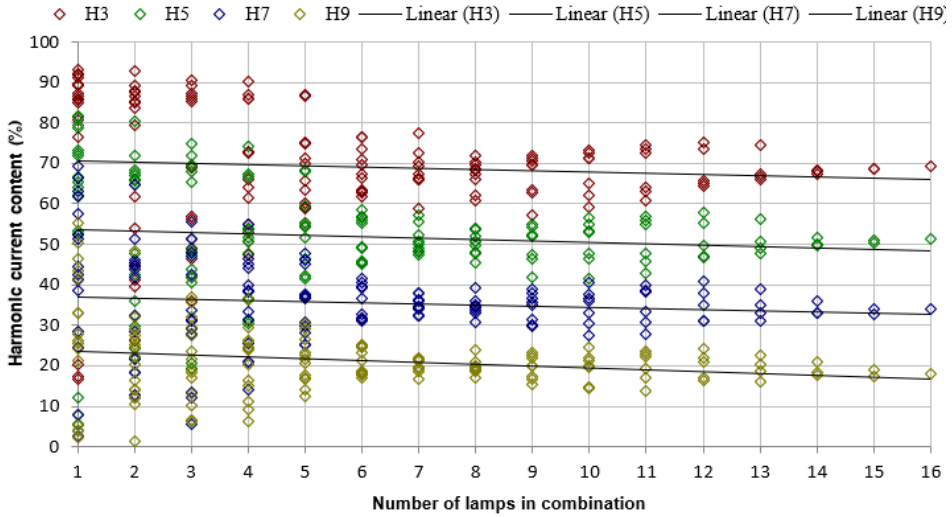Figure 5.7 – Phase difference between measured and aggregated values

Figure 5.8 – Harmonic current content for 3rd to 9th harmonic order in relation to the number of lamps in a combination [IX]
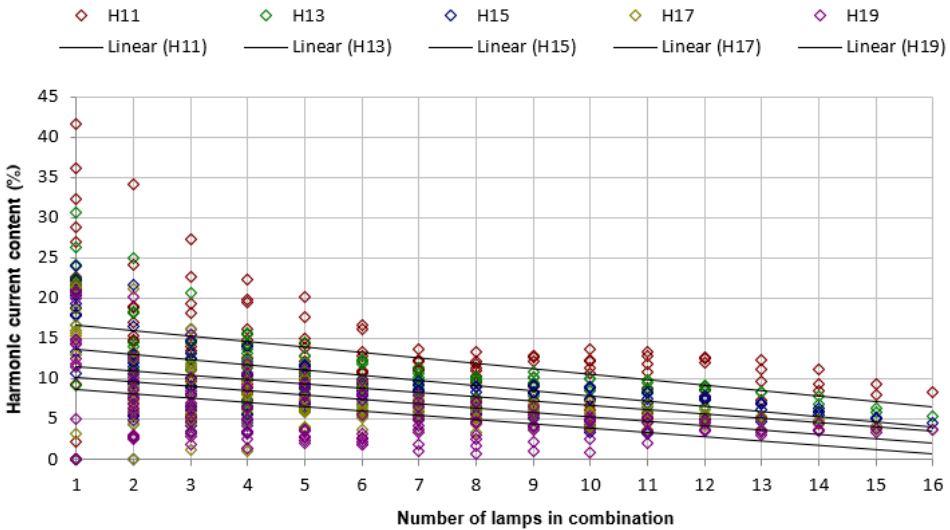

Figure 5.9 – Harmonic current content for 11th to 19th harmonic order in relation to the number of lamps in a combination [IX]

and cannot supply current to more than two LED lamps at the same time; therefore, only two lamp combinations are used to evaluate the aggregation error. The box plot in Fig. 5.6 and Fig. 5.7 shows the difference between magnitude and phase angles of measured values and mathematical aggregated values. The box's upper edge shows 95th percentile values, while the lower edge shows the 5th percentile. The red centre dotted line shows the mean difference. The whiskers are extended towards extreme values.

The magnitude difference is shown in percentage, and the mean difference is less than 0.002%. The maximum difference for the 19th harmonic is almost 0.21%. The maximum

phase difference is between -0.3 to 0.65 degrees, while the mean difference is reaching a maximum value of 0.1 degrees. The graph shows that the difference increases from the lower order to higher-order harmonics.

Fig. 5.8 shows the harmonic cancellation effect. The harmonic content is shown in the percentage relative to the fundamental component for each lamp. As the number of lamps increases in a combination, the average value of the low order harmonics decreases and is shown by black lines. The average reduction is between 4-5% for low order harmonics, while the higher-order harmonics show an average reduction of 8-10%. It shows that higher-order harmonics have a widespread in contrast to low order harmonics. Fig. 5.9 shows the harmonic cancellation for higher order harmonics.

5.4 Device operating mode variations
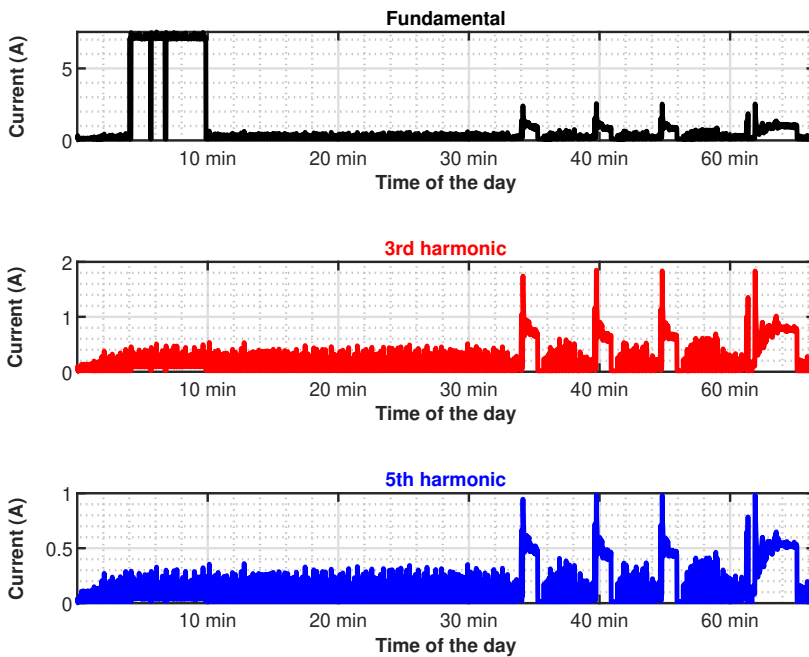
Figure 5.10 – Harmonic current variation of washing machine

The advancement in power electronics has enabled manufacturers to improve the functionality and power management of the appliances. Electric motors are an integral part of many household devices such as washing machines, blenders, vacuum cleaners, and air conditioners. Induction motors were the only choice for many years until the commercial availability of power electronic converters. These days many appliances contain DC motors with drives that provide better speed and torque control. Mostly, pre-programmed device operating modes are provided by the manufacturer and each mode consist of several sub-cycles. For example, a typical operating mode of a modern washing machine consists of heating, spinning, washing and rinsing sub-cycles. The harmonic emission of the device in each sub-cycle is different, and for harmonic estimation models, the measurement of the entire working cycle must be taken into account. Fig. 5.10 shows

the variation in current harmonics for a complete washing cycle of a washing machine.
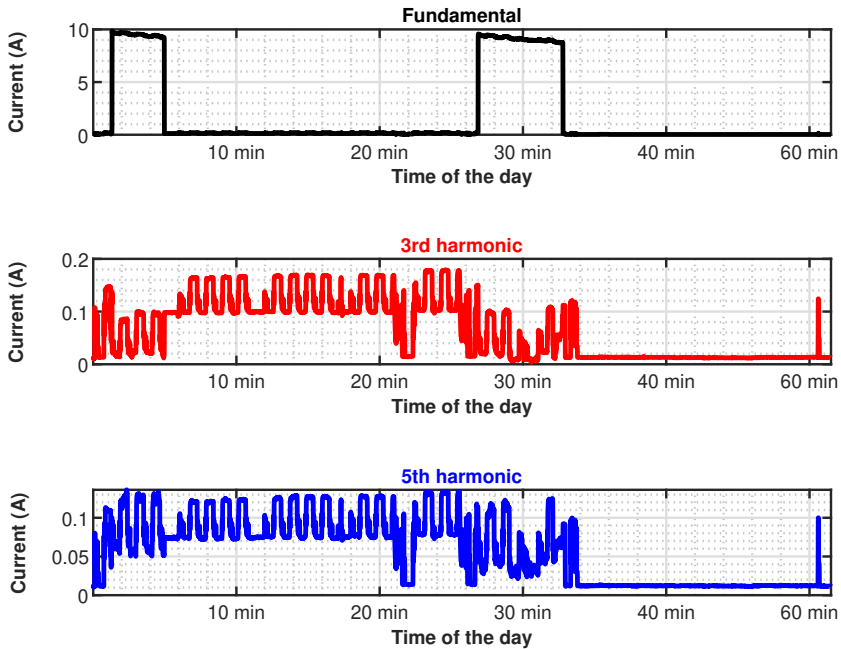

Figure 5.11 – Harmonic current variation of a dishwasher

The fundamental component shows large values between 4-10 minutes because of the heating sub-cycle. The harmonic current variation is in a constant range between 10 to 35 minutes during the washing sub-cycle. In the rinse sub-cycle, the harmonic currents are changing continuously in a cyclic manner. The 3rd and 5th harmonic variation during the heating and washing cycle is approximately the same because it does not affect the high-frequency currents. The cyclic variations can also be observed in the rinse cycle for the 3rd and 5th harmonic current. Another example of a similar device is a dishwasher. Fig. 5.11 shows the variation in fundamental, 3rd and 5th harmonic current of a dishwasher.

5.5 Impact of thermal stability

The studies related to harmonic analysis and estimations have considered uncertainties like harmonic cancellation and network uncertainties; however, time-dependent variations of the harmonic currents due to thermal stability are often neglected. A recent study reported notable variation in current harmonics magnitude and phase angles of LED lamps when 230 V sinusoidal voltage is applied [VIII]. The LED lamps contain rectifier circuits and draw a nonlinear current waveform. The study concludes that using measurements performed during the period when LED lamps were unstable leads to a significant error in harmonic current estimation.

LED lamps and switch-mode power supplies are measured on sinusoidal voltage to observe the impact of thermal stability on current harmonics variation. The measurement setup described in section 3.1.1 is used for this experiment. The measurements were performed for one hour, and current harmonics magnitude and phase variations were ob-

served.

5.5.1 Thermal stability time estimation

The current harmonic magnitude and phase angles measured during the experiment were analysed to find stability time. Odd current harmonics up to the 19th harmonic are considered in this experiment. The power supply may add unwanted small variation in the harmonics, and it can affect the current harmonics measurements [102]. To avoid these variations and to simplify the process, the trend fitting curves are applied to all current harmonics and phase angle variations over time. This approach has enabled us to calculate the stability time as the magnitude, and phase angles of all current harmonics observe an exponential rise or decay with time. Eq. (5.9) shows the exponential curve fitting that is applied to the magnitude and phase angles variations [I].

$$y = d_{Ah} \times e^{(-\frac{x}{\tau})} + Ah_f \tag{5.9}$$

Eq. (5.9) provides the values of fitting curve y for each value of original data x. Here, Ah_f is the final value of the magnitude or phase when the device becomes fully thermally stable. The difference between the initial value of magnitude or phase (during 1st minute) and the final value is represented by d_{Ah}, as given by Eq. (5.10).

$$d_{Ah} = Ah_f - Ah_o \tag{5.10}$$

The time constant τ in Eq. (5.9) is the time required by the exponent to decay by $1/e$ or grow by the factor e. The time constant is calculated by using Eq. (5.11) for all the harmonics up to the 19th.
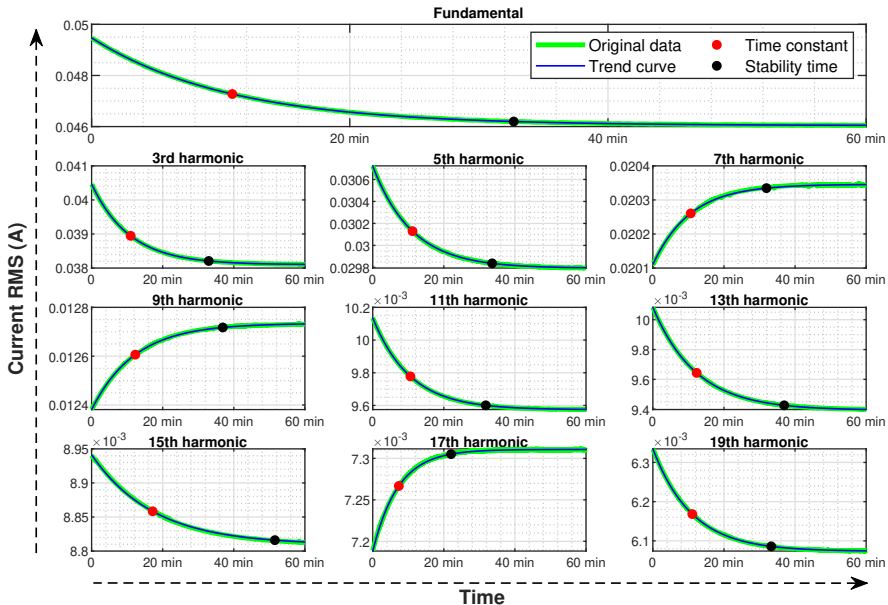

Figure 5.12 – 9.5W (type A) LED lamp magnitude (RMS) variations over time and trend curves [I]

$$\tau = \frac{T_{80} - T_o}{1 - \ln(\frac{1-\gamma}{d_{Ah}})} \qquad (5.11)$$

Where T_{80} is the time when the magnitude or phase angle reaches 80% of the final value. T_o is the starting time, and its value is, therefore, 1. The γ is the difference between 80% of the final value of magnitude or phase and the initial value, as indicated by Eq. (5.12).

$$\gamma = Ah_{80\%} - Ah_o \qquad (5.12)$$

After finding the time constant, the stability time of a device can be estimated. is assumed to have reached thermal stability after duration of 3 time-constants from the power-on and can be calculated by Eq. (5.13).

$$T_s = 3 \times \tau \qquad (5.13)$$

Fig. 5.12 shows the current magnitude (RMS) and trend fitting curve for a 9.5 watt LED lamp. The green line indicates the RMS values of the current for fundamental and odd harmonics up to the 19th. The blue line is the trend fitting curve applied by using Eq. (5.9). The time constant τ is indicated by the red dot and calculated by using Eq. 5.11. The thermal stability time T_s is shown by the black dot and is calculated by Eq. 5.13. The trend curves provide a close fit to the original current data and have applied to all the LED lamp's magnitude and phase variations to estimate their thermal stability time. The stability time T_s will change if we changed γ in Eq. 5.10.

5.5.2 Thermal stability impact on LED lamps

The measurement results of 163 LED lamps available in the market were used to evaluate their thermal stability time. The LED lamps were classified based on the driver circuit topology. Table 5.7 summarises the average price per watt, average light output efficacy, the number of lamps measured, and the number of manufacturers for each LED type used in this study.

Table 5.7 – LED lamp characteristics [I]

	Type 1	Type 2	Type 3	Type 4	Total
No. of lamps	140	15	4	4	163
No. of manufacturers	27	7	2	1	28
Average price (euro/W)	0.53	0.51	0.41	0.45	0.48
Lumens (lm/W)	90	81	82	92	86

Almost 88% of the measured LED lamps have the current waveform of type A as shown in Fig. 5.13 with a pink line. Such a lamp driver circuit contains a simple rectifier circuit. The conduction time of type B LED is greater than type A. The current waveform of type B LED lamp is shown by the black line in Fig. 5.13.

The C type LED laps has a square shape current waveform and is shown by the green line in Fig. 5.13. A constant current regulator maintains a constant flow of current over wide range of voltage[103]. Type D LED lamps contain power factor correction (PFC) circuits and their current waveform is closest to the sinusoidal, as shown by the red line in Fig. 5.13.

During each measurement cycle, sixteen LED lamps were connected to the test bench. Each lamp is measured over one hour and switched automatically for each measurement
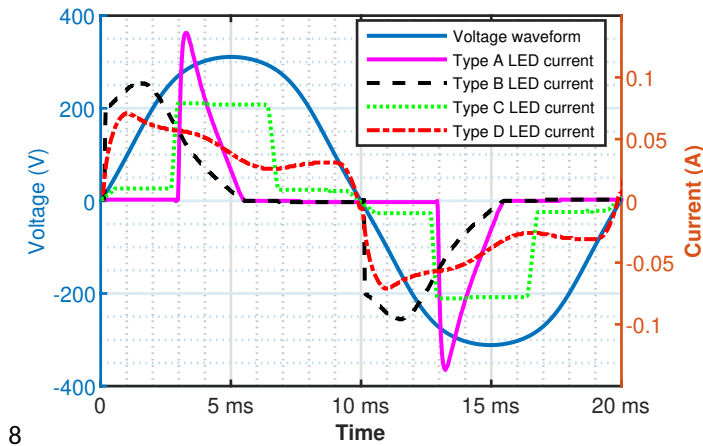
Figure 5.13 – Current waveform drawn by different types of LED [I]

cycle. The distance between the LED lamp measured in each cycle was more than 1 m from the lamp measured in the previous cycle to maintain a constant temperature. The lamps are connected through relays, and only one lamp is switched ON during each measurement cycle. It will eliminate additional primary and secondary harmonics due to several loads sharing the same power source [104]. The data extracted for analysis comprises THDI, current harmonic magnitude and phase angles, active power, reactive power, and power factor. Current waveforms are also recorded for each LED lamp. The THDI of the LED lamp changes continuously until it becomes thermally stable. The THDI of a thermally stable LED lamp is different than the initial value of THDI when it is turned ON. This difference can be up to 10%. Figure 5.14a shows the histogram of the percentage difference between thermally stable and cold LED lamps. For the majority of the lamps (95%), the difference in THDI before and after thermally stability is between 2 and 8%. Only 3.6% of lamps have less than 1% difference, and 1.84% have more than 10% difference.
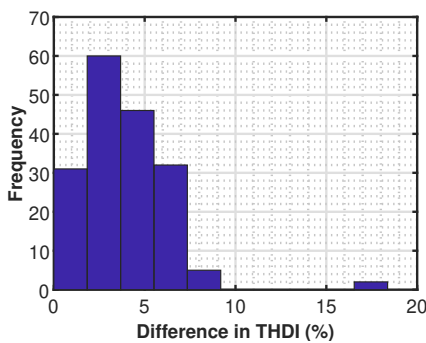
(a) THDI difference (%) histogram of 163 LED lamps
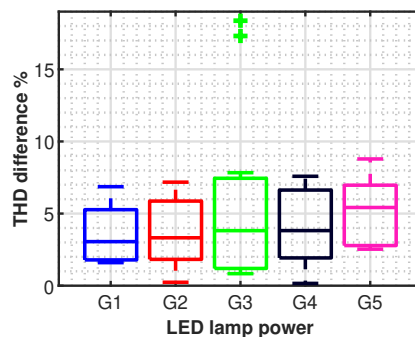
(b) Boxplot of THDI difference (%) and active power

Figure 5.14 – THDI variations of LED lamps [I]

The percentage difference in THDI between thermally stable and cold states increases with the increase of the active power of the lamps. A total of 163 LED lamps are divided into five groups based on the active power. The group G1 include LED lamps with power

ratings between 3.3 to 5 W. Similarly, in groups G2, G3, G4 and G5 LED lamps with power ratings between 5.1 to 7 W, 7.1 to 9 W, 9.1 to 12 W, and 12.1 to 20 W are included, respectively. Fig. 5.14b shows the box plot of percentage difference in THDI between cold and thermally stable LED lamps of all groups. The central line indicates the median, and the bottom and top edges of the box indicate the 10th and 90th percentiles. The whiskers are extended to extreme values. It is clear from Fig. 5.14b that as the power of the lamp increases, the percentage difference of THDI between thermally stable and cold lamps also increases. The G1 and G2 groups show a relatively large variation as most of the type A lamps include in these groups.

Thermal stability time variations   The stability time T_s of all the current harmonic magnitude and phase angle are estimated by applying trend fitting curve using Eq. (5.9). The trend curves provide a close fit to the original current data and have applied to all the LED lamps to find out the thermal stability time of each lamp. The stability time T_s will change if γ is changed in Eq. (5.11). The γ is selected by using 80% of the final value. However, γ value can be changed by changing $Ah_{80\%}$ in Eq (5.12), with 70 or 90% of the final value ($Ah_{70\%}$, $Ah_{90\%}$). However, the magnitude variation will become less than 1% as it reaches 80% of the final value. Similarly, the stability time of the phase angles can be calculated. This procedure is applied to the measurement data of all 163 LED lamps, and thermal stability time is estimated for current harmonics magnitude and phase angles.

The trend fitting curve has enabled to estimate the thermal stability time T_s of all the LED lamps. The thermal stability time may depend on many factors like temperature, lamp driver topology, the variation in the magnitude or phase angles of current harmonics, and the active power of the lamp. To investigate the reason that may influence this variance, a comparison between thermal stability time T_s of all LED lamps with active power and d_{Ah} is made.

(a) Magnitude stability   (b) phase angles stability
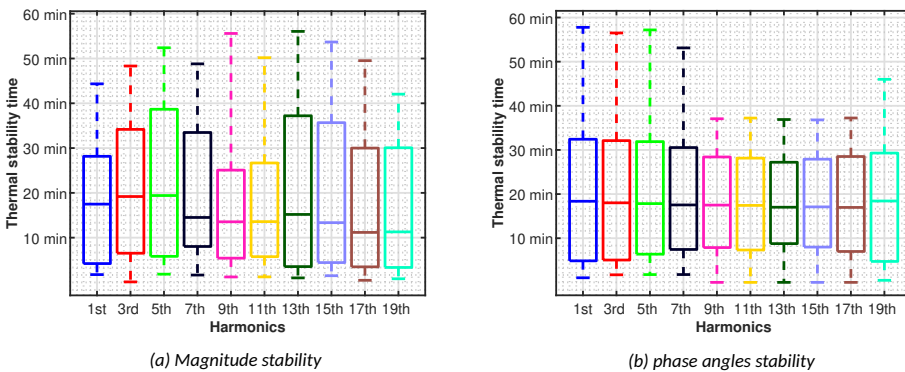
Figure 5.15 – Box plot of stability time [I]

The box and whisker plot for the magnitude of the current harmonics against the stability time is shown in Fig. 5.15a. The box top edge represents 95th percentile, and the bottom edge is equal to 5th percentile of the T_s values. The line between the top and bottom edge of the box shows median values. The upper whisker is extended to 99th percentile value, and the bottom whisker represents 1 percentile value. The plot shows that for 95th percent of the lamps, the magnitude of all harmonics becomes stable bellow 40 minutes. The fundamental magnitude becomes thermally stable quickly than most of

the higher-order harmonics except for the 9th and 11th harmonic. However, the upper whisker of the 9th and 11th harmonic is more than 55 minutes in contrast to the fundamental where it is less than 45 minutes. The 5th, 13th and 15th harmonic have the most significant spread between 5 to 95th percentile values of T_s. The stability time extends up to 38, 37 and 36 minutes for 5th, 13th, and 15th harmonic respectively.

The phase angles, on the other hand, have a different spread in comparison to the magnitude. Fig. 5.15b shows the box and whisker plot of the phase angles versus the thermal stability time for the odd harmonics. The 3rd and 5th harmonics have the highest value of the stability time T_s around 33 minutes at 95th percentile. For the 7th to 19th harmonic the T_s is between 31 to 27 minutes for 95th percentile of LED lamps. The upper whiskers of 3rd to 7th harmonic lies between 53 to 58 minutes. Therefore, it can be concluded that the phase angles of 95% of LED lamps get thermally stable before 35 minutes. The maximum time required for some lamps to have stable phase angles is 58 minutes. The magnitude takes more time to get stable and 95% of LED lamps have a stable magnitude before 40 minutes. The magnitude takes 5 minutes more time to get stable in comparison to the phase angles. The maximum time taken by the lamps to have stable magnitude for all the harmonic is 56 minutes.
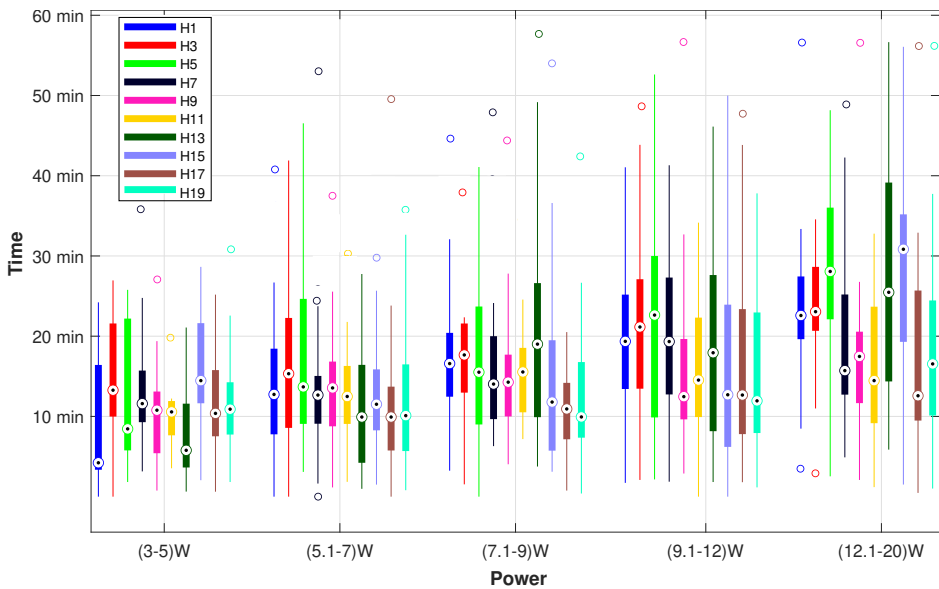

Figure 5.16 – Boxplot of active power against thermal stability [I]

The stability time may also be affected by the power of the LED lamp, although it is not a valid assumption for all LED lamps. Some high power LED lamps have shorter stability times in comparison to the low power LED lamps. However, the overall trend shows that in general high power LED lamps have a slightly higher thermal stability time in comparison to the low power LED lamps for the fundamental and higher harmonics. Fig. 5.16 shows this trend. All 163 LED lamps are divided into five groups. The group one contains LED lamps with power between 3.3 to 5 watts. Similarly, groups 2, 3, 4 and 5 contain LED lamps with active power between 5.1 to 7 watts, 7.1 to 9 watts, 9.1 to 12 watts, and 12.1 to 20 watts respectively. The box and whisker plot is made for fundamental and higher-order harmonics for the aggregate data of LED lamps in each group. The individual harmonics are represented by different colors as shown in Fig. 5.16. The top of the box indicates 75th

percentile value and the bottom indicates 25th percentile. The circle between the box represents the median value. The whiskers are extended up to the most extreme data points and outer circles represent out-liners.

It is evident from the Fig. 5.16, the median value for the fundamental component increases linearly from around 5 minutes for group 1 to 22 minutes for group 5. Hence, there is more than a three times increase in the median value of fundamental magnitude from group 1 to group 5. Similarly, the 3rd and 5th harmonics show a similar trend with 0.76 and 2.3 times increase respectively. The 7th harmonic shows an increase in the median value up to group 4, but then it decreases for group 5. The higher harmonics do not show an increasing or decreasing trend. However, the overall trend of the 25 to 75 percentile boxes shows an upward moment from group 1 to group 5. The large spread of stability time indicates its dependence on factors related to lamp architecture. These factors include cooling and electrical structures of LED lamps. However, Fig. 5.16 shows a general trend of an increase in the thermal stability time as the LED lamp's active power increases.

The d_{Ah} in eq. (5.10) shows the difference between 80% of the final value of magnitude or phase and the initial value. It means that if the d_{Ah} is large than the difference between the harmonic magnitude or phase angle is more between thermally stable state and cold state. Fig. 5.17 shows the plot of percentage change between 80% of the final value and the initial value (% d_{Ah}) against the stability time. Different markers are used to indicate types of LED lamps based on their current waveform. The colors are used to indicate the power of the lamp. Although most lamps in this study are of type A, the trend between percentage d_{Ah} and thermally stability time is independent of the LED lamp types based on the current waveform.

Fig. 5.17 shows the percentage change in d_{Ah} against thermal stability time for the fundamental and higher-order odd harmonics. The green circle in each plot indicates the majority trend. The fundamental component of magnitude shows an incremental linear trend. The 3rd, 7th, and 15th harmonics also show a similar trend to the fundamental
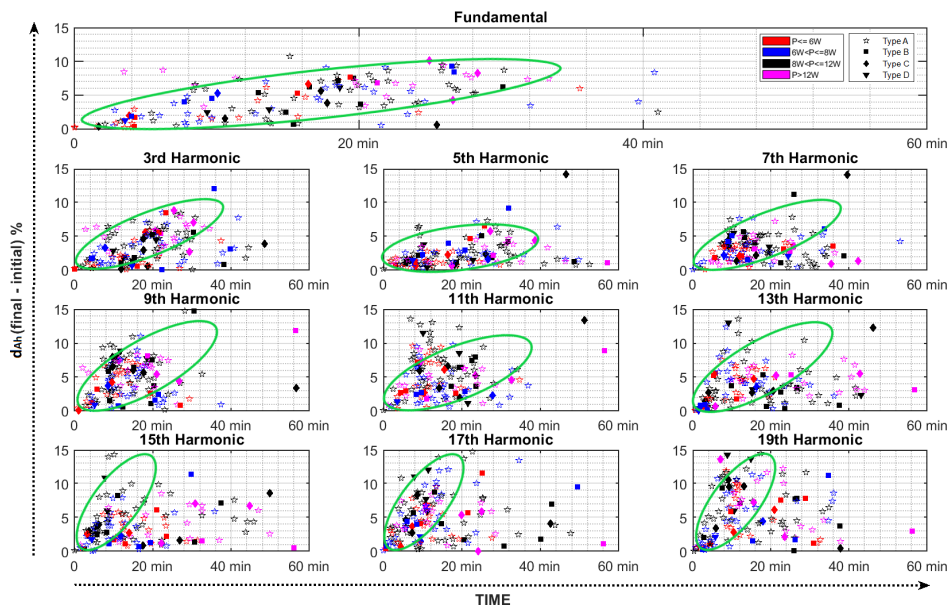

Figure 5.17 – d_{Ah} (%) against time for all LED lamp types [I]

component. The trend for 5th harmonic is somewhat linear but the growth is very flat. It means most lamps with a low d_{Ah} percentage of magnitude also have a higher stability time. The 9th harmonic has a high concentration of stability time between 10 and 20 minutes. Also, the percentage of d_{Ah} is between 1-10% during the stability time. Hence the trend is close to a uniform distribution of stability time between 10-20 minutes for different values of d_{Ah} percentage. The 11th and 19th harmonic has a linear incremental trend but between 8 to 13 minutes, the percentage of the d_{Ah} has a wide range of 1 to 15 percent. For the 17th harmonic, the trend is indicates a linear increase in thermal stability time against a change in d_{Ah} percentage.

To evaluate the impact of thermal stability on harmonic current estimation, device usage model is used to generate lighting usage profiles for 60 houses. A Monte-Carlo approach is used by selecting random lamps based on the light output needed in each room. The light output is calculated by the type of lamps used in the building measured for the data collection. During each run, lamps were selected randomly form uniform distribution. The cold and thermal stable measurements for each lamp were used to find the current harmonics for 60 houses during each run. The number of lamps in each house may vary from 5 to 11.
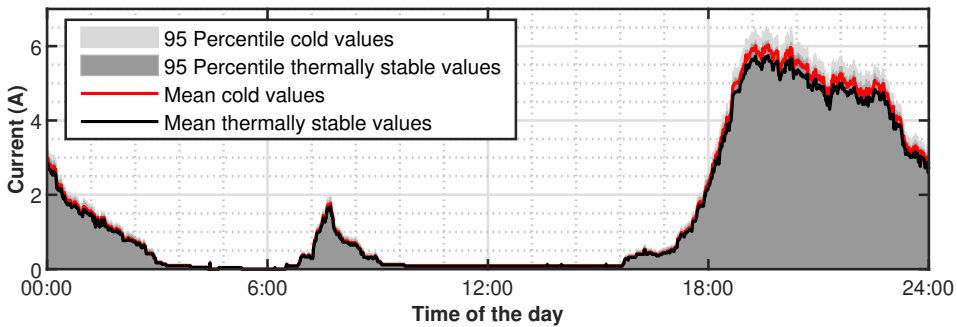

Figure 5.18 – Estimated fundamental current difference for cold and thermally stable measurements [I]

Fig. 5.18 shows the fundamental component variation of lighting usage in 60 houses. The bold black line shows the mean value of the fundamental current when thermally stable values are used in the simulation model for calculation. The red line shows the mean value when cold lamp measurement data is used. The difference is more noticeable during the evening peak. It is evident from Fig. 5.18 that the mean value difference is quite significant. Therefore, the cold measurements will result in inaccuracy in the estimation of current harmonics. The boundary of the light grey shaded area indicates the 95th percentile values of the 100 run Monte-Carlo model simulation when cold lamps measurements are used. The dark grey area boundary indicates the 95 percentile values of fundamental current magnitude when thermal stable values are used. A comparison is made between the harmonic currents estimated using measurements with thermally stable and normal values with a cooling effect in a previous study, but the results show a negligible difference [VIII]. Although lamp cooling may affect the current harmonics, however, the mean variation will be between black and red lines as shown in Fig. 5.18.

Fig. 5.19 shows the difference between the mean current magnitude estimated using cold and thermally stable measurements for the higher-order harmonics. All current harmonics show a significant difference in the magnitude estimated using cold and stable values. The 7th and 9th harmonic current magnitude show a higher value for thermally

stable measurements in contrast to the cold measurements. For the remaining harmonics, the estimated current magnitude is higher when the value of the cold measurement is used.

Therefore, for an accurate estimation of power quality indexes, the thermal stability of the lamps is critical; otherwise, it could lead to noticeable deviations in the estimation. Hence, the measurements for the estimation of the current harmonic emission levels should be taken once the LED lamps become thermally stable.
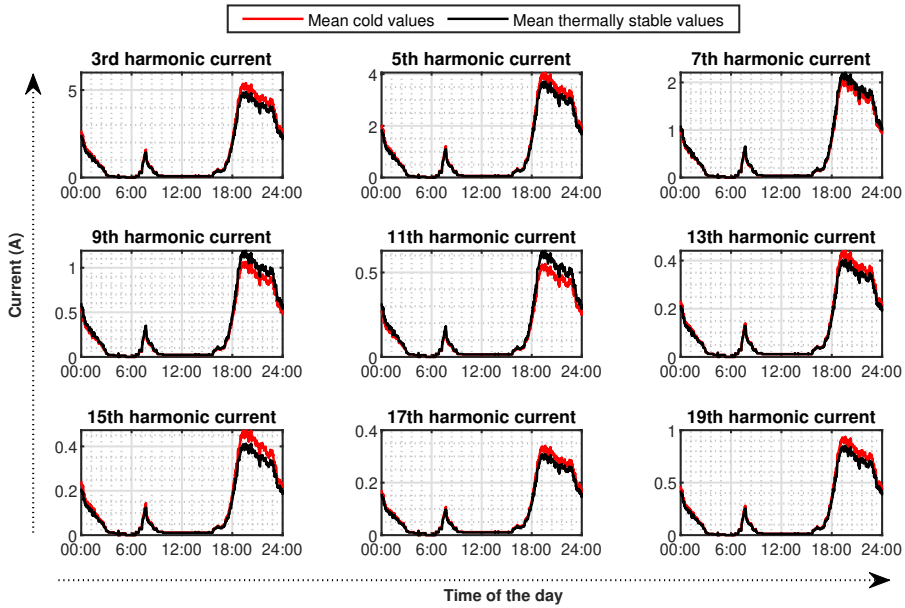

Figure 5.19 – Higher harmonic current difference for cold and thermally stable measurements [I]

5.5.3 Thermal stability of switch mode power supplies

Switch-mode power supplies (SMPS) are widely used as industrial, commercial and domestic loads. These nonlinear devices inject current harmonics, and their aggregated impact on power quality in the distribution grid could be devastating. The electronic loads may also be categorised based on the topologies of their SMPS circuits [II].

Various studies about the harmonic emissions of SMPS loads are available in the literature. The phenomena of harmonic cancellation for multiple SMPS operating at the same time is studied in [105]. The harmonic emission of these SMPS is aggregated using a Monte Carlo simulation. The harmonic cancellation was more prominent in the SMPS with high power ratings. In another study, the losses due to harmonic emission from SMPS in commercial buildings are evaluated [106]. Harmonic emissions from modern electronic load result in overheating of cables, neutral conductor overloading and power factor reduction. The wiring losses were shown to have increased by nearly 250%. The study estimates additional losses due to harmonic emission from the switch-mode power supplies. A significant portion of the electronic load includes personal computers that contain switch-mode power supplies. The harmonic losses caused by SMPS inside personal computers can increase up to 2.4 times compared to the resistive load.

The majority of the studies related to harmonic emission from SMPS have considered

Table 5.8 – Switch-mode power supplies (SMPS) characteristics [II].

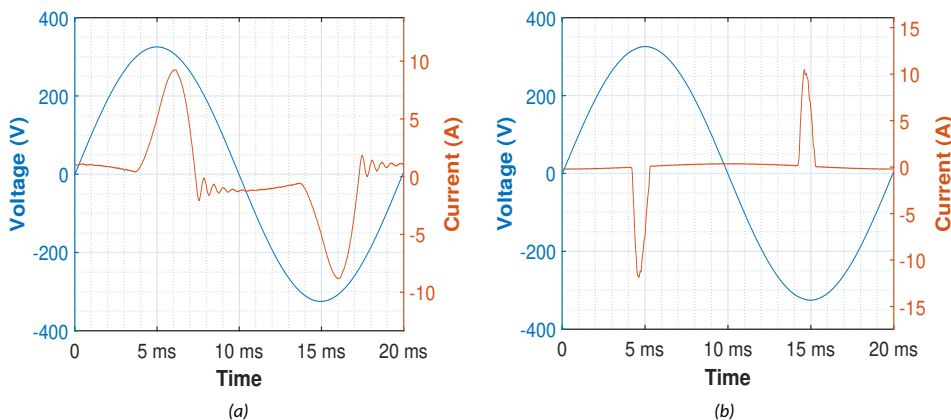| Power supply no.	Input current AC (A)	Output current DC (A)	Output voltage DC (V)
1	0.83	5	24
2	0.63	5	24
3	0.30	2	24
4	0.60	1.3	24
5	0.70	1.3	24
6	0.67	2.5	24

*Figure 5.20 – Current waveform drawn by SMPS (**a**) Type 1 (**b**) Type 2 [II].*

the impact of harmonic cancellation and circuit topology variation; however, the effect of thermal stability is generally ignored. The thermal stability of the electronic circuit may cause time-dependent variations of the harmonic currents that can contribute to significant errors in the harmonic estimation results [II].

The switch-mode power supplies can be categorised based on the type of filters used. The majority of the power supplies that are less than 75 W do not include any PFC circuits. However, the high power SMPS employs active or passive filter circuits to improve the power factor and reduce harmonic emissions. The devices with passive PFC include large inductors to reduce current variations due to switching circuits. The active power factor correction circuits inject fewer harmonics in comparison to passive power factor correction circuits.

The impact of thermal stability on the variation of current harmonic emission from SMPS is presented here. Six single-phase power supplies are selected from various manufacturers in the range of 30 W to 120 W. The detailed specification of the power supplies is listed in Table 5.8. The current waveform drawn by these power supplies depends on their circuit topologies; therefore, categorised into two groups. Fig. 5.20 shows the current waveform of both types of switch-mode power supplies. Type 2 SMPS shows a typical current waveform drawn by rectifier circuits that do not include any filtering circuits. In contrast, type 1 power supplies contain passive filters and have a different current waveform. A programmable electronic load is used, and a 60% rated load current is applied to all SMPS for the power quality measurements.

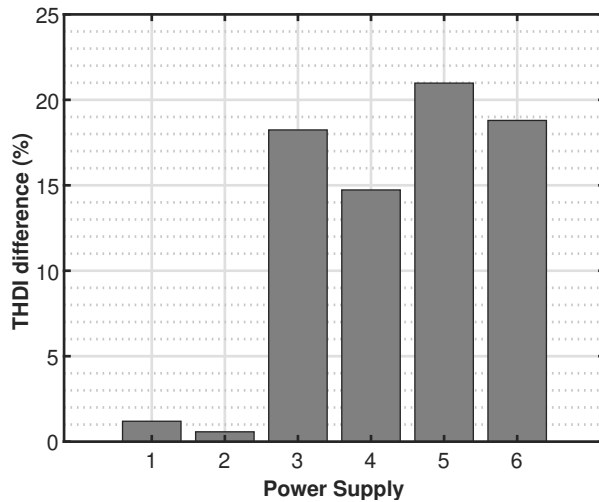The measurement setup described in section 3.1.1 is used to test all six SMPS on 230

Figure 5.21 – Histogram of total current harmonic distortion (THDI) difference between cold and stable state of all power supplies [II].

V sinusoidal voltage. The measurement is performed for 60 minutes with a rated load of 60% using a controllable electronic DC load TENMA 72-13210. Currents harmonics and THDI measurements are analysed to estimate the impact of thermal stability. The absolute percentage difference in the THDI measurements of the power supplies during the cold and thermally stable states are shown in Fig. 5.21. During the first five minutes, the measurements are referred to as cold state measurements, while the stable state indicates when the THDI variation is less than 0.25%. Power supply 1 and 2 show the THDI difference between the cold and thermally stable state of 1.2% and 0.6%, respectively%. However, significant variations in the THDI values between cold and stable states are shown by the remaining power supplies. The highest THDI variation was about 21% for the 5th power supply, while third and sixth power supplies show the THDI difference between 18 to 19% between cold and stable states. The fourth power supply shows a THDI difference of almost 15%.

Trend curves are used to estimate the stability time of all power supplies. Eq. (5.9) is used to apply exponential trend curves for variations in the phase and magnitude of the current harmonics for all power supplies. The stability time is calculated using Eq. (5.13). The magnitude variation in the fundamental current and odd harmonics for the third power supply is shown by Fig. 5.22. The green and blue lines show the measurement data and trend curve, respectively. The time constant is indicated by the red dot, while the black dot shows the stability time. This approach is applied to the current harmonics magnitude and phase variations for all power supplies, and thermal stability time is evaluated.

Type 2 power supplies show relatively high variations in harmonic magnitude and phase compared to type 1 power supplies. The magnitude difference of less than 1% was observed between cold and stable states for type 1 power supplies. The first power supply has shown the most considerable difference of 1.2% for the fundamental and 17th current harmonic magnitude. On the other hand, the second power supply shows the 1.7% difference in the 11th harmonic magnitude. The type 2 power supplies have shown a significant difference in the phase and magnitude, especially for the higher harmonics. The highest difference of 194% was observed in the magnitude of the 17th harmonic current for the
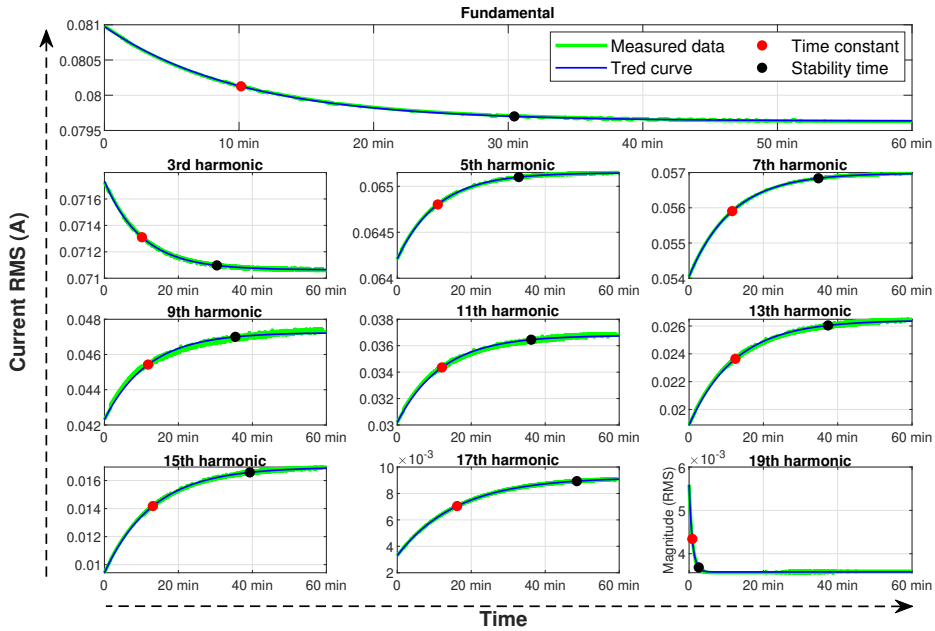
Figure 5.22 – Current harmonic magnitude variation over time for power supply 3 [II].

third power supply.

The maximum, minimum and average difference between the values of current harmonic magnitudes of type 2 power supplies are shown in Table 5.9. The phase variations of harmonic currents at cold and stable states are also less in type 1 power supply. A difference of only 1-degree was observed for the 3rd, 5th and 7th harmonic current in power supply one, while the second power supply has shown the 1-degree phase difference for the 15th, 17th, and 19th harmonic current. On the contrary, type 2 power supplies have shown a noteworthy phase difference in current harmonics measured at cold and stable states.

Table 5.9 – Difference between cold and stable state current harmonics magnitude for type 2 SMPSs (%) [II].

Harmonics	Current harmonics magnitude difference									
	F	H3	H5	H7	H9	H11	H13	H15	H17	H19
Minimum	0.4	0.1	0.8	2.3	4.5	7.6	11.8	17.6	26.2	11.1
Maximum	1.6	1.4	3.7	7.5	13.4	23.8	43.4	88.2	194.7	97.0
Average	0.8	0.6	2.0	5.2	10.0	17.6	30.0	54.7	105.4	39.9

The phase variation between cold and stable states of type 2 power supplies is significantly higher. The third power supply shows slightly fewer phase variations between 1 – 2 degrees among all type 2 SMPS. The remaining power supplies have phase variations in the range of 2 to 35 degrees. As the harmonic cancellation depends on the phase angles of harmonics, the IEC 61000-3-2 standards do not define any limits for phase variation and may result in inaccurate harmonic estimations.

The stability time for current harmonics magnitudes of all power supplies is shown

in Fig. 5.23a. The magnitude stability time for type 1 power supplies is significantly less as they show minor variations in harmonic magnitudes at cold and stable states. The stability time of power supply 1 and 2 for up to the 7th harmonics is between 20 and 43 minutes. However, the 11th and 13th harmonics took more than 60 minutes to stabilise for the power supply 2. All other magnitudes of current harmonics for these two power supplies are less than the magnitude stability time of type 2 power supplies.

(a) Magnitude stability   *(b) Phase stability*
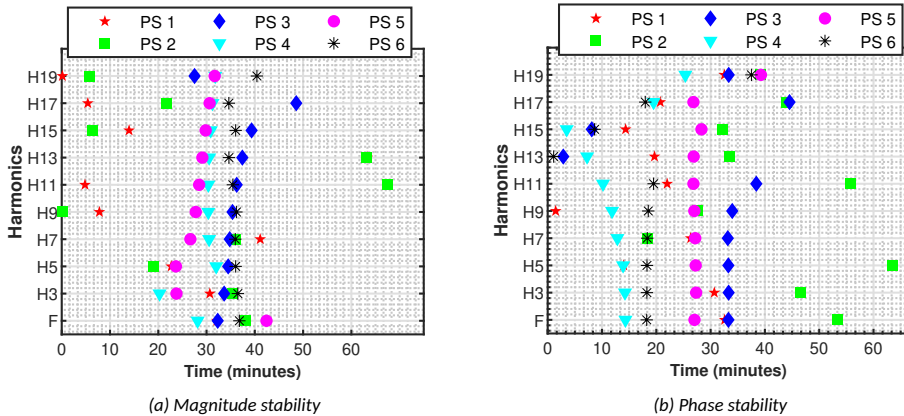
Figure 5.23 – Stability time of current harmonics for all SMPS [II]

Type 2 power supplies have a stability time range of 20-40 minutes except for the 17th harmonic of the third power supply. The third and sixth power supplies show a similar trend of the current harmonic magnitude stability time. The fourth and fifth power supplies also follow the same trend; however, their stability time is less in contrast to the third and sixth power supplies. The harmonic phase stability of all power supplies for harmonics up to the 19th is shown by Fig. 5.23b. The majority of the power supplies have achieved phase stability in less than 35 minutes except for a few high order harmonics.

The stability time is independent of the active power of the SMPS. The relation between the active power and the stability time of the magnitude of the current harmonic is shown by Fig. 5.24 . Interestingly, SMPS with high active power has less stability time than SMPS with low active power consumption. This trend is more noticeable for the higher-order harmonics.

In the real-time scenario, the harmonic current estimations could be affected significantly by the thermal stability of the loads. The probabilistic harmonic estimation models rely on the measurement data and may lead to errors in the harmonic estimation when thermal stability is not considered. The percentage difference in the RMS current calculated at the cold and thermally stable state for all six power supplies is shown in Fig. 5.25. Type 1 power supplies show a relatively small difference of nearly 1% while type 2 power supplies show a difference of more than 8% between RMS current calculated at the cold and stable states. The fifth and sixth power supply shows the maximum difference of more than 13%. Consequently, in the distribution network, many power supplies operating in an idle or working state, the estimation of current harmonics would result in an erroneous outcome because of their time-dependent thermal variation.
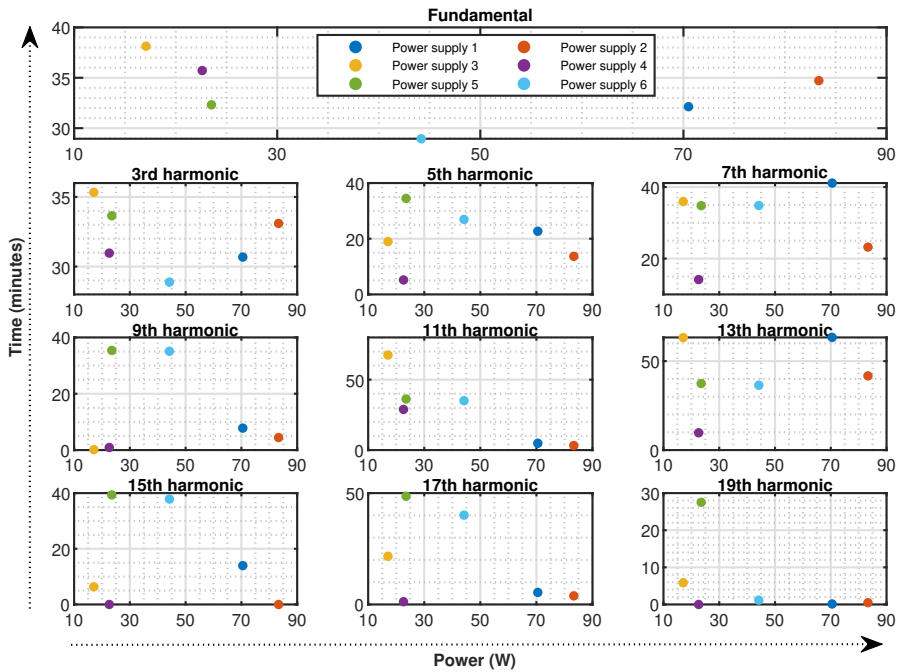
Figure 5.24 – Current harmonic stability time (T_{stable}) variation against active power of all SMPS [II].

5.6 Impact of cable impedance

Various lengths of cables are associated with each domestic, commercial, and industrial load in a distribution network. Cables may alter the magnitude or phase angle of the current harmonics. However, the extent to which the installation cable length may affect the power quality is not reported in the literature. An experiment is performed using LED lamps with different cable lengths to evaluate the impact of installation cables on current harmonics. The LED lamps are selected as their current harmonic emission profile is quite
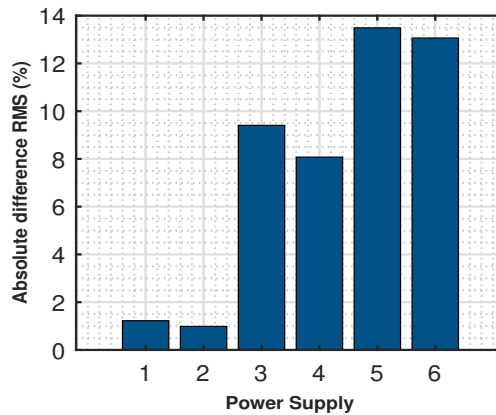

Figure 5.25 – Current RMS difference between Cold and Stable state [II].

stable. The results are compared with the measurements taken using the same lamps without cables [XI].

Four different LED lamps and three cable lengths are used in this experiment. A 230 V sinusoidal input voltage is applied, and harmonic phase angles and magnitude up to the 19th harmonic are measured. The characteristics of the LED lamps used in this study are summarised in Table 5.10. The current waveform drawn by all four LED lamps when pure sinusoidal voltage is applied is shown in Fig. 5.26a.

Table 5.10 – Summary of LED lamp parameters [I]

Lamp No.	Energy ratings	Power (W)	Lumens (lm)	THDI	Price (€)
1	A+	6	470	136.04	4
2	A+	12	1055	150.69	5
3	A+	12	1055	137.42	4.5
4	A+	6	470	133.51	3.5

(a) Current waveform drawn by the LED lamps   *(b) LED lamps THDI (%) difference for different cables*
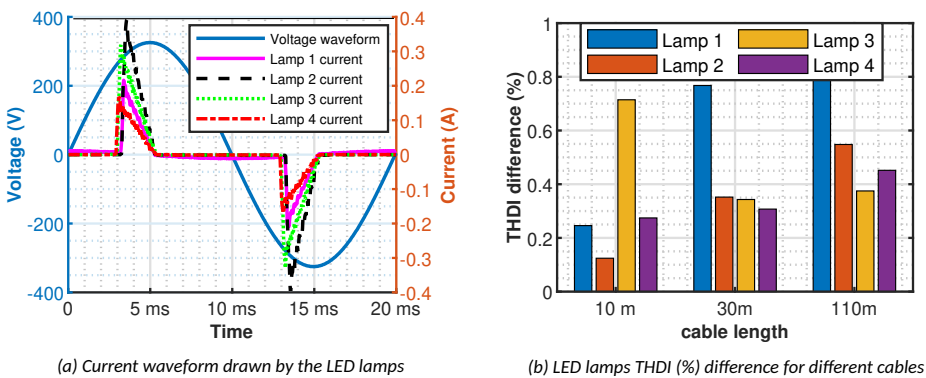
Figure 5.26 – Current waveforms of lamps and their THDI difference with cables [XI]

The cables used in this experiment are three core-stranded 3G 1.5 mm with 10, 30, and 110-meter lengths. The LED lamps are also tested by using the cable parameters for a 1000 meter long cable. All LED lamps are warmed for 1 hour to make sure there is no variation in the measurement results due to thermal stability issues.

LED lamps are tested on different cable lengths, and THDI, current harmonics magnitude, and phase angles were measured and compared with the results without cables. A difference of 0.2 to 1% in THDI was observed when lamps were measured using different cable lengths. Fig. 5.26b shows the absolute percentage change in the THDI when measurements for all LED lamps with three different cables are compared with measurements without cables. For the lamp 1, 2 and 3, the THDI difference has increased as the cable length increase. However, in the case of lamp 3, the THDI difference with 10 m cable is more in comparison to 30 m and 110 m cables.

The current harmonics magnitude shows a maximum difference of 3% between measurements taken with and without cables. The magnitude variation in fundamental components of the current up to the 11th harmonics is relatively small. The mean value and 90th percentile values of the magnitude difference is less than 0.25% and 1.5%, respectively, as shown in Fig. 5.27a. The lower and upper boundary of the dark grey box represents the 10th percentile and mean values, respectively. The upper boundary of the
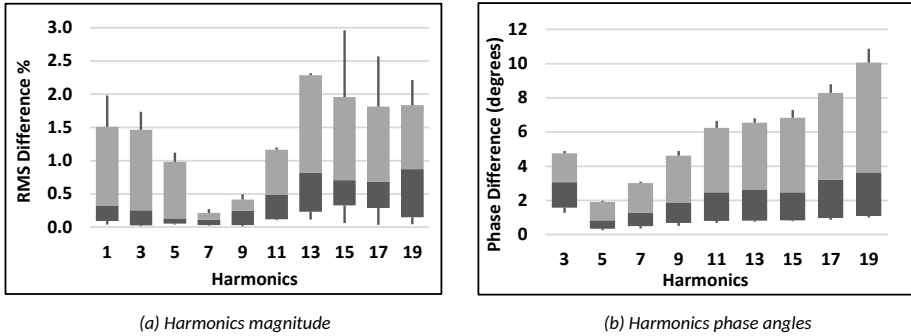
(a) Harmonics magnitude   (b) Harmonics phase angles

Figure 5.27 – Boxplot of current harmonics difference with cables [XI]

light grey box shows the 90th percentile values. The lower and upper whiskers extend to the extreme low and high values. The higher current harmonics from the 13th to the 19th shows more variation. The mean value of percentage change is between 0.7 to 0.9% with and without cables. The 90th percentile value of magnitude difference is also more in comparison to lower harmonics and is between 1.5% to 2.5%. The phase difference of current harmonics is up to 11 degrees when cables are used with LED lamps, as shown in Fig. 5.27b. The mean difference of the phase angle for the 3rd harmonic is 3 degree and more than the mean difference of higher harmonics. The variation in the phase angle increases as we observed from the 5th to the 19th harmonic. The mean difference increases from 1 degrees for the 5th harmonic to 3 degrees for the 19th harmonic. The 90th percentile of phase difference also shows an incremental increase from 2 to 10 degree from the 5th to the 19th harmonic. For the 3rd harmonic, the 90th percentile of phase difference is 5 degree.
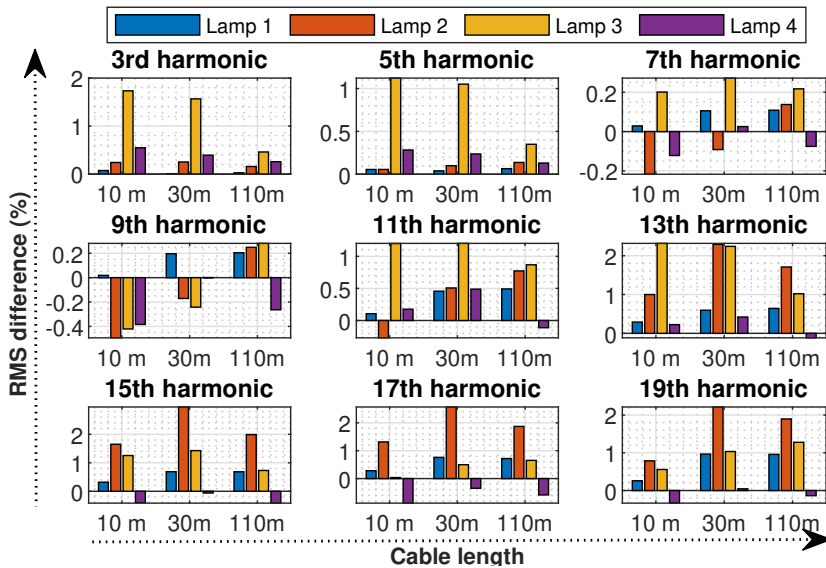

Figure 5.28 – Current magnitude difference for all LED lamps with different cables [XI]

Fig. 5.28 shows the variations of current magnitude percentage difference for all lamps from 3rd to the 19th harmonic when measurements at different cables length are compared without cables. The variation of each lamp is different from the other and there is no general trend of harmonic current variation. The lamp 1 and 4 have same power consumption but different variation in current harmonics. The lamp 1 shows less difference in harmonic current variation in comparison with other lamps. This percentage difference in magnitude also increases from 3rd to the 19th harmonic gradually. Also, it shows an increase in the magnitude difference as the cable length increases. The 4th lamp although has the same power consumption as of lamp 1 but shows a different trend for magnitude variations. There is no specific pattern observed, however, the magnitude difference is more for the 3rd to 11th harmonic and less for 11th to 19th harmonic in comparison to lamp 1. Similarly, the lamp 2 and 3 have same power consumption but the percentage of magnitude difference with and without cables does not show a similar trend. The lamp 3 shows a significantly large difference from 3rd to 11th harmonic in contrast to lamp 2. For the higher harmonics, lamp 2 shows more difference in the current magnitude than lamp 3.

The phase difference of the current harmonics for different lengths of the cables is shown in Fig. 5.29. For lamp 1, the difference tends to increase as the length of the cable is increased while lamp 2 shows a decrease in phase angles as cable length increases. The lamp 4 shows significantly more deviations in the phase angles in contrast to lamp 1. The phase deviation for lamp 4 is between 1 to 5 degrees while for lamp 1 its between 0 to 1 degrees. The lamp 2 and 3 shows a different trend and phase difference is more for 10m and 30 m cable in comparison to the 110 m cable. Except for the 15th harmonic, lamp 2 shows a large phase deviation for the 30 m cable while the phase difference is nearly same for 10 m and 110 m cables. On the other hand, the lamp 3 shows the almost same difference for 10 m and 30m cable but a significantly lower phase deviation for the 110 m cable.
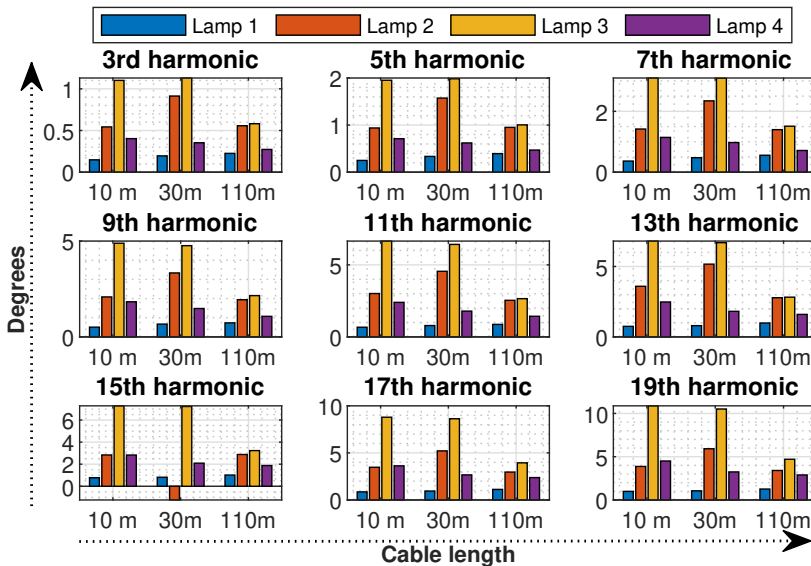

Figure 5.29 – Phase (degree) difference for all LED lamps with different cables [XI]

Table 5.11 – Current harmonics difference for 1000m cable [XI]

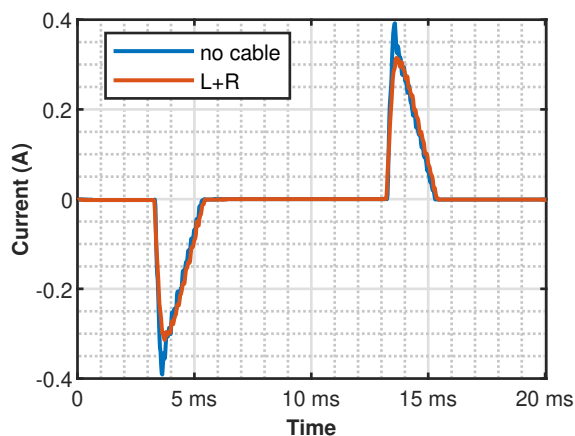| Magnitude difference											
	THDI	I_f	I_3	I_5	I_7	I_9	I_{11}	I_{13}	I_{15}	I_{17}	I_{19}
Lamp 1	3.3%	0.5%	0.4%	1.3%	2.9%	5.6%	9.4%	10.6%	10.1%	12.1%	15.8%
Lamp 2	5.9%	-0.2%	0.5%	2.1%	4.9%	9.8%	17.3%	21.8%	21.3%	23.9%	30.4%
Phase difference											
	THDI	ϕ_1	ϕ_3	ϕ_5	ϕ_7	ϕ_9	ϕ_{11}	ϕ_{13}	ϕ_{15}	ϕ_{17}	ϕ_{19}
Lamp 1	3%	0 °	3 °	6 °	8 °	2 °	11 °	11.3	13 °	15 °	18 °
Lamp 2	5.9%	0 °	5 °	9 °	13 °	16 °	18 °	16 °	10 °	20 °	23 °

Figure 5.30 – Current waveform with and without cable of lamp 2 [XI]

To observe the effect of large cable length on current harmonics, electrical parameters of 1000 m long cable are used for current harmonics measurements. The electrical parameters were measured for a 3 m long 1.5 mm 3G stranded cable. The inductance, capacitance and resistance values are calculated. These values are used to estimate the inductance and resistance of a 1000 m long cable. The inductance value is 135 µH, and the resistance is 13.3 ohms. The capacitance value is ignored as its effect is negligible. The inductance and resistance were connected with lamp 1 and lamp 2, and measurements were performed to observe the variation in the current harmonic spectrum. The current waveform shows a significant change when compared with the current waveform drawn by the lamp without any installation cables, as shown in Fig. 5.30. The THDI for both lamps shows a change of 3 and 6% when compared to the results without cables. The fundamental current shows a change of 0.5 and 0.2% for lamp 1 and 2, respectively. The percentage difference for both lamps increases for the higher harmonics. The magnitude and phase difference for both lamps are indicated in Table 5.11. The maximum difference was for the 19th harmonic for both lamps. The current magnitude shows a change of 15% and 30%, respectively, for lamp 1 and 2. The phase deviation is also 15 to 20 degrees for both lamps.

5.7 Network uncertainties

The amount and type of load connected to the network are changing continuously. The voltage at the PCC is directly affected by the supply voltage in the MV line supplying the distribution transformer, as well as load current itself due to voltage drop on resistance

Table 5.12 – Harmonic content of voltage waveforms

| Harmonics	Sinusoidal	Flat Top 1	Flat Top 2	Pointed Top 1	Pointed Top 2	Grid 1	Grid 2	Grid 3
H1	230.0	229.9	229.0	229.8	229.0	233.8	233.0	230.6
Ph1	-	-	-	-	-	-	-	-
H3	-	5.450	18.753	6.620	18.320	0.478	0.345	0.154
Ph3	-	-	-	-	180	57	51	80
H5	-	3.828	7.951	4.730	11.450	1.073	1.028	1.546
Ph5	-	180	180	180	-	295	224	296
H7	-	2.040	0.082	1.440	-	1.113	0.972	0.792
Ph7	-	-	-	180	-	26	15	37
H9	-	0.565	2.324	-	-	0.480	0.268	0.301
Ph9	-	180	0	-	-	211	248	241
H11	-	0.308	0.998	-	-	0.402	0.353	0.430
Ph11	-	180	180	-	-	311	316	318
H13	-	0.557	0.673	-	-	0.176	0.249	0.310
Ph13	-	0	180	-	-	87	90	115
H15	-	0.375	0.832	-	-	0.101	0.073	0.123
Ph15	-	180	0	-	-	331	51	43
H17	-	0.051	0.015	-	-	0.049	0.111	0.161
Ph17	-	0	0	-	-	105	158	152
H19	-	0.182	0.524	-	-	0.1017	0.032	0.088
Ph19	-	0	180	-	-	78	42	95
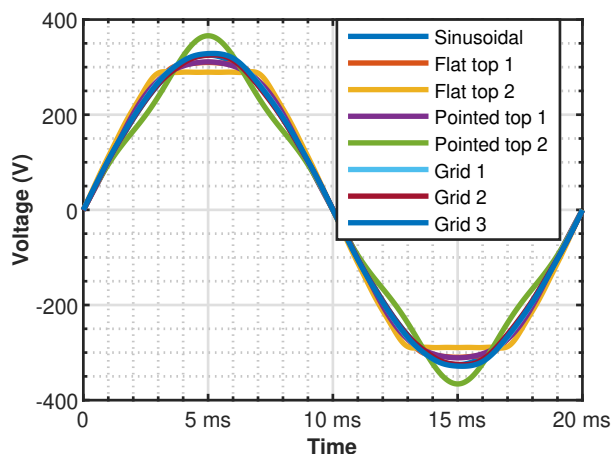
Figure 5.31 – Different voltage waveforms

and reactance. The voltage may also increase or decrease in the weak networks. These voltage variations will affect the load and its harmonic emission profile. Therefore, the harmonic emission of a constant load will also be different under dynamic network conditions.

Compact fluorescent lamps (CFL) were measured on different voltage distortions to evaluate the effect of network voltage variations. A total of eight different voltage profiles are used, and the harmonic content of each waveform is listed in Table 5.12. Fig. 5.31 shows the signal cycle of each voltage waveform.

The device usage model is used to simulate the lighting load of 60 houses. Each house is populated with random CFL lamps from the measurement portfolio, and aggregated harmonic emission is estimated using Monte Carlo simulation. The harmonic measurement results for a single voltage distortion are used during each iteration, and the aggregated harmonic are estimated. Fig. 5.32 shows the aggregated 3rd and 5th harmonic current of 60 houses for a day. The results indicate a significant difference in the harmonic content at few voltage distortions. Therefore, it is essential to analyse the impact of network uncertainties on harmonic emission in the low voltage network.
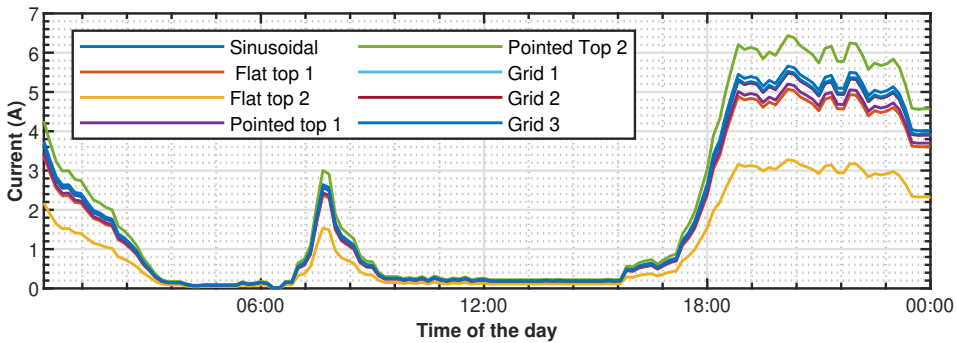
(a) 3rd harmonic current
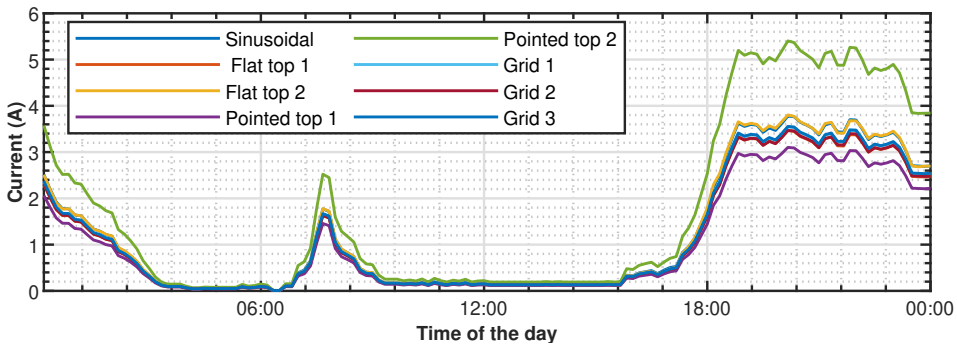
(b) 5Th harmonic current

Figure 5.32 – Comparison of harmonic emission on different voltage distortions

6 Harmonic aggregation models for LV Networks

The type and number of nonlinear loads are increasing in residential networks continuously. It is crucial to evaluate the harmonic emission impact of these devices on the operation of the distribution network. These evaluations would also be vital for planning the new or up-gradation of the existing networks to accommodate the high penetration of nonlinear loads, including EVs and PV based electricity generating units. However, the complexity associated with the network and loads influences the harmonic emission and propagation through the network. A bottom-up harmonic aggregation approach is used to estimate the current harmonic emission profile for the stochastic load usage models developed in chapter 4. The result would provide an estimate of the current harmonic emission in the presence of current and future nonlinear loads for different voltage distortions.

6.1 Methodology

The total load connected to the residential network is changing continuously depending on the consumer's usage behaviour. It will result in a dynamic harmonic emission profile of individual households. The network condition, including voltage magnitude and waveform distortions, also affects the load's harmonic emission profile. Therefore, the deterministic estimation of current harmonics is not effective, and a probabilistic approach can provide a border perspective for the network planners and operators. In this chapter, stochastic load usage profiles are used to estimate the aggregated impact of the nonlinear loads on the current harmonic emission. Time series plots are used to show the range of current harmonics magnitude estimated at different times during a day.

The harmonic emission of a device depends on many factors, including its operating technology, circuit topologies and power ratings. The outdated technologies such as incandescent lamps, cathode ray tube (CRT) based televisions (TVs) were not energy efficient in comparison to their modern-day counterparts but had harmonic emission of low intensity or with little variance. Present devices include high efficiency nonlinear power supplies and the harmonic emission can be different for the devices having the same power ratings but different circuit topologies. The residential LV networks are composed of several individual households containing numerous devices with different usage behaviour depending on the dweller's occupancy, socioeconomic status, and building structures. The harmonic emission of the network will be the aggregated sum of harmonic currents of individual devices connected to the network. The aggregated sum depends on the magnitude and phase angles of the harmonic vectors. The aggregation of several appliances will result in harmonic cancellation depending on the phase angles. The dynamic network conditions may affect the magnitude and phase variations of the current harmonics injected by the loads.

A Monte-Carlo approach is used to calculate the mean and 95th percentile values of aggregated harmonic emission of devices simulated over several days. This approach provides a range of harmonic magnitudes likely to exist at a particular time of the day. 60 houses are simulated over 100 days and each house has assigned appliances based on the ownership statistics provided by the national surveys. Simulation is performed to estimate the impact of technology evolution, circuit topology and high EV penetration on the harmonic emission profiles in the LV residential network.

6.2 Impact of technology on current harmonic emission

The improvement in the efficiency of electrical appliances can reduce the overall electricity consumption by 27% [107]. Policy making institutions are promoting practices that can improve energy efficiency to reduce power consumption. The European parliament has also emphasised the importance of adopting energy-efficient appliances and lighting in its regulation [108].

The advancement of electronics has enabled the appliances manufacturer to replace inefficient technologies such as incandescent lamps and CRT TVs to improve performance and reduce power consumption. To provide an effect on harmonic current emission by the gradual replacement of efficient appliances, the impact of LED and CFL penetration in the low voltage residential grid is estimated [XII].

Lighting ingests a significant part of electricity in residential, commercial, and industrial electricity consumption. Incandescent lamps have been in use for many years as a conventional light source. However, they have a short life span and poor efficiency. During the last two decades, most incandescent lamps are replaced by CFL and LED lights. The share of IL lamps was almost 77% in the UK residential lighting market by 2010, while the CFL share was only 6.7% [109]. Similarly, in the United States (US), 96% of the homes still have at least one IL, and 13% of households have all lamps of incandescent type [110]. The projections indicate a significant shift in the lighting market towards LED lamps in the last few years. LED lamps share will increase from 3% for indoor lamps in the US to 42% by the end of 2020. By the end of 2030, the projected LED lamps share for indoor and outdoor installations is expected to be 81% and 99%, respectively. LED lamps will replace 46% of all indoor lights and 75% of all outdoor lights in the US by the end of 2020. The penetration of LED lamps in Europe is around 46% of the total installed lighting by 2020 [111]. It shows the significant potential of LED lamps in the future.

The mass adoption of CFL and LED lamps will significantly affect the utility grid in terms of power quality. A comparison has been presented between CFL adoption in the grid and incandescent lamp usage in [112]. The CFL lamps are divided into good, average, and poor categories based on the driver circuit topology. The author reports a significant saving in power consumption by using any type of CFL. However, poor quality CFL injects more harmonics in the distribution network than good quality CFL as it does not include any filters in the driver circuit. The reduction of peak current and losses was observed while replac-
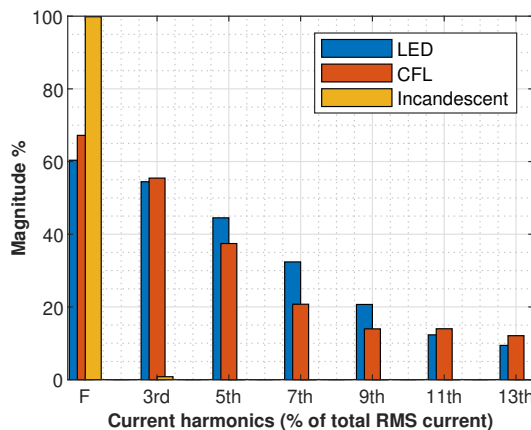

Figure 6.1 – Harmonic current comparison of IL, CFL and LED [XII]

ing incandescent lamps with CFL and LED [113]. The experiment was performed in the laboratory-based residential building model; however, the building's actual lighting usage patterns were not considered. In another study, a comparison has been made between harmonic emission by CFL and LED lamps in the distribution network [114]. The measurements were taken for 50 LED lamps usage simultaneously and, therefore, do not represent real-time lighting usage in a building. The author reported that few LED lamps cause a DC in the network. Measurements of different combinations of incandescent, CFL, and LED lamps were performed to compare the effect on power quality in [115]. The measurement results are also used in a computer simulation of a distribution network to compare CFL, LED, and IL usage in the grid. The results show poor power factor and high total harmonic current distortion for CFL and LED lamps. Most of the studies available in the literature show various limitations. The building models have not considered the real-time lighting usage patterns by the occupants. The lamp's thermal stability affects the current harmonics magnitude and phase angles that could affect the power quality estimation [I]. Also, the harmonic cancellation may vary the results under different combinations of load. The harmonic current magnitude could be varied between 2.5 to 5%, and phase angles may vary between 2 to 3% for different combinations of LED lamps [IX].

To evaluate the impact of energy-efficient lamp integration in the residential network, 194 lamps, including LED, CFL, and IL, were measured on sinusoidal voltage. LED, CFL, and IL lamps with the same lumen output are selected to compare the current harmonic emission from different lighting technology. Fig. 6.1 shows the current harmonic magnitude comparison of different lamps with the same light output. The graphs show the percentage of current harmonic RMS relative to the lamp's total RMS current. This will provide the comparison of the share of fundamental component in the total RMS current. Both CFL and LED lamps show a significant 3rd, 5th, and 7th harmonic component. The IL lamp shows a higher fundamental component in contrast to LED and CFL but shows no higher harmonics.

The lighting usage model is used to generate each lamp's switching profiles for all 60 houses. Six different scenarios are created in which each house is populated with a different mix of LED, CFL, and IL.

1. Scenario 1: 30% IL and 70% CFL

2. Scenario 2: 10% IL, 20% LED and 70% CFL
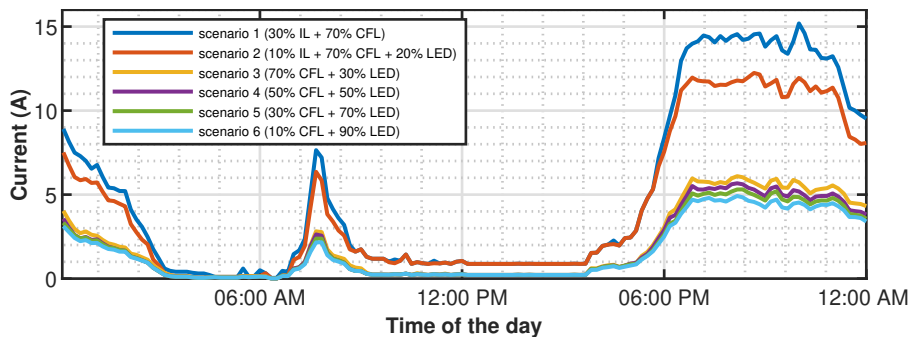
3. Scenario 3: 70% CFL and 30% LED

Figure 6.2 – Fundamental current estimated for 60 households lighting load with different scenarios [XII]

4. Scenario 4: 50% CFL and 50% LED

5. Scenario 5: 30% CFL and 70% LED

6. Scenario 6: 10% CFL and 90% LED

During each scenario, lamps are selected based on the same light output to have a fair comparison of current harmonic emission and power consumption. Fig. 6.2 shows the fundamental current drawn by 60 houses for different scenarios. The peak current during the evening interval has been significantly reduced by the replacement of IL with CFL and LED lamps.

The peak current was in the range of 14-16 A for 30% IL usage and dropped to 10-12 A range for 10% IL usage. For the remaining scenarios, all IL are replaced by CFL and LED lamps. As a result, a significant reduction in peak current is observed and now in the range of 4 to 6 A. In the last four scenarios, LED lamps are gradually replacing the CFL with a 30% share in scenario three, towards a 90% share in scenario six. The peak current also dropped with an increasing share of LED lamps in the houses. Fig. 6.3 and Fig. 6.4 shows the graph of current harmonics from 3rd to 9th for different scenarios. Although the power consumption of IL is significantly higher than CFL and LED, but it behaves like a resistive load. The 3rd harmonic current is low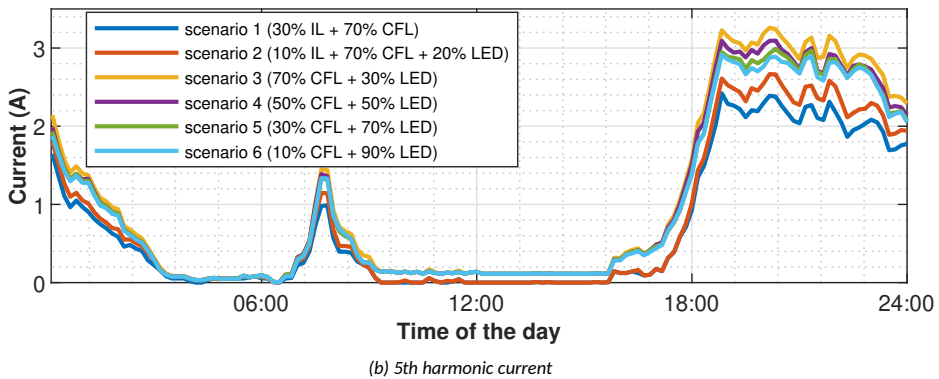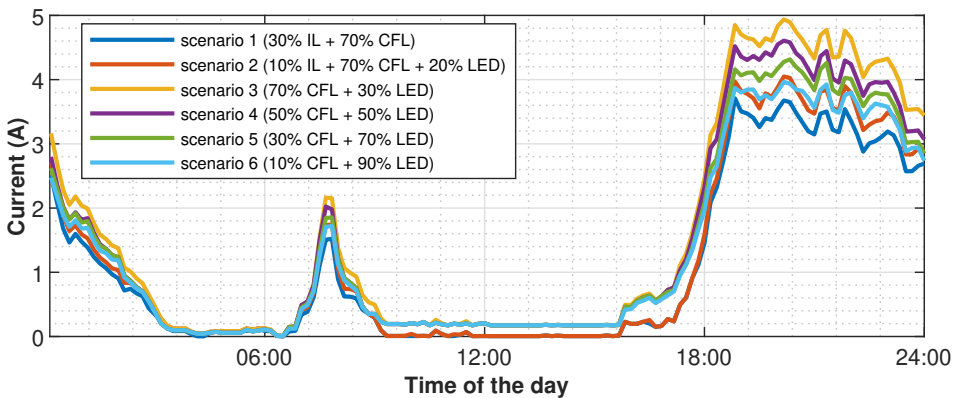est for scenario 1, with a 30% share of IL and 70% CFL. When only LED and CFL combinations are used to evaluate the 3rd harmonic

(a) 3rd harmonic current

(b) 5th harmonic current

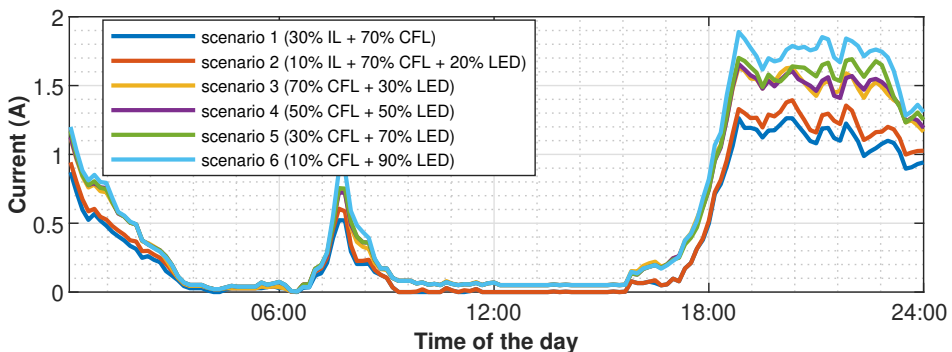*Figure 6.3 – Comparison of 3rd and 5th harmonic emission from lighting for different scenarios [XII]*

current magnitude, scenarios with higher shares of CFL inject higher 3rd harmonic current. As the CFLs are replaced with LED lamps, the 3rd harmonic current magnitude also drops. A similar pattern is observed for the 5th harmonic current, where scenarios with a higher share of IL generate less harmonic current. The 7th and 9th harmonic current increases with the increase in the percentage of LED lamps. For the 6th scenario, the 7th and 9th harmonic current is higher as the share of LED lamps is 90% in the houses.

It is clear from the results that although energy-efficient lamps consume significantly less power but are responsible for harmonic injection in the grid. Both CFL and LED lamps use a similar driver circuit and include rectifiers. However, LED lamps are more energy-efficient and consume 50% less electricity for the same light output. As a result, the 3rd and 5th harmonic magnitude were more for the scenarios with a greater CFL share than LED lamps in the houses. For higher harmonics, LED lights generate more harmonic content in contrast with CFL.

6.3 Impact of circuit topology on current harmonic emission

6.3.1 Classification based on circuit topology

Similarly to other electronic loads the LED and CFL lamps can be classified based on the internal circuit topologies of the power supplies. The classification can be based on the type of power factor correction circuits employed in the power supplies and their design topology [116, 117, 118, 119]. To observe the impact of the circuit topology employed inside

(a) 7th harmonic current
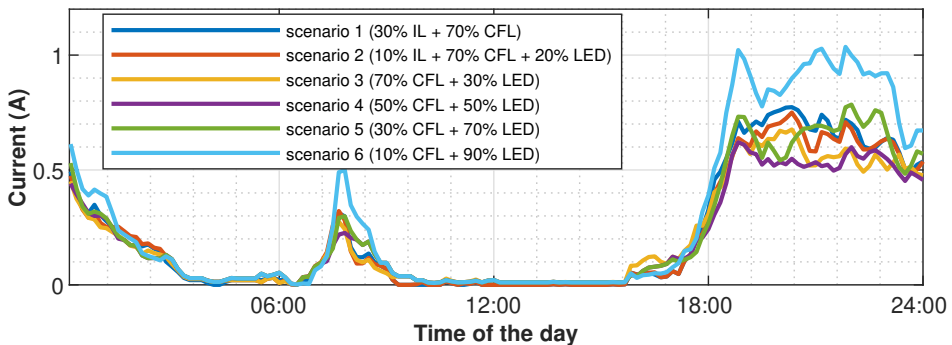
(b) 9th harmonic current

Figure 6.4 – Comparison of 7th and 9th harmonic emission from lighting for different scenarios [XII]

the power supplies on the current harmonic emission, over 200 LED lamps are tested and classified based on their current waveforms and internal topology of the driver circuit. Fig. 6.5a shows the current waveform drawn by LED lamps with four different driver circuits.

Type A The bold pink line in Fig. 6.5a shows a plus-like current waveform drawn by the type A LED lamp. This type of LED driver is based on a full-wave rectifier circuit. The PFC circuits are not used and a large smoothing capacitor controls the out-voltage ripples [117]. These circuits may also include an input EMI filter to reduce electromagnetic interference. The THDI values of type A circuits are high, as shown in Fig. 6.5b. The box's top and bottom lines indicate 90th and 10th percentile values, while the middle line shows the mean value of the THDI. The upper and lower whiskers are extended towards the maximum and minimum values. Most CFL and low-quality LED lamps contains a similar circuit in their drivers.

Type B Type B LED driver circuits include a Zener diode Dz that limits the LED lamp's forward voltage, as shown in Fig. 6.6. The black dotted line shows the current waveform drawn by these LED lamps in Fig. 6.5a. The rectifier starts to conduct around zero crossings of the input voltage and continues until the input voltage reached the peak value. The increase in conduction time will decrease the THDI values of these lamps in comparison to type A, as shown in Fig. 6.5b. The red boxplot shows the mean, 10th and 90th percentile values that are significantly lower than the type A LED. Most commercially available LED lamps contain these types of driver circuits.

Type C The current drawn by the C type LED lamps have a square shape, as shown by the green dotted line in Fig. 6.5a. The circuit contains a constant current regulator (CCR). It provides a constant current flow over a wide voltage range and therefore protects the LED [103]. Their THDI values spread is lower than the type B LED driver circuits, although the mean values are nearly the same, as shown in Fig. 6.5b. The lower number of type C lamp availability during power quality testing may also result in a higher mean value.

Type D The current waveform drawn by type D LED is close to sinusoidal and shown by the orange dotted line in Fig. 6.5a. These LED driver circuits contain a power factor correction (PFC) converter [119]. The resistor can also be added to the LED string to minimise
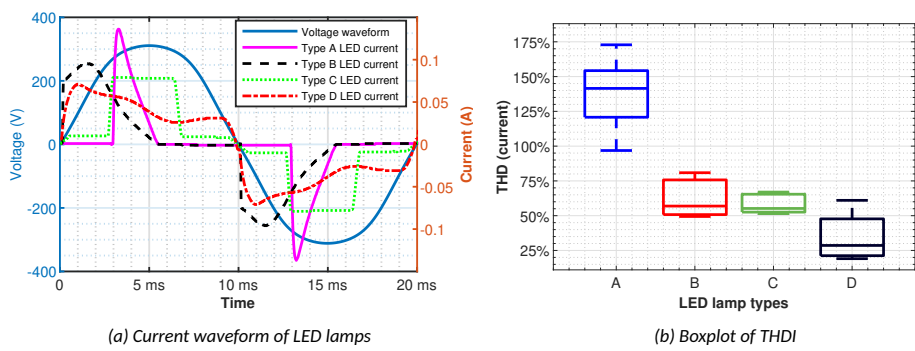

(a) Current waveform of LED lamps   *(b) Boxplot of THDI*

Figure 6.5 – Current waveform and THDI of LED lamps with different driver circuit topology
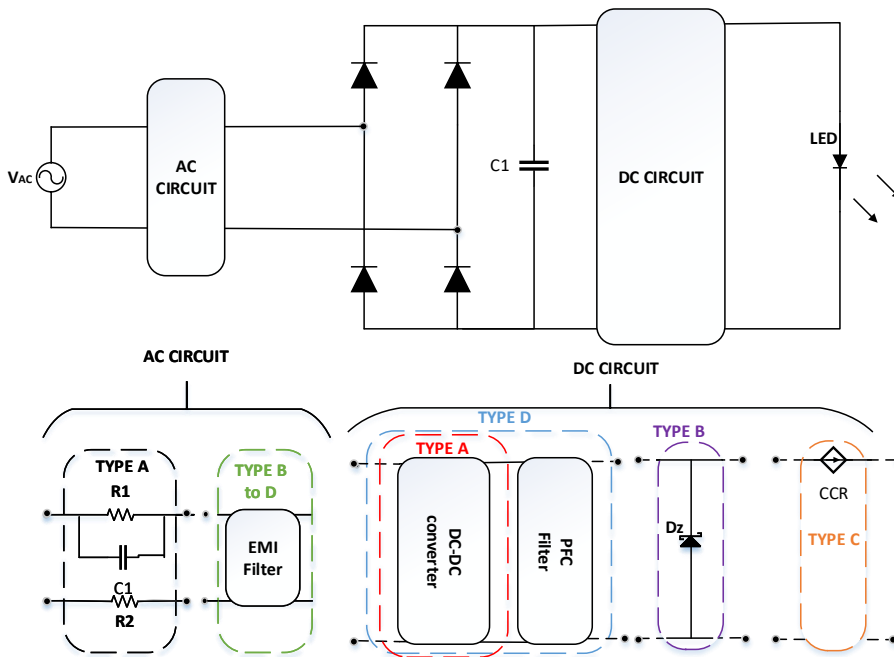
Figure 6.6 – Circuit topologies of different LED drivers [I]

the current difference. Type D LED driver circuit shows the lowest THDI values in comparison to the other three types, as shown in Fig. 6.5b. This topology is common in modern high-power energy-efficient appliances.

6.3.2 Comparison of harmonic emission

Monte-Carlo simulation is used along with the lighting usage model to evaluate the impact of power supplies circuit topology on the current harmonic emission. Over 200 LED lamps with different power ratings are measured on a 230 V sinusoidal voltage and categorised based on their circuit topology. Table 6.1 summarises the average price per watt, average light output efficacy, the number of lamps measured, and the number of manufacturers for each LED type used in this study. The circuit topology for different types of LED lamps are shown in Fig. 6.6.

Table 6.1 – LED lamp portfolio summary [I]

	Type 1	Type 2	Type 3	Type 4	Total
No. of lamps	160	18	12	15	205
No. of manufacturers	27	7	4	6	34
Average price (euro/W)	0.53	0.55	0.53	0.60	0.55
Lumens (lm/W)	90	85	88	91	88

In order to compare the harmonic emission of different topologies, LED lamps are selected based on similar power ratings. 60 houses are simulated, and during each run, all homes are populated with an equal share of 6, 9 and 12 Watt lamps of a single topology.

The current harmonics are aggregated by vector addition in the complex plane using both real and imaginary components of each harmonic. The results of individual odd harmonics up to the 19th are compared for different LED driver circuit topology. Fig. 6.7 shows the total RMS current drawn by 60 houses for different LED driver topologies. The solid line shows the mean value while the dotted line indicates the 90th percentile values of the RMS current drawn by 60 houses for 100 days. The evening peak shows that RMS current of type A LED lamps indicated by blue line is higher in comparison to the other lamps. The type C LED lamps have drawn the lowest RMS current.
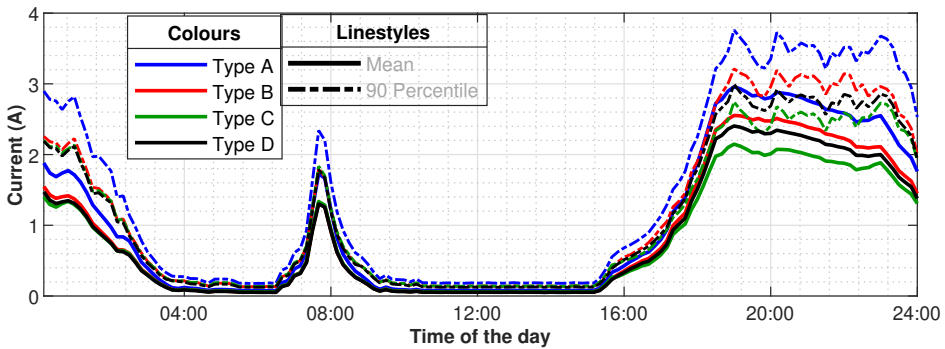

Figure 6.7 – RMS current of 60 houses over 100 days for different LED driver topologies

Fig. 6.8a shows the mean and 90th percentile absolute values of the 3rd harmonic current drawn by 60 houses for 100 days. The type A LED lamps have significantly higher values of the 3rd harmonic current with a peak value of more than 1.5 A while type D lamps have the lowest value among all four types of LED lamps and has a peak value of only 0.5 A. The type B and C shows the second and third highest values for the 3rd harmonic respectively. The mean values of type B LED has a maximum value of 1 A which is 28% less than type A LED lamps and 35% more than type C LED lamps.

For the 5th harmonic current, type A LED lamps shows substantially higher values in contrast to the other types, as shown in Fig. 6.8b. The maximum value of the mean and 90th percentile values for type A LED lamps are exceeding 1 and 1.5 A, respectively. The remaining three types show very less 5th harmonic emission in comparison to type A LED lamps. The mean values in the evening peak are in the range of 0.2 – 0.3 A for type B, C and D lamps and show similar trends for the 5th harmonic. A similar trend can be observed for the 7th harmonic where type A LED lamps show significantly large values than other types. The mean and 90th percentile values of the 7th harmonic during the evening peak exceeds 1 A, for type A LED lamps while the harmonic emission of the remaining lamps is in the range of 0.2 to 0.3 A for both mean and 90th percentile values.

The 9th harmonic emission show a similar pattern with type A LED lamps having the highest emission followed by type C LED lamps. The emission patterns of type B and D are close to each other, however, type D LED shows slightly higher values in comparison to type B.

## 6.4 Impact of EV integration on current harmonic emission

The rapid integration of EV technology is leading towards large-scale vehicle electrification. The EV charging is based on power electronic circuits and will result in additional load and harmonic emission in the low voltage residential network. This imminent increase in charging load is urging stakeholders to plan up-gradation in the electric power
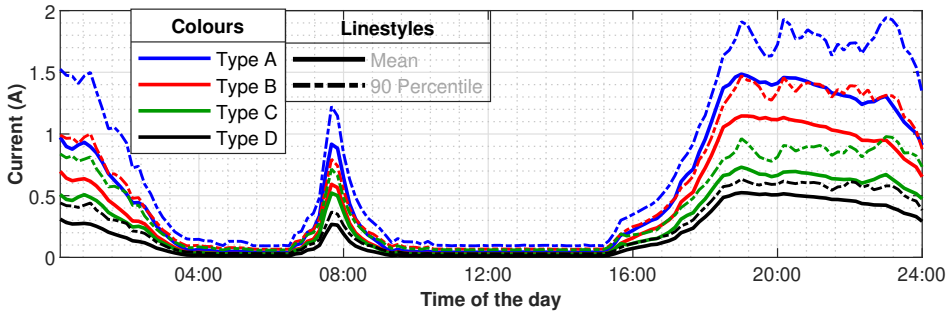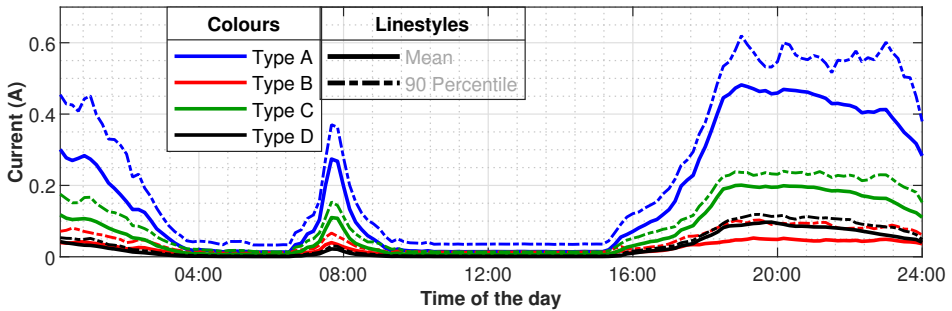
(a) 3rd harmonic current
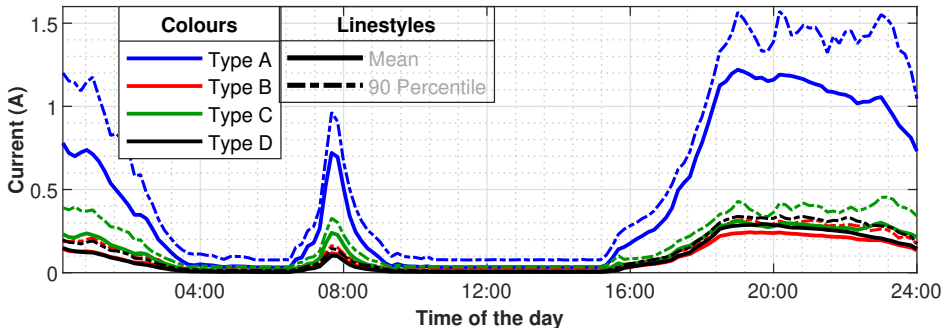
(b) 5th harmonic current
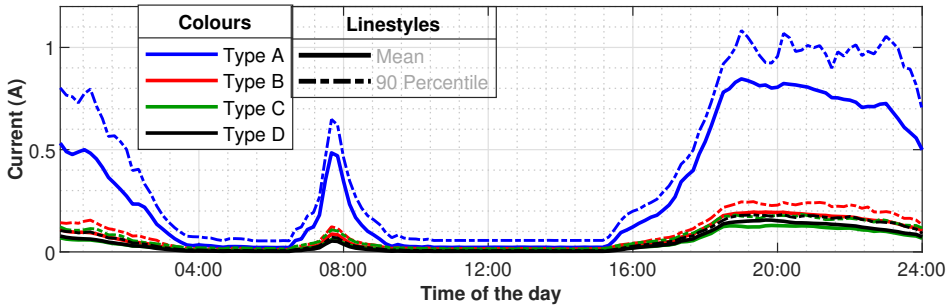
(c) 7th harmonic current

(d) 9th harmonic current

Figure 6.8 – Circuit topology impact on harmonic emission

system infrastructure. However, for efficient planning to support the additional load, an accurate assessment of the electric vehicle load and power quality indices is required. Although several EV models to estimate the charging profile and additional electrical load are available. Still, they cannot provide a high-resolution evaluation of charging current, especially at higher frequencies. For an accurate assessment of the EV charging impact on the LV network's operation, cautious evaluation of charging modes under supply voltage variation should be considered. As several EVs are available in the market offered by various manufacturers, it is a challenging task to evaluate the power quality index of every vehicle. A typical EV battery charging cycle consists of two modes: constant current (CC) and constant voltage (CV) mode. The charging at home can take several hours; therefore, an increase in EV penetration will significantly increase the LV network load.

The charging decision of an EV is a stochastic process and depends on several factors related to its owner's travel pattern. The EV load model is developed to estimate the charging load using travel statistic in the chapter 4. The EV load model and the power quality measurement data of EV charging at different voltage distortions are used to estimate the additional charging current and current harmonic emission in the residential network.

6.4.1 EV characteristics

The PQ measurement data of EVs is measured in the laboratory using the test setup described in section 3.1.1. The vehicles are measured on the sinusoidal, flat top and pointed top voltage waveforms. Some data is also included from the PANDA database. The summary of the vehicle's characteristics is listed in Table 6.2.

Table 6.2 – Summary of EV characteristics [V]

Number	Type	Battery capacity (kWh)	Driving range (km)
EV1	BEV	22	170
EV2	BEV	16.8	100
EV3	BEV	31	160
EV4	BEV	40	220
EV5	BEV	14.5	171
EV6	PHEV	11.2	50
EV7	BEV	18.7	165
EV8	PHEV	9.4	36
EV9	BEV	17.6	145
EV10	BEV	58	335
EV11	PHEV	8.8	26

6.4.2 Simulation results

The EV load model is used to simulate usage patterns of 50 EVs for 100 days. The EVs are selected randomly (uniform distribution) from Table 6.2 for each consumer. The current harmonics are aggregated in the complex plane using both magnitude and phase angles of each current harmonic. To observe the impact of supply voltage distortions, the current harmonic data recorded at different supply voltage waveform is used to simulate the overall impact of EV charging in the residential grid.

The magnitude of individual harmonic currents of EVs are mostly greater than the aggregated sum of typical household appliances. Therefore, the large scale EV integration will significantly increase the current harmonic emission in the low voltage distribution
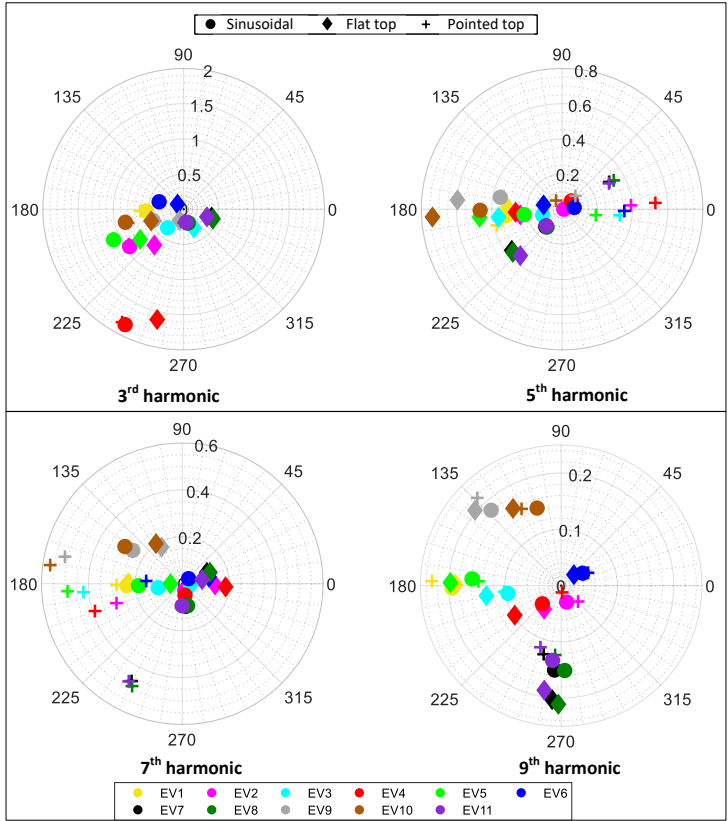
Figure 6.9 – Current harmonic emission of individual EVs [V]

network. The impact of voltage waveform distortions on the individual harmonics is presented in Fig. 6.9. The vectors of the 3rd harmonic current shows that the spread will change slightly for the flat top voltage waveform while the harmonic spread is nearly identical for sinusoidal and pointed top voltage waveforms. The harmonic spread for 5th harmonic on pointed top voltage waveform is almost shifted 180 in contrast to sinusoidal or flat top voltage waveform for majority of the EVs. On the flat top voltage waveform, the 5th harmonic current is slightly increased in magnitude; however, the phase angles are almost same as on sinusoidal voltage waveform. The 7th harmonic current spread on pointed top voltage waveform shows a significant change in terms of magnitude in comparison to sinusoidal or flat top voltage profiles. The 9th harmonic shows a wide spread for different EVs but the change in magnitude or phase in not very high for different voltage waveforms [V].

High ownership of 83% is selected while simulating the EV load in the residential grid. It means 50 out of 60 houses owns an EV. The EVs are assigned randomly from the list provided in Table 6.2. The EV load model is used to simulate the travel activities to generate charging profiles based on the distance travelled during each trip. For each EV, the outgoing and incoming times of each trip during a day is estimated. The final destination is assumed to be the home. Based on the distance travelled during each trip, the state
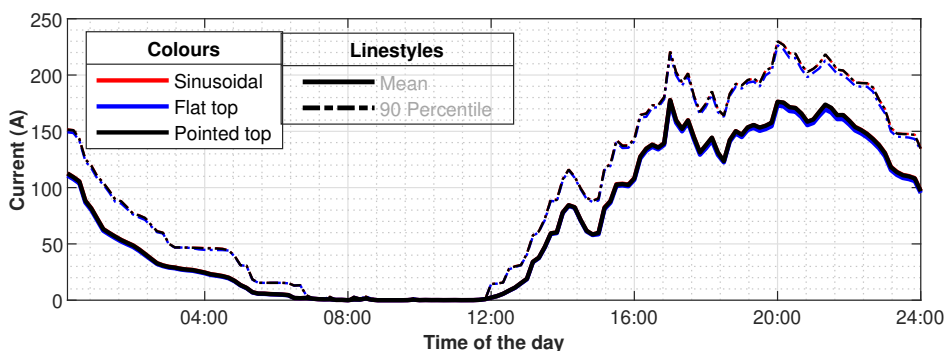
Figure 6.10 – RMS current of electric vehicles [V]

of charge of the battery is estimated. The decision of charging depends upon the state of SOC. While the EV is at home and does not have sufficient SOC to make a new trip, the EV charging will take place. The simulation is performed for weekdays only, therefore, the EV charging takes place during the evening time. Fig. 6.10 shows the mean and 90th percentile values of total RMS current for different voltage distortions.

The bold lines indicate the mean values while the dotted line shows the 90th percentile value of the RMS current. The RMS values does not show a significant variation for different voltage waveforms and only slight variation can be observed. The mean and 90th percentile values of 3rd harmonic current drawn over 100 days for 50 EVs is shown in Fig. 6.11a. No significant variation in the 3rd harmonic current can be observed between sinusoidal and pointed top voltage waveforms, however, the values on flat top voltage waveforms are significantly less for both mean and 90th percentile values. The mean value increases to its maximum value of 7 A around 21:30. The mean values on flat top voltage waveform at the same time is only 4.5 A which 33% less. The 5th harmonic emission values are more for flat top voltage waveform as shown in Fig. 6.11b. On sinusoidal voltage waveform, the 5th harmonic current has lowest values during the 24 hours. The values slightly increase on pointed top voltage waveform shown by black bold line in Fig. 6.11b. The mean and 90th percentile values of the 5th harmonics crosses 4.5 and 5.5 A, respectively, during the evening peak. On the sinusoidal and pointed top voltage waveforms, the mean value increases to a maximum value of 2 and 3 A only.

The 7th harmonic emission on pointed top voltage waveform is very high in comparison to sinusoidal and flat top voltage waveforms as shown in Fig. 6.11c. The mean value exceeds 4 A for pointed top voltage waveform during the evening peak while the mean values at sinusoidal and flat top voltage waveforms are around 1 A. The values for the 9th harmonic current are more on the flat top voltage waveform with the mean value crossing 1 A during the evening time. For sinusoidal and pointed top voltage waveform, the mean values of the 9th harmonic are quite close during the whole day with the maximum value of 0.83 A. Fig. 6.11d shows the mean and 90 percentile values of the 9th harmonic current on different voltage distortions.

6.5 Aggregated impact of nonlinear devices on current harmonic emission in LV network

Mostly all modern appliances include power electronic converters, including refrigerators, dishwashers and washing machines. The converters and electronics circuits inside modern and future appliances may significantly impact the current harmonic emission levels;
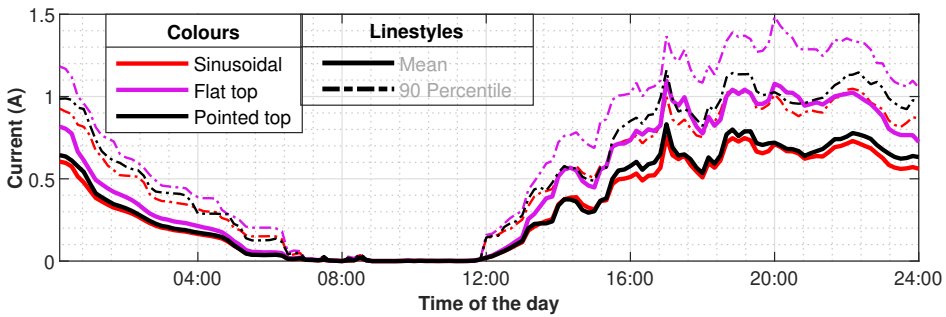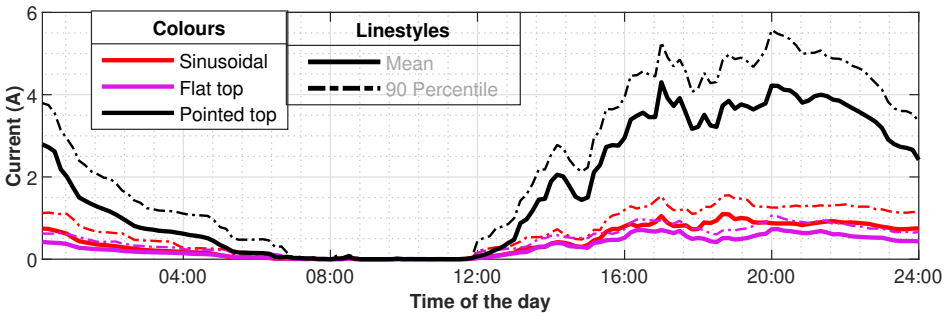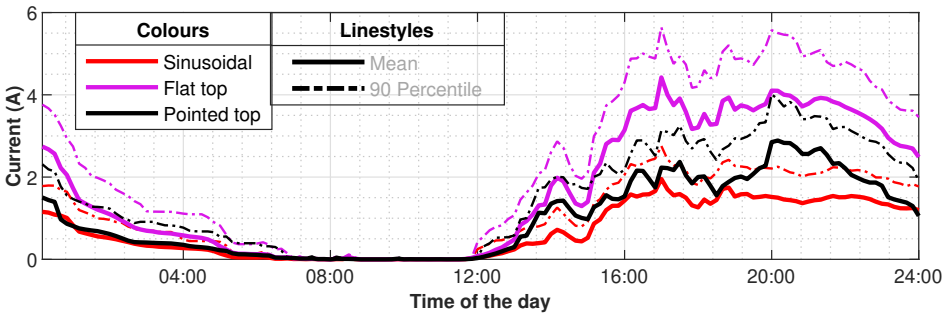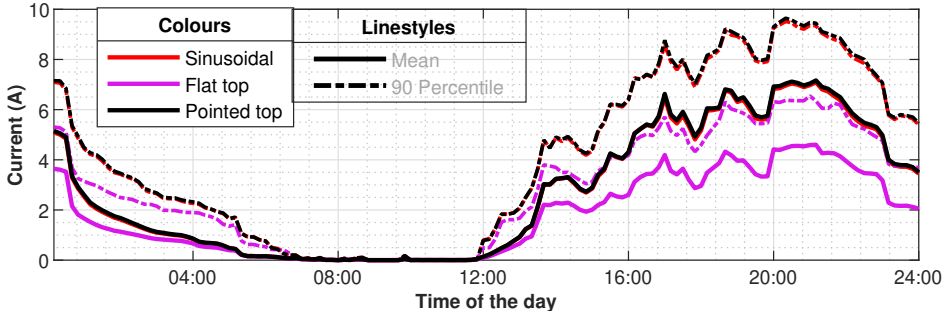
(a) 3rd harmonic current

(b) 5th harmonic current

(c) 7th harmonic current

(d) 9th harmonic current

Figure 6.11 – EV harmonic emission [V]

therefore, it is essential to evaluate their impact. The usage profiles of different domestic appliances generated using the DU model have made the harmonic estimation model compatible with any present and future variant of the home appliances.

6.5.1 Appliance stock

The number and type of appliances in a house depend on occupant needs and preferences. Researchers have used various national surveys about appliance ownership in residential building to construct their energy models. CREST model has used appliances from a set of 33 common appliances found in the residential building based on national ownership statistics in the UK [60]. American housing survey , English housing survey and Estonian household energy consumption survey are examples of similar surveys conducted on a national level to determine the household energy consumption trends [120, 121, 122].

For harmonic estimation, the household appliances are selected from the appliance ownership statistics provided by the Household Energy Consumption Survey (HECS) [122]. The HECS results were based on the data collected in 2010 from more than 6000 homes in different parts of Estonia. The data was collected by interviewing the occupants face to face and, therefore, more reliable. The list of most common appliances, along with their ownership share, is presented in Table 6.3.

Table 6.3 – Appliance ownership data

Type of the appliance	Share %
Refrigerator	99
Vacuum cleaner	93
TV	97
Washing machine	89
Electric cooker	72
Microwave oven	61
Coffee machine	21
Electric storage water heater	37

The majority of the household include refrigerators, vacuum cleaners and television sets, as their ownership share in more than 96%. Washing machines also have high ownership while electric cookers have a 72% ownership. The other cooking appliances include microwave ovens and coffee machines, with an ownership share of 61% and 21%, respectively.

Apart from the appliances in Table 6.3, the other common household appliance's ownership has been assumed. The list of these appliances with assumed ownership statistics is provided in Table 6.4.

Table 6.4 – Assumed ownership data

Type of the appliance	Assumed ownership share %
Blender	40
Hand blender	30
Toaster	40
Kettle	70
Food factory	20
Floor heaters in WC	35

6.5.2 Measurement and simulation

Fifteen common household appliances presented in Table 6.3 and 6.4 are measured in the laboratory on different voltage distortions to record their current harmonic emission. Based on the current harmonic emission profiles, the appliances are divided into static appliances and dynamic appliances.

The static appliances have a nearly constant harmonic emission profile under a constant operating mode. These devices include vacuum cleaners, refrigerators, floor heaters, kettles, electric cookers and other kitchen appliances. The operating mode may include the thermostat or power mode settings of a device. The interaction of occupants with the operating mode of static appliances is limited. Therefore, it is assumed that the harmonic profile of these appliances does not change for the entire length of their operation.

The dynamic appliances have a high variation in their harmonic emission profile. These devices include washing machines and dishwashers. They operate for a fixed length depending on the operating mode selected by the user. A single usage cycle can be divided into sub-cycles such as heating, spinning and rinsing etc. The harmonic emission of these sub-cycles can be very different and explained in section 5.4. These devices are measured over the full complete operating cycle. The dynamic current harmonic profiles of the devices are used in the simulation to estimate the aggregated impact of current harmonics by 60 houses.

It is also assumed that all houses only have LED TV sets as the old models such as LCD, plasma, CRT are rarely used these days. The harmonic emission of LED TV also changes in a small range during their operation. The TVs are measured over 1 hour by playing a video with a constant volume setting. The complex values of harmonics are selected using bivariate harmonic modelling approach to simulate of the TV load of 60 houses.

Numerous models of each appliance are available in the market and households with various power ratings and utility. It a challenging task to measure several models of an appliance. The measurement database is improved by using the PANDA (equiPment hArmoNic DAtabase) database that provides current harmonic measurements of different household appliances.

60 houses are populated with fifteen appliances based on the ownership data. A Monte Carlo approach is used to simulate 60 for 100 days using the appliance usage data
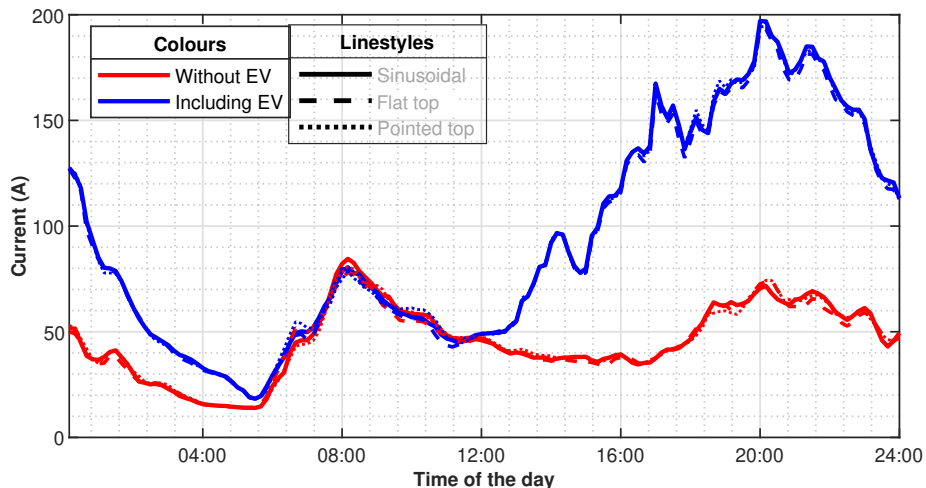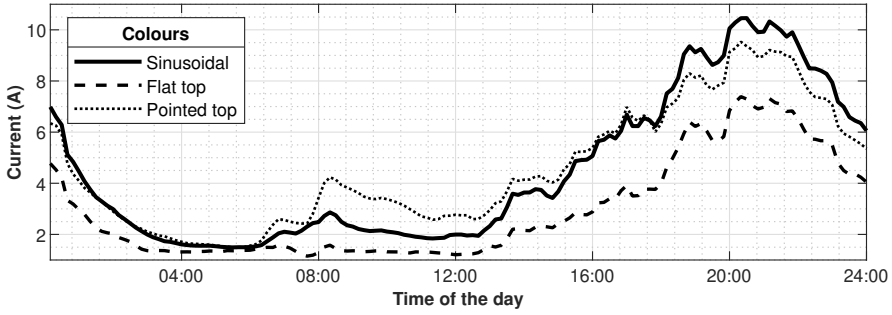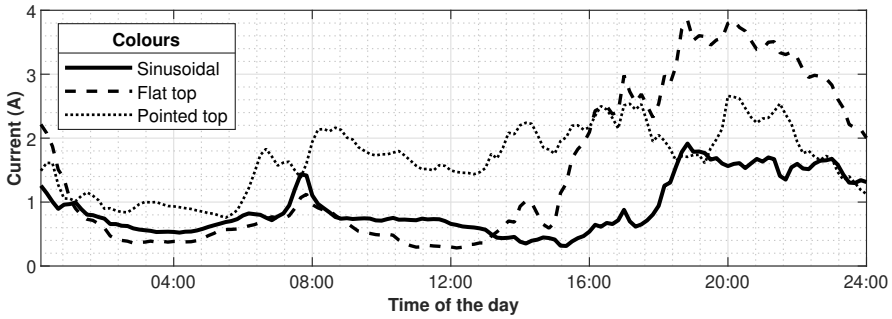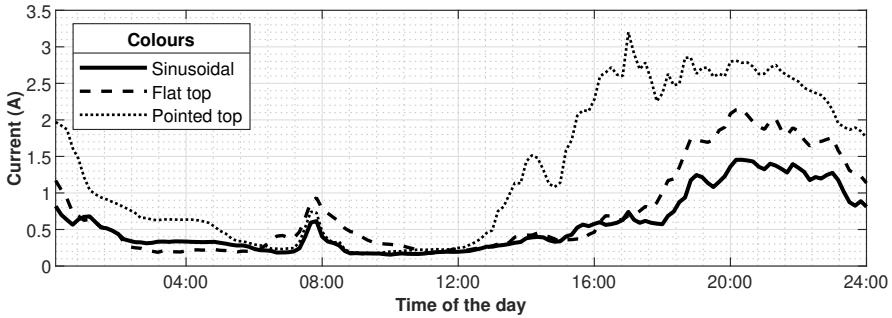

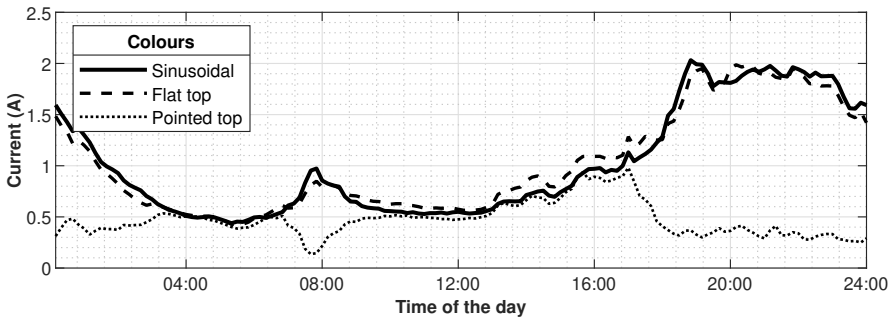*Figure 6.12 – RMS current of non linear loads with and without EV load*

(a) 3rd harmonic current

(b) 5th harmonic current

(c) 7th harmonic current

(d) 9th harmonic current

Figure 6.13 – Aggregated harmonic emission of nonlinear devices and EVs

generated from the DU model. Each current harmonic is aggregated using vector addition in complex plane. Harmonic emission of the lighting and EVs is simulated separately and aggregated into the appliance's current harmonics. Fig. 6.12 shows the mean and 90th percentile values of the total RMS current drawn by lighting, appliances and EVs by 60 houses for 100 days. The red bold and the dotted line show the mean and 90th percentile values of the total RMS current of appliances and lighting only. Both morning and evening peaks are visible. The morning peak load is high because of the frequent usage of water heater between 06:00 to 09:00. The blue bold and dotted line show mean and 90th percentile values of combined total RMS current of EVs, lighting and appliances load. It shows the impact of unmanaged charging of EVs on the distribution grid. The total RMS current has been increased by nearly 174% when EV load is taken into account.

Fig. 6.13 shows the 3rd, 5th, 7th, and 9th harmonic current drawn by lighting, appliances and EV load. The harmonic emission comparison of sinusoidal, flat top, and pointed top voltage distortions can be observed. The flat-top voltage distortion has increased the 5th harmonic current significantly. The peak value has been increased almost 2 and 1.4 times in comparison to harmonic emission on sinusoidal and peak top voltage, respectively. The pointed top voltage distortion has a major impact on the 7th harmonic. The maximum value has been increased by nearly 120% and 50% from the values on sinusoidal and flat top voltage waveforms. Fig. 6.13 provides an estimate of harmonic current emission for nonlinear loads in the LV residential network. The 3rd harmonic could be between 7 and 11 A during the evening peak for 60 houses connected to the network. The harmonic cancellation could be observed for 9th harmonic current at pointed top voltage distortion. The aggregated 9th harmonic current of the EV load is cancelling and reducing the 9th harmonic current in the low voltage network. Similarly, the 5th, 7th, and 9th harmonic currents can be in the range of 1 - 4 A, 1 – 3 A, and 0.3 - 2 A, respectively. The impact on high-order harmonic can also be observed using this harmonic estimation model.

7 Conclusions and future work

7.1 Conclusion

This doctoral thesis provides a stochastic approach to estimate harmonic propagation in the low voltage network. So far, most of the available models have provided a top-down measurement approach or offer the worst-case aggregated harmonic emission impact from the network's nonlinear load. The load and network conditions, however, are changing continuously in an LV network. An accurate assessment must consider various uncertainties and the stochastic nature of the load itself but also variations in the distribution network. The probabilistic approach can provide a better estimation of the impact of nonlinear loads in the distribution network. Therefore, a stochastic current harmonic estimation model is developed based on devices' usage patterns and power quality measurements of various appliances on different voltage distortions.

Within the present thesis, a device usage model was elaborated with a target to have sufficient capability and granularity for power quality analysis. The core of this model is relying on the device usage model, developed to generate the usage patterns of various household appliances with fine time resolution. The device-level measurement data and the results of multiple surveys are used to construct a bottom-up stochastic device usage model. The appliances were categorised based on the nature of their usage and operating principles. The main groups of load devices included lighting, EV and domestic loads with nonlinear characteristics. Each of these groups had specifics and were considered separately. For lighting and domestic appliances, it is presented that the empirical stochastic approach is the favourable one. The lighting model was presented with more detail, to include the manageability of short-duration operation scenes. For this, a Markov chain model was selected to reflect the frequent switching of the different lamps. However, the EV load model is based on a totally different set of assumptions where trip distance, incoming and outgoing times are estimated from the probability distribution functions defined for each variable. The device usage model is flexible enough to include any current or future model of load devices.

The measurement data is used to provide an estimation of the current harmonic emission. Every load device is presented with its characteristic harmonic patterns, respective to their operating modes. Some of the domestic devices are really low-power loads which are pushing the measurement methodology to the limits. The effect of various inaccuracies and uncertainties on the harmonic current measurement and estimation is discussed in detail. The accuracy of the measurement setup is determined using signal processing techniques. The current and voltage waveforms are recorded using a calibrated instrument, and signal processing results are compared with the measurement results obtained from the primary measurement device. The results confirm the repeatability and accuracy of the harmonic current measurements. Here several other considerations emerge that could affect measurement result accuracy for the modelling output. The thesis discusses the dispersion estimation due to the thermal stability of operating load devices and network topology effects. It is presented that the thermal stability conditions hold the key for more accurate harmonic estimation. In the cold state, the LED lamps, for example, produce THDI in the range of 2% to 15%, different from the stable state. The dispersion effect is observed for the modelling outcome, and it is presented that warmed-up state load measurements provide a better accuracy margin. Thus, loads measurements would have to be done using warmed-up loads operating for at least 60 minutes before measurement.

For the distribution network harmonic current emission estimation, the measurement data would be used along with the load utilisation patterns. Different load connection

points and various supply voltage waveforms would be supplied to loads. The thesis also presents an estimation of deviations due to cable length variation. The cable presence variations are relatively low; however, the noticeable effect is seen for longer cables. The magnitude variations up to 30% have been observed for higher current harmonics when the longer cable length is attached during measurements. Similarly, phase angles could vary up to 20 degrees.

The harmonic estimation model's flexibility provides various opportunities to study several impacts of nonlinear loads on the distribution network. The technological advancements of the loads also affect the current harmonic emission. The thesis provides a case example comparison of LED and CFL penetration impact on current harmonics in the distribution network. The impact of circuit topologies on harmonic emission has been studied, and results show that harmonic filters and power factor correction circuits can reduce the current harmonics. Another model usage case example shows the influence of the high penetration of EVs on the distribution network. The unmanaged charging will drastically increase the load and harmonic currents in the distribution network. The EV load model is used to generate the charging schedule. The power quality measurement data at various voltage distortions are used to estimate the current harmonic emission range in the LV network. The aggregated harmonic emission from most common household appliances and EVs is estimated using the device usage model and measurement data. The results provide a range for harmonic currents during the day under various network uncertainties.

The results from various case studies demonstrate the effectiveness and flexibility of the harmonic estimation model developed. With input data inaccuracies discussed, it is pointed out that the main variation in the results would be originating due to device usage model output. It is also expected for the real distribution networks and load variation of the domestic household. Results indicate that in the statistical approach, the results provide stable harmonic current margins for a high number of simulated days. The stochastic model relying on the Monte-Carlo method and provides the occurrence probability for extreme values. Thus the model is appropriate to use for the estimation of critical parameters.

The model provides a vital tool to estimate harmonic emissions. The results are of great importance for improving the low voltage network operation characteristics by enhancing performance in harmonic propagation estimation from nonlinear loads. These estimations are essential to support the network operators to plan up-gradation or expansion of their network, especially considering the imminent nonlinear devices penetration in the grid (inverters, battery storage devices).

7.2 Future work

The distribution networks, especially on the LV levels, face abrupt and complex set of challenges. On the one hand, the policymakers encourage everyone to provide their effort towards a more sustainable power supply network. The proposals include building near-zero energy dwellings, high renewable production capacity, more modern and efficient loads and domestic electric energy storage. All this includes powerful nonlinear power supply units, converters and inverters. The distribution network has to support these units and continue operating under specified operating characteristics, i.e., providing sufficient hosting capacity.

The rapid turn to support the Green Deal and climate neutrality targets will put more pressure on the distribution grids. The hosting capacity of more powerful units will likely see limits resulting in the limitation of the new technologies until improved. Therefore,

the load model essentially provides a base to evaluate the impact of various policies and technologies on the performance of power supply systems. It allows testing solutions such as energy conservation, distributed generation, smart buildings, electric vehicles and smart grids. These estimations could provide valuable information about the significance of these policies on the power system operation prior to real-time implementation.

The model as presented in this thesis does not incorporate, at this time, PV production data. Similarly, battery storage possible implementation would be feasible if not a mandatory part of the future development. At this time, the model can be used to evaluate the effect of demand-side management on the peak load and current harmonics. It may include scheduling large loads such as EVs to reduce evening peaks. The model could be extended to include commercial loads to observe their impact on harmonic emission. The effect of seasonal variation can also be added to estimate the harmonic current range for the whole year.

Another range of topics is to extend the model to include a stochastic network model. This could be proposed based on the current harmonic estimation model results. The current and voltage values may provide network impedance values at different frequencies. The network parameters and load model will provide the influence of harmonics on the grid operation parameters. A more detailed voltage waveform influence to load current harmonics emission model is already under development.

References

[1] I. of Electrical and E. Engineers, "IEEE Std 519-2014: IEEE Recommended Practice and Requirements for Harmonic Control in Electric Power Systems," standard, International Electrotechnical Commission, New York, US, 2014.

[2] T. Gonen, *Electric Power Distribution Engineering*. CRC Press, aug 2015.

[3] E. L. Owen, "A history of harmonics in power systems," 1998.

[4] S. Santoso, *Fundamentals of Electric Power Quality*. Createspace Independent Pub, 2012 ed., 2009.

[5] IEC, "IEC 61000-1-1: Electromagnetic compatibility (EMC) - Part 1: General - Section 1: Application and interpretation of fundamental definitions and terms," tech. rep., International Electrotechnical Commission, Geneva, 2000.

[6] IEEE, *Std 1100:2005 - IEEE Recommended Practice for Powering and Grounding Electronic Equipment*. IEE, 2006.

[7] S. Rönnberg and M. Bollen, "Propagation of Suraharmonics in the Low Voltage Grid," tech. rep., ENERGIFORSK AB, STOCKHOLM, 2017.

[8] D. Agudelo-Martinez and A. Pavas, "Measurement and simulation of power quality disturbances between 2–150 kHz from compact fluorescent lamps," in *2018 18th International Conference on Harmonics and Quality of Power (ICHQP)*, pp. 1–6, IEEE, may 2018.

[9] E. O. Larsson and M. H. Bollen, "Measurement result from 1 to 48 fluorescent lamps in the frequency range 2 to 150 kHz," in *ICHQP 2010 - 14th International Conference on Harmonics and Quality of Power*, 2010.

[10] Á. Espín-Delgado, S. Rönnberg, T. Busatto, V. Ravindran, and M. Bollen, "Summation law for suraharmonic currents (2–150 kHz) in low-voltage installations," *Electric Power Systems Research*, 2020.

[11] D. Ritzmann, S. Lodetti, D. de la Veg, V. Khokhlov, A. Gallarreta, P. Wright, J. Meyer, I. Fernandez, and D. Klingbeil, "Comparison of Measurement Methods for 2–150-kHz Conducted Emissions in Power Networks," *IEEE Transactions on Instrumentation and Measurement*, vol. 70, no. Lv, pp. 1–10, 2021.

[12] A. Baggini, *Handbook of Power Quality*. WILEY, 2008.

[13] S. Chattopadhyay, M. Mitra, and S. Sengupta, *Electric Power Quality*. Power Systems, Dordrecht: Springer Netherlands, 2011.

[14] A. Elmoudi, M. Lehtonen, and H. Nordman, "Effect of Harmonics on Transformers Loss of life," in *Conference Record of the 2006 IEEE International Symposium on Electrical Insulation*, pp. 408–411, IEEE, 2007.

[15] M. A. Masoum and E. F. Fuchs, *Power Quality in Power Systems and Electrical Machines: Second Edition*. Academic Press, 2015.

[16] M. H. Bollen and I. Y. H. Gu, *Signal Processing of Power Quality Disturbances*. Wiley-IEEE Press, 2005.

[17] L. Czarnecki, "Comments on active power flow and energy accounts in electrical systems with nonsinusoidal waveforms and asymmetry," *IEEE Transactions on Power Delivery*, vol. 11, pp. 1244–1250, jul 1996.

[18] CENELEC, "EN 50160: Voltage characteristics of electricity supplied by public distribution networks," standard, European Committee for Electrotechnical Standardization, Brussels, Belgium, 2005.

[19] IEC, "Electromagnetic compatibility (EMC) - Part 1-4: General - Historical rationale for the limitation of power-frequency conducted harmonic current emissions from equipment, in the frequency range up to 2 kHz," standard, International Electrotechnical Commission, Geneva, Switzerland, 2005.

[20] IEC, "Electromagnetic compatibility (EMC) - Part 2: Environment - Section 1: Description of the environment - Electromagnetic environment for low-frequency conducted disturbances and signalling in public power supply systems," standard, International Electrotechnical Commission, Geneva, Switzerland, 1990.

[21] IEC, "Electromagnetic compatibility (EMC) - Part 2-2: Environment - Compatibility levels for low-frequency conducted disturbances and signalling in public low-voltage power supply systems," standard, International Electrotechnical Commission, Geneva, Switzerland, 2002.

[22] IEC, "Electromagnetic compatibility (EMC) - Part 2-4: Environment - Compatibility levels in industrial plants for low-frequency conducted disturbances," standard, International Electrotechnical Commission, Geneva, Switzerland, 2002.

[23] IEC, "Electromagnetic compatibility (EMC) - Part 2-5: Environment - Description and classification of electromagnetic environments," standard, International Electrotechnical Commission, Geneva, Switzerland, 2017.

[24] IEC, "Electromagnetic compatibility (EMC) - Part 3-2: Limits - Limits for harmonic current emissions (equipment input current $\leq$ A per phase)," standard, International Electrotechnical Commission, Geneva, Switzerland, 2018.

[25] IEC, "Electromagnetic compatibility (EMC) - Part 3-4: Limits - Limitation of emission of harmonic currents in low-voltage power supply systems for equipment with rated current greater than 16 A," standard, International Electrotechnical Commission, Geneva, Switzerland, 1998.

[26] IEC, "Electromagnetic compatibility (EMC) - Part 3-12: Limits - Limits for harmonic currents produced by equipment connected to public low-voltage systems with input current >16 A and ≤75 A per phase," standard, International Electrotechnical Commission, Geneva, Switzerland, 2011.

[27] IEC, "Electromagnetic compatibility (EMC) - Calibration and verification protocol for harmonic emission compliance test systems," standard, International Electrotechnical Commission, Geneva, Switzerland, 2016.

[28] IEC, "Electromagnetic compatibility (EMC) - Part 4-13: Testing and measurement techniques - Harmonics and interharmonics includingmains signalling at a.c. power port, low frequency immunity tests," standard, International Electrotechnical Commission, Geneva, Switzerland, 2016.

[29] IEC, "Electromagnetic compatibility (EMC) - Part 4-30: Testing and measurement techniques - Power quality measurement methods," standard, International Electrotechnical Commission, Geneva, Switzerland, 2015.

[30] A. C. Henao-Muñoz and A. J. Saavedra-Montes, "Comparison of two mathematical models for nonlinear residential loads," in *Proceedings of International Conference on Harmonics and Quality of Power, ICHQP*, 2016.

[31] A. M. Blanco, S. Yanchenko, J. Meyer, and P. Schegner, "Impact of supply voltage distortion on the current harmonic emission of non-linear loads," *DYNA*, vol. 82, pp. 150–159, aug 2015.

[32] A. S. Koch, J. M. Myrzik, T. Wiesner, and L. Jendernalik, "Evaluation and validation of Norton approaches for nonlinear harmonic models," in *2013 IEEE Grenoble Conference PowerTech, POWERTECH 2013*, 2013.

[33] C. F. M. Almeida and N. Kagan, "Harmonic coupled norton equivalent model for modeling harmonic-producing loads," in *Proceedings of 14th International Conference on Harmonics and Quality of Power - ICHQP 2010*, pp. 1–9, IEEE, sep 2010.

[34] E. E. Ahmed, W. Xu, and G. Zhang, "Analyzing systems with distributed harmonic sources including the attenuation and diversity effects," *IEEE Transactions on Power Delivery*, 2005.

[35] J. Cunill-Sola and M. Salichs, "Study and Characterization of Waveforms From Low-Watt (<25 W) Compact Fluorescent Lamps With Electronic Ballasts," *IEEE Transactions on Power Delivery*, vol. 22, pp. 2305–2311, oct 2007.

[36] Y. Baghzouz and O. T. Tan, "Probabilistic Modeling of Power System Harmonics," *IEEE Transactions on Industry Applications*, vol. IA-23, pp. 173–180, jan 1987.

[37] G. Ye, M. Nijhuis, V. Cuk, and J. F. Cobben, "Stochastic residential harmonic source modeling for grid impact studies," *Energies*, 2017.

[38] D. Salles, C. Jiang, W. Xu, W. Freitas, and H. E. Mazin, "Assessing the collective harmonic impact of modern residential loads-part I: Methodology," *IEEE Transactions on Power Delivery*, 2012.

[39] P. Caramia, D. Proto, A. Russo, and P. Varilone, "Probabilistic Harmonic Analysis for Waveform Distortion Assessment of Low Voltage Distribution Systems with Plug-in Hybrid Electric Vehicles," in *2019 1st International Conference on Energy Transition in the Mediterranean Area (SyNERGY MED)*, pp. 1–6, IEEE, may 2019.

[40] M. T. Au and J. V. Milanović, "Establishing harmonic distortion level of distribution network based on stochastic aggregate harmonic load models," *IEEE Transactions on Power Delivery*, 2007.

[41] M. T. Au and J. V. Milanović, "Stochastic assessment of harmonic distortion level of medium voltage radial distribution network," in *2006 9th International Conference on Probabilistic Methods Applied to Power Systems, PMAPS*, 2006.

[42] M. T. Au and J. V. Milanović, "Development of stochastic aggregate harmonic load model based on field measurements," *IEEE Transactions on Power Delivery*, 2007.

[43] F. Nasrfard-Jahromi and M. Mohammadi, "Probabilistic harmonic load flow using an improved kernel density estimator," *International Journal of Electrical Power and Energy Systems*, 2016.

[44] S. Ray and B. G. Lindsay, "The topography of multivariate normal mixtures," *Annals of Statistics*, 2005.

[45] J. Meyer and P. Schegner, "Characterization of power quality in low voltage networks based on modeling by mixture distributions," in *2006 9th International Conference on Probabilistic Methods Applied to Power Systems, PMAPS*, 2006.

[46] Z. I. Botev, J. F. Grotowski, and D. P. Kroese, "Kernel density estimation via diffusion," *Annals of Statistics*, 2010.

[47] S. Węglarczyk, "Kernel density estimation and its application," *ITM Web of Conferences*, 2018.

[48] F. Nasrfard-Jahromi and M. Mohammadi, "A sampling-based method using an improved nonparametric density estimator for probabilistic harmonic load ow calculation," *Turkish Journal of Electrical Engineering and Computer Sciences*, 2016.

[49] Z. Li, H. Hu, Y. Wang, L. Tang, Z. He, and S. Gao, "Probabilistic Harmonic Resonance Assessment Considering Power System Uncertainties," *IEEE Transactions on Power Delivery*, vol. 33, pp. 2989–2998, dec 2018.

[50] K. Sun, D. Yan, T. Hong, and S. Guo, "Stochastic modeling of overtime occupancy and its application in building energy simulation and calibration," *Building and Environment*, vol. 79, pp. 1–12, 2014.

[51] H. Yoshino, T. Hong, and N. Nord, "IEA EBC annex 53: Total energy use in buildings—Analysis and evaluation methods," *Energy and Buildings*, 2017.

[52] R. C. Sonderegger, "Movers and stayers: The resident's contribution to variation across houses in energy consumption for space heating," *Energy and Buildings*, vol. 1, pp. 313–324, apr 1978.

[53] X. Feng, D. Yan, and T. Hong, "Simulation of occupancy in buildings," *Energy and Buildings*, vol. 87, pp. 348–359, 2015.

[54] E. A. Essah, E. L. Ofetotse, E. A. Essah, and R. Yao, "Domestic energy models : complexities in defining specific tools Domestic energy models : Complexities in defining specific tools," in *International Conference of SuDBE2013, 25-28 Oct 2013, Chongqing, China.*, pp. 1–9, October 2016.

[55] F. Causone, S. Carlucci, M. Ferrando, A. Marchenko, and S. Erba, "A data-driven procedure to model occupancy and occupant-related electric load profiles in residential buildings for energy simulation," *Energy and Buildings*, 2019.

[56] Z. D. Tekler, R. Low, L. Blessing, D. Chen, S. Barker, A. Subbaswamy, D. Irwin, P. Shenoy, S. Hattori, and Y. Shinohara, "Actual consumption estimation algorithm for occupancy detection using low resolution smart meter data," in *SENSORNETS 2017 - Proceedings of the 6th International Conference on Sensor Networks*, 2019.

[57] A. Molina-Markham, P. Shenoy, K. Fu, E. Cecchet, and D. Irwin, "Private memoirs of a smart meter," in *BuildSys'10 - Proceedings of the 2nd ACM Workshop on Embedded Sensing Systems for Energy-Efficiency in Buildings*, pp. 61–66, 2010.

[58] W. Kleiminger, C. Beckel, and S. Santini, "Household occupancy monitoring using electricity meters," in *Proceedings of the 2015 ACM International Joint Conference on Pervasive and Ubiquitous Computing - UbiComp '15*, (New York, New York, USA), pp. 975–986, ACM Press, 2015.

[59] I. Richardson, M. Thomson, and D. Infield, "A high-resolution domestic building occupancy model for energy demand simulations A high-resolution domestic building occupancy model for energy demand simula- tions. Energy and," *Buildings*, vol. 40, no. 8, pp. 1560–1566, 2008.

[60] J. L. Ramírez-Mendiola, P. Grünewald, and N. Eyre, "The diversity of residential electricity demand – A comparative analysis of metered and simulated data," *Energy and Buildings*, vol. 151, pp. 121–131, 2017.

[61] S. Firth, K. Lomas, A. Wright, and R. Wall, "Identifying trends in the use of domestic appliances from household electricity consumption measurements," *Energy and Buildings*, vol. 40, no. 5, pp. 926–936, 2008.

[62] W. Kleiminger, C. Beckel, T. Staake, and S. Santini, "Occupancy Detection from Electricity Consumption Data," in *Proceedings of the 5th ACM Workshop on Embedded Systems For Energy-Efficient Buildings - BuildSys'13*, (New York, New York, USA), pp. 1–8, ACM Press, 2013.

[63] M. Jin, R. Jia, and C. J. Spanos, "Virtual Occupancy Sensing: Using Smart Meters to Indicate Your Presence," *IEEE Transactions on Mobile Computing*, vol. 16, pp. 3264–3277, nov 2017.

[64] Z. D. Tekler, R. Low, and L. Blessing, "Using smart technologies to identify occupancy and plug-in appliance interaction patterns in an office environment," in *IOP Conference Series: Materials Science and Engineering*, 2019.

[65] D. Chen, S. Barker, A. Subbaswamy, D. Irwin, and P. Shenoy, "Non-Intrusive Occupancy Monitoring using Smart Meters," in *Proceedings of the 5th ACM Workshop on Embedded Systems For Energy-Efficient Buildings - BuildSys'13*, (New York, New York, USA), pp. 1–8, ACM Press, 2013.

[66] F. Farokhi and H. Sandberg, "Fisher Information as a Measure of Privacy: Preserving Privacy of Households With Smart Meters Using Batteries," *IEEE Transactions on Smart Grid*, vol. 9, pp. 4726–4734, sep 2018.

[67] OECD, "Global ev outlook 2018," tech. rep., IEA, Paris, France, 2018.

[68] R. Sell, A. Rassõlkin, R. Wang, and T. Otto, "Integration of autonomous vehicles and Industry 4.0," *Proceedings of the Estonian Academy of Sciences*, vol. 68, no. 4, p. 389, 2019.

[69] D. B. Richardson, "Electric vehicles and the electric grid: A review of modeling approaches, Impacts, and renewable energy integration," 2013.

[70] L. Pieltain Fernández, T. Gómez San Román, R. Cossent, C. Mateo Domingo, and P. Frías, "Assessment of the impact of plug-in electric vehicles on distribution networks," *IEEE Transactions on Power Systems*, 2011.

[71] J. Balcells and J. García, "Impact of plug-in electric vehicles on the supply grid," in *2010 IEEE Vehicle Power and Propulsion Conference, VPPC 2010*, 2010.

[72] D. T. Roger Duncan Fred Beach, "Electric vehicle charging infrastructure," tech. rep., The University of Texas, 2019.

[73] "Report on the assessment of the member states national policy frameworks for the development of the market as regards alternative fuels in the transport sector and the deployment of the relevant infrastructure pursuant to article 10 (2) of directive 2014," tech. rep., EUROPEAN COMMISSION, 2019.

[74] M. S. Maarten Matthias Spöttle, Korinna Jörling and Staats, "Research for tran committee - charging infrastructure for electric road vehicles," tech. rep., Policy Department for Structural and Cohesion Policies, European Parliament, 2018.

[75] S. W. Hadley, "Impact of Plug-in Hybrid Vehicles on the Electric Grid," Tech. Rep. October, U.S. DEPARTMENT OF ENERGY, Oak Ridge, Tennessee, 2006.

[76] G. Pareschi, L. Küng, G. Georges, and K. Boulouchos, "Are travel surveys a good basis for EV models? Validation of simulated charging profiles against empirical data," *Applied Energy*, 2020.

[77] Y. Xiang, S. Hu, Y. Liu, X. Zhang, and J. Liu, "Electric vehicles in smart grid: a survey on charging load modelling," *IET Smart Grid*, vol. 2, pp. 25–33, mar 2019.

[78] N. Daina, A. Sivakumar, and J. W. Polak, "Modelling electric vehicles use: a survey on the methods," 2017.

[79] S. Huang, H. Safiullah, J. Xiao, B. M. S. Hodge, R. Hoffman, J. Soller, D. Jones, D. Dininger, W. E. Tyner, A. Liu, and J. F. Pekny, "The effects of electric vehicles on residential households in the city of Indianapolis," *Energy Policy*, 2012.

[80] J. Axsen and K. S. Kurani, "Anticipating plug-in hybrid vehicle energy impacts in California: Constructing consumer-informed recharge profiles," *Transportation Research Part D: Transport and Environment*, vol. 15, pp. 212–219, jun 2010.

[81] C. B. Harris and M. E. Webber, "An empirically-validated methodology to simulate electricity demand for electric vehicle charging," *Applied Energy*, 2014.

[82] N. H. Tehrani and P. Wang, "Probabilistic estimation of plug-in electric vehicles charging load profile," *Electric Power Systems Research*, vol. 124, pp. 133–143, jul 2015.

[83] F. Salah, J. P. Ilg, C. M. Flath, H. Basse, and C. van Dinther, "Impact of electric vehicles on distribution substations: A Swiss case study," *Applied Energy*, 2015.

[84] P. Grahn, J. Munkhammar, J. Widen, K. Alvehag, and L. Soder, "PHEV home-charging model based on residential activity patterns," *IEEE Transactions on Power Systems*, 2013.

[85] M. Nourinejad, J. Y. Chow, and M. J. Roorda, "Equilibrium scheduling of vehicle-to-grid technology using activity based modelling," *Transportation Research Part C: Emerging Technologies*, 2016.

[86] T. Bellemans, B. Kochan, D. Janssens, G. Wets, T. Arentze, and H. Timmermans, "Implementation Framework and Development Trajectory of FEATHERS Activity-Based Simulation Platform," *Transportation Research Record: Journal of the Transportation Research Board*, vol. 2175, pp. 111–119, jan 2010.

[87] L. Knapen, B. Kochan, T. Bellemans, D. Janssens, and G. Wets, "Activity-based modeling to predict spatial and temporal power demand of electric vehicles in flanders, Belgium," *Transportation Research Record*, 2012.

[88] J. Stiasny, T. Zufferey, G. Pareschi, D. Toffanin, G. Hug, and K. Boulouchos, "Sensitivity analysis of electric vehicle impact on low-voltage distribution grids," *Electric Power Systems Research*, vol. 191, p. 106696, feb 2021.

[89] D. Fischer, A. Harbrecht, A. Surmann, and R. McKenna, "Electric vehicles' impacts on residential electric local profiles – A stochastic modelling approach considering socio-economic, behavioural and spatial factors," *Applied Energy*, vol. 233-234, pp. 644–658, jan 2019.

[90] E. Pashajavid and M. A. Golkar, "Non-Gaussian multivariate modeling of plug-in electric vehicles load demand," *International Journal of Electrical Power and Energy Systems*, 2014.

[91] B. M. Hodge, A. Shukla, S. Huang, G. Reklaitis, V. Venkatasubramanian, and J. Pekny, "Multi-paradigm modeling of the effects of PHEV adoption on electric utility usage levels and emissions," *Industrial and Engineering Chemistry Research*, 2011.

[92] M. Balmer, K. Meister, M. Rieser, K. Nagel, and K. W. Axhausen, "Agent-based simulation of travel demand : Structure and computational performance of MATSim-T," in *2nd TRB Conference on Innovations in Travel Modeling (ITM 2008), Portland, OR, USA, June 22-24, 2008*, (Portland), p. 33, ETH Zurich, Institute for Transport Planning and Systems, 2008.

[93] Finnish Transport Agency, "National Travel Survey 2016," tech. rep., Traficom, 2018.

[94] J. Su, T. Lie, and R. Zamora, "Modelling of large-scale electric vehicles charging demand: A New Zealand case study," *Electric Power Systems Research*, vol. 167, pp. 171–182, feb 2019.

[95] M. J. Chihota and C. T. Gaunt, "Impact of Input Model Accuracy on Probabilistic Load Flow Outputs," in *2018 IEEE International Conference on Probabilistic Methods Applied to Power Systems (PMAPS)*, pp. 1–6, IEEE, jun 2018.

[96] R. Herman and J. Kritzinger, "The statistical description of grouped domestic electrical load currents," *Electric Power Systems Research*, vol. 27, pp. 43–48, may 1993.

[97] R. Singh, B. Pal, and R. Jabr, "Statistical Representation of Distribution System Loads Using Gaussian Mixture Model," *IEEE Transactions on Power Systems*, vol. 25, pp. 29–37, feb 2010.

[98] J. Meyer, P. Schegner, and K. Heidenreich, "Harmonic summation effects of modern lamp technologies and small electronic household equipment," *21st International Conference on Electricity Distribution (CIRED)*, 2011.

[99] J. Meyer, A.-M. Blanco, M. Domagk, and P. Schegner, "Assessment of Prevailing Harmonic Current Emission in Public Low-Voltage Networks," *IEEE Transactions on Power Delivery*, vol. 32, pp. 962–970, apr 2017.

[100] B. Peterson, J. Rens, and J. Desmet, "Harmonic emission assessment on a distribution network: The opportunity for the prevailing angle in harmonic phasors," in *CIRED - Open Access Proceedings Journal*, 2017.

[101] A. Abd El-Mageed Elhenawy, M. Mohamed Sayed, and M. Ibrahim Gilany, "Harmonic Cancellation In Residential Buildings," in *2018 Twentieth International Middle East Power Systems Conference (MEPCON)*, pp. 346–351, IEEE, dec 2018.

[102] P. Janiga and D. Gasparovsky, "Power Quality in Public Lighting Installations," in *Power Quality*, ch. 3, pp. 45–66, InTech, apr 2011.

[103] ON Semiconductor, "Direct-AC , Linear LED Driver Topology : CCR Straight Circuit (120 V AC & 230 V AC)," tech. rep., ON Semiconductor, 2015.

[104] M. H. J. Bollen and S. K. Ronnberg, "Primary and secondary harmonics emission; harmonic interaction - a set of definitions," in *2016 17th International Conference on Harmonics and Quality of Power (ICHQP)*, vol. 2016-Decem, pp. 703–708, IEEE, oct 2016.

[105] A. J. Collin, C. E. Cresswell, and S. Ž. Djokić, "Harmonic cancellation of modern switch-mode power supply load," in *ICHQP 2010 - 14th International Conference on Harmonics and Quality of Power*, 2010.

[106] T. S. Key and J. S. Lai, "Costs and benefits of harmonic current reduction for switch-mode power supplies in a commercial office building," *IEEE Transactions on Industry Applications*, 1996.

[107] J. Trifunovic, J. Mikulovic, Z. Djurisic, M. Djuric, and M. Kostic, "Reductions in electricity consumption and power demand in case of the mass use of compact fluorescent lamps," *Energy*, vol. 34, no. 9, pp. 1355–1363, 2009.

[108] European Commission, "Regulation EU 1194/2012 - implementing Directive 2009/125/EC of the European Parliament and of the Council with regard to ecodesign requirements for directional lamps, light emitting diode lamps and related equipment," 2012.

[109] J.-P. Zimmermann, M. Evans, T. Lineham, J. Griggs, G. Surveys, L. Harding, N. King, and P. Roberts, "Household Electricity Survey: A study of domestic electrical product usage," tech. rep., Intertek Testing & Certification Ltd, Milton Keynes, 2012.

[110] EIA, "RESIDENTIAL ENERGY CONSUMPTION SURVEY (RECS)," tech. rep., U.S. Department of Energy, 2015.

[111] G. Bertoldi, "Status of LED-Lighting world market in 2017," tech. rep., Joint Research Centre (JRC), European Commission, 2018.

[112] N. Watson, T. Scott, and S. Hirsch, "Implications for Distribution Networks of High Penetration of Compact Fluorescent Lamps," *IEEE Transactions on Power Delivery*, vol. 24, pp. 1521–1528, jul 2009.

[113] S. K. Rönnberg, M. H. Bollen, and M. Wahlberg, "Harmonic emission before and after changing to LED and CFL - Part I: Laboratory measurements for a domestic customer," in *ICHQP 2010 - 14th International Conference on Harmonics and Quality of Power*, 2010.

[114] C. Keyer, R. Timens, F. Buesink, and F. Leferink, "DC pollution of AC mains due to modern compact fluorescent light lamps and LED lamps," in *IEEE International Symposium on Electromagnetic Compatibility*, 2013.

[115] M. S. Islam, N. A. Chowdhury, A. K. Sakil, A. Khandakar, A. Iqbal, and H. Abu-Rub, "Power quality effect of using incandescent, fluorescent, CFL and LED lamps on utility grid," in *2015 First Workshop on Smart Grid and Renewable Energy (SGRE)*, pp. 1–5, IEEE, mar 2015.

[116] A. J. Collin, S. Z. Djokic, J. Drapela, R. Langella, and A. Testa, "Light Flicker and Power Factor Labels for Comparing LED Lamp Performance," *IEEE Transactions on Industry Applications*, 2019.

[117] X. Xu, A. Collin, S. Z. Djokic, R. Langella, A. Testa, and J. Drapela, "Experimental evaluation and classification of LED lamps for typical residential applications," in *2017 IEEE PES Innovative Smart Grid Technologies Conference Europe, ISGT-Europe 2017 - Proceedings*, 2017.

[118] O. Florencias Oliveros, A. M. Blanco, J. Meyer, J. J. González de la Rosa, and A. Agüera Pérez, "Automatic classification of circuit topologies of appliances based on higher order statistic," *Renewable Energy and Power Quality Journal*, vol. 17, pp. 516–521, jul 2019.

[119] X. Xiao, A. J. Collin, S. Z. Djokic, S. Yanchenko, F. Moller, J. Meyer, R. Langella, and A. Testa, "Analysis and Modelling of Power-Dependent Harmonic Characteristics of Modern PE Devices in LV Networks," *IEEE Transactions on Power Delivery*, 2017.

[120] Z. Sprociński, W. Szymański, R. Adamczak, G. Ludwikowski, M. Przeperski, and M. Gruszka, "[Evaluation of incidence of Chlamydia trachomatis infections among the group of infertile women diagnosed by laparoscopy, and based on properties of Chlamydia trachomatis in the cervical canal, peritoneal fluid and ovarian cyst puncture].," *Ginekologia polska*, vol. 72, pp. 224–7, apr 2001.

[121] DCLG, "Summary for Policymakers," in *Climate Change 2013 - The Physical Science Basis* (Intergovernmental Panel on Climate Change, ed.), pp. 1–30, Cambridge: Cambridge University Press, 2015.

[122] S. Estonia, "Household Energy Consumption Survey," tech. rep., Statistics Estonia, Talinn, 2013.

Acknowledgements

Abstract

Measurement Based Approach for Residential Customer Stochastic Current Harmonic Modelling

This thesis provides a stochastic methodology to evaluate the low-voltage distribution network's current harmonic levels due to the operation of nonlinear loads. With the advancement of power electronics, nearly every household device contain nonlinear circuits. High penetration of nonlinear power electronic loads with on-site electricity generating units could deteriorate the distribution grid's voltage quality to a critical level for operation. The current harmonics injected by different nonlinear loads affect voltage distortions.

The thesis addresses current harmonic level estimations using a probabilistic bottom-up modelling approach. One of the core parts of the model is the device usage model that provides the lighting load, electric vehicle and general domestic appliances usage patterns for the households. The device usage model allows the modelling of the stochastic nature of the domestic load. Measurement-based data is collected for the devices to be connected to the grid for harmonic current values estimations. Lighting model presented through switching schedule of the lamps, electric vehicle model through travel activity characterisation and domestic appliances with the custom probability distribution functions in the proposed methodology.

Measurement device uncertainty assessment is carried out to support the measurement results and provide a clear indication of the sufficient accuracy margin. Another set of uncertainty is observed in the load's thermal stability and operating behaviour responsible for significant variation in the harmonic currents of the load device. Warm-up is advised prior to any device harmonic current emission measurement. Various uncertainties related to networks and loads are considered.

Case examples of the model developed include estimation on the impact of the high penetration of electric vehicles on harmonic emission. The influence of circuit topologies of nonlinear loads is also estimated. The replacement of appliances with their efficient power substitutes to reflect the impact of continuous increase of the nonlinear device's penetration is also discussed.

Kokkuvõte

Mõõtmispõhine lähenemine olmetarbijate vooluharmoonikute juhusliku esinemise modelleerimiseks

Käesolev doktoritöö esitab madalpinge-jaotusvõrkudes mittelineaarsete koormuste talitlusega kaasnevate vooluharmoonikute tasemete hindamise stohhastilise metoodika. Erinevate mittelineaarsete tarvitite poolt vooluharmoonikute sisestamine mõjutab jaotusvõrgu pingemoonutusi. Jõuelektroonika arengute tulemusena sisaldab iga kodutarviti mittelineaarset toiteallikat. Suur jõuelektroonikal põhinevate koormuste määr võrgus ning kohalike elektrienergia tootmisseadmete lisamine võib halvendada jaotusvõrgu pingekvaliteeti talitluse seisukohast kriitilise tasemeni.

Doktoritöö käsitleb vooluharmoonikute tasemete hindamist läbi tõenäosusliku lähenemisega alt-üles modelleerimise. Selle mudeli üks tuumosa on seadmete kasutusmudel, milline esitab valgustuskoormuse, elektrisõidukite laadimise ja üldistatud koduseadmete kasutusmustrid majapidamise kontekstis. Seadmete kasutusmudel võimaldab käsitleda kodutarvitite kasutamise stohhastilist iseloomu. Mõõtmistel põhinevad lähteandmed on koondatud võrku ühendatavate seadmete harmoonikute tasemete hindamiseks. Väljapakutud metodoloogia esitab valgustuse mudeli lülitamise ajastuse, elektrisõidukite mudeli läbitud teekonna iseloomustuse ja kodutarvitid eri-jaotustihedusfunktsioonidena alusel. Mõõtetulemuste toetamiseks ja mõõtetäpsuse piisavale tasemele selge hinnangu andmiseks viiakse läbi mõõteseadmete määramatuse hinnang. Täiendavaid määramatuse komponente vaadeldakse seadme soojuslikus talitluses ja talitlusviisides, millised põhjustavad olulist vooluharmoonikute taseme varieeruvust. Vooluharmoonikute emissiooni mõõtmisele eelnevalt soovitatakse seadmetele töötemperatuurile soojenemist. Vaadeldakse võrgu ja seadmete ühendustega seotud määramatust.

Välja töötatud mudeli kasutamise näitejuhtumiteks on elektriautode kõrge osakaalu mõju harmoonikute emissionile. Samuti hinnatakse mittelineaarsete koormuste ahelate topoloogiate mõju. Et kajastada jätkuvat mittelineaarsete tarvitite osakaalu kasvu mõju, käsitletakse ka tarvitite väljavahetamist vastavate energiatõhusamate toodete vastu.

Appendix 1

I

M. N. Iqbal, L. Kütt, B. Asad, N. Shabbir, and I. Rasheed, "Time-dependent variations in current harmonic emission by LED lamps in the low-voltage network," Electrical Engineering, vol. 103, p. 1525–1539, 2021

ORIGINAL PAPER

Time-dependent variations in current harmonic emission by LED lamps in the low-voltage network

Muhammad Naveed Iqbal[1] · **Lauri Kütt[1]** · **Bilal Asad[1]** · **Noman Shabbir[1]** · **Iftikhar Rasheed[1]**

Abstract

This paper presents the variation in current harmonics injected by the LED lamps and their effect on harmonic estimation in the low-voltage network. Lighting consumes a significant portion of total electricity consumption in residential, commercial and industrial sectors. The energy-efficient lights, for example, light-emitting diode lamps, are reducing this share significantly over the last few years. These nonlinear LED lamps are the source of current harmonics and reduce the power quality in the low-voltage grid. The estimation of the magnitude by which they affect the power quality is essential for network operators. However, the thermal stability of the lamps is a prime consideration for the accurate assessment of the power quality. This paper investigates the effect of thermal stability on current harmonics injected by LED lamps.

Keywords Power quality · Harmonics · Thermal stability · LED lamps · Lighting modeling

1 Introduction

Commercial and home appliances are now more energy efficient with improved energy ratings. However, energy-efficient appliances often include nonlinear power electronic units that can contribute to poor power quality by sourcing non-sinusoidal current, thus adding load of the current harmonics. It is, therefore, necessary to estimate the magnitude by which they can influence the power quality in a low-voltage (LV) network.

One of the major areas where energy efficiency brings immediate impact would be lighting, as it consumes 19% of the total electricity in the world and 14% in the EU [1]. Lighting accounts for more than 20% of total electricity consumption in the residential sector [2]. The wide dissemination of energy-efficient lights, for example, LED lamps in recent years, has shrunk the lighting power consumption. The dwindling prices and improved reliability have made them very popular amid residential consumers. Policies to scale down inefficient lamps in different countries also contributed in this regard [3]. Many countries, including, for example, EU,

Australia, Canada, Colombia, Russia, and Malaysia, have set policies aimed at prohibiting the sale of inefficient lamps [4]. Better life cycle cost and absence of mercury makes LED an efficient and environment-friendly lamp [5].

The selection of a lamp by the customer is influenced by the price tag, power ratings, lumens, and light quality. However, they are not aware of the lamp characteristics, power quality information, and design technology. Incandescent lamp (IL) was the most popular choice for many years, although they have poor efficiency. Slightly better technologies, such as halogen (HL) or discharged lamps [6], latter including fluorescent (FL) and compact fluorescent (CFL) lamps, are more energy-efficient and have a longer life span in comparison with IL. Apart from all the efforts by governments and policy-making institutes, many households still have inefficient lamps.

During the last decade, LED lamps are getting more popular because of more competitive prices, better efficacy, and improved light quality. In 2012, the share of CFL and LED lamps in the UK residential sector was 7.9% and 0.2%, respectively [7]. The projected growth of LED lamps market share indicates that by 2020, 42% of the indoor and 75% of the outdoor lamps will be LED. The LED uptake will further increase to 81% of the total indoor lamps and 99% of the total outdoor lamps by 2030. In Europe, the LED penetration will be in the range of 42–46% of the total lamps installed by 2020 [8].

Muhammad Naveed Iqbal
miqbal@taltech.ee

1   Department of Electrical Power Engineering
    and Mechatronics, Tallinn University of Technology,
    Ehitajate tee 5, 19086 Tallinn, Estonia

Both CFL and LED lamps include power electronic circuits and reduce power quality by adding nonlinear current load in the network, which in turn can be one of the main reasons for voltage distortions. The presence of a sine waveform in the distribution network voltage is one of the critical power quality indexes. As the voltage becomes distorted from the sine wave, the periodic deviations are characterized as harmonics. The presence of significant share of voltage harmonics can lead to several unwanted consequences, such as decrease of transformer lifetime and reliability of the distribution line [9], even up to malfunction of protection equipment such as relays and circuit breakers; the capacitor banks can be overloaded because of their low impedance at higher frequencies; electrical equipment including motors may produce additional noise and vibration; added interference in communication lines may be observed [10]. Very often, the reason for the distorted voltage is high distorted load current in the network components, lines, and transformers. It is therefore vital for the distribution network operator to assess, how the power quality indexes are met during the network operation. One of the key inputs to this is the estimation of expected distorted current levels, i.e., current harmonic levels.

Although the current harmonic load by individual LED lamp is minimal, but the overall effect of all the lamps operating in the distribution network can be significant. Still, there are a lot of challenges to estimate and mitigate the harmonics caused by the lamps as well as, for example, the other high-power power electronic devices such as inverters.

While the LED lamps can be considered rather stable units in their illuminance, initial research has shown that their power ratings tend to be variable in time [11]. The variations can be explained by their inherent process of heating up to their stable thermal operating point, related also to their internal losses. It is evident that this heating process would result in variations both in the fundamental power draw but also relates to the levels of the load current harmonics.

This paper focuses on the aspects of the LED lamps, especially related to the thermal stability of the load current harmonics. The magnitude of the inaccuracies due to the thermal stability of the LED lamps in the measurement and estimation of power quality is discussed in this paper. In Sect. 2, a literature overview is presented. A detailed overview of led lamps has been provided concerning efficiency, types, and performance in Sect. 3. The various performance indicators of LED lamps have been compared with CFL and IL. Types of LED lamps have been categorized based on the circuit topologies and current waveforms drawn by the LED lamps. In Sect. 4, a measurement setup used to evaluate the power quality indexes of the LED lamps is described. The current harmonics and phase angles analysis approach to estimate the thermal stability of the LED lamps is discussed in Sect. 5. The results of the comparison

between thermal stability time and other vital parameters are presented in detail. Section 6 shows the difference between current harmonics estimation with or without thermal stability is taken into consideration. The conclusions are discussed in Sect. 7.

2 Literature overview

Literature reports are available on the effect of large-scale penetration of energy-efficient lamps in the distribution grid. The implication of the mass adoption of CFL on the New Zealand distribution system is presented in [10] where the effect of CFL on the grid was presented with a bottom-up Norton equivalent model of the distribution grid. It was reported that although the active power saving was the same for all CFLs, the lamps with filters had lower harmonic losses. Different proportions of CFL, LED, and IL were considered for lighting load applied to a distribution grid using computer software in [12]. It is described that while LED lamps have the lowest power factor, but total current harmonic distortion (THD$_i$) was less in comparison with CFL. A CFL is modeled, and MATLAB simulation is used to study the impact of large-scale adoption of CFL in the LV distribution grid [13]. However, in this study, only one lamp is considered, and therefore, harmonic cancellation was not included in the study. The results show the negative impact on power quality, reduced power factor, and harmonic distortion. Another set of results to compare THD$_i$ and power consumption for different lighting technologies is made in another study [14] indicate that LEDs had higher THD$_i$ values than CFL. Here, still different types of LED lamps were not considered. A comparison between IL load and CFL load presented in [15] reported possible distribution transformer overloading by 30% in the case of the CFL load due to the high current harmonic levels.

The aforementioned studies have to be observed in their limitations and usually do not provide generalization on a level that would provide reasonable accuracy for analyzing the effects of added LED lamps in the distribution network. Furthermore, the detail level is not so fine to take into account different heating models of the LED units. Only a few recent studies done on the adoption of energy-efficient lamps in the distribution network report aspects of thermal stability on the operation. A distribution grid simulation is used to assess the effect of CFL and LED penetration where lamps were stabilized for 15 and 30 min, respectively, in [16]. High voltage distortion was reported, and THD$_v$ was even above the limits defined in the standard IEEE 519-1992 for the unbalanced network. CFL lamps were measured at room temperature and cold state in [17] to evaluate the effects on the distributed grid. A computer model of the distribution grid is used to compare the effect of CFL adoption in the grid. An increase in the odd

Table 1 IEC Class C harmonic limits

Harmonics (h)	P > 25 Current harmonic limit (%)	P ≤ 25 Harmonic current per watt (mA/W)
3	30 × p.f	3.4
5	10	1.9
7	7	1
9	5	0.5
11	3	0.35
13	3	3.85/h

current harmonics except for the 5th and 7th harmonics due to harmonic compensation is reported. Harmonic current levels observed for LED lamps during dimming operation in [18] had used lamps switched for 10 min to stabilize them before measurement. The study concludes an increase in the harmonic levels with an increase of dimming angle to reduce the brightness. High-power (25 W) street LED lamp was measured in [19] to compare power quality issues with other lamps. Measurement was taken after the steady-state warm-up of the lamp, where it failed to achieve a steady-state even after 30 min because of its dependence on temperature. The power factor was 0.96, and a current was nearly sinusoidal. In the current harmonic spectrum, 3rd harmonic was the most dominant 5.4% of the fundamental following 9th, 13th, and 15th harmonics with 2.5%, 1,6%, and 1.25%, respectively. The results were compared with more powerful street light LEDs of 68 W and 144 W. The magnitude of current harmonics and THD_i were much higher in the latter case.

In the incandescent lamps, over 90% of the input power is lost in the form of heat [20]. The efficacy and lifetime have been increased by adding halogen gas in the incandescent lamps, resulting in two times longer lifespan and 70% better efficacy in comparison with IL [21]. Still, these lamps are of resistive load type and usually are not associated with particular nonlinear characteristics.

A typical CFL lamp could have a 15 times longer life span and use 70% less energy in contrast to IL [22]. However, their operation requires lamp driver circuits that act as non-linear load and are the source of current harmonics. While electromagnetic lamp drivers are recyclable and have better reliability and longer life span, their poor efficiency and lower power factor [23] make electronic lamp driver more favorable with better input power factor, lower THD_i and ability to eliminate the flickering effect of the lamps.

The LED lamps are the semiconductor-based light sources and require a constant current to generate stable and efficient light output. Their light color is managed by types of materials used as coatings to generate visible light. These materials are known as luminescent and convert parts of input energy into the electromagnetic waves in the visible, ultraviolet, or infrared spectrum [24]. The other method is an RGB (red,

green, blue) system that utilizes a mixture of red, green and blue LEDs to produce white light. The RGB systems are more complicated because of the electrical control system involved [25]. In an LED lamp, radiation emission is almost negligible, and heat is mainly removed through conduction or convection methods. Therefore, heat sinks are present in most of the high-power LED lamps.

The lamp driver circuits provide a (near) constant DC current source to the LED string and are the most critical part of the lamp. Rectification and current control refer to power electronic circuits that operate as nonlinear load. This means they will inject load current harmonics into the grid. This may also depend on the supply voltage. The distortion of the voltage waveform may further alter the harmonic emission profile of the nonlinear loads [26].

To limit the possible effects of the high levels of harmonic currents, IEC 61000-3-2 standard states limits to electrical equipment harmonic current emissions. The lighting equipment falls under Class C, while based on active power consumption, a distinction is made for ratings from 5 to 25 W and greater than 25 W. Table 1 shows the harmonic current limits percentage to the fundamental for load greater than 25 W. The lamps less than 25 W must observe one of the following conditions.

- The harmonic currents shall observe the power limits shown in Table 1.
- The 3rd and 5th harmonic currents should not exceed 86% and 61% of the fundamental frequency, respectively
- The THD must not be greater than 70%, and the 3rd, 5th, and 7th harmonic currents must be equal or below 35%, 25% and 20%, respectively [27].

While the IEC 61000-3-2 standard does not indicate any limits for the harmonic angles, the harmonic current addition or cancellation may result in unexpected current harmonic emissions. The current harmonic levels for the lamps can be high, as pointed out in [28]. Levels of injection from the commercially available LED and CFL lamps depend on the control strategy and topology of the power supply. Newer lamps include filters and power factor correction circuits to

Table 2 LED lamp portfolio summary

	Type 1	Type 2	Type 3	Type 4	Total
No. of lamps	140	15	4	4	163
No. of manufacturers	27	7	2	1	28
Average price (euro/W)	0.53	0.51	0.41	0.45	0.48
Lumens (lm)	90	81	82	92	86

reduce current harmonics and improve the power factor. In another study, the performance of LED lamps was monitored for normal voltage and voltage sags [27]. The experiment results show THD$_i$ values from 30 to 175% for the LED lamps. THD$_i$ injection depends on the type of filter used in the lamps. For the active filter, valley-filled circuits, and passive filters, the THD$_i$ injection was found between 30–35%, 63–70%, and 100–175%, respectively. It has been proposed that LED lamps could be classified based on the types of components present in the LED driver circuit. A typical LED driver circuit contains rectifier circuits that convert primary AC supply to low-voltage DC. For a constant current supply to the LED, the DC–DC converter is used. Electromagnetic interference (EMI) filter and power factor correction (PFC) filters may also be present to improve the current waveform.

3 LED lamp overview

For this study, measurement results of 163 LED lamps available in the market were used, and the shape of the current waveform when pure sinusoidal voltage is applied was used for classification. Table 2 summarizes the average price per watt, average light output efficacy, the number of lamps measured, and the number of manufacturers for each LED type used in this study. The circuit typology for different types of LED lamps is shown in Fig. 1.

Almost 88% of the measured LED lamps have the current waveform of type A as shown in Fig. 2. It is a pulse-like shape and similar to the CFL current waveform [29]. Such a lamp driver circuit contains a rectifier circuit, a DC–DC converter to regulate the input voltage to the LED and EMI filters. In type B LED shown in Fig. 2, the rectifier starts to conduct around zero crossings of the input voltage and continues until the input voltage reached the peak value. It has 50% more conduction time than type A LED. The Zener diode D$_z$ limits the forward voltage to the LED. Variations in the input voltage can affect the DC voltage at the LED in these lamps [29]. The current drawn by the C type has a square shape, as shown in Fig. 2. The circuit contains a constant current regulator (CCR). It provides a constant current flow over a wide voltage range and therefore protects the LED [30]. The current waveform drawn by type D LED in Fig. 2 is close to sinusoidal, which is achieved through active power

factor correction (PFC) converter [31]. The resistor can also be added in the LED string to minimize the current difference [32].

4 Measurement setup

A test bench has been developed for this experiment. It consists of sixteen lamp sockets connected to a bus-bar through relays. The relays are controlled by the control box consists of a DC power supply and sixteen transistor switches. It provides a 12 V DC voltage to the relays when a digital input is applied to the transistor switch. A National Instrument (NI) data acquisition module (DAQ) is used to provide the digital inputs to the control box and analog reference signal to the controllable power supply. A 4-kVA Chroma 61505 power supply is used in this experiment. This power supply is programmable and can be controlled via reference signal V_{REF}.

$$V_{REF} = \frac{V_{out}}{V_{RANGE}} \times V_{coef} \tag{1}$$

Here, V_{coef} is 7.072 and V_{RANGE} is 300 V. A MATLAB program is used to generate this reference voltage and digital signals for the control box through the DAQ module. Amplitude and phase angles for each odd harmonic are used to calculate the reference signal for the programmable power supply. Equation (2) is used to calculate the V_{out} from the given amplitude and phase angle of the fundamental and odd harmonics up to the 19th harmonic.

$$V_{out} = \sum_{i=1}^{n} \sqrt{2} \times A_i \sin(2\pi f_i t_s + \alpha_i) \tag{2}$$

Here, A_i is the RMS value of harmonic magnitude and f_i is its frequency. The α_i is the phase difference between the harmonic and the fundamental component. t_s is the sampling interval for which the calculation has to be made. It is calculated from the sampling frequency f_s as shown in Eq. (3).

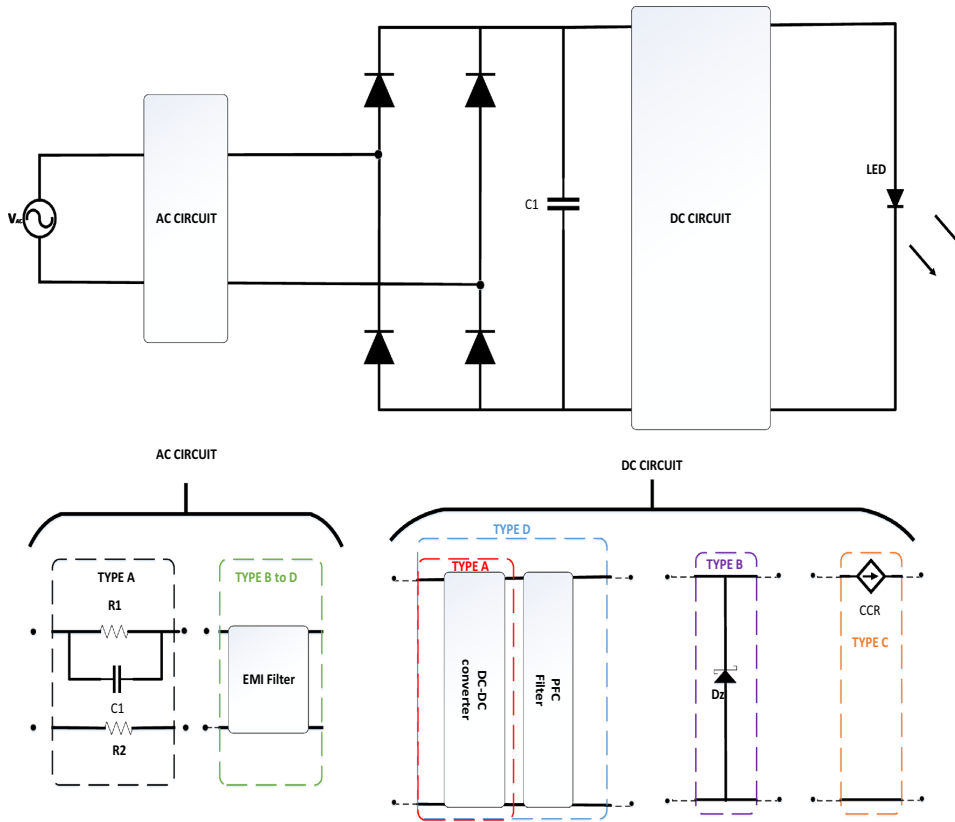$$t_s = \frac{1}{f_s} \tag{3}$$

Fig. 1 Schematics of different types of LED lamps

The sampling frequency can be calculated by the time duration T_m of the waveform to be generated and the number of samples in that interval N as shown by Eq. (4).

$$f_s = \frac{N}{T_m} \tag{4}$$

This setup has enabled us to generate a pure sinusoidal voltage with a sampling frequency of 100 kHz. For power quality measurements, A-Eberle PQ-BOX 200 is used to record harmonic magnitude and phase angles with 41 kHz sampling frequency. The PQ-BOX 200 is capable of recording power quality data with a 1-s resolution. The 1-s data are based on the average values calculated at 200 ms according to IEC 61000-4-30 standard. The experiments were performed under a constant laboratory environment at 24°C with an unforced ventilation system. Figure 3 shows the block diagram of our measurement setup.

5 Measurement and analysis

We have used our measurement setup to test 163 LED lamps. During each measurement cycle, sixteen LED lamps were connected to the test bench. Each lamp is measured over 1 h and switched automatically for each measurement cycle. The distance between the LED lamp measured in each cycles was more than 1 m from the lamp measured in the previous cycle to maintain a constant temperature. The lamps are connected through relays, and only one lamp is switched ON during each measurement cycle. It will eliminate additional primary and secondary harmonics due to several loads sharing the same power source [34]. The data extracted for analysis comprises THD_i, current harmonic magnitude and phase angles, active power, reactive power, and power factor. Current waveforms are also recorded for each LED lamp.

The THD_i of LED lamp changes continuously until it become thermally stable. The THD_i of a thermally stable
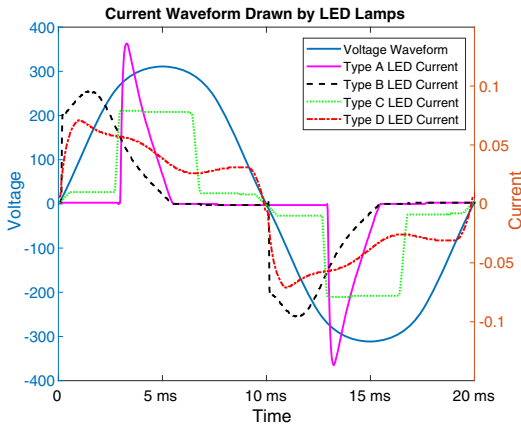
Fig. 2 Current waveform drawn by different types of LED

LED lamp is different than the initial value of THD_i when it is turned ON. This difference can be up to 10%. Figure 4a shows the histogram of the percentage difference between thermally stable and cold LED lamps. For the majority of the lamps (95%), the difference in THD_i before and after thermally stability is between 2 and 8%. Only 3.6% of lamps have less than 1% difference, and 1.84% have more than 10% difference.

The percentage difference in THD_i between thermally stable and cold states increases with the increase of the active power of the lamps. A total of 163 LED lamps are divided into five groups based on the active power. Figure 4b shows the box plot of percentage difference in THD_i between cold and thermally stable LED lamps of all groups. The central line indicates the median, and the bottom and top edges of the box indicate the 10th and 90th percentiles. The whiskers are extended to extreme values. It is clear from Fig. 4b that as the power of the lamp increases, the percentage difference of THD_i between thermally stable and cold lamps also increases. The (3–5) W and (7.1–9) W groups show a relatively large variation as most of the type A lamps include in these groups.

5.1 Thermal stability time estimation

The current harmonic magnitude and phase angles measured during the experiment were analyzed to find the stability time of each LED lamp. We have considered up to the 19th current harmonic magnitude and phase angles in this study. The power supply may add unwanted small variation in the harmonics, and it can affect the current harmonics measurements [35]. To avoid these variations and to simplify the process, the trend fitting curves are applied to all current harmonics and phase angle variations over time. This approach has enabled

us to calculate the stability time as the magnitude and phase angles of all current harmonics observe an exponential rise or decay with time. Equation (5) shows the exponential curve fitting that is applied to the magnitude and phase angles of LED lamps.

$$y = d_A \times e^{(-\frac{x}{\tau})} + A_f \qquad (5)$$

Equation (5) provides the values of fitting curve y for each value of original data x. Here, A_f is the final value of the LED lamp magnitude or phase when the lamp becomes fully thermally stable. The difference between the initial value of magnitude or phase (during 1st minute) and the final value is represented by d_A, as shown by Eq. (6).

$$d_A = A_f - A_o \qquad (6)$$

The time constant τ in Eq. (5) is the time required by the exponent to decay by $1/e$ or grow by the factor e. The time constant is calculated by using Eq. (7) for all the harmonics up to the 19th.

$$\tau = \frac{T_{80} - T_o}{1 - \ln(\frac{1-\gamma}{d_A})} \qquad (7)$$

where T_{80} is the time when the magnitude or phase angle reaches 80% of the final value. T_o is the starting time, and its value is, therefore, 1. The γ is the difference between 80% of the final value of magnitude or phase and the initial value, as indicated by Eq. (8).

$$\gamma = A_{80\%} - A_o \qquad (8)$$

After finding the time constant, the stability time of the LED lamp can be estimated. LED lamps will become thermally stable when Eq. (5) is decayed by $1/3e$ or increased by $3e$. It will be equal to 3τ. Hence, the stability time T_s can be calculated by Eq. (9).

$$T_s = 3 \times \tau \qquad (9)$$

5.2 Thermal stability time variations

The stability time T_s of all the current harmonic magnitude and phase angle is estimated by the same approach. As an example, Fig. 5 shows the current magnitude (RMS) and trend fitting curve for a 9.5 watt (type A) LED lamp. The green line indicates the RMS values of the current for fundamental and odd harmonics up to the 19th. The blue line is the trend fitting curve applied by using Eq. (5). The time constant τ is indicated by the red dot and calculated by using Eq. (7). The thermal stability time T_s is shown by the black dot and is calculated by Eq. (9). The trend curves provide a close fit
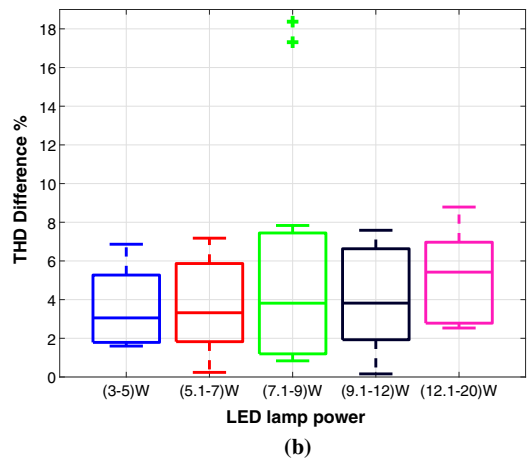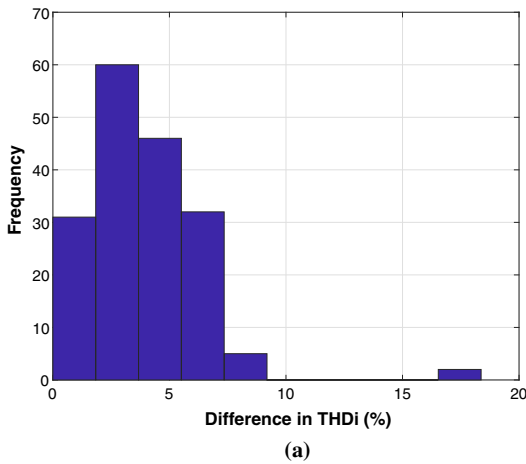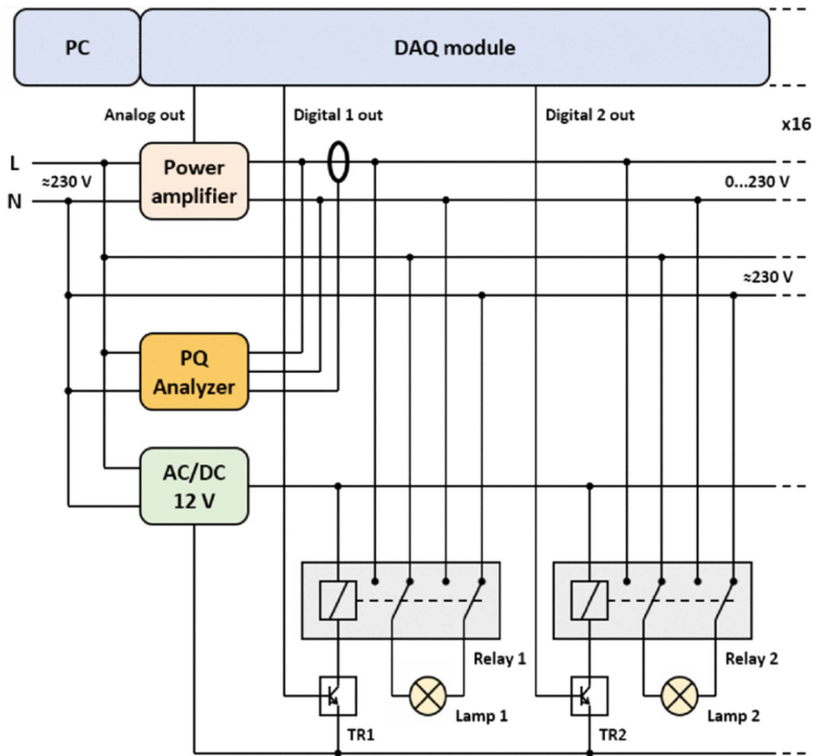
Fig. 3 Block diagram of measurement setup [33]

Fig. 4 **a** THD$_i$ difference (%) histogram of 163 LED lamps. **b** Box plot of THD$_i$ difference (%) and active power

to the original current data and have applied to all the LED lamps to find out the thermal stability time of each lamp. The stability time T_s will change if we changed γ in Eq. (6). In our study, we have selected γ by using 80% of the final value. However, γ value can be changed by changing $A_{80\%}$ in Eq. (8), with 70–90% of the final value ($A_{70\%}-A_{90\%}$). However, the magnitude variation will become less than 1% as it reaches 80% of the final value. Similarly, we can find the stability time of the phase angles for the fundamental and odd harmonics. Figure 6 shows the original data, trend
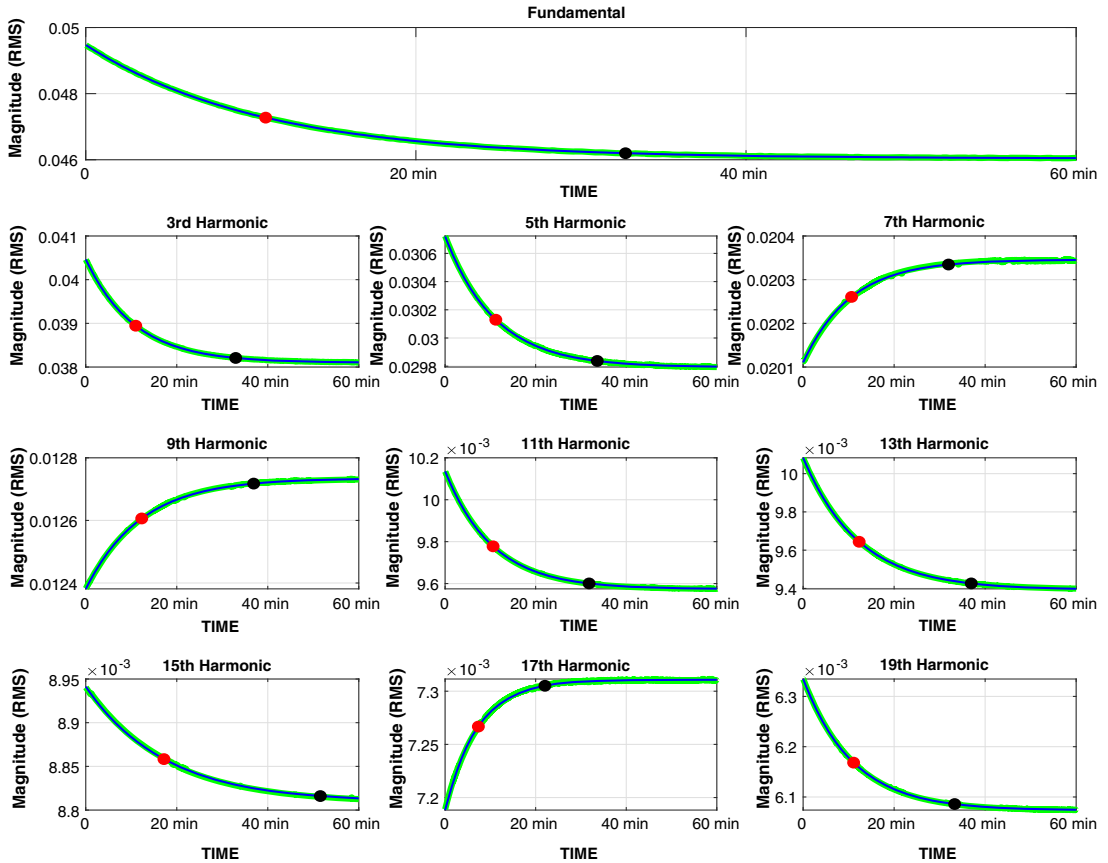
Fig. 5 A 9.5W (type A) LED lamp magnitude (RMS) variations over time

fitting curve, the time constant τ, and stability time T_s for the phase angles of fundamental and up to the 19th odd harmonic. This procedure is applied to the measurement data of all 163 LED lamps, and thermal stability time is estimated for current harmonics magnitude and phase angles.

The trend fitting curve has enabled us to estimate the thermal stability time T_s of all the LED lamps. The thermal stability time may depend on many factors like temperature, lamp driver topology, the variation in the magnitude or phase angles of current harmonics, and the active power of the lamp. To investigate the reason that may influence this variance, we have compared thermal stability time T_s of all LED lamps with active power and d_A.

The box and whisker plot for the magnitude of the current harmonics against the stability time is shown in Fig. 7a. The box top edge represents 95 percentile, and the bottom edge is equal to 5 percentile of the T_s values. The line between the top and bottom edges of the box shows median values. The upper whisker is extended to 99 percentile value, and the bottom whisker represents 1 percentile value. The plot shows that for 95% of the lamps, the magnitude of all harmonics becomes stable below 40 min. The fundamental magnitude becomes thermally stable quickly than most of the higher-order harmonics except for the 9th and 11th harmonics. However, the upper whisker of the 9th and 11th harmonics is more than 55 min in contrast to the fundamental where it is less than 45 min. The 5th, 13th, and 15th harmonics have the most significant spread between 5 and 95 percentile values of T_s. The stability time extends up to 38, 37 and 36 min for 5th, 13th, and 15th harmonics, respectively.

The phase angles, on the other hand, has a different spread in comparison with the magnitude. Figure 7b also shows the box and whisker plot of the phase angles versus the thermal stability time for the fundamental and odd harmonics. The fundamental component has the highest value of the stability time T_s around 33 min at 95 percentile. It is very close to the 3rd and 5th harmonics. For the 7th to 19th harmonics, the T_s is between 31 and 27 min for 95 percentile of LED
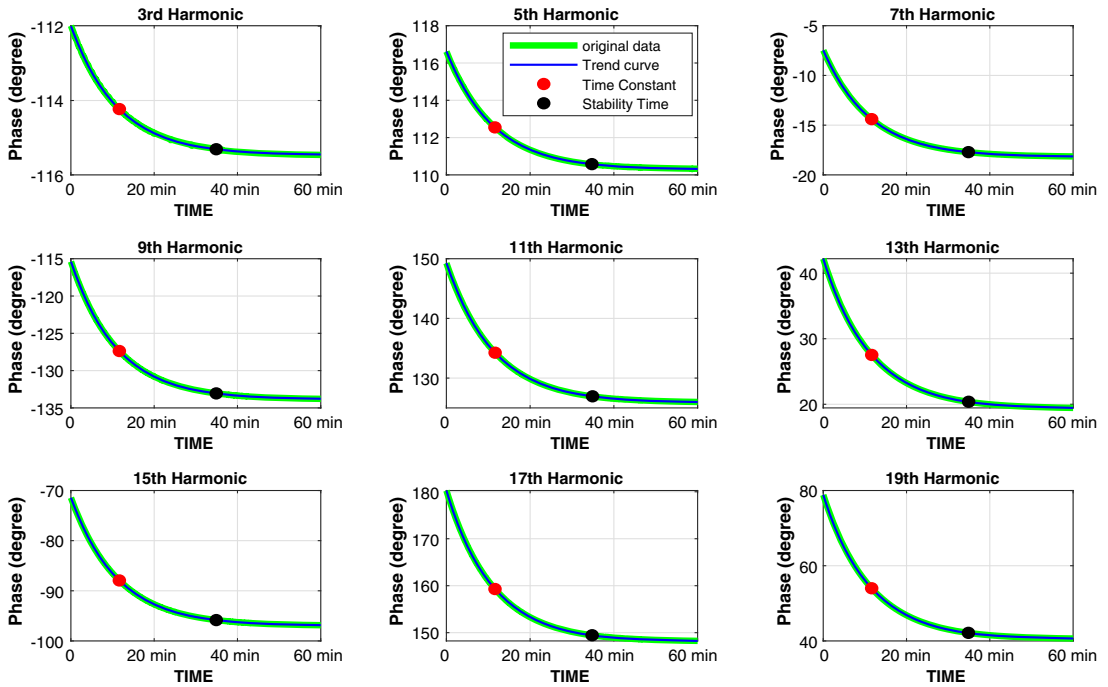
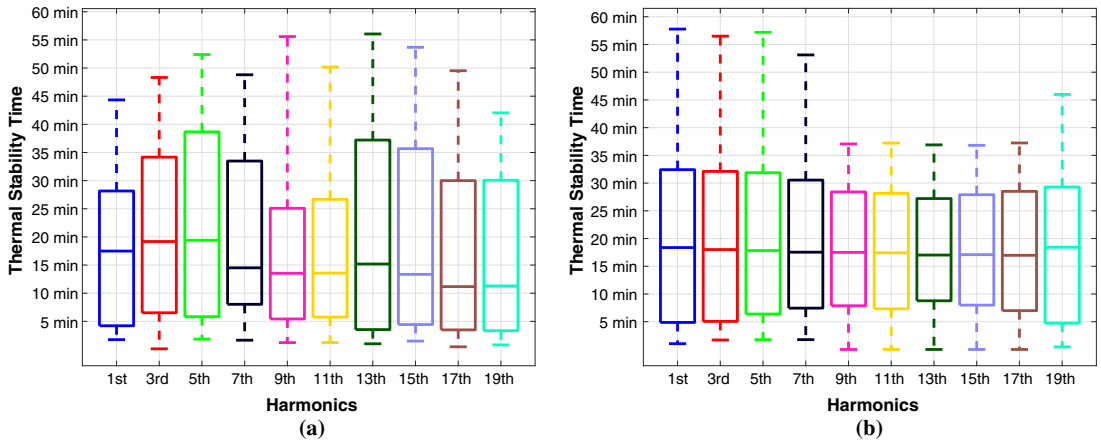**Fig. 6** A 9.5W (type A) LED lamp phase variations over time

Fig. 7 Box plot of stability time against **a** harmonics magnitude and **b** harmonics phase angles

lamps. The upper whiskers of fundamental to 7th harmonic lies between 53 and 58 min. Therefore, it can be concluded that the phase angles of 95% of LED lamps get thermally stable before 35 min. The maximum time required for some lamps to have stable phase angles is 58 min. The magnitude takes more time to get stable and 95% of LED lamps have a stable magnitude before 40 min. The magnitude takes

5 min more time to get stable in comparison with the phase angles. The maximum time taken by the lamps to have stable magnitude for all the harmonic is 56 min. Figure 8 shows the stability achieved over time for the magnitude and phase angles from fundamental to the 19th harmonic for all the LED lamps. During the first 10 min, the percentage of LED lamps with a stable magnitude is more than the lamps with stable

phase angles. For the phase angle, 24–29% of LED lamps have achieved thermally stable for some or all harmonics during the first 10 min. On the other hand, the lamps with stable RMS values are between 32 and 58% for few or all harmonic during the same time. After 20 min, the total percentage of lamps with thermally stable magnitude and phase angles are in the same range. Now, 57–87% of LED lamps have achieved stability for the magnitude of one or more harmonics. The phase angle is stable for 67–76% of LED lamps for any odd harmonic. After 30 min, 88–97% of lamps have stable magnitude harmonics, and 90–96% have stable phase angles.

5.3 Stability time and active power

The stability time may also be affected by the power of the LED lamp, although it is not a valid assumption for all LED lamps. Some high-power LED lamps have shorter stability times in comparison with the low power LED lamps. However, the overall trend shows that in general high-power LED lamps have a slightly more thermal stability time in comparison with the low-power LED lamps for the fundamental and higher harmonics. Figure 9 shows this trend. All 163 LED lamps are divided into five groups. The group one contains LED lamps with power between 3.3 and 5 W. Similarly, groups 2, 3, 4, and 5 contain LED lamps with active power between 5.1–7 W, 7.1–9 W, 9.1–12 W, and 12.1–20 W, respectively. The box and whisker plot is made for fundamental and higher-order harmonics for the aggregate data of LED lamps in each group. The individual harmonics are represented by different colors as shown in Fig. 9. The top of the box indicates 75 percentile value, and the bottom indicates 25 percentile values. The circle between the box represents the median value. The whiskers are extended up to the most extreme data points and outer circles represent outliners.

It is evident from Fig. 9 that the median value of fundamental increases linearly from around 5 min for group 1 to 22 min for group 5. Hence, there is more than a three times increase in the median value of fundamental magnitude from group 1 to group 5. Similarly, the 3rd and 5th harmonics show a similar trend with 0.76 and 2.3 times increase, respectively. The 7th harmonic shows an increase in the median value up to group 4, but then it decreases for group 5. The higher harmonics do not show an increasing or decreasing trend. However, the overall trend of the 25–75 percentile boxes shows an upward moment from group 1 to group 5. The large spread of stability time indicates its dependence on factors related to lamp architecture. These factors include cooling and electrical structures of LED lamps. However, Fig. 9 shows a general trend of an increase in the thermal stability time as the LED lamp's active power increases.

5.4 Stability time and d_A

The d_A in (6) shows the difference between 80% of the final value of magnitude or phase and the initial value. It means that if the d_A is large, then the difference between the harmonic magnitude or phase angle is more between thermally stable state and cold state. Figure 10 shows the plot between percentage change between 80% of the final value and the initial value (% d_A) against the stability time. Different markers are used to indicate types of LED lamps based on their current waveform. The colors are used to indicate the power of the lamp. Although most lamps in this study are of type A, the trend between percentage d_A and thermally stability time is independent of the LED lamp types based on the current waveform. Figure 10 shows the percentage change in d_A against thermal stability time for the fundamental and higher-order odd harmonics. The green circle in each plot indicates the majority trend. The fundamental component of magnitude shows an incremental linear trend. The 3rd, 7th, and 15th harmonics also show a similar trend to the fundamental component. The trend for 5th harmonic is somewhat linear, but the growth is very flat. It means most lamps with a low d_A percentage of magnitude also have a higher stability time. The 9th harmonic has a high concentration of stability time between 10 and 20 min. Also, the percentage of d_A is between 1 and 10% during the stability time. Hence, the trend is close to a uniform distribution of stability time between 10 and 20 min for different values of d_A percentage. The 11th and 19th harmonic has a linear incremental trend but between 8 and 13 min, the percentage of the d_A has a wide range of 1–15%. For the 17th harmonic, the trend is indicated by two circles. The upper circle contains more data and hence shows a slow incremental linear change of thermal stability time against a substantial change in d_A percentage. The lower circles have fewer values but have a more rapid linear increase of stability time against d_A percentage.

6 Effect on harmonic estimations

The lighting load has a significant share in the total end-users electricity consumption in the residential sector. Therefore, switching to energy-efficient lamps has a substantial impact on energy savings. To observe the current harmonics and the impact of thermal stability in the residential sector, we have constructed a lighting usage model. This model is based on the real-time measurement of lighting load in a residential building, occupancy profiles, and the number of lamps in the building. This model can simulate lighting usage of each lamp at a high resolution of 1 min in the residential building.

Lighting load modeling in the residential buildings is a challenging task. Lighting load is highly variable in nature and depends on many factors, including the building struc-

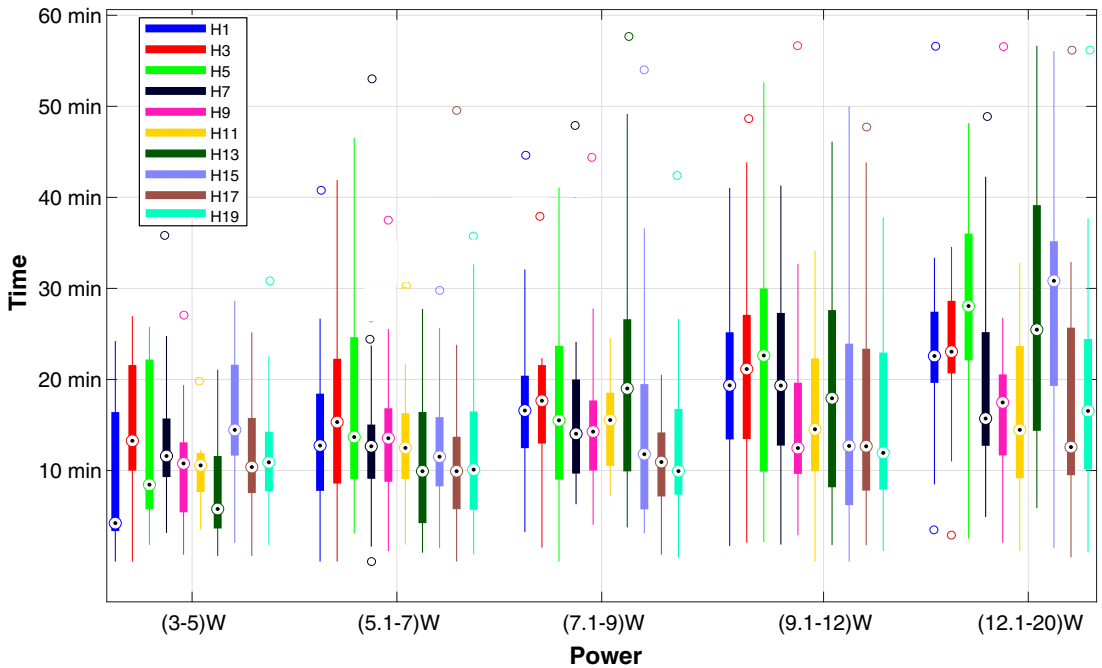**Fig. 8** Magnitude and phase
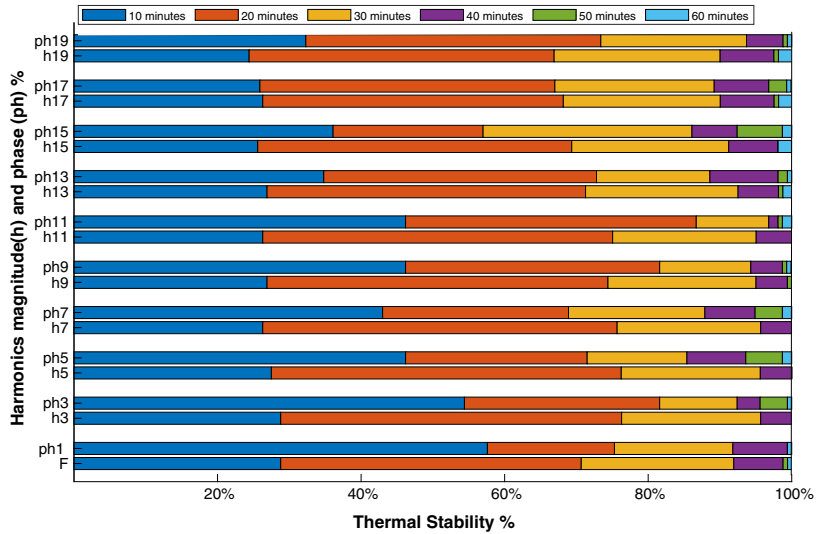stability achieved over time

Fig. 9 Box plot of active power against thermal stability

ture, occupancy profile, weather, and solar cycles [36]. We
have used a bottom-up approach to formulate a model based
on end-user appliance usage patterns. A residential building
is measured with sub-meters at the device level for a month.
The power consumption data are analyzed to study the usage
patterns of each device. For the lighting load, a single sub-

meter provided us the aggregated power consumption of all
the lights in the building.

The aggregated consumption data for lighting load are
compared with the active power of individual lamps in the
building to find the usage patterns of each lamp. The total con-
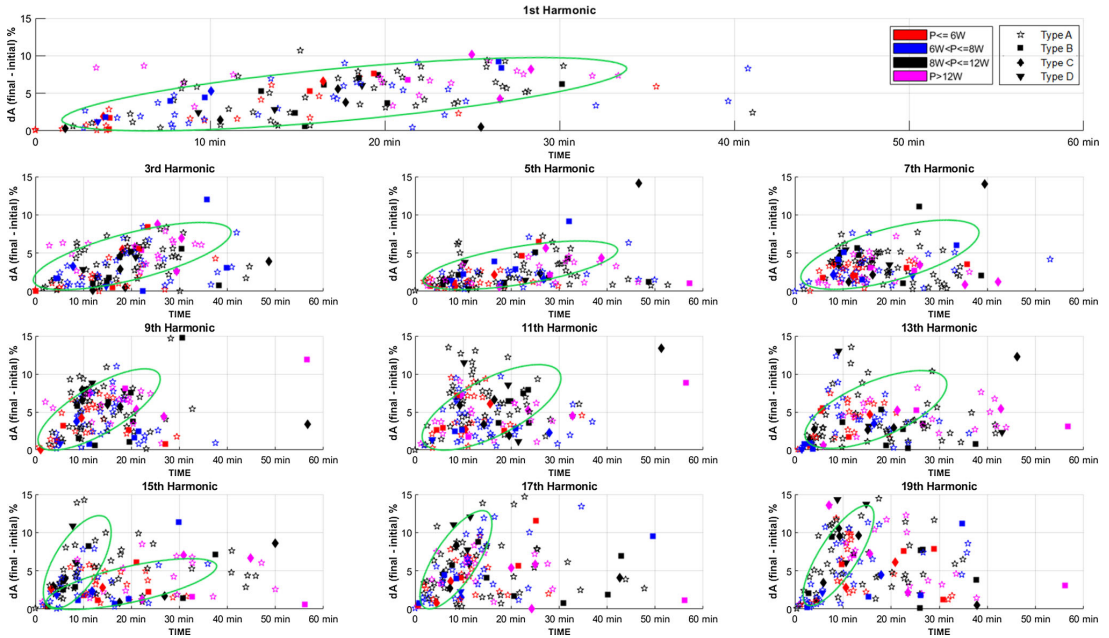sumption is further divided into three intervals: morning, day,

Fig. 10 d_A (%) against time for all LED lamp types

and evening cycles. The measurement data shows an identical usage pattern during these intervals. The consumption patterns during weekdays and weekends were also different. The occupancy profiles were created by studying the electrical appliance usage data that comes in direct contact with the occupants. For example, lighting, cooking, washing, cleaning, and media appliances are the active appliances used by the occupants directly. The usage pattern of each lamp is divided into switching and noise events. A switching event occurs when the lamp is used for more than 10 min. When the lamp is used for less than 10 min, it is accounted for a noise event. The switching and noise events during the morning, day, and evening intervals are calculated for all the lamps. Based on this input data, a statistical model is formulated to determine the lighting load in a residential building.

Empirical distribution function (ECDF) is used to calculate the probability density function of occupancy profiles, the number of switching and noise cycles in the morning, day, and evening intervals. Equation (10) is used to calculate the ECDFs.

$$P_n\,(X \leq x) = \frac{1}{n} \sum_{i=1}^{n} 1\,[x_i \leq t] \tag{10}$$

Here n is the sample size of possible values and $1[x_i \leq t]$ is the indicator function. The indicator function has two possi-

ble values and is given by Eq. (11).

$$1\,[x_i \leq t] = \begin{cases} 1 & \text{for } x_i \leq x \\ 0 & \text{for } x_i > x \end{cases} \tag{11}$$

Therefore, by calculating all the data less or equal to the given value x, we can find the probability P_n by dividing it with the sample size. The ECDFs for the number of switching events and noise events are calculated for each interval for all days. The duration of each switching event D_{sw} and noise events d_{ns} is used to find the total lighting demand of each house for a day with the 1-s resolution, as shown by Eq.(12).

$$P_T = \sum_{sw=1}^{n} (D_{sw} \times P_{sw}) + \sum_{ns=1}^{n} (d_{ns} \times P_{ns}) \tag{12}$$

The lighting power consumed during each switching and noise events P_{sw} and P_{ns} is calculated by Eq. (13) and Eq. (14).

$$P_{sw} = \sum_{s=1}^{n} \sum_{L=1}^{m} P_L \times T_s \tag{13}$$

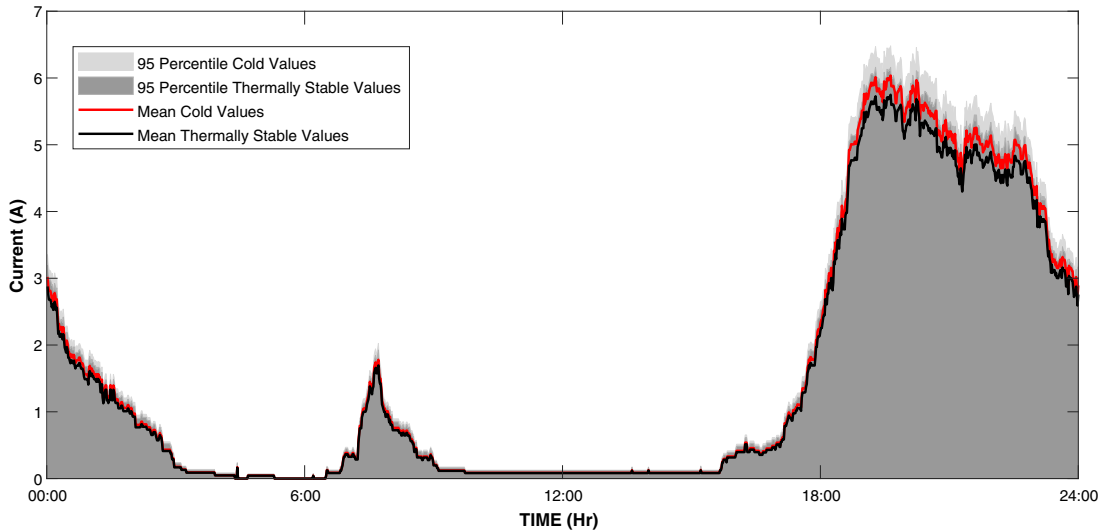$$P_{ns} = \sum_{N=1}^{n} \sum_{L=1}^{m} P_L \times T_N \tag{14}$$

Fig. 11 Estimated fundamental current difference for cold and thermally stable measurements

The T_s and T_N are the time duration for each individual switching and noise event, respectively. A Monte Carlo approach is used by selecting random lamps based on the light output needed in each room. The light output is calculated by the type of lamps used in the building measured for the data collection. During each run, lamps were selected randomly form uniform distribution. The cold and thermal stable measurements for each lamp were used to find the current harmonics for 60 houses during each run. The number of lamps in each house may vary from 5 to 11.

Figure 11 shows the fundamental component variation of lighting usage in 60 houses. The bold black line shows the mean value of the fundamental current when thermally stable values are used in the simulation model for calculation. The red line shows the mean value when cold lamp measurement data are used. The difference is more noticeable during the evening peak. It is evident from Fig. 11 that the mean value difference is quite significant. Therefore, the cold measurements will result in inaccuracy in the estimation of current harmonics. The boundary of the light grey shaded area indicates the 95 percentile values of the 100 run Monte Carlo model simulation when cold lamps measurements are used. The dark grey area boundary indicates the 95 percentile values of fundamental current magnitude when thermal stable values are used. A comparison is made between the harmonic currents estimated using measurements with thermally stable and normal values with a cooling effect in a previous study, but the results show a negligible difference [11]. Although lamp cooling may affect the current harmonics, the mean variation will be between black and red lines as shown in Fig. 11.

Figure 12 shows the difference between the mean current magnitude estimated using cold and thermally stable measurements for the higher-order harmonics. All current harmonics show a significant difference in the magnitude estimated using cold and stable values. The 7th and 9th harmonic current magnitudes show a higher value for thermally stable measurements in contrast to the cold measurements. For the remaining harmonics, the estimated current magnitude is higher when the value of the cold measurement is used.

Therefore, for an accurate estimation of power quality indexes, the thermal stability of the lamps is critical; otherwise, it will lead to significant errors in the estimation. Hence, the measurements should be taken once the LED lamps become thermally.

7 Conclusion

A detailed analysis of the time-dependent variation in the harmonic current emission by LED lamps during power quality measurements is discussed in this paper. It is evident that the difference between the measurements taken in the cold state and the thermally stable state is quite significant. This will result in a substantial error while estimating the magnitude of current harmonics in the real-time scenarios where a large number of LED lamps are involved. The thermal stability time is independent of the type of LED driver circuit topology as different types of LED lamps show a similar range of stability time. However, stability time depends on the active power of the lamp. High-power lamps show more difference
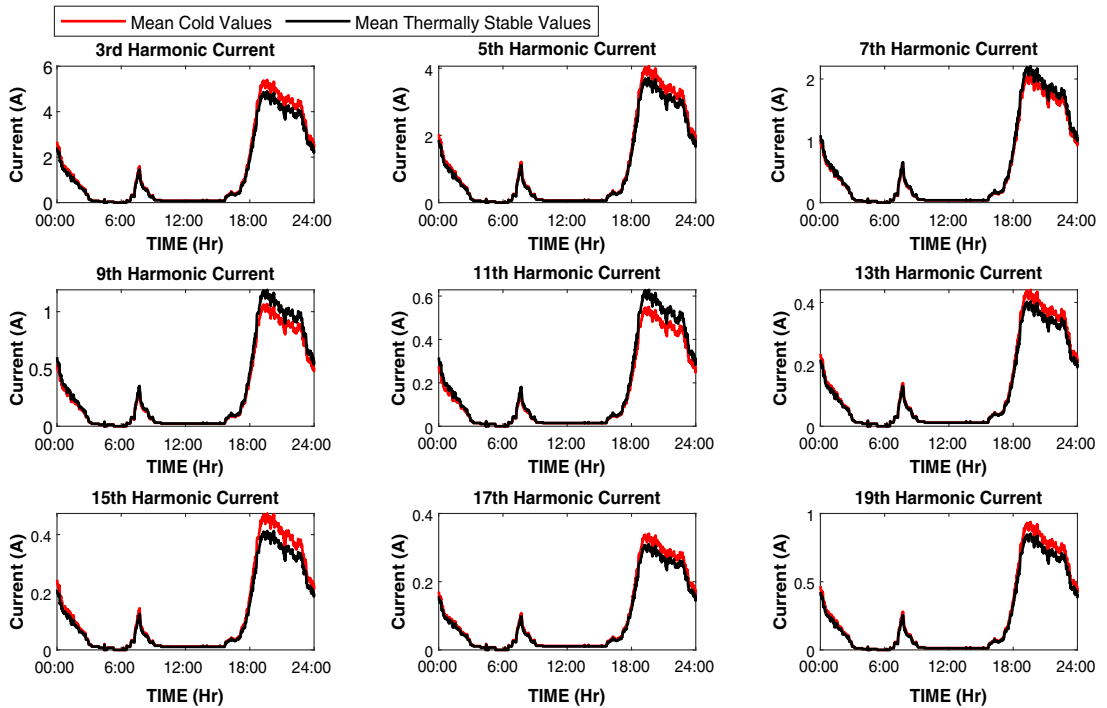
Fig. 12 Higher harmonic current difference for cold and thermally stable measurements

between the current harmonics magnitude and phase angles measured at the cold and thermally stable state. The THD_i difference between a cold and thermally stable state of LED lamps also increases with the active power. Therefore, the stability time tends to be higher for more powerful LED lamps. 95% of LED lamps have stable current harmonics magnitude and phase angles after 40 and 35 min, respectively. Therefore, majority of the LED lamps under 25 W achieve a thermally stable state in 40 min. The maximum time taken by the lamp to become thermally stable was 57 min. However, the lamps with active power more than 25 W may take more time to get thermally stable. LED lamps with significant differences in the current harmonics at cold and thermally stable state have longer stability time.

A lighting usage model is used to observe the effect of time variation of current harmonics in the distribution grid. The results show a notable difference for estimated fundamental and odd current harmonics for sixty houses. Therefore, the time-dependent variations in current harmonics measurements lead to a significant error, and LED lamps should be warmed for 60 min before performing power quality measurements.

References

1. European Commission (2011) Lighting the future: accelerating the development of innovative lighting technologies. Technical report, European Commission
2. Bladh M, Krantz H (2008) Towards a bright future? Household use of electric light: a microlevel study. Energy Policy. https://doi.org/10.1016/j.enpol.2008.06.001
3. Blanco AM, Stiegler R, Meyer J (2013) Power quality disturbances caused by modern lighting equipment (CFL and LED). In: IEEE grenoble conference PowerTech, POWERTECH 2013, pp 1–6. https://doi.org/10.1109/PTC.2013.6652431
4. Strack JL, Suárez JA, Fabián G, Mauro D, Jacob SB, Strack J, Suárez J, Mauro GD, Jacob S (2014) Impact of efficient residential lighting on power quality of a distribution network. Rev Inge CuC 10:9–19
5. European Commission (2015) Guidelines accompanying Regulation (EU) No 874/2012 with regard to the energy labelling of lighting products, and Regulations (EC/EU) No 244 and 245/2009 and 1194/2012 with regard to ecodesign requirements for lighting products-July 2015. DOI OJ L 224, 27.8.2015
6. The European Parliament (2009) Commission Regulation (EC) No 244
7. Zimmermann JP, Evans M, Lineham T, Griggs J, Surveys G, Harding L, King N, Roberts P (2012) Household electricity survey: a study of domestic electrical product usage. Intertek, London
8. Bertoldi G (2018) Status of LED-lighting world market in 2017. Technical report, Joint Research Centre (JRC), European Commission

9. Clement-Nyns K, Haesen E, Driesen J (2010) The impact of charging plug-in hybrid electric vehicles on a residential distribution grid. IEEE Trans Power Syst 25(1):371. https://doi.org/10.1109/TPWRS.2009.2036481

10. Watson NR, Scott TL, Hirsch SJ (2009) Implications for distribution networks of high penetration of compact fluorescent lamps. IEEE Trans Power Deliver 24(3):1521. https://doi.org/10.1109/TPWRD.2009.2014036

11. Naveed Iqbal M, Jarkovoi M, Kutt L, Shabbir N (2019) Impact of LED thermal stability to household lighting harmonic load current modeling. In: Electric power quality and supply reliability conference and 2019 symposium on electrical engineering and mechatronics, PQ and SEEM. https://doi.org/10.1109/PQ.2019.8818226

12. Islam MS, Chowdhury NA, Sakil AK, Khandakar A, Iqbal A, Abu-Rub H (2015) Power quality effect of using incandescent, fluorescent, CFL and LED lamps on utility grid. In: 1st Workshop on smart grid and renewable energy, SGRE 2015. IEEE, pp 1–5. https://doi.org/10.1109/SGRE.2015.7208731. http://ieeexplore.ieee.org/document/7208731/

13. Nohra AF, Kanaan HY, Al-Haddad K (2012) A study on the impact of a massive integration of compact fluorescent lamps on power quality in distribution power systems. In: International conference on renewable energies for developing countries, REDEC 2012. IEEE, pp 1–6. https://doi.org/10.1109/REDEC.2012.6416700. http://ieeexplore.ieee.org/document/6416700/

14. Ogunjuyigbe AS, Ayodele TR, Idika VE, Ojo O (2017) Effect of lamp technologies on the power quality of electrical distribution network. In: Proceedings of IEEE PES-IAS PowerAfrica conference: harnessing energy, information and communications technology (ICT) for affordable electrification of Africa. PowerAfrica 2017, pp 159–163. https://doi.org/10.1109/PowerAfrica.2017.7991216

15. Sadek MH, Abbas AA, El-Sharkawy MA, Mashaly HM (2004) Impact of using compact fluorescent lamps on power quality. In: Proceedings of international conference on electrical, electronic and computer engineering, ICEEC'04, pp 941–945. https://doi.org/10.1109/iceec.2004.1374641

16. Blanco AM, Parra EE (2010) Effects of high penetration of CFLS and LEDS on the distribution networks. In: Proceedings of 14th international conference on harmonics and quality of power–ICHQP 2010. IEEE, pp 1–5. https://doi.org/10.1109/ICHQP.2010.5625420. http://ieeexplore.ieee.org/document/5625420/

17. Matvoz D, Maksic M (2008) Impact of compact fluorescent lamps on the electric power network. In: 13th International conference on harmonics and quality of power. IEEE, pp 1–6. https://doi.org/10.1109/ICHQP.2008.4668864. http://ieeexplore.ieee.org/document/4668864/

18. Uddin S, Shareef H, Mohamed A, Hannan MA (2012) An analysis of harmonics from dimmable LED lamps. In: IEEE international power engineering and optimization conference, PEOCO 2012–conference proceedings, pp 182–186. https://doi.org/10.1109/PEOCO.2012.6230857

19. Gil-De-Castro A, Moreno-Munoz A, Larsson A, De La Rosa JJ, Bollen MH (2013) LED street lighting: a power quality comparison among street light technologies. Light Res Technol 45(6):710. https://doi.org/10.1177/1477153512450866

20. Brunner EJ, Ford PS, McNulty MA, Thayer MA (2010) Compact fluorescent lighting and residential natural gas consumption: testing for interactive effects. Energy Policy 38(3):1288. https://doi.org/10.1016/j.enpol.2009.11.003

21. Tetri E, Bhusal P (2010) Annex 45 guidebook on energy efficient electric. Technical report, International Energy Agency. www.lightinglab.fi/IEAAnnex45

22. Khan N, Abas N (2011) Comparative study of energy saving light sources. https://doi.org/10.1016/j.rser.2010.07.072

23. Chen N, Chung HSH (2011) A driving technology for retrofit LED lamp for fluorescent lighting fixtures with electronic ballasts. IEEE Trans Power Electron 26(2):588. https://doi.org/10.1109/TPEL.2010.2066579

24. Kasap S, Capper P (eds) (2017) Springer handbook of electronic and photonic materials. Springer, Cham. https://doi.org/10.1007/978-3-319-48933-9

25. Nardelli A, Deuschle E, de Azevedo LD, Pessoa JLN, Ghisi E (2017) Assessment of Light Emitting Diodes technology for general lighting: a critical review. Renew Sustain Energy Rev. https://doi.org/10.1016/j.rser.2016.11.002

26. Thallam RS, Doyle MT, Krein SD, Samotyj MJ, Mansoor A, Grady WM (1995) Effect of supply voltage harmonics on the input current of single-phase diode bridge rectifier loads. IEEE Trans Power Deliv. https://doi.org/10.1109/61.400924

27. Uddin S, Shareef H, Mohamed A (2013) Power quality performance of energy-efficient low-wattage LED lamps. Meas J Int Meas Confed 46(10):3783 10.1016/j.measurement.2013.07.022

28. Dolara A, Leva S (2012) Power quality and harmonic analysis of end user devices. Energies 5(12):5453. https://doi.org/10.3390/en5125453

29. Xu X, Collin A, Djokic SZ, Langella R, Testa A, Drapela J (2017) Experimental evaluation and classification of LED lamps for typical residential applications. In: IEEE PES innovative smart grid technologies conference Europe, ISGT-Europe 2017-proceedings. https://doi.org/10.1109/ISGTEurope.2017.8260292

30. Power I (2015) Direct-AC, linear LED driver topology: CCR straight circuit (120 V AC, 230 V AC). Technical report, ON Semiconductor

31. Xiao X, Collin AJ, Djokic SZ, Yanchenko S, Moller F, Meyer J, Langella R, Testa A (2017) Analysis and modelling of power-dependent harmonic characteristics of modern PE devices in LV networks. IEEE Trans Power Deliv. https://doi.org/10.1109/TPWRD.2016.2574566

32. Uddin S, Shareef H, Mohamed A, Hannan MA, Mohamed K (2011) LEDs as energy efficient lighting systems: a detail review. In: Proceedings of IEEE student conference on research and development, SCOReD 2011. https://doi.org/10.1109/SCOReD.2011.6148785

33. Jarkovoi M, Naveed Iqbal M, Kutt L (2019) Analysis of harmonic current stability and summation of LED lamps. In: Electric power quality and supply reliability conference and 2019 symposium on electrical engineering and mechatronics, PQ and SEEM 2019. IEEE. https://doi.org/10.1109/PQ.2019.8818237

34. Bollen MHJ, Ronnberg SK (2016) Primary and secondary harmonics emission; harmonic interaction—a set of definitions. In: 17th International conference on harmonics and quality of power (ICHQP), vol 2016-Decem, vol 2016-Decem, pp 703–708. IEEE. https://doi.org/10.1109/ICHQP.2016.7783333. http://ieeexplore.ieee.org/document/7783333/

35. Janiga P, Gasparovsky D (2011) Power quality in public lighting installations, chap. 3. In: Eberhard A (ed) Power quality. IntechOpen, Rijeka. https://doi.org/10.5772/14581

36. Iqbal MN, Kutt L, Rosin A (2018) Complexities associated with modeling of residential electricity consumption. In: IEEE 59th Annual international scientific conference on power and electrical engineering of Riga Technical University, RTUCON 2018-Proceedings. IEEE, pp 1–6. https://doi.org/10.1109/RTUCON.2018.8659812. https://ieeexplore.ieee.org/document/8659812/

II

M. N. Iqbal, L. Kütt, B. Asad, T. Vaimann, A. Rassõlkin, and G. L. Demidova, "Time dependency of current harmonics for switch-mode power supplies," Applied Sciences, vol. 10, p. 7806, Nov 2020

Time Dependency of Current Harmonics for Switch-Mode Power Supplies

Muhammad Naveed Iqbal [1,*], **Lauri Kütt [1]**, **Bilal Asad [1,2]**, **Toomas Vaimann [1,3]**, **Anton Rassõlkin [1,3]** and **Galina L. Demidova [3]**

1   Department of Power Engineering and Mechatronics, Tallinn University of Technology, Ehitajate tee 5, 19086 Tallinn, Estonia; lauri.kutt@taltech.ee (L.K.); bilal.asad@aalto.fi (B.A.); toomas.vaimann@taltech.ee (T.V.); anton.rassolkin@taltech.ee (A.R.)
2   Department of Electrical Engineering and Automation, Aalto University, 02150 Espoo, Finland
3   Faculty of Control Systems and Robotics, ITMO University, 197101 Saint Petersburg, Russia; demidova@itmo.ru
*   Correspondence: miqbal@taltech.ee

check for updates

Featured Application: The time-dependent variations in current harmonic emission from switch mode power supplies are often not considered during power quality measurements. It can affect the results of the current harmonic estimation models as switch-mode power supplies constitute a significant portion of domestic, commercial, and industrial electrical loads.

Abstract: This paper presents the time-dependent variance in the current harmonics emission by power supplies during power quality measurements. Power quality problems are becoming more significant with the adoption of power electronic-based circuits such as power supplies. The switch-mode power supplies are widespread as industrial, commercial, and domestic electrical loads. They draw non-sinusoidal current from the utility and inject current harmonics. Therefore, they are the reason for poor power quality and reduction in the power factor. The current harmonics emission from these power supplies depends on the circuit topology, operating conditions, and filter inside them. The harmonic emission estimations are critical for network operators; however, various uncertainties have made it a complicated task. The time-dependent stability affects the magnitude and phase angle of the harmonic current measurements and estimation of power quality indices. This paper investigates the variation in current harmonics emitted by the power supply during the initial unstable period under constant load and operating conditions.

1. Introduction

Power quality issue is becoming critical for the network operators and electrical equipment manufacturers in the last few years. The electronics-based switching devices are burgeoning and escalating the current harmonics emission level in the electric supply system. With the enhancement in power electronics, the efficiency of domestic, commercial, and industrial electronic equipment has been boosted with a substantial reduction in their size. Almost every modern electrical equipment, such as personal computers (PC), battery chargers, household appliances, large commercial and industrial electrical systems encompasses a converter based power supply. These power supplies incorporate rectifiers and nonlinear components, thus polluting the distribution system with current harmonics. Therefore, current harmonic estimation is critical for power quality assessment. Probabilistic models

for current harmonic estimation are based on the measurements of the electrical loads [1] and most of the non-linear loads can be modeled as different switch-mode power supplies [2]. However, the time-dependent stability of the current harmonics generated by the power supplies may alter the outcome of such estimations. This paper deals with the deviation in the current harmonics magnitude and phase angles of switch-mode power supplies over time under constant load and input voltage.

The direct current (DC) power supply takes input from the utility or local DC source such as a battery. It maintains an interminable voltage level within the designed current limits and can be regulated or unregulated. The regulated power supplies uphold the output voltage close to the desired nominal value for the variations in voltage, load current, and temperature [3]. The switch-mode power supplies (SMPS) are regulated power supplies and contain alternating current to direct current (AC-DC) converters. Because of the nonlinear components in the SMPS, they are the source of power quality problems and feed current harmonics in the network.

These current harmonics prompt voltage distortion and the power factor reduction in the network. The current harmonics and voltage distortion cause overloading of the transformers. Their lifespan is reduced, and reliability is compromised. Excessive harmonic emission overheats electrical appliances and causes additional noise. Moreover, protection equipment, such as relays and circuit breakers, can also malfunction. Apart from polluting the network, these harmonics also affect the performance of SMPS itself [4]. Therefore, it is essential to estimate the impact of current harmonics emission in the network added by nonlinear power supplies. However, various uncertainties are associated with the power system that may affect the power quality estimations. Supply voltage variation and load operating modes can alter the harmonic emission in the grid [5]. The components present inside various electrical appliances may provide a variation because of material properties [6]. The aging of the components also affects the output [7]. The variation in power system operating conditions also results in variation of the network impedance [8,9]. However, uncertainties in the measurement of power quality indices like thermal stability of the components and transients are mostly ignored in the harmonic estimation models available in the literature.

Since SMPS are widely used in industrial, commercial and domestic loads, their collective impact could be devastating. Household loads in a residential distribution grid can be categorized into the linear load and the electronic load. However, electronic appliances are responsible for the majority of the current harmonic emission. These devices can be modeled as SMPS loads. Household appliances are categorized based on the SMPS circuit topologies in [2]. Consequently, for an accurate power quality assessment, every uncertainty during measurements of SMPS should be taken into account.

Several studies are available related to harmonic emission associated with the SMPS load. The harmonic cancellation between multiple SMPS operated at the same time has been presented in [10]. A Monte Carlo simulation is used to aggregate numerous SMPS loads. The author concludes that harmonic cancellation is more prominent in high power SMPS. The losses due to harmonic current injected by SPMS in a commercial building are discussed in [11]. The harmonic losses generated by modern electronics in the commercial buildings are responsible for neutral conductor overloading, overheating of the cables, and power factor reduction. The author projected an 8 kW of additional losses due to harmonic loading caused by SMPS. It will increase the total building wiring losses by up to 250%. The wiring loss caused by personal computers without harmonic elimination is 2.4 times compared to resistive loads. The comparison of electromagnetic interference in the grid due to series and parallel configuration of SMPS load is presented in another study [12]. A computer simulation is used to estimate the noise effectuated by SMPS in [13]. Topologies of SMPS are simulated to find the dimension that can impede noise emission defined by the standards. A Simulink model is used to scrutinize the current harmonics generated by the SMPS in another study [14]. The nonlinear loads can be imitated as parallel harmonic current sources with magnitude and phase angles [15]. A total harmonic distortion between 150% to 200% for different 3-phase balanced and unbalanced schemes was reported. The harmonic current injection was influenced by the number of equipment, circuit topologies, and type of equipment. The imbalance of the phase lines also altered the harmonic

injection. The current harmonic generation due to SMPS inside computers and other electronic equipment and the harmonic mitigation effects in the large office building is presented in [16].

Although, the studies mentioned above have considered uncertainties like harmonic cancellation, none of them discuss the effect of time-dependent variations of the harmonic currents due to thermal stability. A recent study reported significant variation in current harmonics magnitude and phase angles of LED lamps when pure sinusoidal voltage is applied [17]. LED lamps also contain rectifier circuits and draw a current waveform similar to the SMPS. The study concludes that by using measurements performed during the period when LED lamps were unstable leads to a significant error in harmonic current estimation.

This paper presents the results of the harmonic current variation of different industrial switch mode power supplies under constant load and operating conditions. A comprehensive overview of SMPS is presented in Section 2. The details of the experimental setup are described in Section 3. Section 4 includes a detailed analysis of the experimental results and framework to estimate the stability time of the power supplies. A comparison of the stability time of power supplies is also described in this section. Conclusions are presented in Section 5.

2. SMPS Overview

The SMPS converts AC to DC power by using switching devices, inductors, and capacitors. They deliver stable power to many industrial, commercial, and domestic electrical systems proficiently, as they contain rectifier circuits, consequently drawing non-sinusoidal current from the grid. As a result, they have low power factor and power quality [18]. SMPS are common in computers and battery chargers of different home appliances. A typical computer SMPS operates at 220V and draws input current with a total current harmonic distortion (THD$_i$) of 80%, and the power factor around 0.6 [19]. The block diagram of an SMPS is shown in Figure 1. The electromagnetic interference (EMI) filter reduces the high-frequency noise, and the inrush current limiter protects the circuit from the initial current surge due to capacitor charging. Most high power SMPS also contains a power factor correction circuits (PFC) to improve voltage regulations. The rectifier converts the input AC power to DC using switching devices like a diode, Insulated gate bipolar transistor IGBT, or MOSFET. The DC to DC converter is used to convert the input DC from one voltage level to another.
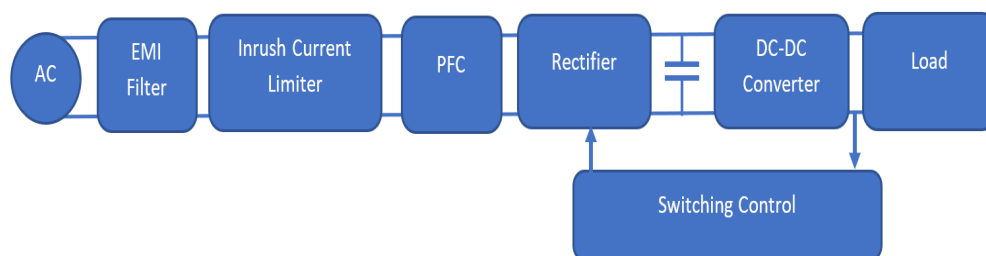

Figure 1. Block diagram of a typical switch-mode power supply.

The latest development in power electronics has enabled us to produce more efficient DC power supplies with improved power factor and stable output [20]. Modern design possesses low conduction losses and synthesizes near sinusoidal current waveform leading to fewer problems related to power quality. The SMPSs are classified based on the converters, power factor correction circuits, and type of switching control strategy [21]. The converter topology classification includes buck, boost, buck-boost, and multilevel converters [3]. The control strategies include pulse width modulation (PWM), proportional integral derivative (PID), sliding mode control (SMC), adaptive control, and neural network controllers. Many other control strategies are also employed and discussed in the literature [22]. The single-stage power supplies are widespread as they implement power conversion using a single switching circuit and simple control [23]. However, in computers and other

advanced applications, the single-stage power supplies are inadequate because of the stress across the switch and poor voltage regulations [22]. The SMPS in computers provides multiple DC outputs, and PFC circuits are used in the first stage for improving power factor and harmonics in the input current [24,25]. The impact of computer power supplies and other electronic equipment on the network has been discussed in [26]. Similar studies have also estimated the impact of computer power supplies and other new harmonic sources on the grid [27,28]. Most computer power supplies incorporate passive PFC circuits due to strict emission standards [29]. Researchers have proposed several designs with improved PFC for SMPS used in computer applications [30,31]

SMPS can be classified based on the type of filter circuits. Mostly low power SMPS (less than 75W) does not contain any PFC circuits. The high power SMPS may contain active or passive PFC. The devices with passive PFC contain a large inductor to smooth the variations in the current. On the other hand, devices with active PFC encompass an additional DC-DC converter. The SMPS with active PFC generates fewer harmonics than SMPS with passive PFC.

We have selected six single-phase SMPS from different manufacturers in the range of 30 W to 120 W. Table 1 shows the detailed specification of all six SMPS. The power supplies are categorized into two types based on the shape of the input current waveforms. Figure 2 shows the current waveform of both types of SMPS. Type 1 power supplies include passive filtering circuits to improve the power factor. The current waveform drawn by type 2 power supplies shows that they contain typical rectifier circuits without filters. We have applied 60% of the rated load current using the programmable electronic load to the power supply and recorded the input current drawn by the SMPS.

Table 1. Switch-mode power supplies (SMPS) characteristics.

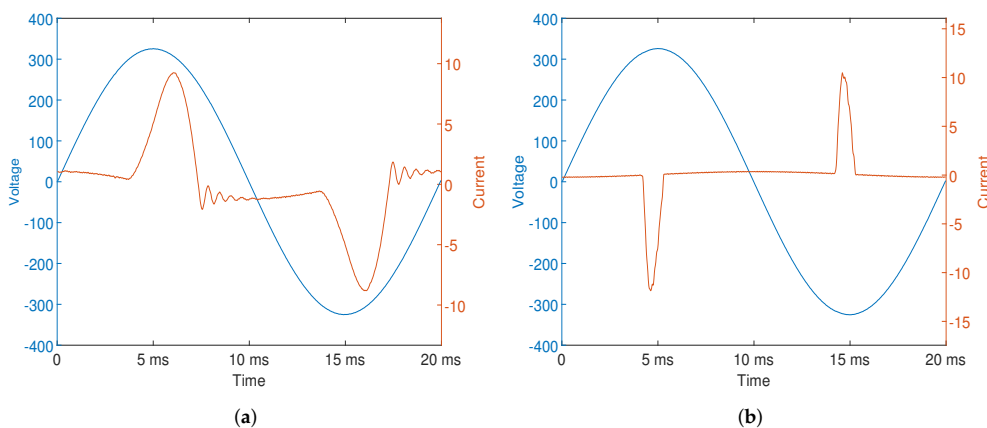| No.	Manufacturer	Model	Input Current AC (A)	Output Current DC (A)	Output Voltage DC (V)
1	ABB, Zürich, Switzerland	CP-E	0.83	5	24
2	Dran, Chinfa Electronics, Taiwan	120-24x	0.63	5	24
3	Entrelec,Germany	Systron 2A	0.30	2	24
4	Omron, Kyoto, Japan	S8VS-03024	0.60	1.3	24
5	Siemens logo, Munich, Germany	6EP1331-1SH03	0.70	1.3	24
6	Siemens, Munich, Germany	6EP1332-1SH71	0.67	2.5	24

Figure 2. Current waveform drawn by SMPS (**a**) Type 1 (**b**) Type 2.

The current harmonic limits are defined in the International Electrotechnical Commission (IEC) 61000-3-2. The SMPS less than 600 W comes under class D equipment. Table 2 represents the maximum allowed harmonic current and harmonic currents per watt for odd harmonics [32].

Table 2. Current harmonic limits for class D devices.

Harmonic Order (h)	Maximum Permissible Harmonic Current per Watt (mA/W)	Maximum Current Harmonic Limit (A)
3	3.4	2.30
5	1.9	1.14
7	1	0.77
9	0.5	0.40
11	0.35	0.33
$13 \leq h \leq 39$	3.85/h	0.15(15/h)

3. Measurement Setup

We have measured six SMPS for 60 min with our test bench and evaluated their THD_i and current harmonics. The test bench involves a personal computer (PC), a 4kVA controllable power supply Chroma 61505 (Chroma system solutions, USA), a data acquisition (DAQ) module (National Instrumentation, United States), controllable electronic DC load TENMA 72-13210 (Premier Farnell, United Kingdom) and power quality measurement device a-eberle PQ-Box 200 (A-Eberle, Germany). The PQ-Box 200 can record at 200 ms resolution according to the standards IEC 61000-4-30 for CLASS A. These 200 ms data points are aggregated to 1-s interval data available to extract from the PQ-Box 200. Relays are used to switch all SMPS automatically. A control box is designed to provide 12V DC to the relays. The 50 Hz reference waveform for the power supply is generated with a sampling frequency of 100 kHz using MATLAB program through the DAQ module. The DAQ module is capable of generating an analog signal corresponding to the digital input. This reference signal (V_{rf}) has enabled us to generate a pure sinusoidal voltage through the programmable power supply as defined by Equation (1).

$$V_{rf} = \frac{V_o}{V_{range}} \times V_{co} \tag{1}$$

Here, V_{range} is 300 V and V_{co} is 7.072. The digital inputs to switch the relays are also generated using the same the MATLAB program via the DAQ module. The reference signal is calculated by using the relation indicated by Equation (2).

$$V_{out} = \sum_{i=1}^{n} \sqrt{2} \times A_i \sin(2\pi f_i t_s + \alpha_i) \tag{2}$$

A_i and α_i are the root mean square values of the harmonics and its phase difference from the fundamental frequency, respectively. The harmonic frequency is shown by f_i and sampling interval by t_s. The number of samples needed for the specific duration (T_m) of the voltage output from the controllable power supply can be calculated by Equation (3).

$$n = T_m \times f_s \tag{3}$$

Here f_s is the sampling frequency and its value is 100 kHz. The controllable DC electronic load is used to operate each SMPS with 60% of its rated capacity. Figure 3 shows the block diagram of our test setup.
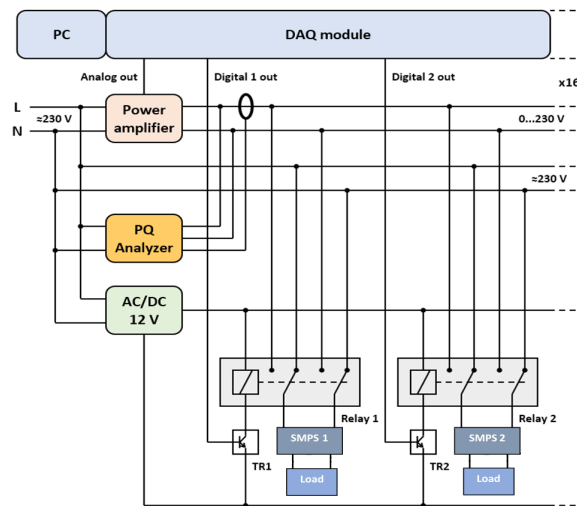
Figure 3. Block diagram of the measurement setup.

4. Results and Discussion

The measurement setup is used to test all six SMPS on pure sinusoidal voltage. The measurement is performed for 1 h, and 60% of the rated load is applied to each SMPS. The THD_i, current harmonics magnitude, and phase angles are analyzed. Figure 4 shows the absolute percentage difference between the THD_i measured when the power supplies are in the cold state and stable state. The term "cold state" indicates the first five minutes of the measurements, and the "stable state" indicates the duration when the harmonic current variation is less than 0.25%. The first two power supplies indicate only 1.2% and 0.6% difference between the THD_i measurements at the cold and stable state. However, the remaining power supplies have shown a significant difference between THD_i values at the cold and the stable state. The fifth power supply shows the highest variance of 21%. Both third and fifth SMPS have a variation of 18 to 19% between cold and stable state. Similarly, the fourth SMPS shows a difference of 14.8%. Hence, Figure 4 indicates that type 1 SMPS shows a minimal difference in contrast to type 2 SMPS.
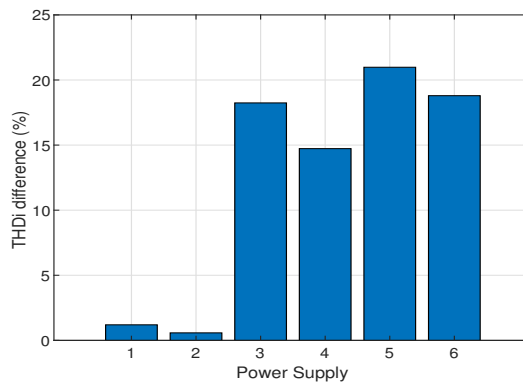

Figure 4. Histogram of total current harmonic distortion (THD_i) difference between cold and stable state of all power supplies.

To estimate the stability time of power supplies, we have used the curve-fitting approach to the current harmonic amplitude and phase angle variations over time. An exponential trend curve is

applied to the current harmonics magnitude, and phase angles up to the 19th harmonic. Equation (4) is used to calculate the parameters of the trend line using measurement data of the current harmonic magnitude and phase angle.

$$T_L = \triangle_i \times e^{\left(-\frac{i_t}{T_C}\right)} + \gamma_{stable} \tag{4}$$

γ_{stable} is the current magnitude or phase value in the stable state. The delta $\triangle_i$ is the difference between the current harmonic magnitude or phase angle in the cold state and the stable state and calculated by Equation (5).

$$\triangle_i = \gamma_{stable} - \gamma_{cold} \tag{5}$$

The time constant in Equation (4) T_C is the time taken by the exponential trend curve to increase or decrease by the factor e. It is calculated by using Equation (6).

$$T_C = \frac{T_{final} - T_{cold}}{1 - \ln(1 - \frac{1-(\gamma_{stable}-\gamma_{cold})}{\triangle_i}} \tag{6}$$

The stability time (T_{stable}) of the current harmonic magnitude and phase angle is three times of the time constant (T_C). Figure 5 shows the current magnitude variation of the fundamental and odd harmonics up to the 19th for the third power supply. The green line shows the measured harmonic current, and the blue line indicates the applied trend curve. The red dot indicates the time constant, and the black dot shows the stability time. A similar approach is applied to the phase angles of odd harmonics up to the 19th, as shown in Figure 6.
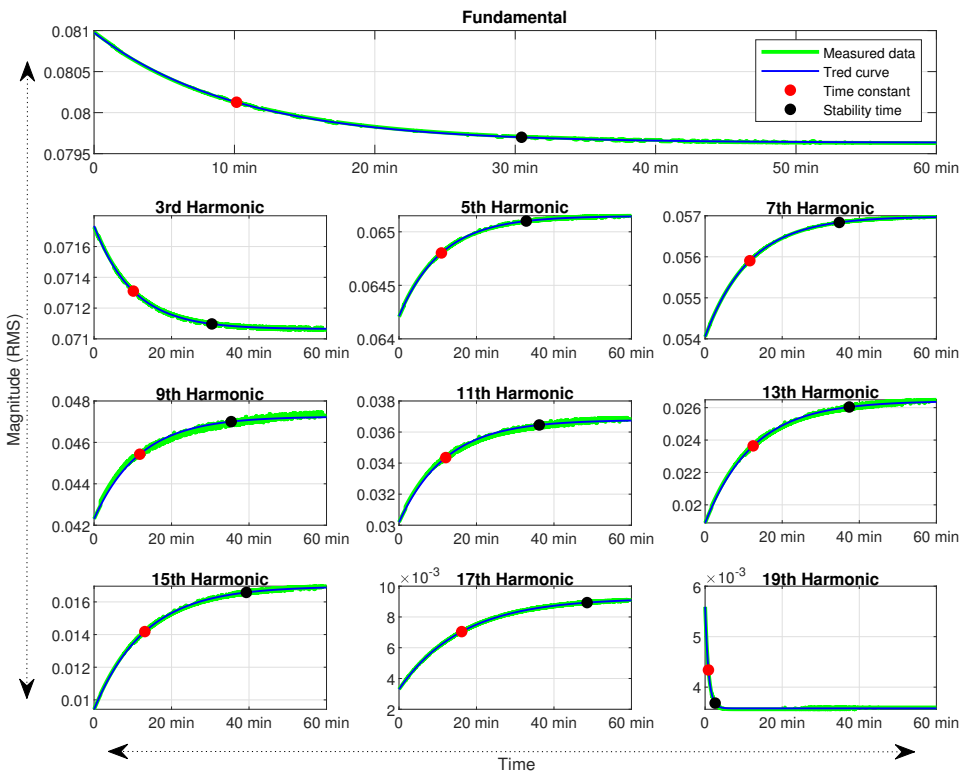

Figure 5. Current harmonic magnitude variation over time for power supply 3.
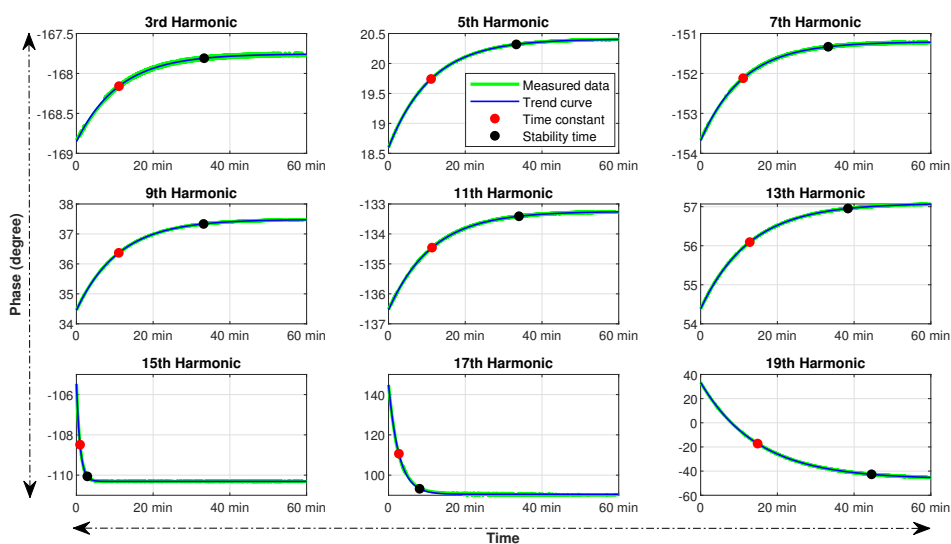
Figure 6. Current harmonic phase variation over time for power supply 3.

The difference between the cold and stable values of harmonic current magnitude and phase angles are more significant for type 2 power supplies. For type 1 power supplies, most of the current harmonics have less than 1% difference in the magnitude. The maximum difference observed for the fundamental and 7th harmonic for the first power supply is 1.2%. The power supply 2 shows the maximum difference of 1.7% for the 11th harmonic. Conversely, the type 2 power supplies exhibit a noteworthy difference, especially for the higher-order harmonics. The maximum difference was up to 194% for the 17th harmonic of power supply 3. Table 3 shows the minimum, maximum, and average deviation of cold and stable current harmonics magnitude for type 2 power supplies. The phase angle variation between cold and stable state is also less for type 1 power supplies. The first power supply only shows more than 1-degree variation for the 3rd, 5th, and 7th harmonic. On the other hand, power supply two shows phase angle variation of more than 1 degree for 15th, 17th and 19th harmonic. The type 2 power supplies show a significant deviation of phase angles between the cold and stable state measurements. Power supply three shows less phase angle variation of between 1–2 degrees among all type 2 power supplies. The other power supplies show a variation of 2 to 35 degrees, increasing from low to higher-order harmonics. Although the IEC 61000-3-2 standards do not define any limits for phase angle variation, the harmonic cancellation depends on current harmonics phase angles.

Table 3. Difference between cold and stable state current harmonics magnitude for type 2 SMPSs (%).

Harmonics	Current Harmonics Magnitude Difference									
	F	**H3**	**H5**	**H7**	**H9**	**H11**	**H13**	**H15**	**H17**	**H19**
Minimum	0.4	0.1	0.8	2.3	4.5	7.6	11.8	17.6	26.2	11.1
Maximum	1.6	1.4	3.7	7.5	13.4	23.8	43.4	88.2	194.7	97.0
Average	0.8	0.6	2.0	5.2	10.0	17.6	30.0	54.7	105.4	39.9

Figure 7a shows the magnitude stability time for all power supplies from fundamental to the 19th odd harmonic. Since the variation between cold and stable state magnitude values for type 1 power supplies is less than type 2, the stability time for type 1 power supplies is also less for most of the current harmonics. The power supply 1 and 2 have maximum stability time for the fundamental and

odd harmonics up to the 7th between 20 and 43 min. However, the 11th and 13th harmonic took more than 60 min to stabilize for the power supply 2. All other magnitudes of current harmonics for these two power supplies are less than the magnitude stability time of type 2 power supplies.
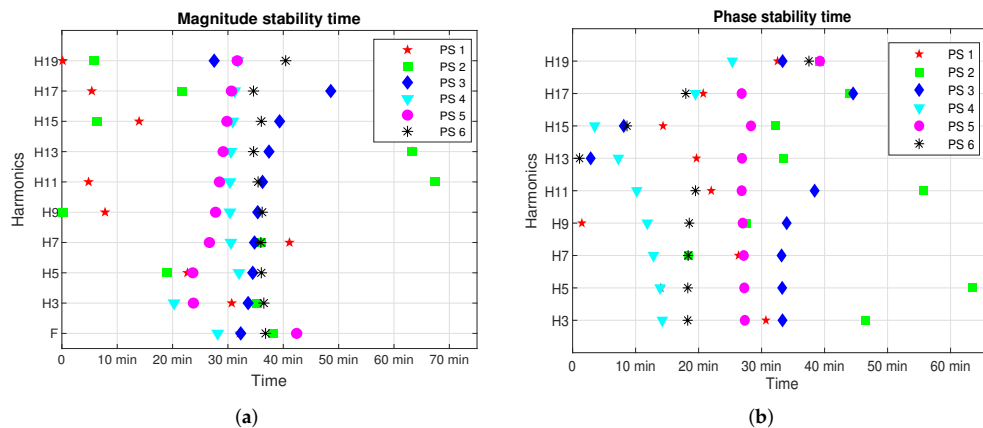

Figure 7. Stability time of current harmonics for all SMPSs (**a**) Magnitude (**b**) Phase.

The stability time for type 2 SMPS is in the range of 20 to 40 min, except for the 17th harmonic of power supply 3. The stability time of power supply 3 and 6 is quite close for most of the current harmonic magnitude. Similarly, the stability time of current harmonics magnitude for power supply 4 and 5 also follows the same trend but less than the power supply 3 and 6. Figure 7b shows the plot for phase angle stability for the odd harmonics for all switch-mode power supplies. Power supply 2 shows the highest value of stability time. For other power supplies, most of the current harmonics achieved stable phase angles before 35 min, except for the few high order harmonics.

The stability time is independent of the active power of the switch-mode power supplies. Figure 8 shows the graph of the active power of the power supplies against the stability time for all current harmonics magnitude up to the 19th harmonic. However, it is interesting to note that power supplies with high active power have less stability time on average in comparison to the power supplies with low active power consumption. This trend is more prominent for the higher-order harmonics.

The overall impact of thermal stability on harmonic current estimation could be significant in the real-time scenario. A similar study had indicated a notable difference for the harmonic current estimation for light-emitting diode (LED) lamps. The RMS current of LED lamps in a stable state was significantly different in comparison to the RMS current in a cold state [10].

Stochastic harmonic estimation models are based on the measurement results of the current harmonics of the electrical appliances. As thermal stability affects the measurement results, it may lead to a significant error in the harmonic analysis results. Figure 9 shows the percentage difference between the current RMS calculated at a cold and stable state for each power supply. Power supply 1 and 2 are type 1; therefore, it shows a small difference of about 1% between cold and stable states. All type 2 power supplies show a significant difference of more than 8% between current RMS values at a cold and stable state. Power supplies 5 and 6 show the maximal difference of more than 13%. Consequently, in a real-time scenario with many power supplies operating in an idle or working state, the estimation of current harmonics would result in an erroneous outcome because of their time-dependent variation.
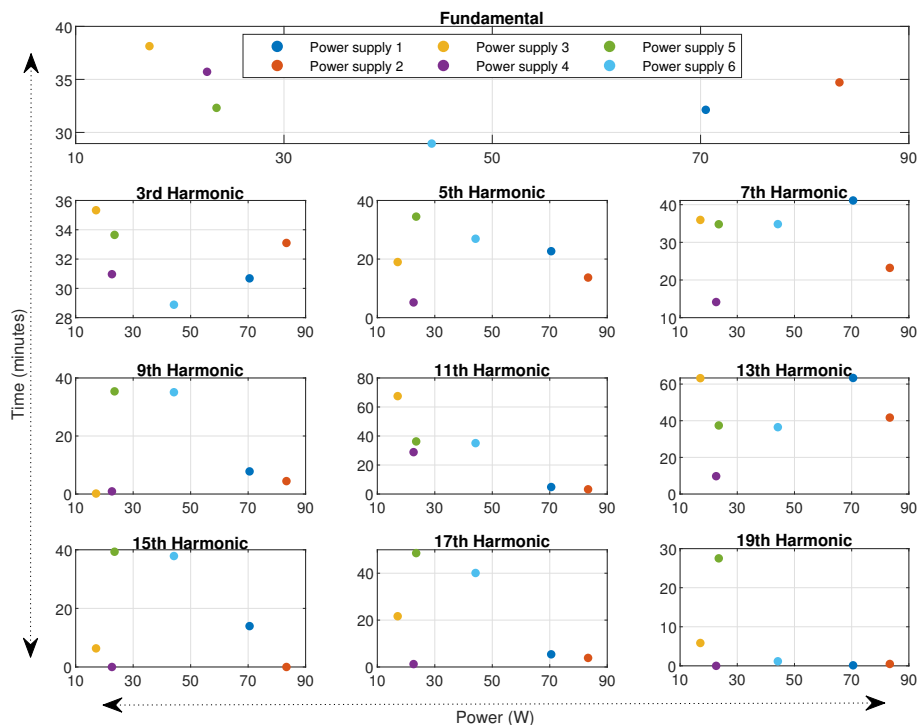
Figure 8. Current harmonic stability time (T_{stable}) variation against active power of all SMPS.
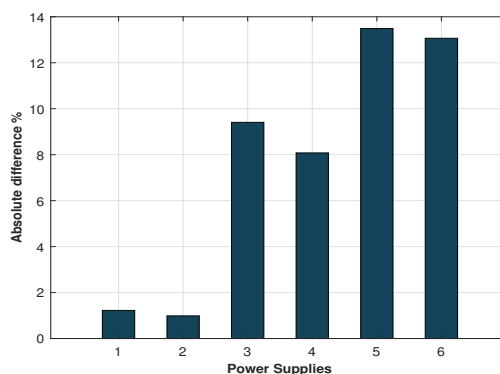

Figure 9. Current RMS difference between Cold and Stable state.

5. Conclusions

As the nonlinear loads are proliferating in the grid, the accurate assessment of power quality problems is becoming vital. The variation in current harmonics for the switch-mode power supplies has been discussed in this paper. The power supplies are categorized into two groups based on the filter circuits. The type 1 power supplies contain filtering circuits, while type 2 power supplies are without filters. The difference between cold and stable state measurements of current harmonics magnitude and phase angles are more significant for type 2 power supplies contrary to type 1. The THD_i values of SMPS also vary with time until they become stable. The power supplies without filters show more difference between THD_i measurements in the cold state and stable state. The THD_i variation was between 15 to 20% for type 2 power supplies and 0.5 to 1.2% for type 1 power

supplies. The maximum time taken by power supplies to have stable current harmonics was 85 min. The absolute difference between cold and stable measurements was more prominent for higher-order harmonics for power supply without harmonic filters. For power quality estimation in the real-time scenario where a large number of power supplies have been involved, this difference may result in a significant error. Therefore, it is recommended to perform power quality measurements when the power supplies become stable. Future work will include power supplies with more rated power and other electronics-based equipment to assess time-dependent variation in harmonic emission.

Author Contributions: Conceptualization, M.N.I. and L.K.; methodology, M.N.I., B.A. and T.V.; validation, A.R. and M.N.I.; data curation, M.N.I. and G.L.D.; writing—original draft preparation, M.N.I. and B.A.; writing—review and editing, A.R. and G.L.D.; supervision, L.K. All authors have read and agreed to the published version of the manuscript.

Conflicts of Interest: The authors declare no conflict of interest.

References

1.　Baghzouz, Y. An overview on probabilistic aspects of harmonics in power systems. In Proceedings of the IEEE Power Engineering Society General Meeting, San Francisco, CA, USA, 12–16 June 2005; Volume 3, pp. 2813–2815. [CrossRef]

2.　Blanco, A.M.; Yanchenko, S.; Meyer, J.; Schegner, P. Impact of supply voltage distortion on the current harmonic emission of non-linear loads. *DYNA* **2015**, *82*, 150–159. [CrossRef]

3.　Singh, B.; Singh, B.N.; Chandra, A.; Al-Haddad, K.; Pandey, A.; Kothari, D.P. A review of single-phase improved power quality AC-DC converters. *IEEE Trans. Ind. Electron.* **2003**, *50*, 962–981. [CrossRef]

4.　Thallam, R.S.; Doyle, M.T.; Krein, S.D.; Samotyj, M.J.; Mansoor, A.; Grady, W.M. Effect of Supply Voltage Harmonics on the Input Current of Single-Phase Diode Bridge Rectifier Loads. *IEEE Trans. Power Deliv.* **1995**. [CrossRef]

5.　Pinceti, P.; Prando, D. Sensitivity of parallel harmonic filters to parameters variations. *Int. J. Electr. Power Energy Syst.* **2015**, *68*, 26–32. [CrossRef]

6.　Preece, R.; Milanovic, J.V. Efficient Estimation of the Probability of Small-Disturbance Instability of Large Uncertain Power Systems. *IEEE Trans. Power Syst.* **2016**, *31*, 1063–1072. [CrossRef]

7.　Nagamani, H.; Ganga, S. A study of electrical endurance of MPPF capacitors and selection of end-point criteria. *IEEE Trans. Electr. Insul.* **1992**, *27*, 1193–1201. [CrossRef]

8.　Cuk, V.; Cobben, J.F.G.; Kling, W.; Ribeiro, P.F. Considerations on harmonic impedance estimation in low voltage networks. In Proceedings of the 2012 IEEE 15th International Conference on Harmonics and Quality of Power, Hong Kong, China, 17–20 June 2012; pp. 358–363. [CrossRef]

9.　Li, Z.; Hu, H.; Wang, Y.; Tang, L.; He, Z.; Gao, S. Probabilistic Harmonic Resonance Assessment Considering Power System Uncertainties. *IEEE Trans. Power Deliv.* **2018**, *33*, 2989–2998. [CrossRef]

10.　Collin, A.J.; Cresswell, C.E.; Djokić, S.Ž. Harmonic cancellation of modern switch-mode power supply load. In Proceedings of the ICHQP 2010—14th International Conference on Harmonics and Quality of Power, Bergamo, Italy, 26–29 September 2010. [CrossRef]

11.　Key, T.S.; Lai, J.S. Costs and benefits of harmonic current reduction for switch-mode power supplies in a commercial office building. *IEEE Trans. Ind. Appl.* **1996**. [CrossRef]

12.　Schlichting, L.; Liz, M.; Raizer, A. Power quality related to switched mode power supplies associations. In Proceedings of the 10th International Conference on Harmonics and Quality of Power, Proceedings (Cat. No.02EX630), Rio de Janeiro, Brazil, 6–9 October 2002; Volume 2, pp. 760–764. [CrossRef]

13.　Sudheer, M.L. Reduction of radiated emission from offline switch mode power supply. In Proceedings of the 15th International Conference on Electromagnetic Interference and Compatibility, INCEMIC 2018, Bangalore, India, 15–16 November 2018. [CrossRef]

14.　Acarkan, B.; Erkan, K. Harmonics modeling and harmonic activity analysis of equipments with switch mode power supply using MATLAB and simulink. In Proceedings of the IEEE International Electric Machines and Drives Conference, IEMDC 2007, Antalya, Turkey, 3–5 May 2007. [CrossRef]

15. Chang, G.; Hatziadoniu, C.; Xu, W.; Ribeiro, P.; Burch, R.; Grady, W.; Halpin, M.; Liu, Y.; Ranade, S.; Ruthman, D.; et al. Modeling devices with nonlinear Voltage-current Characteristics for harmonic studies. *IEEE Trans. Power Deliv.* **2004**, *19*, 1802–1811. [CrossRef]

16. Lai, J.S.; Key, T. Effectiveness of harmonic mitigation equipment for commercial office buildings. *IEEE Trans. Ind. Appl.* **1997**, *33*, 1104–1110. [CrossRef]

17. Naveed Iqbal, M.; Jarkovoi, M.; Kutt, L.; Shabbir, N. Impact of LED thermal stability to household lighting harmonic load current modeling. In Proceedings of the 2019 Electric Power Quality and Supply Reliability Conference and 2019 Symposium on Electrical Engineering and Mechatronics, PQ and SEEM 2019, Kardla, Estonia, 12–15 June 2019. [CrossRef]

18. Lai, J.S.; Hurst, D.; Key, T. 6 Switch-mode supply power factor improvement via harmonic elimination methods. In Proceedings of the IEEE APEC '91: Sixth Annual Applied Power Electronics Conference and Exhibition, Dallas, TX, USA, 10–15 March 1991; pp. 415–422. [CrossRef]

19. Singh, S.; Singh, B.; Bhuvaneswari, G.; Bist, V. Improved Power Quality Switched-Mode Power Supply Using Buck–Boost Converter. *IEEE Trans. Ind. Appl.* **2016**, *52*, 5194–5202. [CrossRef]

20. Wang, C.M.; Lin, C.H.; Yang, T.C. High-Power-Factor Soft-Switched DC Power Supply System. *IEEE Trans. Power Electron.* **2011**, *26*, 647–654. [CrossRef]

21. Bhat, A.H.; Agarwal, P. Three-phase, power quality improvement ac/dc converters. *Electr. Power Syst. Res.* **2008**, *78*, 276–289. [CrossRef]

22. Singh, B.; Singh, S.; Chandra, A.; Al-Haddad, K. Comprehensive study of single-phase AC-DC power factor corrected converters with high-frequency isolation. *IEEE Trans. Ind. Inform.* **2011**, *7*, 540–556. [CrossRef]

23. Huber, L.; Jovanovic, M. Single-stage, single-switch, isolated power supply technique with input-current shaping and fast output-voltage regulation for universal input-voltage-range applications. In Proceedings of the IEEE APEC 97—Applied Power Electronics Conference, Atlanta, GA, USA, 27 February 1997; Volume 1, pp. 272–280. [CrossRef]

24. Abe, S.; Yamamoto, J.; Zaitsu, T.; Ninomiya, T. Extension of bandwidth of two-stage DC-DC converter with low-voltage/high-current output. In Proceedings of the IEEE 34th Annual Conference on Power Electronics Specialist, PESC '03, Acapulco, Mexico, 15–19 June 2003; Volume 4, pp. 1593–1598. [CrossRef]

25. Moore, P.; Portugues, I. The influence of personal computer processing modes on line current harmonics. *IEEE Trans. Power Deliv.* **2003**, *18*, 1363–1368. [CrossRef]

26. Chakravorty, D.; Meyer, J.; Schegner, P.; Yanchenko, S.; Schocke, M. Impact of Modern Electronic Equipment on the Assessment of Network Harmonic Impedance. *IEEE Trans. Smart Grid* **2017**, *8*, 382–390. [CrossRef]

27. Sharma, H.; Rylander, M.; Dorr, D. Grid Impacts Due to Increased Penetration of Newer Harmonic Sources. *IEEE Trans. Ind. Appl.* **2016**, *52*, 99–104. [CrossRef]

28. Collin, A.J.; Tsagarakis, G.; Kiprakis, A.E.; McLaughlin, S. Simulating the time-varying harmonics of the residential load sector. In Proceedings of the International Conference on Harmonics and Quality of Power, ICHQP, Bucharest, Romania, 25–28 May 2014. [CrossRef]

29. IEC. *IEC TR 61000-Electromagnetic Compatibility (EMC)—Part 3-14: Assessment of Emission Limits for Harmonics, Interharmonics, Voltage Fluctuations and Unbalance for the Connection of Disturbing Installations to LV Power Systems*; Technical Report; International Electrotechnical Commission: Geneva, Switzerland, 2011.

30. Singh, S.; Singh, B.; Bhuvaneswari, G.; Bist, V. Power Factor Corrected Zeta Converter Based Improved Power Quality Switched Mode Power Supply. *IEEE Trans. Ind. Electron.* **2015**, *62*, 5422–5433. [CrossRef]

31. Singh, S.; Singh, B.; Bhuvaneswari, G.; Bist, V.; Chandra, A.; Al-Haddad, K. Improved-Power-Quality Bridgeless-Converter-Based Multiple-Output SMPS. *IEEE Trans. Ind. Appl.* **2015**, *51*, 721–732. [CrossRef]

32. IEC. *Electromagnetic Compatibility (EMC)—Part 3-2: Limits—Limits for Harmonic Current Emissions (Equipment Input Current ≤16 A per Phase)*; IEC: Geneva, Switzerland, 2019.

III

M. N. Iqbal, L. Kütt, M. Lehtonen, R. J. Millar, V. Püvi, A. Rassõlkin, and G. L. Demidova, "Travel activity based stochastic modelling of load and charging state of electric vehicles," Sustainability, vol. 13, p. 1550, Feb 2021

Article

Travel Activity Based Stochastic Modelling of Load and Charging State of Electric Vehicles

Muhammad Naveed Iqbal [1,*] , Lauri Kütt [1] , Matti Lehtonen [2] , Robert John Millar [2] , Verner Püvi [2] , Anton Rassõlkin [1] and Galina L. Demidova [3]

1   Department of Power Engineering and Mechatronics, Tallinn University of Technology, Ehitajate tee 5, 19086 Tallinn, Estonia; lauri.kutt@taltech.ee (L.K.); anton.rassolkin@taltech.ee (A.R.)
2   Department of Electrical Engineering and Automation, Aalto University, Maarintie 8, 02150 Espoo, Finland; matti.lehtonen@aalto.fi (M.L.); john.millar@aalto.fi (R.J.M.); verner.puvi@aalto.fi (V.P.)
3   Faculty of Control Systems and Robotics, ITMO University, 197101 Saint Petersburg, Russia; demidova@itmo.ru
*   Correspondence: miqbal@taltech.ee

Abstract: The uptake of electric vehicles (EV) is increasing every year and will eventually replace the traditional transport system in the near future. This imminent increase is urging stakeholders to plan up-gradation in the electric power system infrastructure. However, for efficient planning to support an additional load, an accurate assessment of the electric vehicle load and power quality indices is required. Although several EV models to estimate the charging profile and additional electrical load are available, but they are not capable of providing a high-resolution evaluation of charging current, especially at a higher frequency. This paper presents a probabilistic approach capable of estimating the time-dependent charging and harmonic currents for the future EV load. The model is based on the detailed travel activities of the existing car owners reported in the travel survey. The probability distribution functions of departure time, distance, arrival time, and time span are calculated. The charging profiles are based on the measurements of several EVs.

Keywords: activity based modelling; EV charging current; EV load model; managed charging; SOC; unmanaged charging

1. Introduction

The climate change and energy security concerns are pushing policy-making institutes towards setting strict targets towards reducing greenhouse gasses (GHG) emissions and dependency on fossil fuels. The transport sector consumes 58 % of the total oil, while 67% of fossil fuel is used to generate electricity [1]. Electric vehicles (EV) are promising an efficient replacement of the conventional transportation system. For a sustainable future with less dependency on fossil fuels and to meet the world's energy demand, the adoption of electric vehicles and renewable energy is essential. As EV's adoption is encouraged to meet energy security and climate-related targets, some challenges are also associated with their rapid integration. It would typically mean reinforcements to the existing grids to support the additional charging load. The EV charging is based on power electronic circuits that can compromise the network's sustainability by adding harmonic pollution. In planning such changes, the future load due to vehicle fleets would need to be known. A probabilistic EV usage model, based on the traffic surveys and the actual vehicle-driven data, can provide estimation of the EV charging load in the distribution grid.

Governments and automobile manufacturers are pushing towards developing efficient designs of electric vehicles. In 2017, electric vehicle's total stock increased to 3 million, including both battery electric vehicles (BEV) and plug-in hybrid electric vehicles (PHEV). This number is expected to surge up to 13 million by 2020 and 130 million by 2030 [2,3]. This growth is anticipated because of the improved life cycle of EVs and a decrease in the

prices. The payback time of EV is expected to reduce from currently 20 years to 5 years compared to internal combustion engine vehicles (ICEV) [4]. However, along with several advantages, this rampant growth of EVs will possess several challenges related to the grid capacity to support this additional load.

The integration of the EVs in the electricity distribution network is quite challenging as it requires additional infrastructure and investment. Because of the inadequate charging infrastructure, it is expected that the majority of the EVs owners will charge their vehicles at homes [4]. The impact of the EVs on the distribution network is widely discussed in the literature. The large residential distribution networks may not be sized for additional EV load added by the customers [5,6]. Therefore, the additional EV charging load is foreseen to affect the power system directly. The unmanaged charging will result in overloading of existing transformers, increase in the losses and power quality problems [7,8].

Despite the improved power electronics circuit, the EV charging load is mostly distorted with high total harmonic distortion up to the range of 60–70% [9]. The major problem of additional current drawn by the EV chargers is the increase of heating in transformers. The increased high-frequency harmonic current will result in losses because of nonuniform current distribution in the transformer winding. These harmonic currents also increase the losses in the cables. The current in the neutral conductor also increases [10,11].

To assess the impact of EV integration on the electric power system, and optimal planning of the investments, accurate forecasting of the EV ownership and usage is critical. Mathematical models of EV usage can provide a detailed insight into their impact on the power system grid operation, environment, and economics. The EV model provides charging profiles to estimate additional electricity load introduced by the EV charging in the distribution grid. The researchers have used different approaches to construct EV charging profiles [12]. In the first approach, simulation models of EV usage are made that are based on available data related to transportation patterns. In the second approach, real-time studies are carried out to understand the behavior of EV usage of individual customers [13]. While real-time studies require significant resources, the simulation models have a limited domain based on the type and amount of data. However, a hybrid approach, where the simulation model is based on the real-time EV usage and measurement along with transportation surveys, is more effective and flexible.

This paper proposes a mathematical model to determine EV's daily usage behavior based on the travel survey conducted in Finland. The commuter's daily routine from the travel survey is used, and a stochastic model has been developed to provide trip details and the state of charge (SOC) of the EVs. The utilization patterns will be based on the daily activities statistics to estimate each vehicle's state of charge upon home arrival. The charging load current patterns will be elaborated using recorded charging data of different vehicles used for the model. The Monte Carlo approach is used to determine the charging load curves of the EVs. The model will provide options to model charging load upon commute mode, type and length variance in the temporal space. With such variations, different models can be created to estimate charging load in different locations and conditions. The detailed state of charge statistics for different vehicles will also allow using the model for estimating the harmonic emissions, unbalancing, and overload conditions. Furthermore, this model can be used in both unmanaged and managed charging (peaks limiting) scenarios with small modifications for different motivators (price, availability, etc.). In the current paper, the scope will be limited to unmanaged and managed charging on weekdays, with the assumption that owners would charge their EVs as soon as they arrive home from the last travel activity. The paper's organization is as follows: Section 2 provides a brief overview of the existing methodologies used by the researcher to develop the EV models. The purpose methodology used in this study is described in Section 3. The results of the mathematical model are discussed in Section 4, while Section 5 presents the conclusion.

2. Overview of the Existing Models

The researchers have used various methodologies to model EV usage and their charging behavior, both in temporal and spatial dimensions. The various factors associated with the EV user behavior has made the EV modeling quite complicated. The climate and traffic conditions affect the EV user's behavior and alter the travel time and distance. Socioeconomic factors, market behavior such as electricity pricing, and policy decisions, including subsidies, influence the electric vehicles' user behavior and charging patterns.

The EV models usually exploit traffic surveys, vehicle ownership statistics, and parking data as a base to make a mathematical model that can provide qualitative and quantitative insights into EV usage and its environmental and economic impact [14]. The modeling approach depends on the research targets and the scope of the study. The models used to evaluate car ownership and annual driven distance are used to forecast the transportation demand and attribute that influence vehicle manufacturer and energy companies business. A similar model, based on a household travel survey (HTS), is used to predict vehicle ownership in Singapore [15]. These models can help the policymakers to estimate the growing demand for EVs but do not provide detailed insight into the vehicle's charging behavior and actual usage patterns.

The four-state approach has been widely discussing in the literature for transport modeling problems [16]. In the first step, the trips are generated in a region based on commuter's daily activities. Trip purpose defines the nature of the trip by indicating the starting and ending point. The trip's starting point is termed as the production end, while the ending point is called attractions. Most trips have their origin or destination as home. Trips are modeled on personal, household, or zonal level. Typically trips are originated from the household because of the activity demands associated with the dwellers. Therefore, the majority of the trips can be defined as home to work, home to others, and non-home based trips. The trip ends are combined geographically into full trip lengths by defining the second step's origin and destination. The general assumption is that most of the trips originated in a certain zone of a city will be attracted to the surrounding zones while some are attracted to the zones at a moderate distance. Only a few trips are destined for the far-off zones. The mode of travel is selected in the third step. A commuter can use a personal vehicle, shared vehicle, or public transport to fully or partially complete the trip. In the final step, the routes taken by the travelers are predicted. The four-state model lack to accommodate the activities affecting trip behavior. The travel activities affect the trip generation part only while the other states have less or no influence. A four-step transport model consists of trip generation, trip distribution, transportation mode, and route selection for travel activities is presented in [17]. The authors determined traffic flow, electricity demand, and the economic impact of EVs.

A better approach to model daily EV usage is to consider the daily travel activity of the commuters. The daily or weekly travel patterns provide a framework that can model EV usage based on the lifestyle of the users and their travel behavior. These activity-based modeling approaches can provide the user's charging behavior that may help to observe the effect of EV charging on the electric power network. The EV models based on the trip behavior can be divided into two categories; direct use of observed activity-travel schedules (DUOATS) and activity-based models (ABS) [12,16].

The DUOATS method uses external travel patterns previously developed for the existing cars to model EV usage and charging behavior. Various travel surveys conducted in different countries provide data related to the user's individual travel behavior. A web-based survey was used in California (US) to generate energy usage profiles of plug-in hybrid electric vehicles in [18]. The participants provide details of their travel using a car for one day. The information includes the number of trips, traveling time for each trip and the distance covered. Another study used the Monte Carlo approach to estimate the electricity demand of EVs using the US Household Travel Survey [19]. The arrival and departure times of vehicles on weekdays are converted in charging demand. A probabilistic approach has been used to determine the charging profiles using empirical cumulative distribution

functions in [20]. The authors also used HTS data and employed queuing theory to estimate when a particular EV required charging. The EV charging impact of the Swiss distribution grid has been presented in [21]. The travel patterns were based on the mobility survey conducted in Switzerland. A large-scale EV charging model based on travel statistics in New Zealand used a multivariate probabilistic approach [22]. The authors report an increase in the peak electricity demand in the case of unmanaged EV charging. Although the DUOATS models based on the travel surveys provide reliable outcomes, most travel surveys are based on the conventional car owners and do not include specific details related to EVs, such as charging behavior.

The activity-based modeling (ABM) approach employs a collection of activities that may influence people's travel behavior. It enables to model the trips based on individual's activity patterns that can be affected by the behavioral preferences rather than individual trips. Several factors, including social and economic structures, influence travel behavior. The travel schedule is generated within the ABM model in comparison to DUOATS, which relies on external travel schedules. In [23], the household activity model is used to generate PHEV load profiles under an unmanaged charging scenario. The model relates the charging load of PHEV to the electricity consumption of other household appliances. Another activity-based modeling approach analyzed the vehicle-to-grid (V2G) impact on power flow of the distribution grid [24]. A dynamic ABM four-stage model has been developed based on the travel diaries and supporting data-set for household activities that can influence travel decisions [25]. This model is further used to simulate the electricity demand of EVs in Belgium [26]. Traffic survey data are used to generate probability density functions (PDF) of trip related parameters such as arrival time, departure time and distance to make EV usage patterns in [27–29]. These travel patterns are later compared with actual EV charging data to generate SOC and EV load profiles.

Transport simulation software can also simulate domestic activity-based travel behavior. A similar study used TRANSIMS to estimate the effect of PHEV penetration on electricity demand [30]. Another approach simulated traffic flow using multi-agent transport simulation (MAT-Sim), a software capable of simulating large-scale transport model. The MAT-Sim based model is used to generate EV penetration scenarios in Switzerland based on the trip and activities in [31]. The model lacks to take account of the driving range factor; therefore, suitable for PHEV only.

3. Methodology

Based on the overview of the existing models provided in the previous section, the ABM modeling approach is more flexible and can address the user activity and travel behavior interdependence with ease of aggregation because of its bottom-up approach. The electric power grid, planning, and perspective load estimations are expected to affect residential areas because of EV's home charging. Due to the expected charging upon home arrival at the end of the day by the majority of vehicle owners, it will be the most convenient option. The model here aims to simplify the load estimation limited only for residential grids.

In our proposed model, direct data input from the national traffic survey (NTS) is used to categorize the car owner's travel patterns into different categories.The probability distribution for arrival and departure times of each travel activity is defined. A trip of the chain is used to evaluate the distance traveled and the time at which the outgoing and the incoming trip took place. The charging decision depends on the SOC of the EV that is calculated based on the distance traveled by the vehicle during different trips. The charging would occur when the vehicle reaches home and does not have enough SOC for the next trip.

The NTS is carried out in Finland every six years [32]. The survey collects one-year travel data, including all days and seasons, from 30,000 people aged six and above. The survey provides details about the mobility of Finnish people, including the reasons for the trips, modes of transportation, and differences in mobility between population

groups. In order to understand the background of mobility, participants have been asked for different background information. The background information has been used to determine, for example, the respondent's age, gender, the form of residence, household members, use and ownership of a passenger car, driving license management, employment and earnings. As complementary data, regional characteristics related to the location of homes, workplaces, schools/kindergartens, study places, second homes, and destinations, as well as information on how the journey would have been folded by public transport or passenger car. Table 1 shows the daily indicators for domestic trips.

Table 1. Daily indicators for domestic travel [32].

Domestic Travel Indicator	Average Value per Day
Number of domestic trips per person	2.89
Travel expense per person	41.4 (euros)
Total journey time per person	65.5 (min)
The average distance of a trip	14.3 (km)
Average travel time per km	22.7 (min)

3.1. Travel Activities

The daily trips are categorized based on the activities responsible for the trip's need. The majority of the trips are related to work or education and shopping. The other activities include business-related trips, leisure activities, and visits or vacation trips. Table 2 shows the number of trips and distance traveled for all trip purposes.

The data shows that the travel activities from Monday to Friday are very similar. The work and school trips dominate these days. All other trips also follow a similar pattern. The visits have a lower share in the first five days of the week. The work and school trips drop significantly over the weekend; however, both visits and leisure trips have increased on weekends. The shopping trip frequency is almost the same for all days of the week except Sunday. The frequency of business trips is also on the higher end during weekdays. The travel activity data provides an excellent base to model the EV trips by assuming that the travel pattern would remain the same for the Evs.

Table 2. Weekly travel information for different trips [32].

Day	Work	School	Business	Shopping	Visits	Leisure	All
			Number of trips				
Monday	0.64	0.27	0.13	1.02	0.04	0.69	2.79
Tuesday	0.62	0.26	0.14	1.14	0.03	0.71	2.9
Wednesday	0.65	0.29	0.16	1.12	0.03	0.75	3.01
Thursday	0.65	0.27	0.13	1.09	0.03	0.64	2.8
Friday	0.54	0.25	0.11	1.11	0.04	0.68	2.72
Saturday	0.13	0.01	0.03	1.03	0.05	0.88	2.13
Sunday	0.12	0	0.02	0.58	0.06	0.81	1.59
Average	**0.48**	**0.19**	**0.11**	**1.01**	**0.04**	**0.74**	**2.56**
			Distance traveled for each trip (km)				
Monday	15.8	7.74	34.04	6.87	40.48	11.18	116.11
Tuesday	16.73	6.04	33.94	6.6	49.11	11.94	124.36
Wednesday	14.92	6.29	36.77	6.87	38.56	9.6	113
Thursday	17.53	7.82	37.55	6.34	57.17	11.84	138.25
Friday	15.28	7.54	58.2	8.3	80.08	19.12	188.52
Saturday	16.55	25.16	53.21	7.99	48.22	19.48	170.59
Sunday	13.13	69.81	95.58	9.03	65.46	16.56	269.56
Average	**15.98**	**7.27**	**41.39**	**7.3**	**55.14**	**14.43**	**141.52**

3.2. Departure Times

We have defined three travel activities based on the six travel activities mentioned in Table 2. The details of these activities are provided below.

- "Work and school" (WS), is described as the most likely routine trip. The departure and arrival times of these trips will have only slight dispersion, and this will be carried out for all weekdays practically with no exceptions. The trip length will also have rather a low variance for a particular vehicle.
- "Shopping and business" (SB) is also a routine trip; however, the dispersion of the likeliness of such a trip will be greater. Furthermore, the average trip length will vary to a greater extent. There could also be several trips of the same type on the same day.
- "Leisure and vacation" (LV) has the most variance included. It means both variance in trip length as well as trip probability and start-time variance. These trips also tend to be one of the longest ones.

The average trip lengths for each travel activity are also available from the traffic survey. The data for the trips distance have been presented in Table 2. For the WS activity, it is assumed that the driver of the vehicle will be participating in vocational or university-level studies. This means a longer trip to the location rather than to the local school. The SB include two activities; shopping and business trips. It is assumed that private business trips are similar to work-related business trips, for example, visiting a specialized shop at a longer distance. The probability of a long trip is low, and it will be tied together with the distribution of the shopping activities (expected at a shorter distance) length and probability. Similar is valid for the VL activities; however, these activities are less probable than the SB. The departure times for each activity are available in the NTS survey. Figure 1a shows the departure time for each travel activity on a weekday. The data is converted into WS, SB, and LV activities, as shown in Figure 1b.
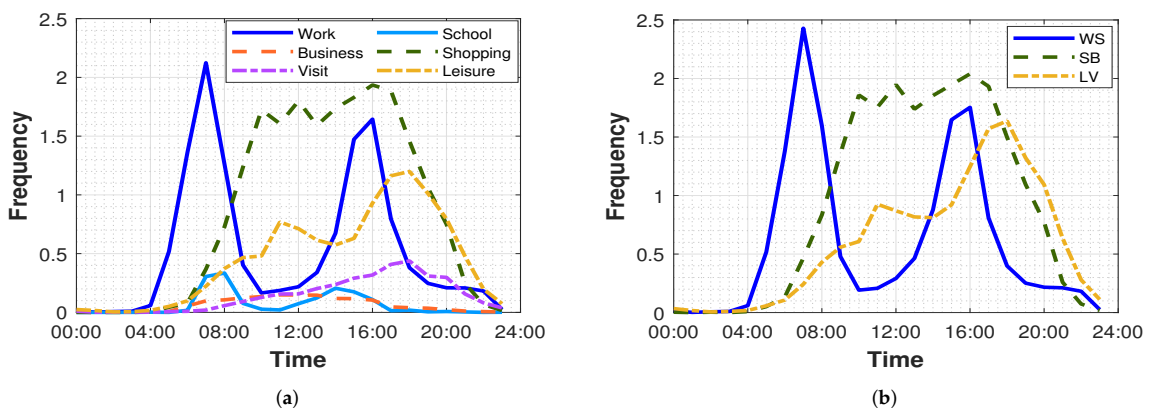

Figure 1. Frequency of departure per hour (**a**) Data from NTS survey (**b**) Data used in the model.

The distribution of the departure times from Figure 1b shows trips cannot distinguish as outgoing or incoming trips for each travel activity. For EV modeling, both incoming and outgoing trips are essential to estimate charging profiles. The time resolution of the initial data is also low, with a 1-h resolution. Therefore, the data interpolation is used to improve the resolution.

3.3. Incoming Trip Estimation

The estimation of an incoming trip to home is critical to model EV charging profiles. The vehicle charging will be initiated once the vehicle returns home and does not have a sufficient battery charge for the next trip. However, the travel activity information does not provide details about the outgoing and incoming trips. Two distinctive peaks are

visible in the WS departure frequency shown in Figure 1b. By assuming a low number of night-shifts workforce, the morning peak will likely indicate the outgoing trips to work, and the evening peak represents the incoming trips from work to home. This assumption will provide us separate distributions for incoming and outgoing WS trips. The evening incoming trips have more spread over a longer time span than the morning outgoing rate. The t location-scale distribution is used to define both incoming and outgoing WS trips separately, as shown in Figure 2. This distribution helps to model data that have a normal distribution with heavier tails. The PDF of the t-location-scale distribution can be calculated by using Equation (1).

$$f(x, v, \sigma, \mu) = \frac{\Gamma\frac{(v+1)}{2}}{\sigma\sqrt{v\pi} \times \Gamma(\frac{v}{2})} \times \left[\frac{v(\frac{x-\mu}{\sigma})^2}{v} \right]^{-(\frac{v+1}{2})} \tag{1}$$

Here v is the shape parameter and σ defines the scale. μ determine the location of the PDF and Γ is the gamma function. As the v approaches towards positive infinity the $f(x, v, \sigma, \mu)$ tends towards the normal distribution. The smaller values of v results in a heavier tail.
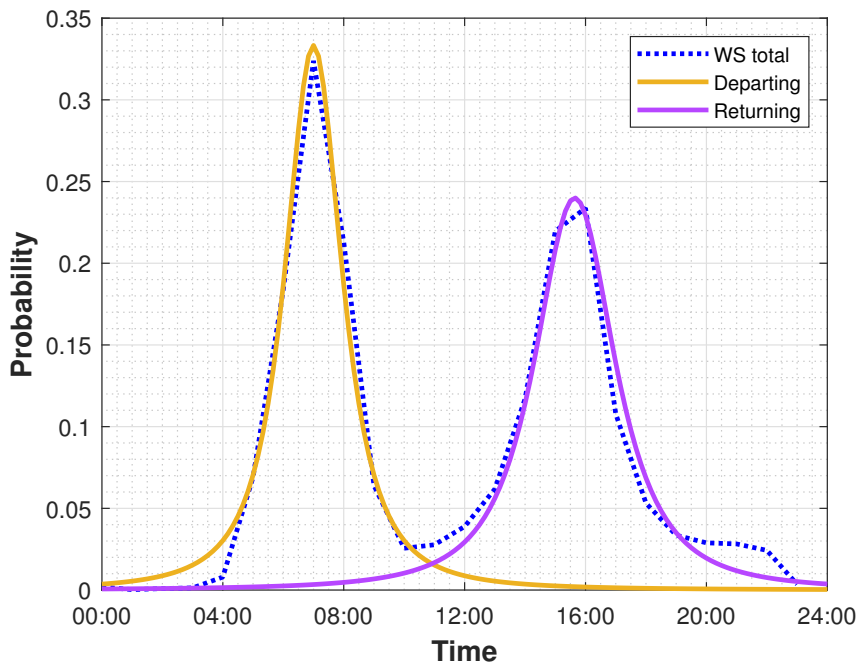

Figure 2. Probability plots of outgoing and incoming trip for WS travel activity.

The LV activity distribution in Figure 1b also shows twin peaks; however, the relation is not straightforward. The higher evening activity in the LV trip frequency is likely due to the vehicle owner's leisure activities after work. The average time at a leisure activity (after the arrival to the place and before the departure from the place) has been observed as 3 h. The duration for the LV activities is calculated using Poisson distribution, as shown in Equation (2).

$$f(x|\lambda) = \frac{\lambda^x}{x!} e^{-\lambda} \tag{2}$$

The λ in Equation (2) shows the variance of the distribution. The detail of the travel distance for different trip activities is also available from the NTS survey. Figure 3a shows

the average distance traveled in kilometers at a different time of the day for various travel activities mentioned in the NTS survey. This data is converted into WS, SB, and VH travel activities used in this model, and the average distance traveled for each activity at a different time of the day is shown in Figure 3b. For each trip, the distance is calculated using Poisson and log-normal distribution defined for the trip distance. Equation (3) represents the log-normal distribution's probability density function, where μ represents the mean and variance is indicated by σ.

$$f(x, \sigma, \mu) = \frac{1}{x\sigma\sqrt{2\pi}} exp(-\frac{(ln(x) - \mu)^2}{2\sigma^2})$$ 　(3)

3.4. Electric Vehicle Characteristics

　　　Another challenging task is to define the electric vehicle mix. Although new EV models are introduced in the market by the major auto manufacturer, EV adoption is still low. The performance evaluation data of these EVs is also not readily available. Therefore, it is a complex task to select the EVs for developing a model in the perspective of future vehicles, and results can be highly inaccurate. However, most of the daily routines likely remain the same; the travel distances would be identical, and vehicle utilization would remain the same. As the energy distribution would be similar in the future; therefore, the charging power limits and current drawn by the EV's is expected to be in the same range. Therefore it could be assumed that the vehicle charging would remain to follow identical patterns as of today.
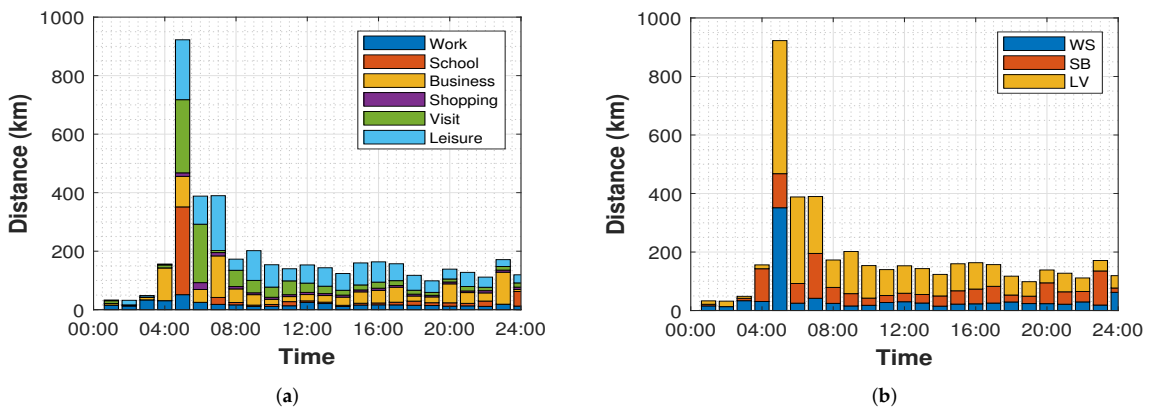

Figure 3. Trip distance frequency per hour for different travel activities (**a**) From NTS survey (**b**) Data used in the model.

　　　In this study, the vehicle mix is created by assuming an equal share of each electric vehicle in the network. Seven different vehicle types are selected, including three Plug-in hybrid vehicles (PHEV) with relatively long electrical driving distance. The EVs are selected based on the ease of market availability. The different parameters of the Evs used in this model are described in Table 3.

Table 3. Type and electrical parameters of the EVs used in the model.

Parameter	EV 1	EV 2	EV 3	EV 4	EV 5	EV 6	EV 7
Type	PHEV	PHEV	PHEV	BEV	BEV	BEV	BEV
Electric-motor power (kW)	111	51	60	80	40	16	16
Charging current RMS (A)	14.9	12.7	9.7	10.3	10.3	13	13
Battery capacity (kWh)	17.1	10.3	8.8	24	16	16	16
Electric range (km)	61	53	54	117	127	127	127

The EV charging would vary based on the different charging patterns; current ramp-up, constant current range, and ramp-down at the end of the charge. Therefore charging current depends on the state of charge (SOC) of the EV. Figure 4 shows the SOC of the EVs used in charging profile modeling in this study. EV 6 and 7, although from different car manufacturers, shows a similar SOC curve as they employed similar specifications for the battery and electric motor.

Energy used by a vehicle for a driven range is assumed to be 180 Wh/km. This assumption is applied after considering the EV manufacturer's data and future vehicles are expected to provide a similar range as the motor and drives are already quite efficient. The variance in energy consumption also depends on the climate conditions, terrain, and region but is not considered in this study. The SOC of an EV is estimated after its arrival at home. For the next trip assigned by the generated travel activity, the SOC is analyzed. If the EV battery SOC drops below the required level for the next trip, the EV will go under the charging state. The EV SOC will be checked before any trip for their estimated range; in case there is not enough energy in the battery for completing the trip, the vehicle will be assumed not to take the trip.
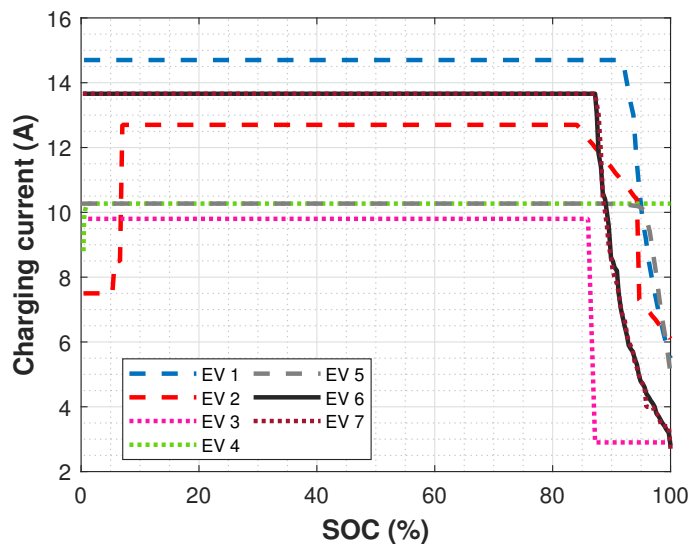

Figure 4. Charging current levels during charging span of 0–100% of the full charge.

3.5. Daily Routine Estimation

The vehicle owners are categorized based on age group and gender in the NTS survey. This data is used to evaluate the number of people going for daily WS travel activity. The remaining vehicle owners are assumed to be on vacation, to be retired, or engaged in other travel activities. For estimating the daily routines for the selected population of vehicles, an array of random seed numbers are assigned to each of the vehicles. In the first step, the permanent routine parameters are created. These routine parameters are used in the later stages for the specification of the daily action. The permanent routine parameters are used to generate the vehicle schedule for each simulated day. The vehicle will be assumed to leave home following the similar outgoing time distribution assigned for each travel activity. If the travel activity is WS, then returning from work will take place during the time following the WS incoming distribution. The other activities after the daily routine will be estimated for each day based on the probabilities of the SB and WS actions. A total of ten different vehicle states are used to describe the vehicle activity. The first state is termed as the home state, while for each type of activity (WS, SB, VL) there will be three states—outgoing, at activity and, incoming state. The vehicle's utilization

will be calculated when the vehicle is in outgoing or incoming states for a trip activity. The incoming state is assumed to always end at home. When the vehicle returns home, the SOC will be dropped because of the trip's energy consumed. The SOC is determined based on distance travel during the trip obtained in Section 3.3. The amount of charge left in the EV battery will determine whether the vehicle can leave to other activity or required charging before the next trip. If the next trip is scheduled for the next day, then the vehicle will be charged until full SOC. The EV load for the given number of EVs is estimated using the Monte Carlo approach. The steps during each iteration are as follows.

- Step 1: Determine the probability of outgoing and incoming for WS travel activity;
- Step 2: Probability of SB or VL travel activity after WS is complete;
- Step 3: Distance traveled for all WS, SB, and VL activities;
- Step 4: Duration for all WS, SB, and VL activities;
- Step 5: EV utilization and the SOC after each trip;
- Step 6: SOC tolerance level, when owner always charges the vehicle;
- Step 7: Probability of the owner to charge after every incoming trip.

The flow chart of the algorithm is shown in Figure 5. During each day, the trip activity is determined for each trip. The departure time, distance, average speed, and trip duration is determined based on each parameter's probability distribution. At the end of each trip, SOC is calculated, and the battery charging decision is made. Another VH or SB trip could also take place if the departure time is less than 22:00, and SOC is enough to support the trip. Any given number of EVs can be simulated for the required number of days.
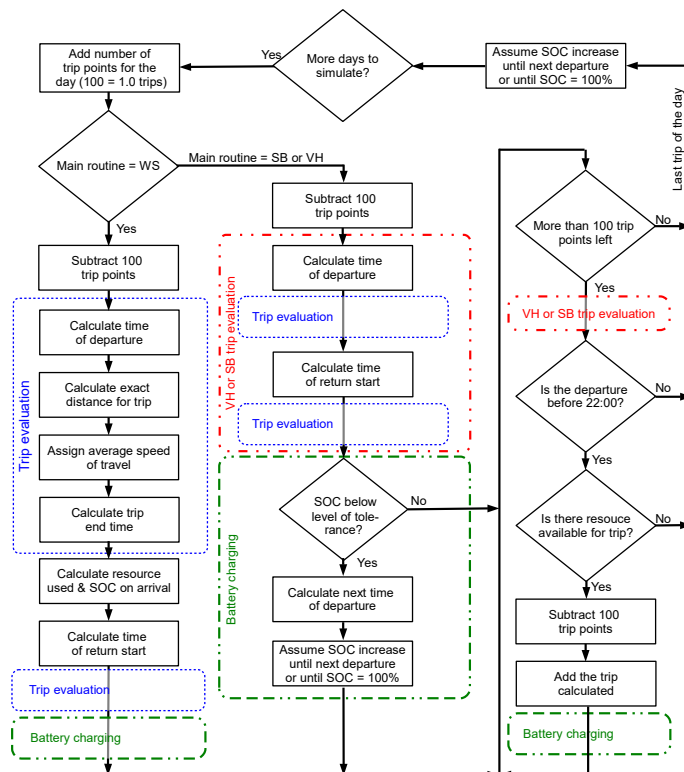

Figure 5. Algorithm of the EV charging profile model.

4. Results and Discussion

The EV model can be used to estimate the load and charging profiles for the required number of EVs and days. To evaluate the outcome of the model, the Monte Carlo approach is used to simulate usage of 50 EVs for 100 days. For each day, vehicle's daily schedule is estimated. The vehicle's daily schedule will provide the vehicle's battery SOC information, including the SOC after arrival at home. Based on the SOC, the respective charging current value is specified for each vehicle, and charging power is calculated for the time instance. Using the charging power, the SOC is calculated for the next time-step until the completion of the charging (SOC = 100%). The total charging current will be the sum of charging currents of all vehicles at any given time.

The model is capable of evaluating the EV load under two charging scenarios. In the first case, an unmanaged charging approach is used where the EV owner can charge the vehicle at any time during the day. Figure 6a shows the EV load for the unmanaged charging scenario. The red dotted line shows the 90th percentile value for the number of vehicles undercharging at a given time, while the black line shows the mean value. The EV load starts appearing around 12:00 and increases exponentially to the maximum value of the charging load. The maximum charging load is around 18:00, as most people came back from the daily routine activities and charged their vehicle. The mean and 90th percentile value of the maximum load is 34 and 42, respectively. The EV load starts decreasing after 18:00 to almost half at 24:00, where the mean and 90th percentile values of the charging vehicle are 14 and 22, respectively. Both mean and 90th percentile values of the charging load are less than ten after 3:00, and the load curve continues to decrease and reaches the minimum value between 06:00 and 08:00.
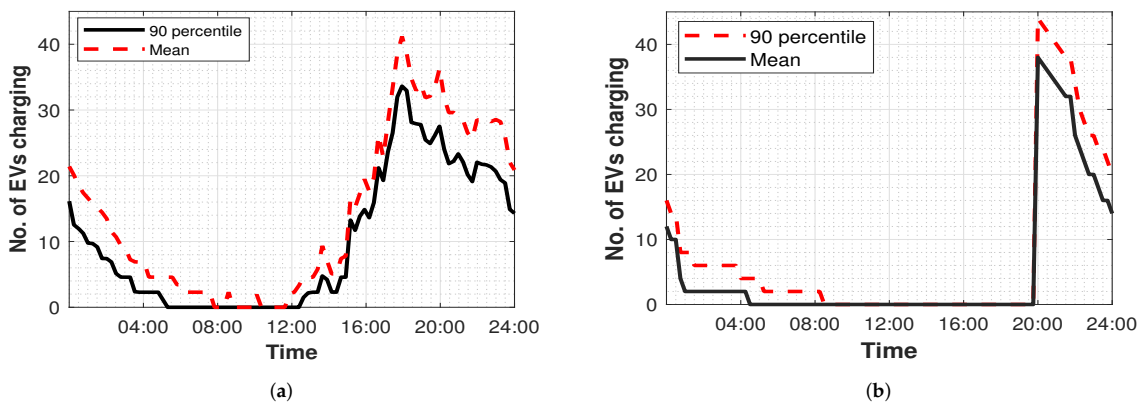

(a)   (b)

Figure 6. EVs load curve for (**a**) Unmanaged charging (**b**) Managed charging.

For the managed charging scenario, the EV owners are forced to charge from 20:00 onwards, and the load curve is shown in Figure 6b. As expected, the maximum load is more in comparison to the unmanaged charging scenario. The mean and 90th percentile charging load is decreased from their maximum value of 38 and 44 to 14 and 22 EV charging at 24:00. The load curve continues to decrease until it reaches a minimum value between 04:00 and 08:00.

The model provides a fast and optimized way to find the expected load curves of EVs under managed (time-driven) and unmanaged charging scenarios. These load curves provide the base to estimate additional current drawn by the electric vehicles during charging in the distribution grid. The estimation is critical for the network operators to plan additional investment to improve the network capacity that can handle EV charging. Additionally, the current harmonic emission by this additional charging load can also be estimated. As a test case, we have estimated the RMS current drawn by the EV charging using the load curves estimated by the model for the unmanaged charging scenario.

The EVs are measured at 230 V sinewave using power quality analyzer. The detail of the measurement setup is provided in [33,34]. The charging current at different SOC is assigned to the EVs and aggregated to find the total current drawn by the EV load at any given time during a particular day. The power consumed by the EV load is also calculated. Figure 7 shows the mean and 90th percentile values of charging current and power for unmanaged charging of 50 vehicles for 100 days.

The results show that the range of current drawn by EV charging could reach 183A in a distribution grid where 50 EV are present and employ home charging. It means an additional 42 kW power is required in the peak hours during the evening. The model can provide results for any given number of EVs under different charging scenarios. The model's EV power consumption estimations follow EV load estimated in [22,27–29]. Particularly, the peak load values and peak load time period, and the load curve form follow nearly identical trends. However, the proposed model provides better flexibility and a simple approach with fewer variables. The results also validate the applicability of the NTS travel survey effectiveness in comparison to the other travel surveys used in various studies to model EV usage patterns.
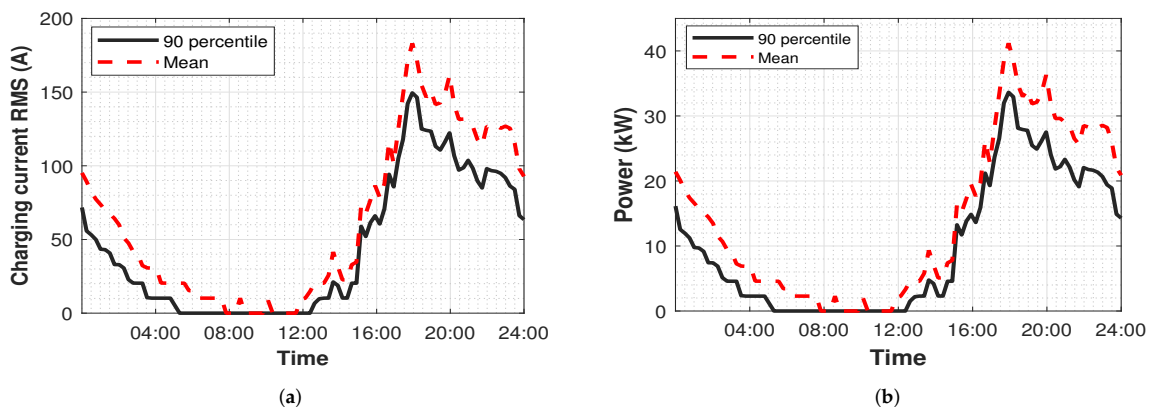

(a) (b)

Figure 7. For unmanaged charging scenario (**a**) EVs charging current (**b**) EVs power consumption.

5. Conclusions

A travel activity-based EV model is presented in this paper based on the National Travel Survey results conducted in Finland. The model provides a simpler and flexible approach and can handle various EVs and travel activities. The travel activity data is used to define three different travel activities during the weekdays. The probability distribution function of the distance traveled, travel time, departure, and arrival time for incoming and outgoing trips are calculated based on the survey data. The EV model is capable of providing the charging load under managed and unmanaged charging scenarios. The model can be also be used to evaluate the load and power quality aspects, including current harmonics and power factor, for the EV integration in the balanced or unbalanced distribution network. Although, at the moment, the scope is limited to home charging of the EVs, however, the model can easily be extended to include charging stations. The model is flexible enough to integrate future models of EVs, including BEV and PHEV.

Author Contributions: Conceptualization, M.N.I. and V.P.; methodology, L.K. and M.N.I; validation, L.K. and R.J.M.; data curation, M.N.I. and G.L.D.; writing—original draft preparation, M.N.I. and L.K.; writing—review and editing, A.R. and G.L.D.; supervision, L.K. and M.L. All authors have read and agreed to the published version of the manuscript.

References

1. IEA. *Key World Energy Statistics 2014*; OECD: Paris, France, 2017; p. 97. [CrossRef]
2. IEA. *Global EV Outlook 2018*; Technical Report; International Energy Agency: Paris, France, 2018. [CrossRef]
3. Sell, R.; Rassolkin, A.; Wang, R.; Otto, T. Integration of autonomous vehicles and Industry 4.0. *Proc. Est. Acad. Sci.* **2019**, *68*, 389–394. [CrossRef]
4. Richardson, D.B. Electric vehicles and the electric grid: A review of modeling approaches, Impacts, and renewable energy integration. *Renew. Sustain. Energy Rev.* **2013**. [CrossRef]
5. Hadley, S.W. *Impact of Plug-in Hybrid Vehicles on the Electric Grid*; Technical Report October; U.S. Department of Energy: Oak Ridge, TN, USA, 2006. [CrossRef]
6. Collin, A.J.; Xu, X.; Djokic, S.Z.; Moller, F.; Meyer, J.; Kutt, L.; Lehtonen, M. Survey of harmonic emission of electrical vehicle chargers in the European market. In Proceedings of the 2016 International Symposium on Power Electronics, Electrical Drives, Automation and Motion, Capri Island, Italy, 22–24 June 2016. [CrossRef]
7. Clement-Nyns, K.; Haesen, E.; Driesen, J. The Impact of Charging Plug-In Hybrid Electric Vehicles on a Residential Distribution Grid. *IEEE Trans. Power Syst.* **2010**, *25*, 371–380. [CrossRef]
8. Rassõlkin, A.; Kallaste, A.; Hõimoja, H. Power factor correction with vehicle-to-grid STATCOM implementation. In Proceedings of the 2014 Electric Power Quality and Supply Reliability Conference (PQ), Rakvere, Estonia, 11–13 June 2014; IEEE: New York, NY, USA, 2014; pp. 177–180.
9. Gómez, J.C.; Morcos, M.M. Impact of EV battery chargers on the power quality of distribution systems. *IEEE Trans. Power Deliv.* **2003**. [CrossRef]
10. Pieltain Fernández, L.; Gómez San Román, T.; Cossent, R.; Mateo Domingo, C.; Frías, P. Assessment of the impact of plug-in electric vehicles on distribution networks. *IEEE Trans. Power Syst.* **2011**. [CrossRef]
11. Balcells, J.; García, J. Impact of plug-in electric vehicles on the supply grid. In Proceedings of the 2010 IEEE Vehicle Power and Propulsion Conference, Lille, France, 1–3 September 2010; VPPC 2010. [CrossRef]
12. Pareschi, G.; Küng, L.; Georges, G.; Boulouchos, K. Are travel surveys a good basis for EV models? Validation of simulated charging profiles against empirical data. *Appl. Energy* **2020**. [CrossRef]
13. Rangaraju, S.; De Vroey, L.; Messagie, M.; Mertens, J.; Van Mierlo, J. Impacts of electricity mix, charging profile, and driving behavior on the emissions performance of battery electric vehicles: A Belgian case study. *Appl. Energy* **2015**. [CrossRef]
14. Xiang, Y.; Hu, S.; Liu, Y.; Zhang, X.; Liu, J. Electric vehicles in smart grid: A survey on charging load modelling. *IET Smart Grid* **2019**. [CrossRef]
15. Basu, R.; Ferreira, J. Understanding household vehicle ownership in Singapore through a comparison of econometric and machine learning models. *Transp. Res. Procedia* **2020**. [CrossRef]
16. Daina, N.; Sivakumar, A.; Polak, J.W. Modelling electric vehicles use: A survey on the methods. *Renew. Sustain. Energy Rev.* **2017**. [CrossRef]
17. Huang, S.; Safiullah, H.; Xiao, J.; Hodge, B.M.S.; Hoffman, R.; Soller, J.; Jones, D.; Dininger, D.; Tyner, W.E.; Liu, A.; Pekny, J.F. The effects of electric vehicles on residential households in the city of Indianapolis. *Energy Policy* **2012**. [CrossRef]
18. Axsen, J.; Kurani, K.S. Anticipating plug-in hybrid vehicle energy impacts in California: Constructing consumer-informed recharge profiles. *Transp. Res. Part Transp. Environ.* **2010**, *15*, 212–219. [CrossRef]
19. Harris, C.B.; Webber, M.E. An empirically-validated methodology to simulate electricity demand for electric vehicle charging. *Appl. Energy* **2014**. [CrossRef]
20. Tehrani, N.H.; Wang, P. Probabilistic estimation of plug-in electric vehicles charging load profile. *Electr. Power Syst. Res.* **2015**, *124*, 133–143. [CrossRef]
21. Salah, F.; Ilg, J.P.; Flath, C.M.; Basse, H.; van Dinther, C. Impact of electric vehicles on distribution substations: A Swiss case study. *Appl. Energy* **2015**. [CrossRef]
22. Su, J.; Lie, T.; Zamora, R. Modelling of large-scale electric vehicles charging demand: A New Zealand case study. *Electr. Power Syst. Res.* **2019**, *167*, 171–182. [CrossRef]
23. Grahn, P.; Munkhammar, J.; Widen, J.; Alvehag, K.; Soder, L. PHEV home-charging model based on residential activity patterns. *IEEE Trans. Power Syst.* **2013**. [CrossRef]
24. Nourinejad, M.; Chow, J.Y.; Roorda, M.J. Equilibrium scheduling of vehicle-to-grid technology using activity based modelling. *Transp. Res. Part Emerg. Technol.* **2016**. [CrossRef]

25. Bellemans, T.; Kochan, B.; Janssens, D.; Wets, G.; Arentze, T.; Timmermans, H. Implementation Framework and Development Trajectory of FEATHERS Activity-Based Simulation Platform. *Transp. Res. Rec. J. Transp. Res. Board* **2010**, *2175*, 111–119. [CrossRef]
26. Knapen, L.; Kochan, B.; Bellemans, T.; Janssens, D.; Wets, G. Activity-based modeling to predict spatial and temporal power demand of electric vehicles in flanders, Belgium. *Transp. Res. Rec.* **2012**. [CrossRef]
27. Stiasny, J.; Zufferey, T.; Pareschi, G.; Toffanin, D.; Hug, G.; Boulouchos, K. Sensitivity analysis of electric vehicle impact on low-voltage distribution grids. *Electr. Power Syst. Res.* **2021**, *191*, 106696. [CrossRef]
28. Fischer, D.; Harbrecht, A.; Surmann, A.; McKenna, R. Electric vehicles' impacts on residential electric local profiles—A stochastic modelling approach considering socio-economic, behavioural and spatial factors. *Appl. Energy* **2019**, *233–234*, 644–658. [CrossRef]
29. Pashajavid, E.; Golkar, M.A. Non-Gaussian multivariate modeling of plug-in electric vehicles load demand. *Int. J. Electr. Power Energy Syst.* **2014**. [CrossRef]
30. Hodge, B.M.; Shukla, A.; Huang, S.; Reklaitis, G.; Venkatasubramanian, V.; Pekny, J. Multi-paradigm modeling of the effects of PHEV adoption on electric utility usage levels and emissions. *Ind. Eng. Chem. Res.* **2011**. [CrossRef]
31. Balmer, M.; Meister, K.; Rieser, M.; Nagel, K.; Axhausen, K.W. Agent-based simulation of travel demand: Structure and computational performance of MATSim-T. In Proceedings of the 2nd TRB Conference on Innovations in Travel Modeling (ITM 2008), Portland, OR, USA, 22–24 June 2008; ETH Zurich, Institute for Transport Planning and Systems: Portland, OR, USA, 2008; p. 33. [CrossRef]
32. Finnish Transport Agency. *National Travel Survey 2016*; Technical report; Traficom: Helsink, Finland, 2018.
33. Iqbal, M.N.; Kütt, L.; Asad, B.; Vaimann, T.; Rassõlkin, A.; Demidova, G.L. Time Dependency of Current Harmonics for Switch-Mode Power Supplies. *Appl. Sci.* **2020**, *10*, 7806. [CrossRef]
34. Iqbal, M.N.; Kütt, L.; Asad, B.; Shabbir, N.; Rasheed, I. Time-dependent variations in current harmonic emission by LED lamps in the low-voltage network. *Electr. Eng.* **2021**. [CrossRef]

IV

M. N. Iqbal, L. Kütt, K. Daniel, M. Jarkovoi, B. Asad, and N. Shabbir, "Bivariate stochastic model of current harmonic analysis in the low voltage distribution grid," Proceedings of the Estonian Academy of Sciences, vol. 70, no. 2, p. 190, 2021

Bivariate stochastic model of current harmonic analysis in the low voltage distribution grid

Muhammad Naveed Iqbal[a]*, Lauri Kütt[a], Kamran Daniel[a,c], Marek Jarkovoi[a], Bilal Asad[a,b] and Noman Shabbir[a]

[a] Department of Power Engineering and Mechatronics, Tallinn University of Technology, Ehitajate tee 5, 19086 Tallinn, Estonia
[b] Department of Electrical Engineering and Automation, Aalto University, 02150 Espoo, Finland
[c] Department of Electrical, Electronics and Telecommunication Engineering, University of Engineering and Technology (FSD Campus), Lahore, Pakistan

Abstract. This paper presents a bottom-up bivariate analysis approach to estimate current harmonics by taking account of network and load variations. The current harmonics assessment in the presence of existing and future nonlinear loads is vital to study their impact on the distribution grid. The traditional harmonic analysis models consider only stable loads while neglecting the harmonic interaction among the devices. Modern nonlinear loads operate under different working modes and configurations. Thermal stability, harmonic cancellation, and dynamic network parameters influence the current harmonic estimations. In this paper, a probabilistic approach is presented to model harmonic emission in the low voltage distribution grid under network and load uncertainties. A case study is used to demonstrate effectiveness of the proposed model.

Key words: probabilistic assessment, network uncertainties, current harmonics, load modelling.

1. INTRODUCTION

Current harmonic emission is becoming a critical power quality issue as the uptake of nonlinear devices in the distribution grid is increasing. Rampant electricity demand, fluctuating fuel prices, and greenhouse gas (GHG) emission is pushing the manufacturer of electrical equipment toward energy-efficient design. Consequently, all modern household appliances incorporate electronic-based converters.These devices draw non-sinusoidal currents and cause voltage distortion in the distribution grid. High penetration of electric vehicles and smart buildings will further increase the share of nonlinear devices in the coming years. The primary task of the network operators is to maintain power quality within the limits for the network and, therefore, a realistic estimation of current harmonics is critical. This paper presents an overview of a probabilistic approach to estimate current harmonics in the low voltage (LV) distribution grid in the presence of different uncertainties.

The power quality indicates an aggregated effect of electromagnetic disturbances that can degrade the voltage and current waveforms. One of the critical parameters of power quality is the sine waveform of the

---

* Corresponding author, miqbal@taltech.ee

network voltage. The periodic variations from the sinewave, characterized as harmonics, are responsible for the voltage waveform deterioration. As the share of these voltage harmonics increases, the reliability of the network is imperiled. The current and voltage distortions may lead to several problems in the distribution network. The incremental higher frequencies amplify the proximity and skin effects in the cables. The performance and life span of transformers, cables, and other network components may be reduced because of the added stress [1,2]. The network protection equipment and electrical appliances can malfunction due to these unwanted harmonics [3]. Furthermore, the neutral conductor can be overloaded and it leads to undesirable consequences in the network [4]. The capacitor banks can also fail as the higher frequencies can alter their impedance [5]. Therefore, details about harmonic sources and their effect on the network are vital for the network operators to understand the power system's smooth operation within the limits of power quality indices.

Although sufficient literature is available related to power flow modelling, nonlinear load modelling and stochastic current harmonic estimations are relatively contemporary. The classical residential load models are developed to predict energy consumption patterns and are, therefore, unable to estimate current harmonic emissions mainly because of their low time resolution. Due to the stochastic nature of the modern nonlinear devices, it is not easy to model their usage and operational behaviour. Typically, a general overview is presented based on assumptions and limited measurements of the harmonic currents. On the other hand, several uncertainties are associated with a probabilistic approach for harmonic estimation. Domestic electrical appliances can operate in different modes and the harmonic emission profile could be very different for each mode. Thermal stability associated with electronic devices causes variation in the current harmonics, leading to an inaccurate assessment of power quality indices [6]. The harmonic cancellation also occurs as voltage or current harmonics are aggregated by geometrical vector addition because of the phase angles associated with them [7]. As a result, the aggregated harmonic content at the point of common coupling (PCC) may increase or decrease [8]. The assumptions and uncertainties linked with harmonic analysis lead to an inefficient modelling approach with inaccurate harmonic estimations.

This paper provides a framework of probabilistic modelling of current harmonics with nonlinear loads in the distribution network. The model relies on comprehensive power quality measurements and a probabilistic approach to model the harmonic current magnitude and phase angles. The electrical appliance usage patterns were developed to evaluate a nonlinear device's impact on the grid by the residential occupants. The load measurements were performed at different voltage waveforms, including sine wave, to observe the harmonic cancellation impact on harmonic aggregation. The harmonic analysis approach at different voltage levels will provide an insight into the real-time effect of electronic load on the network. The network impedance provides the way to calculate harmonic emission limits and is often estimated by using short circuit impedance [9]. The modern electronic load contains additional passive components that may affect the network impedance. The current harmonic measurements of electronic loads with different voltage waveforms will enable us to estimate the change in the load's impedance at various frequencies. Figure 1 shows how to estimate the change in network impedance when the electronic load is connected at the point of
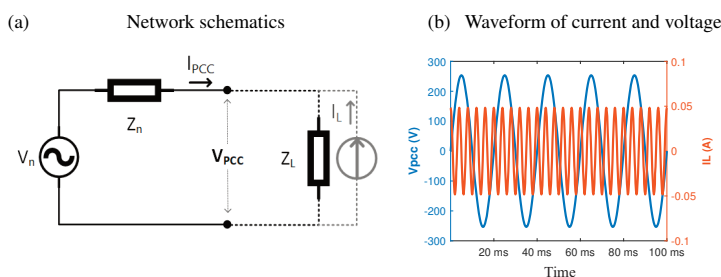

Fig. 1. Current and voltage waveforms at the PCC.

common coupling at a particular frequency. In the first stage, the voltage V_{PCC} and the current I_{PCC} from the network at the PCC are measured before connecting the load. The current I_L (150 Hz) is then injected and new measurements of the voltage V'_{PCC} and the current I'_{PCC} are taken at the PCC. The network impedance can be detected at the frequency f by using Eq. 1:

$$Z_f = \frac{V'_{PCC} - V_{PCC}}{I'_{PCC} - I_{PCC}}. \tag{1}$$

The existing harmonic estimation methods are presented in Section 2. Accuracy and uncertainties are analysed in Section 3 and Section 4 describes the proposed modelling approach for current harmonic estimation. A case study used to evaluate harmonic emission from the lighting load in the distribution grid is introduced in Section 5. Conclusions are presented in Section 6.

2. HARMONIC ESTIMATION METHODS

The distribution network is designed to provide sinusoidal voltage to the consumers. The modern nonlinear loads distort the voltage by adding current harmonics. A detailed harmonic analysis could provide insight into the power system behaviour under these voltage and current distortions. Researchers have made different models to estimate the current harmonics for the residential network. These models can be classified into time or frequency domain equivalent load models or measurement-based models.

The frequency-domain models are easier to compute and consider the frequency domain attributes of the electrical equipment. The simplest frequency domain model is the current source model based on the current magnitude and phase measurement of each harmonic under consideration. Any nonlinear load can be represented by the sum of constant current sources for each frequency [10]. Each current harmonic source is independent of the input voltage. However, in the distribution grid, the voltage distortions can alter the harmonic emissions of electrical equipment [11]. As the voltage waveform in a distribution network changes continuously depending on the type and amount of the connecting load, current source models are not effective for harmonic analysis. The Norton model addresses this problem by considering the admittance matrix. The model parameters are estimated by switching the operating condition of the power system with the assumption that the impedance and current of the Norton model will be constant and will not change with the shape of the voltage waveform. Two different sets of current and voltage harmonics are used to estimate the model parameters by means of Eq. 2 and Eq. 3:

$$Z_{n,h} = \frac{V'_h - V_h}{I'_h - I_h}, \tag{2}$$

$$I_{n,h} = \frac{V_h}{Z_{h,k}} - I_h. \tag{3}$$

Here, $Z_{n,h}$ and $I_{n,h}$ are the impedance and current of the Norton equivalent model for the harmonic h calculated by using two sets of current and voltage measurements V_h, I_h and V'_h, I'_h. Although this approach provides some advantages over the current source model, it is unable to consider the cross dependency of harmonics. The harmonic currents only depend on the corresponding voltage harmonics and not on the voltage waveform itself.

This shortcoming was improved by employing a crossed frequency admittance matrix in the Norton coupled (NC) model. The estimated harmonic currents using this model will depend not only on the voltage harmonics of the same frequency but also on the other frequencies. Eq. 4 and Eq. 5 represent the mathematical form of the NC model. The verification and comparison of frequency-domain models are presented in [12,13].

$$\vec{I} = \vec{Y} \times \vec{V}, \tag{4}$$

$$
\begin{bmatrix} \vec{I}_{1m} \\ \vec{I}_{2m} \\ \vec{I}_{3m} \\ \dots \\ \vec{I}_{nm} \end{bmatrix} = \begin{bmatrix} \vec{Y}_{11} & \vec{Y}_{12} & \vec{Y}_{13} & \dots & \vec{Y}_{1m} \\ \vec{Y}_{21} & \vec{Y}_{22} & \vec{Y}_{23} & \dots & \vec{Y}_{2m} \\ \vec{Y}_{31} & \vec{Y}_{32} & \vec{Y}_{33} & \dots & \vec{Y}_{3m} \\ \vdots & \vdots & \vdots & \dots & \vdots \\ \vec{Y}_{n1} & \vec{Y}_{n2} & \vec{Y}_{n3} & \dots & \vec{Y}_{nm} \end{bmatrix} \cdot \begin{bmatrix} \vec{V}_{1m} \\ \vec{V}_{2m} \\ \vec{V}_{3m} \\ \dots \\ \vec{V}_{nm} \end{bmatrix}. \tag{5}
$$

The time-domain models are based on the load's actual circuits and provide in-depth information about the load harmonic emission profile. A time-domain harmonic analysis approach was applied to nonlinear loads categorized based on their circuit topologies in [11]. Most electronic devices contain switch mode power supplies (SMPSs), for which reason time-domain models equivalent to the SMPS were created. The current harmonic estimation was provided on simulated and measured waveforms. In another study, a harmonic model was formulated for computer loads connected to a single transformer [14]. The results show harmonic cancellation and voltage waveform distortion at the transformer. The mathematical models of low power compact fluorescent lamps (CFLs) were made to study harmonic penetration in [15]. The voltage and current waveforms were recorded and analysed by means of circuit simulation software. Although the time-domain models provide an accurate harmonic analysis approach, they have limited application as it is challenging to model every load connected to the grid using its circuit schematic.

In the electrical model-based approach, the load connected to the network is categorized based on their electrical properties, and the probability distribution of each group is defined to estimate the overall harmonic emission. For example, the network load can be divided into linear or nonlinear devices. These devices can be additionally categorized according to circuit topology and power quality characteristics. A similar probabilistic harmonic analysis model was proposed in 1987 [16]. The model categorized nonlinear loads into four categories based on the switching state and operating mode. The harmonic aggregation analysis was performed using the Monte Carlo approach with probability density functions (PDFs) of harmonic magnitude and phase angles. Based on the appliance measurement data and their usage patterns, a harmonic analysis approach was applied to study the harmonic impacts of the household appliance in the low voltage distribution grid [17]. The results obtained from the harmonic model were then compared with the real-time measurements of the network. A similar bottom-up probabilistic harmonic estimation modelling approach was presented in [18]. The model generated a household appliance's usage patterns based on occupant behaviour, and the appliance's equivalent circuits were used to analyse the harmonic emission. The simulation results of harmonic loads were compared with the actual grid measurement results to extract correlated data. In another study, a probabilistic model to analyse waveform distortions was presented under the influence of high penetration of electric vehicles (EVs). The authors highlight the importance of this approach as uncertainties associated with the EV charging patterns can be easily accounted for [19]. The single and three-phase nonlinear loads were divided into groups based on their current THD (total harmonic distortion) in [20]. The participation of these load groups was obtained based on energy usage patterns at different times of the day. The author selected the customer database parameters by assuming that the data of any particular device type belonged to a normal distribution. The voltage distortion in the low voltage network was evaluated based on this probabilistic method.

In the measurement-based models, current harmonic emission is analysed from the probability distributions of harmonic current measurement data. The measurements could be taken at the electrical appliance level in a bottom-up approach, and aggregated harmonic analysis could provide the harmonic estimation at the point of common coupling. In the top-down approach, measurements are taken at the distribution transformer. In both cases, extensive measurement data is usually compared with an appropriate probability distribution. The voltage distortion in the distribution network was estimated by using Monte Carlo simulation of the aggregated harmonic current in [21]. The measurement data was assumed to fit a normal distribution. The harmonic currents were measured of residential and commercial loads at the point of common coupling in [22]. The measurements were divided into low, medium, and high demand subgroups and compared with the normal distribution and uniform distributions.

Two different approaches can be applied to construct a probabilistic model based on the type and amount of data [23]. The first approach could be termed as a parametric model where a finite set of data parameters can be compared with predefined distributions. In the second non-parametric approach, the model is based on distributions calculated from the data itself [24]. The parametric models mostly employ the normal distribution defined by mean and variance. The probability density function of a normal distribution is indicated by Eq. 6:

$$f_x = \frac{1}{\sqrt{2\pi\sigma^2}} \times e^{-\frac{(x-\mu)^2}{2\sigma^2}}. \tag{6}$$

Here, σ is the standard deviation and μ represents the mean value of x.

In the early harmonic models, the normal distribution was used to describe both magnitude and phase angles as independent variables. However, this assumption is not accurate for harmonic analysis. Therefore, a joint or bivariate probabilistic approach is more effective where the estimated variable depends on the probability density function of two variables. In [10], the load current for residential buildings was estimated using beta bivariate distributions. In [11,12], the joint normal distribution (JNB) was employed for the forecasting of harmonic emissions. The parameters of the normal joint distribution, σ (standard deviation) and μ (mean value) are calculated by Eq. 7 and Eq. 8 using the complex components of the current i_x and i_y:

$$\mu_{xy} = \begin{bmatrix} i_x \\ i_y \end{bmatrix}, \tag{7}$$

$$\sum xy = \begin{bmatrix} \sigma^2 i_x & \sigma(i_x, i_y) \\ \sigma(i_x, i_y) & \sigma^2 i_y \end{bmatrix}. \tag{8}$$

Figure 2a shows the 15th harmonic current when normal distribution fitting parameters are applied in a complex plane for a display monitor. The individual probability density of the real and imaginary parts of the current harmonics is indicated by red and blue lines, respectively. The green circle encloses the part of the distribution responsible for 95 percentile of the estimated values. Although the joint probability distribution provides better results than the individual normal distribution for x and y values, it can, however, be effective only when both components are linearly dependent. The nonlinear devices with multiple operating modes result in different harmonic currents. The resultant distribution fit of these devices could be very different from the normal distribution. Figure 2b shows the 9th harmonic current spread of a personal computer (PC) stress test in a complex plane where three different clusters are clearly visible. The normal joint distribution cannot represent this data efficiently. This problem can be addressed by clustering the data and applying the JNB to respective clusters. This approach is known as a multivariate normal mixture and provides a more flexible distribution fit [25]. The distribution mixture approach was applied in [26] to study power quality impact in low voltage distribution. The PDFs of the current harmonics were calculated by finite normal distribution components with their associated weights. The drawback of this approach is that the model requires predefined cluster information.

An adaptive kernel density estimation (KDE) with a plug-in bandwidth selection approach is presented in [27]. The KDE algorithm designates probability distribution for every data point using a kernel function and bandwidth, also known as the smoothing parameter, indicated in Eq. 9:

$$f_h = \frac{1}{N} \sum_{i=1}^{N} K_b(h - h_i) = \frac{1}{N_b} \sum_{i=1}^{N} K \frac{(h - h_i)}{b}. \tag{9}$$

Here, f_h provides the PDF of h for N observations. K is the kernel and b is the bandwidth. The sum of kernels provides the total probability density of a variable. The optimal bandwidth selection is critical in a KDE model. A large bandwidth will smooth the probability density curve but results in fewer data points in each kernel. As a result, information about data variation will be lost. The optimal methods for finding bandwidth are introduced in [28]. The KDE algorithm, along with the Monte Carlo simulation, was used to
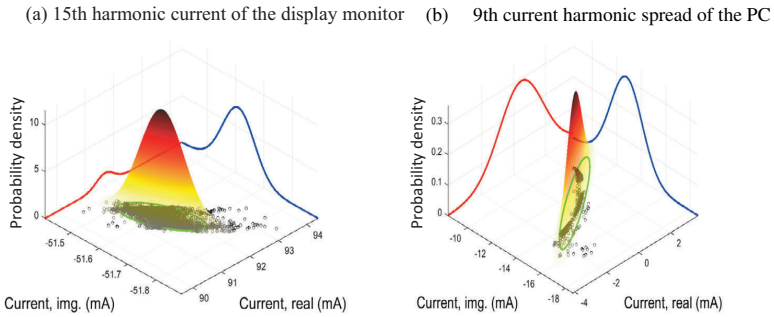
(a) 15th harmonic current of the display monitor   (b)   9th current harmonic spread of the PC

Fig. 2. Joint probability distribution applied to harmonic currents drawn by the monitor and PC [23].

estimate harmonic load flow in [24] and [29]. However, harmonic current magnitude and phase angles were estimated independently, which would provide inaccurate phasor data results. A joint distribution from the KDE algorithm can generate better results where multidimensional vectors represent the parameters. In Fig. 3a, the KDE is applied to the 5th harmonic current measured during the PC stress test. This method requires intensive calculations, and high computational power is needed for even a small-scale harmonic analysis.

Empirical bivariate histogram (EBH) distribution is another approach that divides data into predefined bins. The EBH distribution data is normalized by using Eq. 10 to create a probability density mesh:

$$P_{x,y} = \frac{C(x,y)}{N \cdot W_x \cdot W_y}. \tag{10}$$

Here, $P_{x,y}$ is the probability density of a bin at (x, y), $C(x, y)$ are the number of samples in the bin and W_x, W_y defines the area of the bin. N defines the total number of data points. Figure 3b demonstrates the histogram distribution applied to the 5th harmonic current of a PC under stress test. The advantage of EBH over KDE distribution is that it requires less computational power. However, both EBH and KDE distributions generate unused data space in the PDF when clusters are present in the data. Data sampling for these techniques is quite challenging.
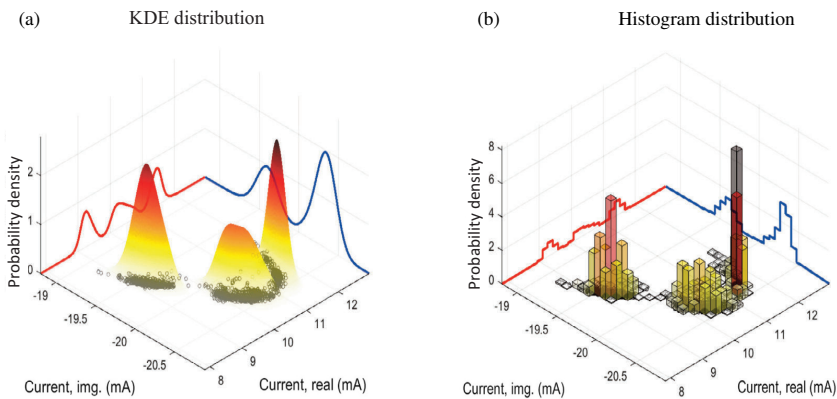

(a)   KDE distribution   (b)   Histogram distribution

Fig. 3. KDE and histogram distributions applied to the 5th harmonic current of the PC [23].

3. ACCURACY AND UNCERTAINTIES

Current harmonic emission could be affected by several factors, including network configurations, load variations, appliance parameters, and measurement uncertainties [30]. The power system uncertainties are widely addressed in the literature. The network uncertainty includes variation in supply voltage, frequency, and resonance. They are difficult to model as various factors, including generation, dispatch, and network topologies, affect the estimations [31,32].

The load connected to each bus in the distribution network is comprised of various linear and nonlinear loads. During different times in the day, various loads are connecting and disconnecting to the buses. The researchers use varied stochastic approaches to predict network load behaviour [33,34]. Modern electrical appliances work in various modes that generate different harmonic emission profiles. Different parameters associated with the appliances also vary due to the variations incorporated during the manufacturing process [35]. The environmental conditions and aging of the equipment play their role as well [36].

The measurement uncertainties are associated with the environment, measuring instrument uncertainties, and variations in the test equipment. As the current harmonic profiles vary under different operating modes of the devices, the measurement results should include these variations. The supply voltage distortion also alters the current harmonics of different loads. Therefore, it is challenging to measure specific electrical equipment on different modes under different supply variations. The thermal stability also changes the current harmonics of the electrical appliances. The thermal stability effect on light-emitting diode (LED) lamps shows a significant variation in current harmonics during the stability time. The effect of current harmonic estimation displays a significant error as well [37]. Similarly, power supplies also show a more than 20% and 12% variation in the THD and the total RMS current, respectively [38]. Likewise, the harmonic current cancellation affects the outcome of harmonic analysis. The higher-order harmonic indicates a more prominent reduction if the harmonic cancellation is taken into account [7]. The harmonic currents are also affected by the cable impedance [39]. Therefore, all of these uncertainties should be included in the model to estimate current harmonic emission.

4. PROPOSED STOCHASTIC MODELLING APPROACH

The modern electronic equipment operates in different modes, and their current harmonic spread is irregular with clustered data. The probabilistic approach of modelling current harmonics has the advantage of tackling any sporadic variations. The stochastic models to estimate the current harmonic described in the previous section have several limitations in terms of accuracy or computational complexity. Most of the models use a normal distribution or joint normal distribution fit, not appropriate for most of the current harmonic measurement data as they show different distribution spreads. The KDE and histogram distribution algorithms require a bandwidth selection and become inefficient if the data has clusters.

A novel empirical bivariate probability distribution (EBPD) approach is applied in this research as a part of the proposed bivariate stochastic (BS) model to estimate the current harmonics in the low voltage network. The current harmonic magnitude data is used to generate the empirical cumulative distribution function (ECDF) for the harmonics under consideration. The ECDF will provide the groups of the real and complex components with their probabilities. The model consists of three parts: appliance usage model, measurement database, and empirical bivariate harmonic current model. The algorithm of the model is described with a flow chart in Fig. 4.

The model will simulate the required number of houses for a given number of days to estimate the magnitude and phase angles of the harmonic currents generated by each house appliance. During each day, all houses are populated with the appliance stock, and the current harmonics of every appliance are estimated using the EBPD model. The appliance stock and usage pattern of that appliance are provided by the appliance usage (AU) model further described in this section. Every appliance is simulated individually, and the total harmonic emission of an individual household is aggregated in each iteration. The harmonic
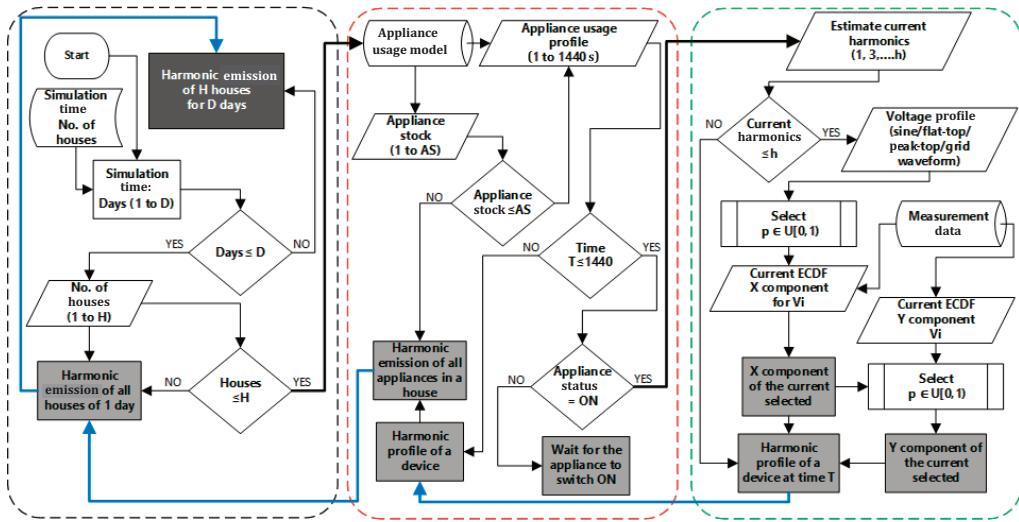
Fig. 4. Flow chart of the proposed model.

currents are aggregated in a complex plane. Therefore, the model also estimates real and complex (X and Y) components of each current harmonic.

4.1. Appliance usage model

An efficient current harmonic estimation model should take into account the load variation in the distribution grid. Harmonic injection in a network at a given time depends on the type and amount of the load connected to the grid on that particular instant. However, the load prediction is a complex task as it is difficult to estimate when the consumer is going to use a particular appliance. The occupant behaviour of using electrical appliances is challenging to model as it depends on many factors. Occupants interact with the electrical and nonelectric systems installed in the building, altering thus the energy usage patterns [40]. The International Energy Agency (IEA) also regards occupant actions as the primary cause of controlling the environmental parameters to maintain a comfortable living atmosphere [41]. These occupant actions are responsible for 71% variation in the building's energy consumption [42]. However, various factors influence the resident's behaviour, including their age, income, social status, and cultural background [43]. The building structure, insulation quality, climate conditions also play their role. Therefore, universal occupancy modelling is near to impossible.

The electricity consumption models can be broadly classified into three categories: top-down models, bottom-up models, and hybrid models [44]. The top-down modelling approach is based on data collected on the macro-level. It may include an electricity billing database, national census, or survey data. The researchers have frequently used the Time Use Survey (TUS) data collected in Europe, Britain, and America for their energy consumption models. These surveys collect data from the targeted groups based on different parameters. The models based on similar data have many drawbacks and lack the capability to provide a detailed analysis of the physical behaviour of the building systems.

The bottom-up models are based on physical measurements at the device or building level. Nevertheless, these models provide accurate information regarding energy consumption in a building but are complicated to construct due to the involvement of several variables. These variables include occupancy, occupant behaviour, climate conditions, building structure, and an extensive database of appliance's measurements. As

it is difficult to consider each variable in detail, a compromise is required to make a specific model for a particular research problem. Another approach is to combine the benefits of both bottom-up and top-down approaches to improve efficiency. These models are termed as hybrid models [45].

We need a residential electricity consumption model to estimate current harmonic emissions from the building. Therefore, a high-resolution bottom-up model is required to provide usage patterns of domestic appliances that can be compared with the power quality (PQ) measurements. Figure 5 illustrates the abstract diagram of our appliance usage model for residential buildings.

For this study, a residential building in Estonia is measured at the device level for one month. The data is used to construct a probabilistic model to estimate the switching behaviour of the appliance. The model consists of active occupancy profiles, appliance stock in the households, and the electricity consumption measurements as shown in Fig. 5.

Active occupancy profiles are created based on the electricity consumption of the appliance that comes under the direct influence of the occupant's activities. The usage of lighting, media, kitchen, cleaning, and laundry appliances directly depends on the occupant's behaviour. Electricity consumption metre data has been used for occupancy modelling in many studies [46–49]. A similar approach is applied here to create a two state active occupancy profile. ECDFs are created for both weekdays and weekends occupancy status based on the electricity consumption data. A survey related to the occupant's daily activities is also used to improve these occupancy profiles.

Every household has different appliances depending on the family size, geographical location and socioeconomic status. Appliances are also available from different manufacturers with various specifications. Manufacturers introduce new models every year with improved functionality and energy ratings. The appliance ownership information can be extracted from several surveys conducted on national level in different countries. A domestic energy model was created on the basis of a set of common appliances based on national ownership statistics for the United Kingdom (UK) in [50]. Similar surveys also conducted in Europe and the USA.

The appliance usage model (AU) will provide the information when a particular appliance is switched ON in the house. The ECDFs are used to generate switching and duration intervals of each appliance in the house. The total electricity consumption of a single housing unit can be determined from the Eq. 11:

$$E = \sum_{day=1}^{D} \left[\sum_{ap=1}^{n} (P_a \times d_a) + (P_s \times d_s) \right]. \tag{11}$$

Here, P_a denotes the active power of the appliance ap in its active mode and P_s is its active power in the standby mode. d_a and d_s are the time duration of an appliance operating in active or standby modes during a day.
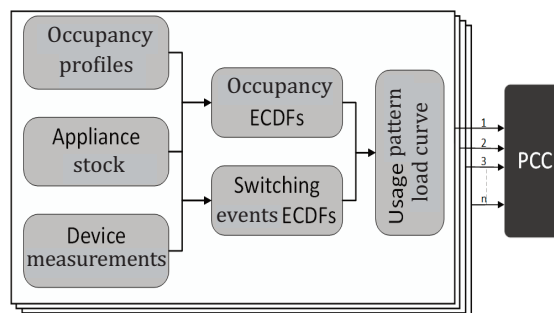

Fig. 5. Abstract diagram of the appliance usage model.

4.2. Measurement database

The measurement database contains the current harmonic measurements of different household appliances operating at different working modes on various voltage waveforms. We have used sinusoidal, peak-top, flat-top, and real-time grid voltage waveforms as an input to measure current harmonics.

For the real-time grid voltage waveforms, a low voltage residential network is measured at 5-minute intervals for a day to record the voltage harmonic magnitude and phase angles. Figure 6 shows the voltage waveform used to measure the current harmonic emission from the household appliances using the measurement test bench.

The measurement test bench consists of a PC with MATLAB program and a data acquisition (DAQ) module from National Instruments to generate a reference signal for the controllable power supply. The reference signal V_R has enabled us to generate the required voltage waveform V_O using Eq. 12:

$$V_O = \frac{V_R \times V_{range}}{V_C}.$$ (12)

Here, V_{range} is 300 V and V_C is 7.07. V_R is generated by using the voltage harmonic magnitudes and phase angles by means of Eq. 13:

$$V_{out} = \sum_{i=1}^{n} \sqrt{2} \times A_i \sin(2\pi f_i t_s + \alpha_i).$$ (13)

Here, A_i represents the root mean square values of the voltage harmonics and α_i indicates the phase difference from the fundamental frequency. f_i, t_s is the harmonic frequency for the ith harmonic and sampling interval, respectively. The sampling frequency of the reference signal is 100 kHz and it is indicated by f_s. Figure 7 demonstrates the schematic of the measurement setup.

The harmonic current estimation model is based on the power quality measurement data of the appliance portfolio. The device usage patterns from Section 3.1 are compared with the harmonic current profiles of each household appliance. The model can be used to evaluate the total harmonic emission of a multiple house as illustrated in Fig. 8.

4.3. Empirical bivariate harmonic current model

The empirical bivariate harmonic current modelling approach is suitable for harmonic analysis of loads with the dynamic profile of harmonic emission and is also capable of addressing different uncertainties responsible
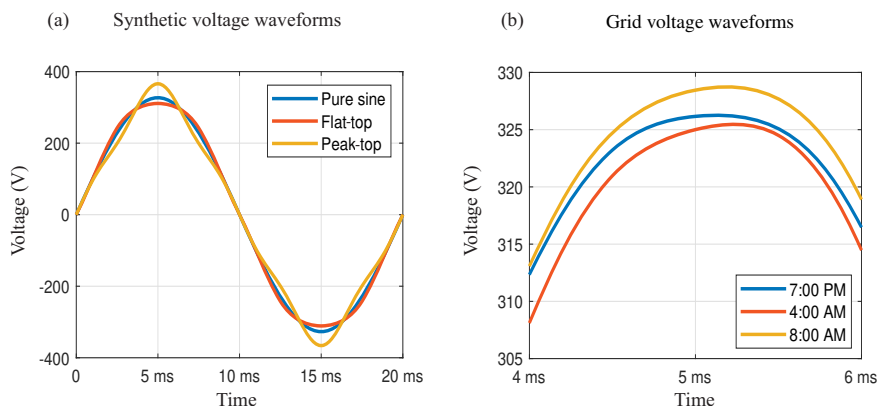

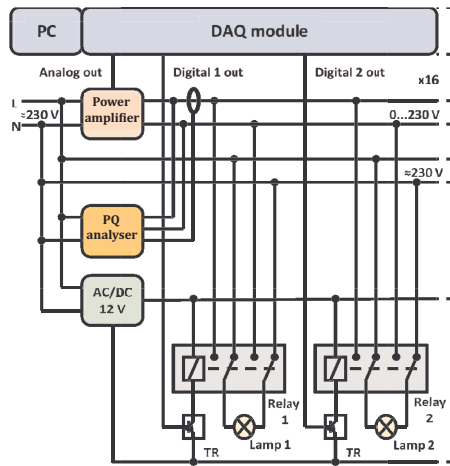Fig. 6. Voltage waveforms used for current harmonics measurements.

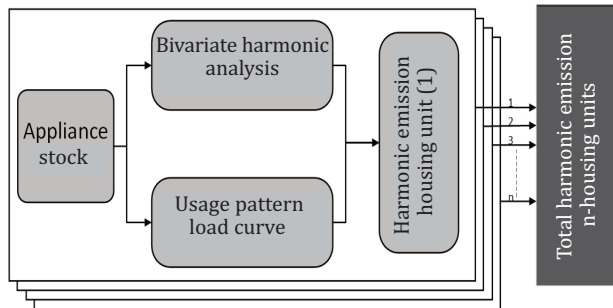**Fig. 7.** Schematic of the measurement setup.

Fig. 8. Harmonic current estimation of multiple households.

for current harmonic variations. The current harmonics of individual appliances will be modelled by means of the ECDF. In the first step, the ECDF for the real part of the current in the complex domain is calculated. Each group of this ECDF is further mapped with the complex part of the variable's data group, and the ECDF of each bivariate data group is calculated. The resolution of the ECDF determines the accuracy of the harmonic estimation model. ECDFs for both real and imaginary components are calculated using Eq. 14:

$$p_m(X \le x) = \frac{1}{m} \sum_{k=1}^{m} 1[x_k \le t].$$ (14)

Here, p_m is the cumulative probability function of m groups. The 1 is called indicator function and has two possible values as shown by Eq. 15:

$$1[x_k \le t] = \begin{cases} 1 & for\ x_k \le x \\ 0 & for\ x_k > x \end{cases}.$$ (15)

Figure 9 demonstrates how ECDFs of real and imaginary components of the current harmonics can be used to create distribution of the current harmonic in the complex plane. The red line shows the ECDF of the real
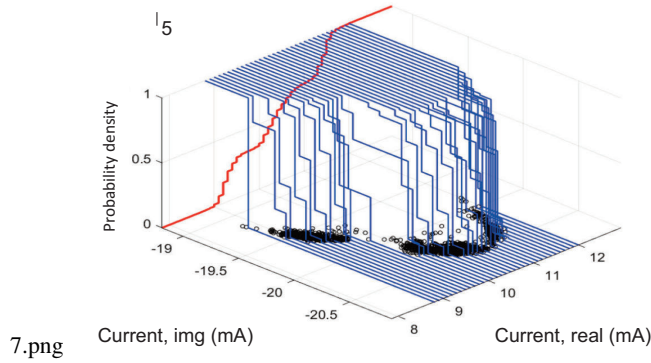
Fig. 9. EBPD applied to the 5th harmonic of the PC under stress test [23].

component of the harmonics and each blue line indicates the ECDF of the imaginary components at each group of the real component's ECDF.

5. CASE STUDY OF HARMONIC ESTIMATIONS

The proposed bivariate stochastic model was used to estimate current harmonic emission from the lighting load in the low voltage residential grid. The lighting usage profiles were made utilizing the AU model with a 1-minute resolution. The lighting measurements from the measured residential building were analysed for this purpose. The active occupancy profiles and electricity consumption data were the inputs of our lighting usage model. Total lighting load was segregated into the usage profile of each switch to control the electrical lights in the building. The load curves were divided into morning, day, and evening cycles. Each cycle was simulated separately.

The ECDFs were created to generate the probability distribution function of the switching and noise events. The switching events occur when a lamp is turned ON for more than 10 minutes. All events with a lamp usage of less than 10 minutes are considered noise events. The time duration of switching and noise events for all lamps in a house can be aggregated to find the total lighting power demand. Equation 16 can be used to calculate the total energy consumed by each lamp during any cycle in a residential building:

$$E_l = \sum_{t=1}^{T} \left[\sum_{se=1}^{m} (d_{se} \times P_l) + \sum_{ne=1}^{n} (d_{ne} \times P_l) \right]. \tag{16}$$

Here, E_l is the total energy consumed by a lamp in one cycle of T minutes duration with m and n switching and noise events, respectively. d_{se} refers to the duration of each switching event and d_{ne} is the duration of one noise event. The 60 houses were simulated for 100 days, and each house was populated with different LED lamps depending on the lumens needed in each room. The usage pattern from the AU model provided the time at which a particular lamp would switch ON as well as the ON time duration. A Monte Carlo based approach was applied to calculate the current harmonics injected by the lighting from all the 60 houses. The lamps operate in a single working mode (ON or OFF state) if dimming circuits are not used. Therefore, bivariate harmonic estimation is simplified. The lamps were measured on different voltage waveforms. These waveforms were regenerated using the measurement test bench described in Section 4.3. Lamps were warmed up for 1 hour to eliminate the measurement variation because of thermal instability. The voltage waveforms included sinusoidal, peak-top, flat-top, and real grid waveforms during different times of a day. The probabilities were assigned to each voltage waveform, as shown in Table 1.

Table 1. Waveform probability used in the model

Waveform	Probability
Sinusoidal	0.15
Flat-top	0.06
Peak-top	0.04
Grid waveform 1	0.25
Grid waveform 2	0.25
Grid waveform 3	0.25

After selecting the voltage waveform during each iteration, the real components of the current harmonics were selected for the particular voltage waveform. In the next step, the complex component of the current harmonics was generated based on the group assigned to the selected real component. The real and imaginary components of current harmonics for all lamps were generated for a day with 1-second resolution. Figure 10 illustrates the total RMS current drawn by the lighting usage of 60 houses. The bold black line shows the mean value of the RMS current, and the blue dotted line indicates the 90 percentile value of the RMS current consumed by the lighting in 60 houses. The minimum value of the RMS current drawn by the lighting usage in all 60 houses is illustrated by the red dotted line.

The high-frequency current harmonics can also be estimated in a similar process. Figure 11 shows the 3rd, 5th, 7th, and 9th current harmonic represented by black, red, blue, and green colours, respectively. The bold line indicates the mean value, and the dotted line shows the 90th percentile value.
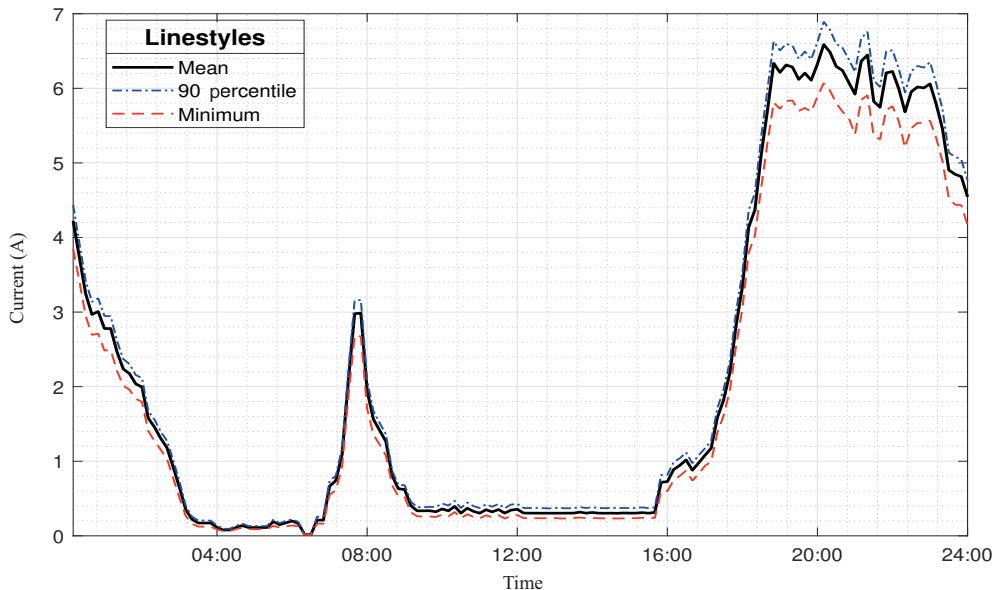
Fig. 10. Total RMS current estimated for the lighting load of 60 houses for 100 days.
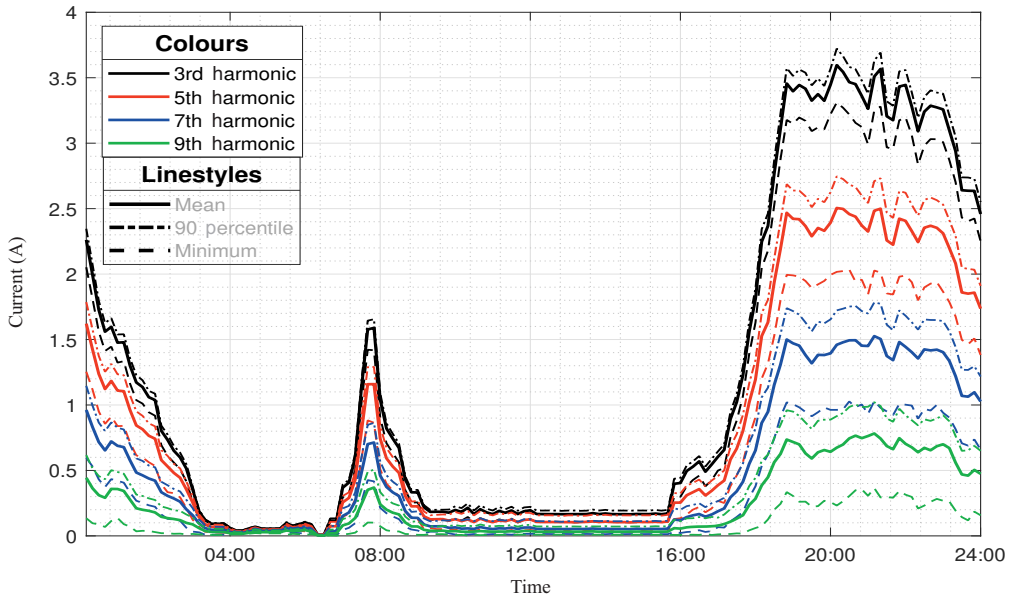
Fig. 11. Harmonic current estimation of the lighting load of 60 houses for 100 days.

The results reveal the effectiveness of the proposed approach as it is simple to evaluate, and any uncertainty could be added at any step. The model provides flexibility to evaluate present and future appliances by expanding the measurement database with power quality measurements of devices on different voltage waveforms.

6. CONCLUSIONS

A novel bottom-up stochastic model to assess the current harmonic emission is presented in this paper. The bivariate empirical distribution approach is used to model harmonic currents. It provides a simple and flexible option to evaluate different aspects of harmonic emission in the distribution grid. The model is capable of handling any uncertainty associated with the distribution grid by considering its stochastic nature.

The stochastic approach has made the model more efficient in handling variations and uncertainties than the traditional numerical or probabilistic methods. The bivariate approach is applied to model current harmonics, making the model capable of processing data with high variations and clusters.

An appliance usage model is also presented based on the real-time measurements at the device level. The occupancy and appliance stock data can be used to create usage profiles of different electrical appliances in a residential building. Thermal stability, cable impedance, and grid side variation are considered during the measurements. The model is flexible to include additional future loads such as electric vehicles. It provides an accurate assessment of the power quality aspects from the perspective of the low voltage distribution under dynamic load and network conditions. The case study provides the effectiveness of the model by estimating the current harmonic emission due to the lighting load of sixty houses. The measurement database could be extended in the future by including measurements of different household appliances.

ACKNOWLEDGEMENTS

REFERENCES

1. Pierce, L. W. Transformer design and application considerations for nonsinusoidal load currents. *IEEE Trans. Ind. Appl.*, 1996, **32**(3), 633–645.
2. Shareghi, M., Phung, B. T., Naderi, M. S., Blackburn, T. R. and Ambikairajah, E. Effects of current and voltage harmonics on distribution transformer losses. In *Proceedings of the IEEE International Conference on Condition Monitoring and Diagnosis, Bali, Indonesia, September 23–27, 2012.* IEEE, 2013, 633–636.
3. Czarnecki, L. S. Comments on active power flow and energy accounts in electrical systems with nonsinusoidal waveforms and asymmetry. *IEEE Trans. Power Delivery*, 1996, **11**(3), 1244–1250.
4. Watson, N. R., Scott, T. L. and Hirsch, S. J. J. Implications for distribution networks of high penetration of compact fluorescent lamps. *IEEE Trans. Power Delivery*, 2009, **24**(3), 1521–1528.
5. Clement-Nyns, K., Haesen, E. and Driesen, J. The impact of charging plug-in hybrid electric vehicles on a residential distribution grid. *IEEE Trans. Power Syst.*, 2010, **25**(1), 371–380.
6. Iqbal, M. N., Jarkovoi, M., Kütt, L. and Shabbir, N. Impact of LED thermal stability to household lighting harmonic load current modeling. In *Proceedings of Electric Power Quality and Supply Reliability Conference (PQ) & Symposium on Electrical Engineering and Mechatronics (SEEM), Kärdla, Estonia, June 12–15, 2019*. IEEE, 2019, 1–6.
7. Jarkovoi, M., Iqbal, M. N. and Kütt, L. Analysis of harmonic current stability and summation of LED lamps. In *Proceedings of Electric Power Quality and Supply Reliability Conference (PQ) & Symposium on Electrical Engineering and Mechatronics (SEEM), Kärdla, Estonia, June 12–15, 2019.* IEEE, 2019, 18957598.
8. Hansen, S., Nielsen, P. and Blaabjerg, F. Harmonic cancellation by mixing nonlinear single-phase and three-phase loads. *IEEE Trans. Ind. Appl.*, 2000, **36**(1), 152–159. https://doi.org/10.1109/28.821810
9. Chakravorty, D., Meyer, J., Schegner, P., Yanchenko, S. and Schocke, M. Impact of modern electronic equipment on the assessment of network harmonic impedance. *IEEE Trans. Smart Grid*, 2017, **8**(1), 382–390.
10. Henao-Muñoz, A. C. and Saavedra-Montes, A. J. Comparison of two mathematical models for nonlinear residential loads. In *Proceedings of the 17th International Conference on Harmonics and Quality of Power (ICHQP), Belo Horizonte, Brazil, October 16–19, 2016.*
11. Blanco, A. M., Yanchenko, S., Meyer, J. and Schegner, P. Impact of supply voltage distortion on the current harmonic emission of non-linear loads. *DYNA*, 2015, **82**(192), 150–159.
12. Koch, A. S., Myrzik, J. M. A., Wiesner, T. and Jendernalik, L. Evaluation and validation of Norton approaches for nonlinear harmonic models. In *Proceedings of IEEE Grenoble Conference PowerTech, Grenoble, France, June 16–20, 2013.* IEEE, 2013, 1–6.
13. Almeida, C. F. M. and Kagan, N. Harmonic coupled norton equivalent model for modeling harmonic-producing loads. In *Proceedings of the 14th International Conference on Harmonics and Quality of Power – ICHQP 2010, Bergamo, Italy, September 26–29, 2010.* IEEE, 2010, 1–9.
14. Ahmed, E. E., Xu, W. and Zhang, G. Analyzing systems with distributed harmonic sources including the attenuation and diversity effects. *IEEE Trans. Power Delivery*, 2005, **20**(4), 2602–2612. https://doi.org/10.1109/TPWRD.2005.855441
15. Cunill-Sola, J. and Salichs, M. Study and characterization of waveforms from low-watt (<25 W) compact fluorescent lamps with electronic ballast. *IEEE Trans. Power Delivery*, 2007, **22**(4), 2305–2311.
16. Baghzouz, Y. and Tan, O. T. Probabilistic modeling of power system harmonics. *IEEE Trans. Ind. Appl.*, 1987, **IA-23**(1), 173–180.
17. Ye, G., Nijhuis, M., Cuk, V. and Cobben, J. F. G. Stochastic residential harmonic source modeling for grid impact studies. *Energies*, 2017, **10**(3), 372. https://doi.org/10.3390/en10030372
18. Salles, D., Jiang, C., Xu, W., Freitas, W. and Mazin, H. E. Assessing the collective harmonic impact of modern residential loads– Part I: methodology. *IEEE Trans. Power Delivery*, 2012, **27**(4), 1937–1946. https://doi.org/10.1109/TPWRD.2012.2207132
19. Caramia, P., Proto, D., Russo, A. and Varilone, P. Probabilistic harmonic analysis for waveform distortion assessment of low voltage distribution systems with plug-in hybrid electric vehicles. In *Proceedings of the 1st International Conference on Energy Transition in the Mediterranean Area (SyNERGY MED), Cagliari, Italy, May 28–30, 2019*. IEEE, 2019, 1–6.
20. Au, M. T. and Milanović, J. V. Establishing harmonic distortion level of distribution network based on stochastic aggregate harmonic load models. *IEEE Trans. Power Delivery*, 2007, **22**(2), 1086–1092. https://doi.org/10.1109/TPWRD.2007.893193
21. Au, M. T. and Milanović, J. V. Stochastic assessment of harmonic distortion level of medium voltage radial distribution network. In *Proceedings of the 9th International Conference on Probabilistic Methods Applied to Power Systems, Stockholm, Sweden, June 11–15, 2006*. IEEE, 2006, 1–6.
22. Au, M. T. and Milanović, J. V. Development of stochastic aggregate harmonic load model based on field measurements. *IEEE Trans. Power Delivery*, 2007, **22**(1), 323–330. https://doi.org/10.1109/TPWRD.2006.881455
23. Jarkovoi, M., Kütt, L. and Iqbal, M. N. Probabilistic bivariate modeling of harmonic current. In *Proceedings of the 19th International Conference on Harmonics and Quality of Power (ICHQP), Dubai, United Arab Emirates, July 6–7, 2020*. IEEE, 2020, 1–6.

24. Nasrfard-Jahromi, F. and Mohammadi, M. Probabilistic harmonic load flow using an improved kernel density estimator. *International Journal of Electrical Power and Energy Systems*, 2016, **78**, 292–298. https://doi.org/10.1016/j.ijepes.2015.11.076

25. Ray, S. and Lindsay, B. G. The topography of multivariate normal mixtures. *Ann. Stat.*, 2005, **33**(5), 2042–2065. https://doi.org/10.1214/009053605000000417

26. Meyer, J. and Schegner, P. Characterization of power quality in low voltage networks based on modeling by mixture distributions. In *Proceedings of the 9th International Conference on Probabilistic Methods Applied to Power Systems, PMAPS, Stockholm, Sweden, June 11–15, 2006*. IEEE, 2007.

27. Botev, Z. I., Grotowski, J. F. and Kroese, D. P. Kernel density estimation via diffusion. *Ann. Statist.*, 2010, **38**(5), 2916–2957. https://doi.org/10.1214/10-AOS799

28. Węglarczyk, S. Kernel density estimation and its application. *ITM Web of Conferences*, 2018, **23**, 00037. https://doi.org/10.1051/itmconf/ 20182300037

29. Nasrfard-Jahromi, F. and Mohammadi, M. A sampling-based method using an improved nonparametric density estimator for probabilistic harmonic load flow calculation. *Turk. J. Elec. Eng. Comp. Sci.*, 2016, **24**, 51113–5123. https://doi.org/10.3906/elk-1505-197

30. Li, Z., Hu, H., Wang, Y., Tang, L., He, Z. and Gao, S. Probabilistic harmonic resonance assessment considering power system uncertainties. *IEEE Trans. Power Delivery*, 2018, **33**(6), 2989–2998.

31. Sainz, L. and Balcells, J. Harmonic interaction influence due to current source shunt filters in networks supplying nonlinear loads. *IEEE Trans. Power Delivery*, 2012, **27**(3), 1385–1393.

32. Barmada, S., Musolino, A., Raugi, M. and Tucci, M. Analysis of power lines uncertain parameter influence on power line communications. *IEEE Trans. Power Delivery*, 2007, **22**(4), 2163–2171. https://doi.org/10.1109/TPWRD.2007.900305

33. Preece, R. and Milanović, J. V. Efficient estimation of the probability of small-disturbance instability of large uncertain power systems. *IEEE Trans. Power Systems*, 2016, **31**(2), 1063–1072.

34. Abu-Hashim, R., Burch, R., Chang, G., Grady, M., Gunther, E., Halpin, M. et al. Test systems for harmonics modeling and simulation. *IEEE Trans. Power Delivery*, 1999, **14**(2), 579–587. https://doi.org/10.1109/61.754106

35. Morales, J. M. and Pérez-Ruiz, J. Point estimate schemes to solve the probabilistic power flow. *IEEE Trans. Power Syst.*, 2007, **22**(4), 1594–1601. https://doi.org/10.1109/TPWRS.2007.907515

36. Pinceti, P. and Prando, D. Sensitivity of parallel harmonic filters to parameters variations. *Int. J. Electr. Power Energy Syst.*, 2015, **68**, 26–32.

37. Iqbal, M. N., Kütt, L., Asad, B., Shabbir, N. and Rasheed, I. Time-dependent variations in current harmonic emission by LED lamps in the low-voltage network. *Electr. Eng.*, 2020, **101**(25), 1277–1293.

38. Iqbal, M. N., Kütt, L., Asad, B., Vaimann, T., Rassõlkin, A. and Demidova, G. L. Time dependency of current harmonics for switch-mode power supplies. *Appl. Sci.*, 2020, **10**(21), 7806.

39. Iqbal, M. N. and Lauri, K. Impact of cable impedance on the harmonic emission of LED lamps. In *Proceedings of the 21st International Scientific Conference on Electric Power Engineering (EPE), Prague, Czech Republic, October 19–21, 2020*. IEEE, 2020, 1–5.

40. Sun, K., Yan, D., Hong, T. and Guo, S. Stochastic modeling of overtime occupancy and its application in building energy simulation and calibration. *Build. Environ.*, 2014, **79**, 1–12. http://dx.doi.org/10.1016/j.buildenv.2014.04.030

41. Yoshino, H., Hong, T. and Nord, N. IEA EBC annex 53: Total energy use in buildings–analysis and evaluation methods. *Energy Build.*, 2017, **152**, 124–136. https://doi.org/10.1016/j.enbuild.2017.07.038

42. Sonderegger, R. C. Movers and stayers: The resident's contribution to variation across houses in energy consumption for space heating. *Energy Build.*, 1978, **1**(3), 313–324.

43. Feng, X., Yan, D. and Hong, T. Simulation of occupancy in buildings. *Energy Build.*, 2015, **87**, 348–359. http://dx.doi.org/10.1016/j.enbuild.2014.11.067

44. Iqbal, M. N. and Kütt, L. End-user electricity consumption modelling for power quality analysis in residential building. In *Proceedings of the 19th International Scientific Conference on Electric Power Engineering (EPE), Brno, Czech Republic, May 16–18, 2018*. IEEE, 2018, 1–6.

45. Ofetotse, E. L., Essah, E. A. and Yao, R. Domestic energy models: complexities in defining specific tools. In *Proceedings of the International Conference of SuDBE2013, Chongqing, China, October 25–28, 2013*.

46. Causone, F., Carlucci, S., Ferrando, M., Marchenko, A. and Erba, S. A data-driven procedure to model occupancy and occupantrelated electric load profiles in residential buildings for energy simulation. *Energy Build.*, 2019, **202**, 109342. https://doi.org/10.1016/j.enbuild.2019.109342

47. Tekler, Z. D., Low, R. and Blessing, L. Using smart technologies to identify occupancy and plug-in appliance interaction patterns in an office environment. *IOP Conf. Ser.: Mater. Sci. Eng.*, 2019, **609**(6), 062010.

48. Molina-Markham, A., Shenoy, P., Fu, K., Cecchet, E. and Irwin, D. Private memoirs of a smart meter. In *BuildSys'10: Proceedings of the 2nd ACM Workshop on Embedded Sensing Systems for Energy-Efficiency in Buildings, Zurich, Switzerland, November 2, 2010*. ACM, New York, NY, 2010, 61–66.

49. Kleiminger, W., Beckel, C. and Santini, S. Household occupancy monitoring using electricity meters. In *UbiComp 2015: Proceedings of the ACM International Joint Conference on Pervasive and Ubiquitous Computing, Osaka, Japan, September 7–11, 2015*. ACM, New York, NY, 2015, 975–986.

50. Richardson, I., Thomson, M. and Infield, D. A high-resolution domestic building occupancy model for energy demand simulations. *Energy Build.*, 2008, **40**(8), 1560–1566.

Madalpinge-jaotusvõrgus esinevate vooluharmoonikute kahemõõtmeline stohhastiline modelleerimine

Muhammad Naveed Iqbal, Lauri Kütt, Kamran Daniel, Marek Jarkovoi, Bilal Asad ja
Noman Shabbir

On esitatud kahemõõtmeline stohhastiline analüüs vooluharmoonikute hindamiseks alt-üles viisil, mis arvestab võrgu ja koormuste muutumist. Vooluharmoonikute hindamine praeguste ja tulevikus rakedatavate mittelineaarsete koormustega on oluline, et määrata nende mõju jaotusvõrgule. Traditsioonilised harmoonikute analüüsi mudelid arvestavad ainult püsivaid koormusi ja jätavad kõrvale harmoonikute omavahelise mõju. Soojuslik stabiilsus, harmoonikute tühistamine ja võrgu dünaamilised parameetrid mõjutavad samuti vooluharmoonikute hinnanguid. Antud artiklis on esitatud tõenäosuslik lähenemine, millega modelleerida vooluharmoonikute emissiooni madalpinge-jaotusvõrkudes võrgu ja koormuse määramatuse korral. Esitatud mudeli tõhusust on näidatud juhtumipõhise analüüsiga.

V

M. N. Iqbal; L. Kütt; K. Daniel; B. Asad; P.S. Ghahfarokhi, "Estimation of harmonic emission of electric vehicles and their impact on low voltage residential network," Sustainability, vol. 13, p. 8551, July 2021

Article

Estimation of Harmonic Emission of Electric Vehicles and Their Impact on Low Voltage Residential Network

Muhammad Naveed Iqbal [1,*] , **Lauri Kütt** [1] , **Kamran Daniel** [1,2] , **Bilal Asad** [1,3] **and Payam Shams Ghahfarokhi** [1,4]

1 Department of Power Engineering and Mechatronics, Tallinn University of Technology, Ehitajate tee 5, 19086 Tallinn, Estonia; lauri.kutt@taltech.ee (L.K.); kamran.daniel@uet.edu.pk (K.D.); bilal.asad@aalto.fi (B.A.); Payam.Shams-Ghahfarokhi@rtu.lv (P.S.G.)

2 Department of Electrical, Electronics and Telecommunication Engineering, University of Engineering and Technology (FSD Campus), Lahore 54890, Pakistan

3 Department of Electrical Engineering and Automation, Aalto University, Maarintie 8, 02150 Espoo, Finland

4 Department of Electrical Machines and Apparatus, Riga Technical University, LV-1658 Riga, Latvia

* Correspondence: miqbal@taltech.ee

Abstract: The EV penetration in the low voltage residential grids is expected to increase rapidly in the coming years. It is expected that EV consumers will prefer overnight home charging because of its convenience and lack of charging infrastructure. The EV battery chargers are nonlinear loads and likely to increase the current harmonic emission in the distribution network. The imminent increase of EV load requires upgrading or managing the existing power system to support the additional charging load. This paper provides the estimation of the current harmonic emission of the EV charging load at different voltage distortions using the stochastic EV load model. The impact of EV charging on the distribution transformer is also presented.

Keywords: electric vehicle; harmonics; transformer derating; power quality

1. Introduction

The transport sector is responsible for 24% of the total CO_2 emission globally, while road transportation has the largest share and accountable for 75% of the emission from transport. The major contributors are passenger and cargo vehicles, with a share of 45.1% and 29.4% [1]. Fossil oil is the primary energy source by providing nearly 92% of the energy demand for transportation. However, rising CO_2 emissions and unstable oil prices have paved the way for alternative technologies such as electric vehicles (EV). Using alternative green energy, the electrification of transport could provide a sustainable solution to address the greenhouse-gas-emission reduction objectives. The EVs provide zero-emission and a high energy conversion efficiency in contrast to traditional combustion engines. However, the rapid high integration of the EVs could pose a severe bottleneck for the existing electric distribution systems as the EV charging infrastructure is still inadequate. At the same time, the overnight home charging of EVs can challenge the network capacity. The EV battery chargers are power electronic-based converters and draw nonlinear currents, thus inject current harmonics into the power supply system. Even with the improved circuits and power factor corrections, the harmonic content after the mass adoption of EVs would be much higher because of the high EV charging current compared to the other domestic or commercial load.

The uptake of EVs has been increased significantly during the last few years, and more than seven million electric vehicles are now in use worldwide [2]. The ambitious policies set by several countries to support the electrification of the transport sector expected to increase EV deployment in coming years. These policies include incentives to decrease the high upfront cost and the development of widespread charging infrastructure. As a result,

the growth in EV stock was nearly 40% in 2019; however, the total global EV stock is still only less than 1% of all the passenger cars in use. The share of EV in total yearly car sales is about 2.6%. Due to the favourable government policies in different countries, the EV uptake is expected to increase to 50 million active units by 2025 and 140 million by the end of 2030.

Private home chargers are nearly 90% of the total low duty electric vehicle chargers installed worldwide [3]. The primary reason for their popularity is the cost-effectiveness and ease of use associated with home chargers. Furthermore, incentives and electricity prices also support home charging. The majority of the EV customers in large EV markets, such as Norway, United Kingdom (UK), United States (US), Japan and China, prefer home charging. It requires no additional infrastructure, and EVs can be charged from the existing electrical sockets. The public charging infrastructure is still not adequate, while only 4% of fast EV chargers are installed worldwide by the end of 2019. The ratio of the number of public chargers to the total number of EVs also shows a slight decline in recent years [4,5].

It is critical to evaluate the ramifications of uncontrolled EV charging on the distribution network. High penetration of EV could affect the capacity and performance of the local power supply network. The constraints on the network can be addressed by adding additional capacity or improve the utilisation of installed capacity. The high EV load may challenge the network's reliability by overloading distribution lines and substation during peak hours [6,7]. Even with abundant electricity generation within the region, the impact of EV charging may bottleneck the transmission and distribution system as it may not have enough capacity to handle this additional charging load. The variability of traditional residential load provides flexibility to the grid. The residential building's load factor is around 20%, while the aggregated load factor of several houses at the distribution transformer may be approximately 30%. However, EV charging could follow relatively consistent patterns as customers would like to charge their vehicle after home arrival. Range anxiety can also contribute here, and the drivers will prefer to charge their EVs overnight for the next day trip even when the battery has sufficient charge [8–10].

Large-scale EV charging can impact the distribution networks in terms of high harmonic distortions, voltage regulation, and transformer overloading. EV batteries require DC for charging; therefore, power electronic converters are employed for AC to DC conversion and charging control. These converters present nonlinear load to the distribution grid as they draw non-sinusoidal currents with high-frequency harmonics. The harmonic emission of an EV charger depends on the circuit topology of the converter. Although the modern battery chargers provide low total current harmonic distortion (THDi) with harmonic content under the limits defined by the relevant standards, the high penetration of EV may result in large aggregated harmonic currents. It may result in high voltage distortion that can affect the performance and harmonic emission of the other loads connected to the network. The voltage and current distortions negatively impact the power grid by introducing additional losses in the transmission and distribution cables [11]. The performance of network components such as transformers will reduce [12]. Electrical appliances and network protection equipment such as relays could malfunction under the influence of harmonics [13]. Therefore, to understand the impact of additional EV charging load on the network, the assessment of harmonic emission is vital for network designers and operators.

This paper provides an assessment of EV harmonic emission in the distribution network based on a stochastic EV usage model. The EV usage model generates the state of charge (SOC) and load profiles for the given number of EVs. Monte Carlo approach is used to estimate the harmonic emission of the EV load and harmonic emission. The impact of EV charging load on the distribution transformer is also estimated for uncontrolled and controlled charging scenarios. Section 2 provides an overview of the existing literature related to EV harmonic emission estimations. The methodology used in this paper is explained in Section 3. EV usage model is described in Section 4 and EV current harmonic emission estimations are provided in Section 5. The conclusions are presented in Section 6.

2. Impact of EV on Harmonic Emission

The impact of EV on the capacity and performance of power system has been widely discussed in the literature. It was found that EV charging load will likely match the peak demand hours in the residential grids [14]. Many countries have sufficient generation capacity to handle additional battery charging load for high EV penetration [15]. However, the capacity of transmission and distribution is insufficient, especially during peak demand hours. Load flow analysis is performed to determine the effect of PHEV charging on the power system losses in [16]. It has been found that for a 30% penetration of PHEV, the network capacity become insufficient to support the additional charging load. The distribution lines also need replacement to support the additional charging load while the voltage deviations are increased up to 10%. In [17], the framework is presented for an intelligent distribution system capable of handling EV charging that can determine the charging schedule and grid operating conditions for the next day. However, the number of EVs required to charge at any particular time is a stochastic process and must be treated accordingly to formulate the EV load. A comparison of uncontrolled, off-peak and smart charging of EV is presented in [18]. A 20% EV penetration increases the peak load by almost 35% for unmanaged charging scenario, while smart charging provides a better grid utilisation. The authors emphasise that a sufficient generation capacity is not a valid parameter to assess the capability of the regional grid to handling EV load.

In [19], a charging strategy is proposed to optimise the grid capacity utilisation in the residential grid. The authors have assumed Poisson distribution to estimate the number of vehicles that arrive in the evening for charging at residential parking lots. The normal distribution is used to estimate the state of charge (SOC) of the incoming vehicles. A charging strategy is proposed by evaluating the number of incoming vehicles and their SOC level and assigning an appropriate charging schedule to avoid evening peaks. However, the estimation of incoming vehicles and SOC is somewhat complex and depends on several factors influenced by the travel patterns. Queuing theory is used to model the charging demand of PHEV in [20]. A random number of PHEV are selected to charge on commercial fast-charging stations or in the residential grid during each iteration. The probability distribution functions are selected based on the data for the charging demand, and power flow analysis is used to analyse the impact of PHEV charging on the distribution grid. The study implies the effect of charging current on the distribution grid; however, high-frequency harmonics are not considered. The impact of EV charging on the residential distribution network is studied in [21]. The authors have modelled the EV load by selecting a constant SOC and fixed charging time to simulate the worst-case scenarios. The impact of current harmonics injected during EV battery charging on the distribution system is estimated in [22]. Although the current harmonics ranges are not estimated at different times during the day, the study provides a relatively simple tool to evaluate the impact of harmonics on transformer ageing.

The aforementioned studies provide valuable insight into EV penetration on LV and MV grids; although, several simplifications were found while modelling the EV load and SOC. The EV demand in the residential grid depends on several factors, including state of charge (SOC) of EV, owner's decision to charge his vehicle and the time required for charging. These events are stochastic in nature and are influenced by the driver's travel patterns or electricity tariff structure. National surveys are used to gather information regarding drivers travel pattern and preferences could provide the foundation of the stochastic modelling of EV load [23].

In [24–26], EV charging strategies are proposed to improve voltage unbalance, network overloading and cost reductions. The controlled and smart charging can improve the network operation significantly without having an additional impact. However, the practical implementation of these strategies is not expected anytime sooner, and uncoordinated charging may be the only mechanism for the time being.

3. Methodology

The travel patterns are the primary influencing factors to estimate the EV load and charging time in a distribution grid. Vehicle usage depends on several factors related to consumer socioeconomic status, where the driving patterns are interrelated to the vehicle ownership and number of occupants in each household. Many studies have assumed the random number of vehicles charging at different parking lots in the residential networks. In fact, the number of EVs present in a residential grid and connected to the grid for battery charging will be different at distinct times during the day. Several variables will contribute to the amount of EV load connected to the grid, such as EV arrival time at home, the number of the trip made during a day, distance travelled during each trip and SOC after the trips.

The selection criteria to estimate the arrival time for the incoming vehicles for charging is crucial to evaluate a realistic impact of charging currents in the distribution grid. Few studies have used queuing theory approach to determine the incoming vehicle for charging at the parking lots in the residential grid, while the Poisson distributions are used to estimate the arrival time [20,27]. Since the nature of various trip by EVs could be different, multiple distributions should be defined to estimate the arrival time of the EVs. Furthermore, the charging decision of EVs depends on the SOC that must be decided based on the distance travelled and energy consumption by the EV during different trips. The daily driving distance of vehicles depends on the driver's routine activities that create the demand for the trips. Therefore, the destination and travel distance are highly stochastic, and the researchers most often use the average trip distance to create EV usage models [28–30]. Travel surveys could provide valuable information in this regard.

The harmonic emission of EVs depends on the charging characteristics that typically include the battery charger circuit topology, network voltage waveforms, and charging time of the battery. The measurement of a selective set of EVs on different voltage waveform may provide a valuable data set because of the identical technology used in the battery chargers in the same time span.

4. EV Usage Model

An EV usage model is developed to estimate the harmonic emission from EV penetration in the distribution grid. The model is based on the data extracted from the national traffic survey (NTS) conducted in Finland. The survey provides data about people mobility using different modes of transportation. It gathers yearly travel data from 30,000 people and provides various travel related statistics. The information related to travel utilising private cars, such as daily distance travelled by individuals, total daily trips, everyday activities that generate the need for trips, and trip starting times, are used in the model. The trip of chain approach is employed to evaluate different parameters of each trip using appropriate probability distributions. A Monte-Carlo simulation is used to simulate the EV trips based on the most common activities responsible to generate trip demand for a given number of days. The charging of EV is decided on the SOC level at the end of each trip. The algorithm of the EV usage model is shown in Figure 1. The details of the EV usage model are presented in [31].

Trips are generated in response to people's everyday activities, including work, school, travel, and leisure. We have selected three major activities for our EV load model. The most likely trip on weekdays is related to travel to work or school (WS). These drips have very low variation in terms of timing and distance. The second category of trips is related to shopping or business (SB) associated activities with significant variation for the trip starting time and travelled distance. The last category of trips is linked with leisure or vacation (LV). In contrast, these trips have a significantly high variance for both start-time and travelled distance and less likely to happen, especially on weekdays.
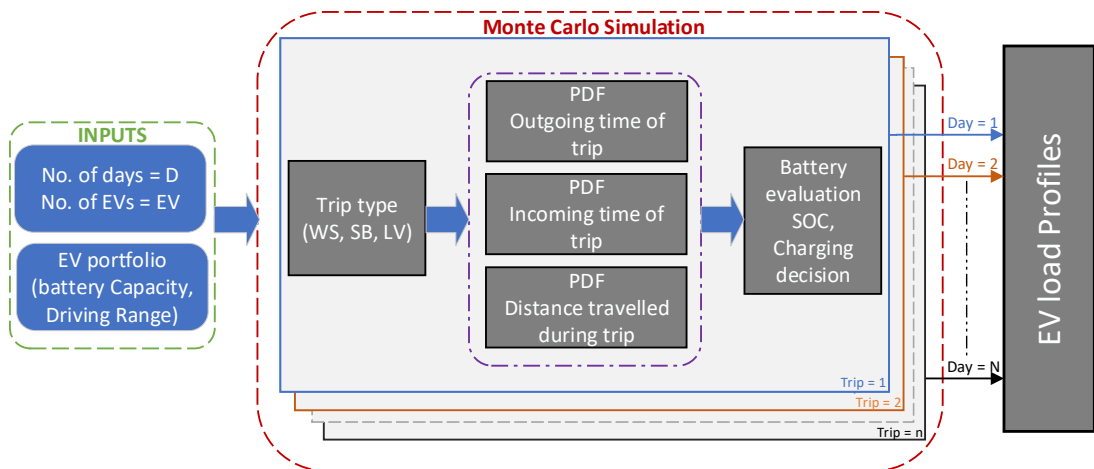
Figure 1. EV usage model algorithm.

The probability distribution functions (PDF) of three essential parameters, trip start-time, trip distance and trip end-time, are defined for different trip categories that provide the base of the EV load model. During each iteration, the number and type of trips are selected for each day. In the next step, the trip characteristics such as start time, end time and distance travelled are estimated from their PDFs. In the last step, battery evaluation is performed after the end of each trip. The SOC is determined based on the energy consumed by the vehicle during the trip.

Figure 2a shows the start-time of different trip categories chosen from the NTS survey, where multiple peaks can be observed. This data is split up into incoming and outgoing trips, and probability distributions are defined for each travel activity. Figure 2b shows the outgoing and incoming time distributions for WS trips extracted from the NTS survey data.
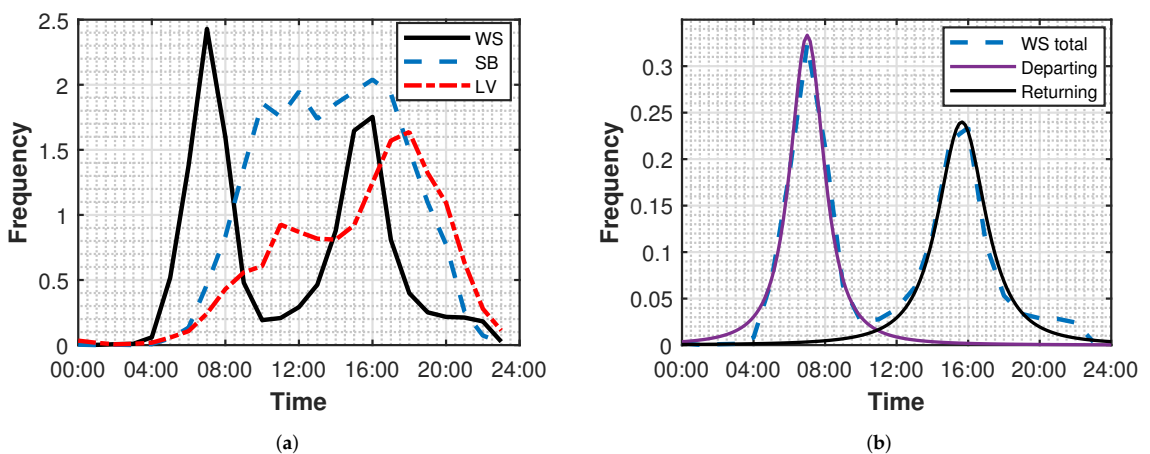

Figure 2. Frequency of trips at different times (**a**) Data obtained from the survey (**b**) Probability distribution of outgoing and incoming trip for WS travel activity [31].

T-location scale distribution is used as it provides a close fit to the incoming and outgoing time data. The probability distribution function of t-location-scale distribution is shown by Equation (1).

$$f(x) = \frac{\Gamma\frac{(v+1)}{2}}{\sigma\sqrt{v\pi} \times \Gamma(\frac{v}{2})} \times \left[\frac{v(\frac{x-\mu}{\sigma})^2}{v}\right]^{-(\frac{v+1}{2})} \tag{1}$$

Here μ and σ represent the location and scale of the PDF while Γ is the gamma function. v is the degree of freedom, and its lower values generate heavier tails. As the value of v increases, t-location-scale distribution approaches a normal distribution. A similar approach is applied to other trip activities to construct a PDF of the start time and end time of trips.

The incoming time of a trip depends on the distance travelled and time spent at the activity for which the trip demand is generated. Duration of leisure and shopping activities is calculated using Poison distribution, where the average time at the leisure and shopping activities is selected randomly between 120–180 and 20–60 min, respectively. The following relation shows the PDF of a Poisson distribution.

$$f(x) = \frac{\lambda^x}{x!}e^{-\lambda} \tag{2}$$

Here λ shows the variance and e is Euler's number. The data of average distance travelled for various trip activities at different times of the day is also taken from the NTS survey and is shown here in Figure 3. The distance travelled for each trip is estimated by using log-normal or Poisson distributions. The PDF of a log-normal distribution is shown by Equation (3).

$$f(x) = \frac{1}{x\sigma\sqrt{2\pi}}exp(-\frac{(ln(x)-\mu)^2}{2\sigma^2}) \tag{3}$$

μ and σ in Equation (3) represents the mean and variance of the input data. The NTS survey provides the data for the number of trips for each activity per day and average trips per day. This data is used to evaluate the probability of trip as shown in Figure 4.
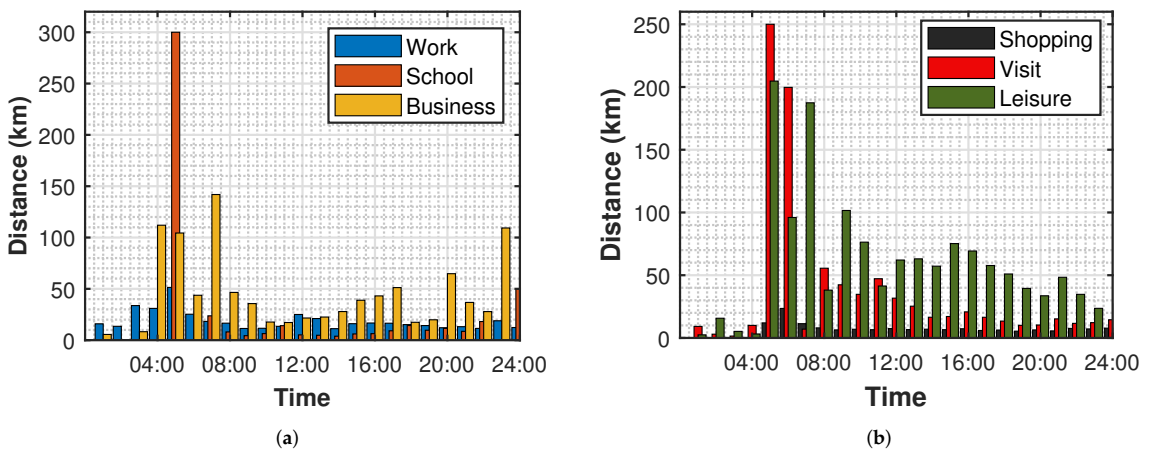

Figure 3. Distance frequency at different times during the day (**a**) Work, school and business related activities (**b**) Shopping, visits and leisure related activities.
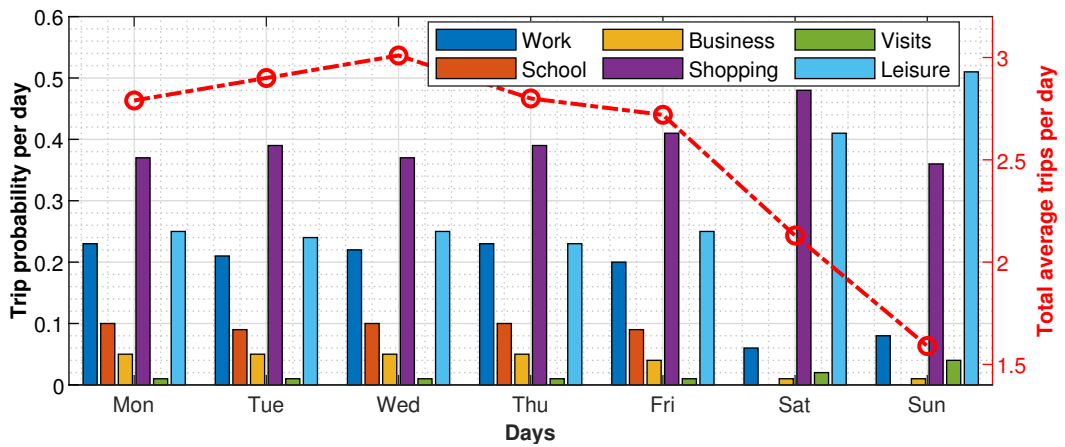
Figure 4. Total number of trip and their probability per day.

5. EV Harmonic Emission Estimation

Accurate evaluation of the EV battery charging impact on the distribution grid requires understanding of charging characteristics dynamics under different operating modes and supply voltage variations. It's a challenging task because several manufacturers are offering EVs in various sizes and battery capacity. The advancement in power electronics has led to notable changes in terms of the design and performance of EV battery chargers. The majority of commercially available EVs are equipped with level 2 chargers and are charged using slow overnight home charging as public fast-charging infrastructure is still inadequate [32]. These chargers provide high efficiency over a wide range of supply voltage variations, including active power factor correction (a-PFC) circuits. Their harmonic emission is well under the limits provided by the standards, and total current harmonic distortions is less than 15% [33,34].

A measurement setup has been made to evaluate the current harmonic emissions of the EV battery charger under various voltage distortions. The setup consists of a 4 kVA controllable power supply Chroma 61505, and the reference signal is provided by the data acquisition module from National Instrument (NI). Figure 5 shows the block diagram of the measurement setup. The voltage distortions are created using a MATLAB program by providing voltage harmonic magnitudes and phase angles as listed in Table 1.
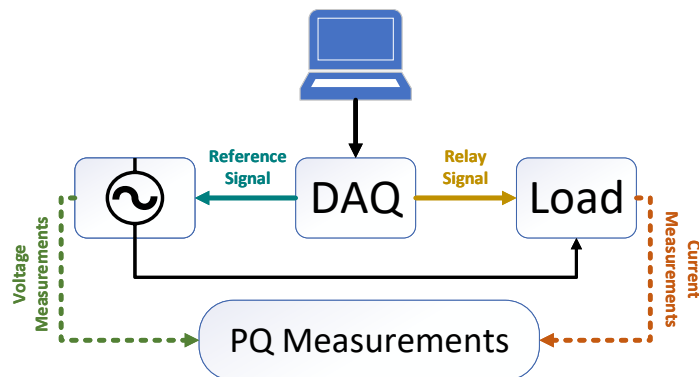

Figure 5. Measurement setup block diagram.

Table 1. Voltage waveform used for EV power quality measurements.

Harmonics	Voltage Waveform 1		Voltage Waveform 2		Voltage Waveform 3	
	RMS (V)	Phase (Degree)	RMS (V)	Phase (Degree)	RMS (V)	Phase (Degree)
H1	230	-	229.89	0	229.85	0
H3	-	-	5.450	0	6.620	0
H5	-	-	3.827	180	4.730	180
H7	-	-	2.040	0	1.440	180
H9	-	-	0.565	180	-	-
H11	-	-	0.308	180	-	-
H13	-	-	0.557	0	-	-
H15	-	-	0.375	180	-	-
H17	-	-	0.050	0	-	-
H19	-	-	0.182	0	-	-

The power supply is controlled by a reference signal using the following relation.

$$V_R = \frac{V_o}{V_{range}} \times V_{coef} \tag{4}$$

The values of V_{range} and V_{coef} is 300 V and 7.072, respectively. V_o is generated at a sampling frequency of 100 kHz using the following equation.

$$V_o = \sum_{i=1}^{n} \sqrt{2} \times v_h \sin(2\pi f_h t_s + \alpha_h) \tag{5}$$

where, v_h is the RMS value of harmonic magnitude and f_h is its frequency. α_h represents the phase difference of the harmonic from the fundamental component of the voltage waveform. The sampling interval t_s is calculated using the sampling frequency f_s as shown by the following relation

$$t_s = \frac{1}{f_s} = \frac{1}{N/T} \tag{6}$$

Here, T is the time duration of the generated waveform and N is the number of samples in that interval. A-Eberle PQ box 200, capable of providing 1-second data averaged over 200 ms recordings, is used to record the current harmonics magnitude and phase angles. The detail of the measurements setup is provided in [35]. Eleven different EVs including both battery-powered electric vehicle (BEV) and plug-in hybrid electric vehicle (PHEV) are measured on the voltage waveforms defined in Table 1. The characteristics of these vehicles are summarised in Table 2.

Table 2. Summary of the measured EVs.

Number	Type	Battery Capacity (kWh)	Driving Range (km)	THDi %
EV 1	BEV	22	170	4.80
EV 2	BEV	16.8	100	7.18
EV 3	BEV	31	160	2.87
EV 4	BEV	40	220	11.66
EV 5	BEV	14.5	171	8.39
EV 6	PHEV	11.2	50	3.10
EV 7	BEV	18.7	165	2.43
EV 8	PHEV	9.4	36	2.47
EV 9	BEV	17.6	145	4.33
EV 10	BEV	58	335	7.07
EV 11	PHEV	8.8	26	2.35

The impact of voltage waveform distortions on the individual harmonics is presented in Figure 6. The vectors of the 3rd harmonic current show that the spread will change

slightly for the flat top voltage waveform while the harmonic spread is nearly identical for sinusoidal and pointy top voltage waveforms. The harmonic spread for the 5th harmonic on pointy top voltage waveform is almost shifted 180 degrees in contrast to sinusoidal or flat top voltage waveform for the majority of the EVs. On the flat top voltage waveform, the 5th harmonic current is slightly increased in magnitude; however, the phase angles are almost the same as on the sinusoidal voltage waveform. The 7th harmonic current spread on the pointy top voltage waveform shows a significant change in terms of magnitude in comparison to sinusoidal or flat top voltage profiles. On the other hand, the 9th harmonic shows a wider spread for different EVs, but the change in magnitude or phase is not very high for different voltage waveforms.
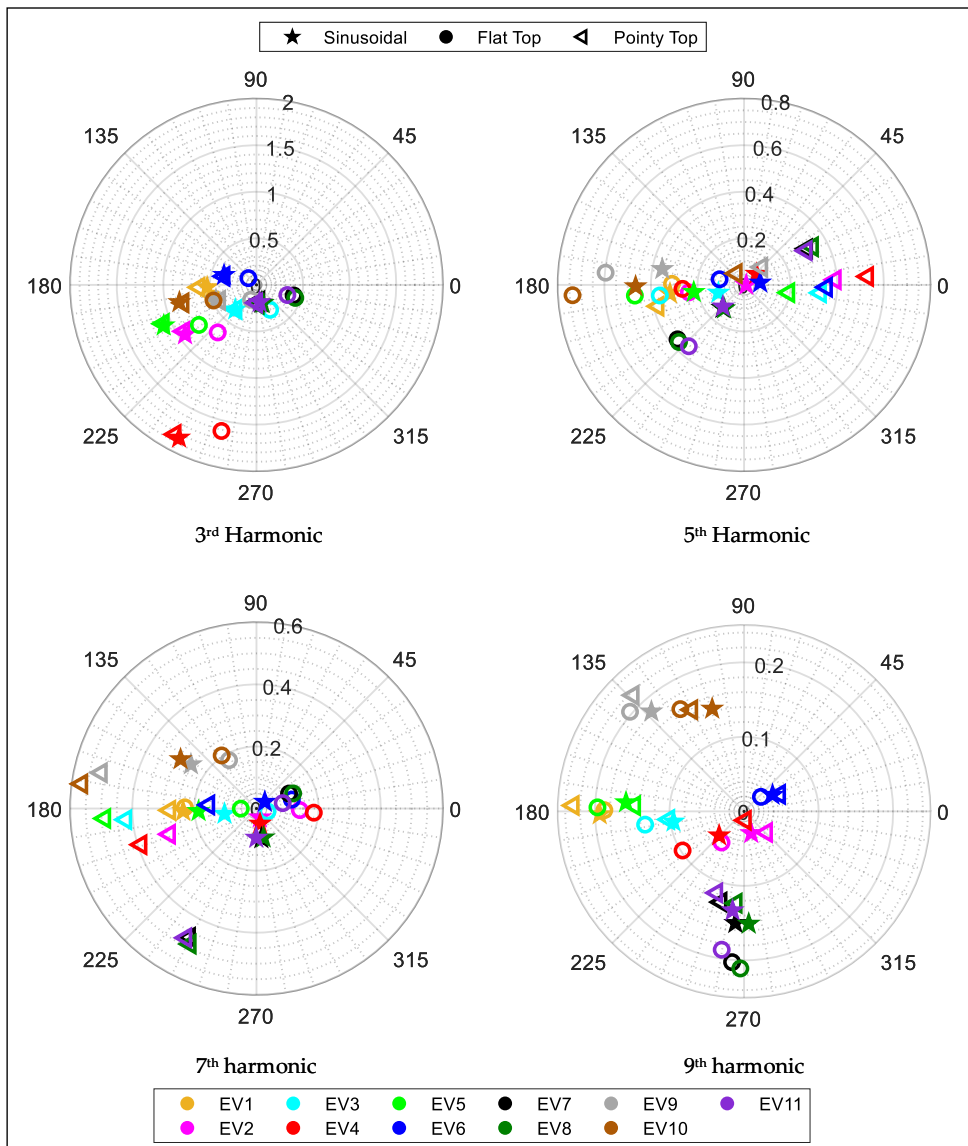

Figure 6. Current harmonic emission of individual EVs.

To observe the impact of the large scale EV integration on the current harmonic emission in the low voltage distribution network, EV load model is used to simulate 50 EVs for 100 days. The EVs are assigned randomly from the list provided in Table 2. The EV load model is used to simulate the travel activities to generate charging profiles based on the distance travelled during each trip. For each EV, the outgoing and incoming times of each trip during a day is estimated. The final destination is assumed to be the home. Based on the distance travelled during each trip, the state of charge of the battery is estimated. The decision of charging depends upon the state of SOC. While the EV is at home and does not have sufficient SOC to make a new trip, the EV charging will take place. The simulation is performed for weekdays only, therefore, the EV charging takes place mostly during the evening time. Figure 7 shows the mean and 90th percentile values of total RMS current for different voltage distortions. The bold lines indicate the mean values while the dotted line shows the 90th percentile value of the RMS current. The RMS values does not show a significant variation for different voltage waveforms and only slight variation can be observed.
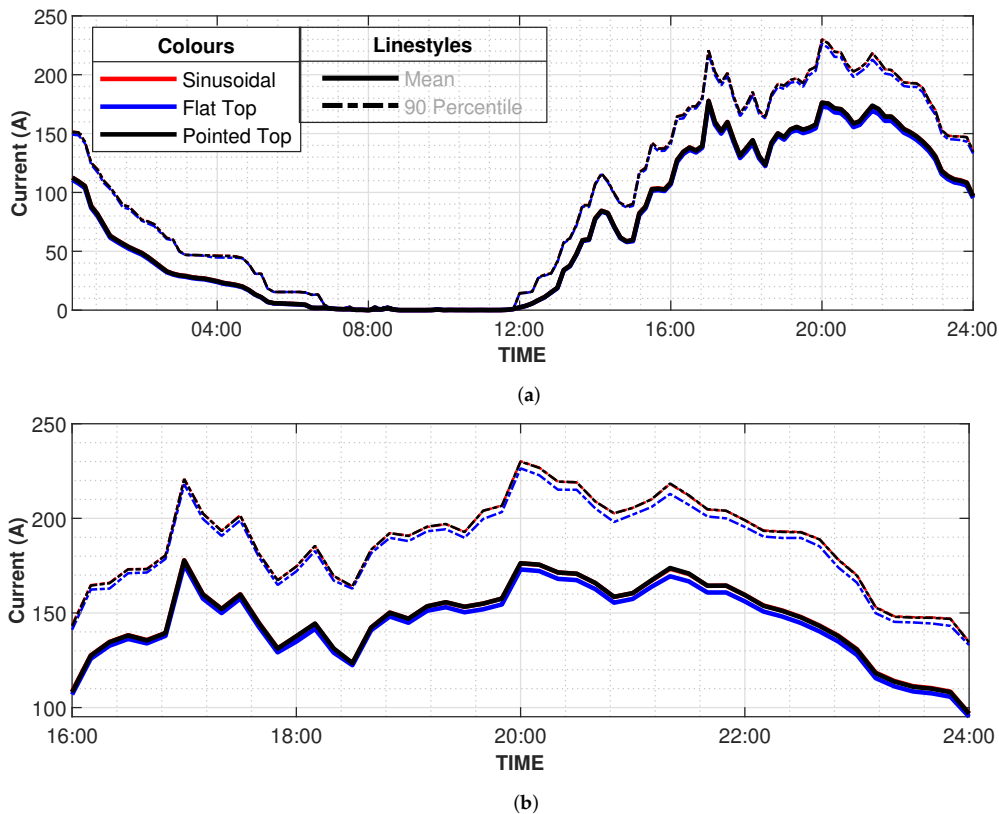

(a)

(b)

Figure 7. RMS current of 50 electric vehicles at different voltage distortions (**a**) Full day (**b**) Evening peak.

The mean and 90th percentile values of 3rd harmonic current drawn over 100 days for 50 EVs is shown in Figure 8a. No significant variation in the 3rd harmonic current can be observed between sinusoidal and pointed top voltage waveforms, however, the values on flat top voltage waveforms are significantly less for both mean and 90th percentile values. The mean value increases to its maximum value of 6.9 A around 21:30. The mean values on flat top voltage waveform at the same time is only 4.60 A which is 33.3% less. The 5th harmonic values are more for flat top voltage waveform as shown in Figure 8b.

On sinusoidal voltage waveform, the 5th harmonic current has lowest values during the 24 h. The values slightly increase on pointed top voltage waveform shown by black bold line in Figure 8b. The mean and 90th percentile values of the 5th harmonics crosses 4.4 and 5.6 A, respectively, during the evening peak. On the sinusoidal and pointed top voltage waveforms, the mean value increases to a maximum value of 1.9 and 2.8 A only.
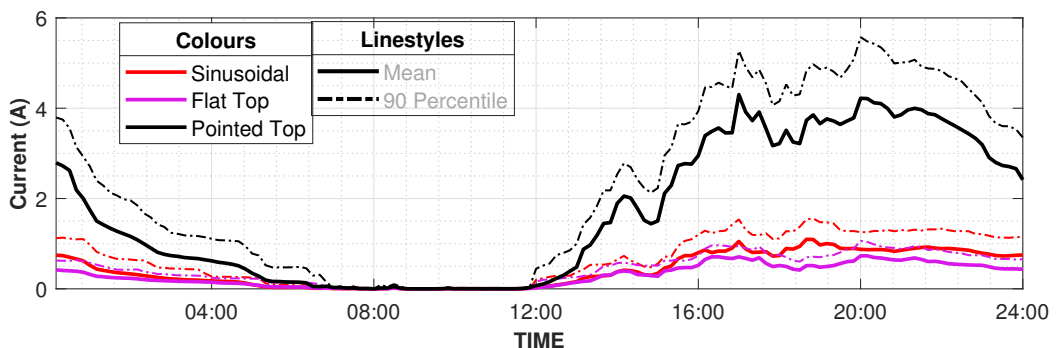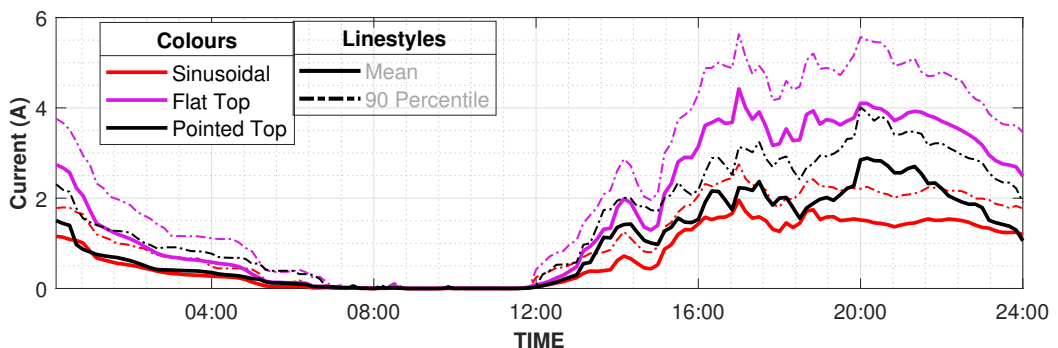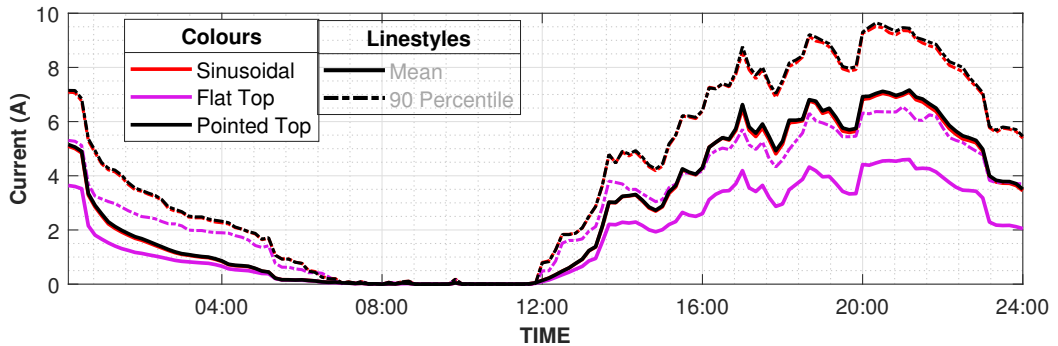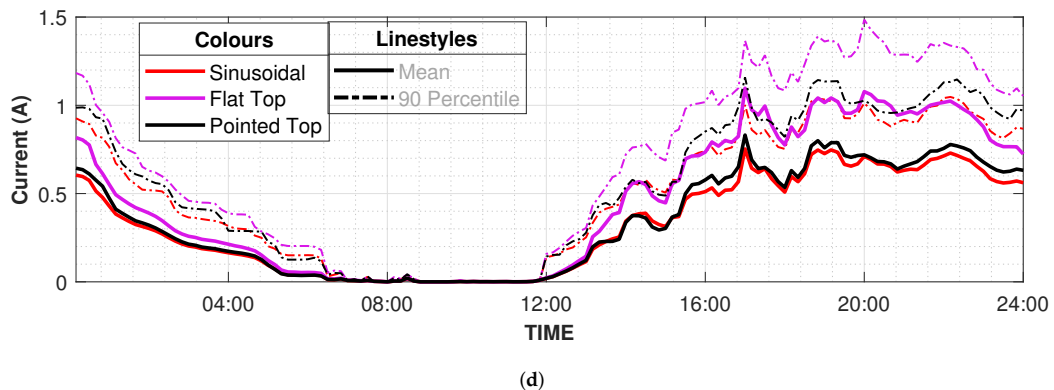

(a)

(b)

(c)

Figure 8. *Cont.*

(**d**)

Figure 8. Estimated harmonic emission of 50 EVs over 100 days (**a**) 3rd harmonic (**b**) 5th harmonic (**c**) 7th harmonic (**d**) 9th harmonic.

The 7th harmonic emission on pointed top voltage waveform is very high in comparison to sinusoidal and flat top voltage waveforms as shown in Figure 8c. The mean value exceeds 4 A for pointed top voltage waveform during the evening peak while the mean values at sinusoidal and flat top voltage waveforms are around 1 A. The values for the 9th harmonic current are more on the flat top voltage waveform with the mean value crossing 1 A during the evening time. For sinusoidal and pointed top voltage waveform, the mean values of the 9th harmonic are quite close during the whole day with the maximum value of 0.83 A. Figure 8d shows the mean and 90 percentile values of the 9th harmonic current on different voltage distortions.

6. EV Charging Impact of Distribution Transformer

The impact of EV charging on the distribution network includes the increase in load and voltage distortions. To assess this impact, the relation between the charging start time and the evening peak should be taken into account. Evening peak load depends on the consumer behaviour of using electricity mainly influenced by regional electricity pricing mechanisms. The primary impact of additional EV load is the heating and overloading of existing distribution transformers. The additional losses may occur because of the skin and proximity effects in the windings and stray losses due to leakage flux. Consequently, the hot spot temperature rise will reduce the operating life span of the transformer and increase the probability of insulation failure. Additionally, the cable efficiency will also be reduced because of the high losses resulting from skin and proximity effects [36].

To evaluate the impact of EV integration in the existing distribution network, a test case has been presented in this section based on the real-time measurement of the distribution grid and EV usage model. A distribution grid in Finland is measured for several days in winter to record current harmonics at the 620 kVA distribution transformer connected in Delta-Wye (Dy) with LV side grounded. In Figure 9, the black line shows the mean value of the existing load at the transformer for approximately 80 houses without any EV usage. The heating load is already shifted to 20:00 to reduce peak loads and take advantage of cheaper electricity tariffs. The heating load scheduling is performed on the user end through time-based switching.

Two different scenarios are simulated using the EV load model to estimate the additional load on the transformer. In the first case, 80% of uncontrolled EV charging load is simulated for 100 days using Monte Carlo simulations. The current harmonics estimated from the simulated EV load are aggregated with the measured current harmonic data at the distribution transformer. The mean value of transformer load is calculated and is shown by the red line in Figure 9. The uncontrolled charging has significantly increased the transformer load by approximately 18% and 25% at 16:00 and 18:00, respectively.

The transformer load significantly increased after 20:00 because of the shifted heating load in winters. The EV charging has caused additionally 15% and 7% transformer loading at approximately 20:00 and 23:30, respectively. The peak loading of the transformer is nearly 89% around 23:30.
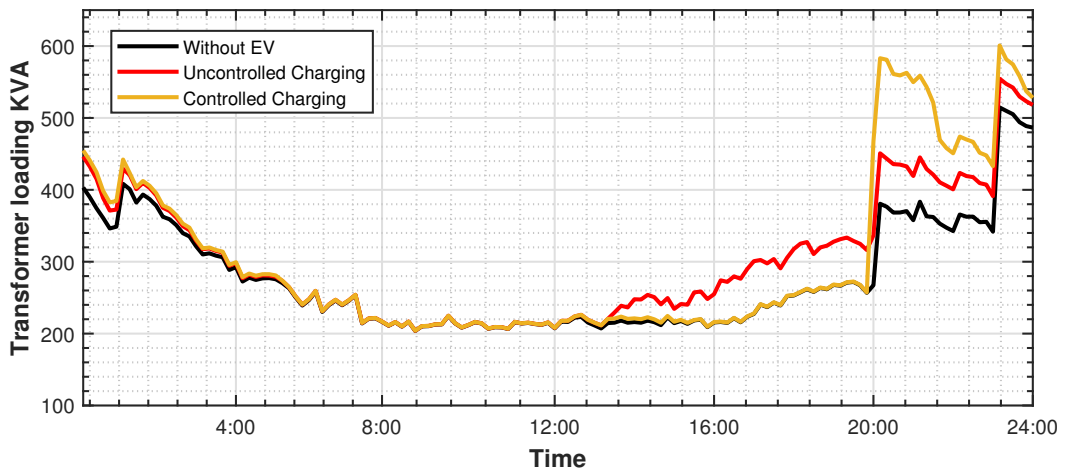

Figure 9. Mean value of distribution transformer load at different times of the day.

In the second case, controlled EV charging is implemented and simulated using the EV load model. In the second case, controlled EV charging is implemented and simulated using the EV load model. Several controlled charging methodologies are available in the literature that provides smart charging algorithms to maximize utility or consumers benefits [37,38]. However, these schemes require additional infrastructures such as data connections and smart meters. These algorithms may also cause inconvenience to the customers and limited practical implementations [21]. We have used controlled charging based on Time-of-Use (TOU) pricing and simulated its impact on the distribution grid using the EV load model. The TOU based controlled charging allow networks to reduce peak load by selecting appropriate peak and off-peak energy prices and required no additional infrastructure [39,40]. It may provide better grid utilization, especially during summertime when the heating load is not present; however, the customers may also take advantage of low price electricity during off-peak hours for their heating load during winter times.

The impact of controlled EV charging is estimated using the EV usage model. The yellow line in Figure 9 shows the transformer loading for controlled charging scenarios. All the EVs are now forced to charge from 20:00 on wards, causing additional strain on the transformer. The transformer load has increased almost 53% at 20:00 and pushing the transformer load to nearly 95%. Furthermore, the peak load is increased to 96% because of the additional 16% EV load at 23:30. The controlled charging for EVs during winters is causing poor load management in contrast to uncontrolled charging because of the shifting of heating load during off-peak hours. The EVs cannot be scheduled between 04:00–08:00 to avoid heating load as the time span is not enough to recharge the batteries fully.

The uncontrolled charging provides better transformer utilisation for the distribution grid under consideration. It means that the time-based tariffs may cause overloading of the transformer as both EV and heating load will take advantage. However, when the heating load is minimal in the summertime, the time-based tariff and controlled charging will improve the transformer utilisation.

The hot-spot temperature of the distribution transformer is estimated using the procedure described in IEEE standard C57.110 [41]. The values of current harmonics estimated using the EV load model for 80% EV penetration along with the measured values of current

harmonics at the distribution transformer are used to calculate the hot spot conductor temperature of the 620 kVA oil-immersed transformer using the Equation (7).

$$\theta_R = \theta_{R(rated)} \times \left[\frac{I_{pu}^2 \times (1 + L_h \times P_{e(rated)})}{1 + P_{e(rated)}} \right]^{0.8} \tag{7}$$

Here θ_R and $\theta_{R(rated)}$ are the hottest spot conductor temperature rise under operating and rated conditions in degree Celsius (°C). $P_{e(rated)}$ is the per unit eddy current loss in the transformer under rated conditions. L_h is the loss factor due to harmonic currents in the transformer winding and calculated by using Equation (8).

$$L_h = \frac{\sum_{h=1}^{h_{max}} \left[\frac{I_h}{I_1} \right]^2 \times h^{0.8}}{\sum_{h=1}^{h_{max}} \left[\frac{I_h}{I_1} \right]^2} \tag{8}$$

Here h is the harmonic number and h_{max} is the highest harmonic order under consideration. I and I_h are the RMS load current and RMS harmonic current, respectively. Figure 10 shows the temperature rise of the hottest spot conductor over ambient temperature for three scenarios. In the first case, the calculation is made only for the mean values of the current harmonic measurement data at the distribution transformer. The black line shows the temperature in the range of 26–52 °C between 00:00 to 20:00 without any EV load. The temperature rises to the maximum value of 77 °C during the time period of 22:00 and 24:00 because of the shifted heating load.
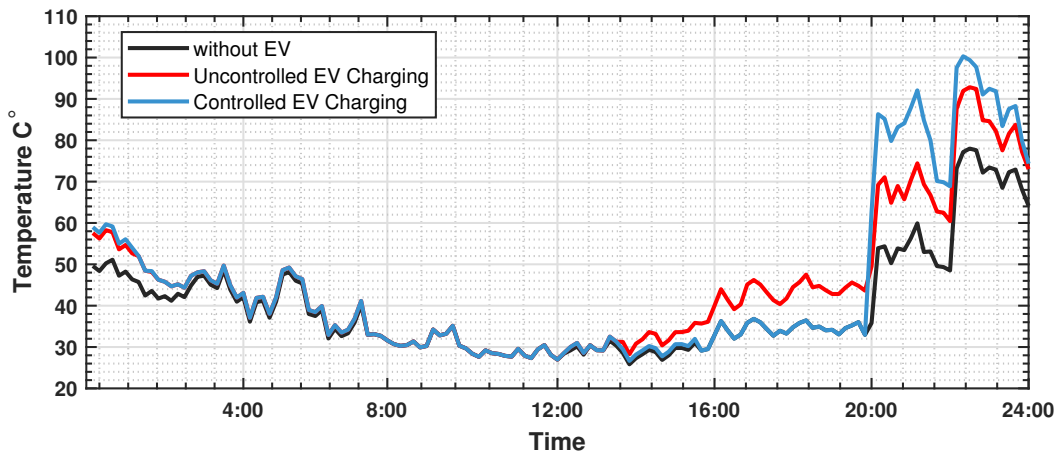

Figure 10. Transformer hottest spot conductor temperature rise above ambient conditions.

In the second scenario, the temperature rise for the hottest spot conductor is calculated when an additional uncontrolled EV charging load is applied. It has increased the temperature range to almost 60 °C between 00:00 to 20:00, while the maximum temperature is now almost 93 °C at 22:30. It means that uncontrolled charging has increased the maximum temperature rise of the transformer by nearly 16 °C. In the controlled EV charging scenario, the maximum temperature of the transformer has increased to more than 100 °C, which is 8 °C more when uncontrolled EV charging is employed. The consistent high hot spot conductor temperature for more than 4 h a day will significantly reduce the transformer life or cause insulation failure.

The results show that EV controlled charging based on TOU electricity tariff to shift the EV load during off-peak hours will not improve the transformer utilisation for high EV penetration in the distribution grids during winter times. A more complex load shifting

procedure is required where heating load and EV charging could be adjusted to improve the transformer utilisation and decrease the hot spot conductor temperature. However, it will require additional infrastructure to support the implementation smart controlled charging schemes. Furthermore, the impact of smart controlled charging algorithms on the EV customers is also unknown at this point. The results also show the validation and capability of our EV load model.

7. Conclusions

A method is proposed in this paper to estimate the current harmonic emission of electric vehicles. The model is based on the EV usage model developed to generate the SOC profiles of individual vehicles. Furthermore, probability distributions functions of various parameters such as outgoing time, distance travelled, and incoming time for different types of trips are calculated based on the data from a travel survey. Various electric vehicles are measured over different voltage waveform to record their current harmonic magnitude and phase angles. Moreover, a Monte Carlo simulation is used to estimate the harmonic emission of fifty EV over one hundred days to estimate their aggregated harmonic emission. The results show that EV harmonic emission also depends on the supply voltage harmonics, which may be affected by various nonlinear loads present in the distribution grid.

The impact of EV integration on the distribution transformer is also evaluated. The current harmonic emission at a distribution transformer, supplying power to approximately 80 households, is measured during winters. Monte-Carlo simulation is used to aggregate the estimated 80% EV charging load to the existing load at the distribution transformer for hundred days. The heating load in the measured distribution grid is shifted because of the time-based electricity tariffs. The EV charging has increased the late-night peak load more in contrast to the uncontrolled EV charging in winters because of the shifted heating load. The hottest spot conductor temperature of the transformer has risen significantly during EV charging. It indicates that TOU controlled charging may not provide the solution to improve transformer utilisation in winters, and smart controlled charging algorithms may be the only solution for the network providers to accommodate additional EV load.

Author Contributions: Conceptualization, M.N.I.; methodology, L.K. and M.N.I.; validation, K.D. and P.S.G.; data curation, M.N.I. and K.D.; writing—original draft preparation, M.N.I.; writing—review and editing, B.A.; supervision, L.K. All authors have read and agreed to the published version of the manuscript.

Institutional Review Board Statement: Not applicable.

Informed Consent Statement: Not applicable.

Data Availability Statement: Data is contained within the article.

Conflicts of Interest: The authors declare no conflict of interest.

References

1. IEA. *CO₂ Emissions from Fuel Combustion 2019 Highlights*; Technical Report; International Energy Agency: Paris, France, 2019.
2. Brand, C.; Anable, J.; Morton, C. Lifestyle, efficiency and limits: Modelling transport energy and emissions using a socio-technical approach. *Energy Effic.* **2019**, *12*, doi:10.1007/s12053-018-9678-9.
3. Beach, F.; Tuttle, D.; Duncan, R. *Electric Vehicle Charging Infrastructure*; Technical Report; The University of Texas: Austin, TX, USA, 2019; doi:10.26153/tsw/2961.
4. *Report on the Assessment of the Member States National Policy Frameworks for the Development of the Market as Regards Alternative Fuels in the Transport Sector and the Deployment of the Relevant Infrastructure Pursuant to Article 10 (2) of Directive 2014*; Technical Report; European Commission: Brussels, Belgium; Luxembourg, 2019.
5. Spöttle, M.; Jörling, K.; Schimmel, M.; Staats, M.; Grizzel, L.; Jerram, L.; Gartner, J. *Research for TRAN Committee—Charging Infrastructure for Electric Road Vehicles*; Technical Report; Policy Department for Structural and Cohesion Policies, European Parliament: Brussels, Belgium, 2018; doi:10.2861/62486.
6. Hadley, S.W. *Impact of Plug-In Hybrid Vehicles on the Electric Grid*; Technical Report; U.S. Department of Energy: Washington, DC, USA, 2006.

7.   Richardson, D.B. Electric vehicles and the electric grid: A review of modeling approaches, Impacts, and renewable energy integration. *Renew. Sustain. Energy Rev.* **2013**, *19*, 247–254, doi:10.1016/j.rser.2012.11.042.

8.   Chen, R.; Liu, X.; Miao, L.; Yang, P. Electric vehicle tour planning considering range anxiety. *Sustainability* **2020**, *12*, 3685, doi:10.3390/su12093685.

9.   Wang, Z.; Zeng, S.; Guo, J. Understanding the influence of state of health on the range anxiety of battery electric vehicle drivers. *IET Intell. Transp. Syst.* **2021**, *15*, 286–296, doi:10.1049/itr2.12023.

10.   Esmaili, M.; Shafiee, H.; Aghaei, J. Range anxiety of electric vehicles in energy management of microgrids with controllable loads. *J. Energy Storage* **2018**, *20*, 57–66, doi:10.1016/j.est.2018.08.023.

11.   Noshahr, J.B.; Meykhosh, M.H.; Kermani, M. Current harmonic losses resulting from first and second generation LED lights replacement with sodium vapor lights in a LV feeder. In Proceedings of the 2017 17th IEEE International Conference on Environment and Electrical Engineering and 2017 1st IEEE Industrial and Commercial Power Systems Europe, EEEIC/I and CPS Europe 2017, Milan, Italy, 6–9 June 2017; pp. 1–5, doi:10.1109/EEEIC.2017.7977429.

12.   Pierce, L. Transformer design and application considerations for nonsinusoidal load currents. *IEEE Trans. Ind. Appl.* **1996**, *32*, 633–645, doi:10.1109/28.502176.

13.   Watson, N.; Scott, T.; Hirsch, S. Implications for Distribution Networks of High Penetration of Compact Fluorescent Lamps. *IEEE Trans. Power Deliv.* **2009**, *24*, 1521–1528, doi:10.1109/TPWRD.2009.2014036.

14.   Heydt, G.T. The impact of electric vehicle deployment on load management strategies. *IEEE Trans. Power Appar. Syst.* **1983**, doi:10.1109/TPAS.1983.318071.

15.   UK Grid Capacity Sufficient for Electric Vehicles, IET Transport Desk. Available online: https://eandt.theiet.org/content/articles/2009/05/uk-grid-capacity-sufficient-for-electric-vehicles/ (accessed on 11 June 2021).

16.   Clement-Nyns, K.; Haesen, E.; Driesen, J. The Impact of Charging Plug-In Hybrid Electric Vehicles on a Residential Distribution Grid. *IEEE Trans. Power Syst.* **2010**, *25*, 371–380, doi:10.1109/TPWRS.2009.2036481.

17.   Sharma, I.; Canizares, C.; Bhattacharya, K. Smart charging of PEVs penetrating into residential distribution systems. *IEEE Trans. Smart Grid* **2014**, *5*, doi:10.1109/TSG.2014.2303173.

18.   Qian, K.; Zhou, C.; Allan, M.; Yuan, Y. Modeling of load demand due to EV battery charging in distribution systems. *IEEE Trans. Power Syst.* **2011**, *26*, doi:10.1109/TPWRS.2010.2057456.

19.   Zheng, J.; Wang, X.; Men, K.; Zhu, C.; Zhu, S. Aggregation model-based optimization for electric vehicle charging strategy. *IEEE Trans. Smart Grid* **2013**, *4*, doi:10.1109/TSG.2013.2242207.

20.   Li, G.; Zhang, X.P. Modeling of plug-in hybrid electric vehicle charging demand in probabilistic power flow calculations. *IEEE Trans. Smart Grid* **2012**, doi:10.1109/TSG.2011.2172643.

21.   Dubey, A.; Santoso, S. Electric Vehicle Charging on Residential Distribution Systems: Impacts and Mitigations. *IEEE Access* **2015**, doi:10.1109/ACCESS.2015.2476996.

22.   Gomez, J.; Morcos, M. Impact of EV battery chargers on the power quality of distribution systems. *IEEE Trans. Power Deliv.* **2003**, *18*, 975–981, doi:10.1109/TPWRD.2003.813873.

23.   Axsen, J.; Kurani, K.S. Anticipating plug-in hybrid vehicle energy impacts in California: Constructing consumer-informed recharge profiles. *Transp. Res. Part D Transp. Environ.* **2010**, *15*, 212–219, doi:10.1016/j.trd.2010.02.004.

24.   Sortomme, E.; El-Sharkawi, M.A. Optimal charging strategies for unidirectional vehicle-to-grid. *IEEE Trans. Smart Grid* **2011**, *2*, doi:10.1109/TSG.2010.2090910.

25.   Farahani, H.F. Improving voltage unbalance of low-voltage distribution networks using plug-in electric vehicles. *J. Clean. Prod.* **2017**, *148*, 336–346, doi:10.1016/j.jclepro.2017.01.178.

26.   Carrión, M.; Zárate-Miñano, R.; Domínguez, R. Integration of electric vehicles in low-voltage distribution networks considering voltage management. *Energies* **2020**, *13*, 4125, doi:10.3390/en13164125.

27.   Garcia-Valle, R.; Vlachogiannis, J.G. Letter to the editor: Electric vehicle demand model for load flow studies. *Electr. Power Compon. Syst.* **2009**, *37*, doi:10.1080/15325000802599411.

28.   ISO, New York. *Alternate Route: Electrifying the Transportation Sector—Potential Impacts of Plug-In Hybrid Electric Vehicles on New York State's Electricity System*; Technical Report; ISO: New York, NY, USA, 2009.

29.   Green, R.C.; Wang, L.; Alam, M. The impact of plug-in hybrid electric vehicles on distribution networks: A review and outlook. *Renew. Sustain. Energy Rev.* **2011**, *15*, 544–553, doi:10.1109/PES.2010.5589654.

30.   Kim, S.; Lee, J.; Lee, C. Does driving range of electric vehicles influence electric vehicle adoption? *Sustainability* **2017**, *9*, 1783, doi:10.3390/su9101783.

31.   Iqbal, M.N.; Kütt, L.; Lehtonen, M.; Millar, R.J.; Püvi, V.; Rassõlkin, A.; Demidova, G.L. Travel Activity Based Stochastic Modelling of Load and Charging State of Electric Vehicles. *Sustainability* **2021**, *13*, 1550, doi:10.3390/su13031550.

32.   Collin, A.J.; Xu, X.; Djokic, S.Z.; Moller, F.; Meyer, J.; Kutt, L.; Lehtonen, M. Survey of harmonic emission of electrical vehicle chargers in the European market. In Proceedings of the 2016 International Symposium on Power Electronics, Electrical Drives, Automation and Motion (SPEEDAM), Capri, Italy, 22–24 June 2016; doi:10.1109/SPEEDAM.2016.7526005.

33.   Müller, S.; Meyer, J.; Schegner, P.; Djokic, S. Harmonic modeling of electric vehicle chargers in frequency domain. *Renew. Energy Power Qual. J.* **2015**, *1*, doi:10.24084/repqj13.337.

34. Kutt, L.; Saarijärvi, E.; Lehtonen, M.; Mõlder, H.; Niitsoo, J. Electric vehicle charger load current harmonics variations due to supply voltage level differences–Case examples. In Proceedings of the 2014 International Symposium on Power Electronics, Electrical Drives, Automation and Motion, Ischia, Italy, 18–20 June 2014; doi:10.1109/SPEEDAM.2014.6872009.

35. Iqbal, M.N.; Kütt, L.; Asad, B.; Vaimann, T.; Rassõlkin, A.; Demidova, G.L. Time Dependency of Current Harmonics for Switch-Mode Power Supplies. *Appl. Sci.* **2020**, *10*, 7806, doi:10.3390/app10217806.

36. Wagner, V.; Balda, J.; Griffith, D.; McEachern, A.; Barnes, T.; Hartmann, D.; Phileggi, D.; Emannuel, A.; Horton, W.; Reid, W.; et al. Effects of harmonics on equipment. *IEEE Trans. Power Deliv.* **1993**, *8*, 672–680, doi:10.1109/61.216874.

37. He, Y.; Venkatesh, B.; Guan, L. Optimal scheduling for charging and discharging of electric vehicles. *IEEE Trans. Smart Grid* **2012**, *3*, 1095–1105, doi:10.1109/TSG.2011.2173507.

38. Xing, H.; Fu, M.; Lin, Z.; Mou, Y. Decentralized optimal scheduling for charging and discharging of plug-in electric vehicles in smart grids. *IEEE Trans. Power Syst.* **2016**, *31*, 4118–4127, doi:10.1109/TPWRS.2015.2507179.

39. Shao, S.; Zhang, T.; Pipattanasomporn, M.; Rahman, S. Impact of TOU rates on distribution load shapes in a smart grid with PHEV penetration. In Proceedings of the 2010 IEEE PES Transmission and Distribution Conference and Exposition: Smart Solutions for a Changing World, New Orleans, LA, USA, 19–22 April 2010; doi:10.1109/TDC.2010.5484336.

40. Weiller, C. Plug-in hybrid electric vehicle impacts on hourly electricity demand in the United States. *Energy Policy* **2011**, *39*, 3766–3778, doi:10.1016/j.enpol.2011.04.005.

41. IEEE Recommended Practice for Establishing Liquid-Immersed and Dry-Type Power and Distribution Transformer Capability When Supplying Nonsinusoidal Load Currents. IEEE Std C57.110(TM)-2018 (Revision of IEEE Std C57.110-2008). 2018, pp. 1–68, doi:10.1109/IEEESTD.2018.8546832. Available online: https://standards.ieee.org/standard/C57_110-2018.html (accessed on 9 June 2021).

Curriculum Vitae

1. Personal data

Name	Muhammad Naveed Iqbal
Date and place of birth	1 August 1988 Punjab, Pakistan
Nationality	Pakistani

2. Contact information

Address	Tallinn University of Technology, School of Engineering, Department of Power Engineering and Mechatronics, Ehitajate tee 5, 19086 Tallinn, Estonia
Phone	+372 56602170
E-mail	miqbal@taltech.ee

3. Education

2017–...	Tallinn University of Technology, Doctoral Student
2010–2011	University of New South Wales, Australia, Electrical Engineering, M.Sc
2004–2008	Islamia University of Bahawalpur, Pakistan, Electronics Engineering, B.Sc

4. Language competence

Urdu	native
English	fluent

5. Professional employment

2017–...	Tallinn University of Technology, Estonia, Early Stage Researcher
2012–2017	Government College University Lahore, Pakistan, Lecturer

6. Main track of research

Power quality, electrical engineering, signal processing, measurements of AC quantities

7. Research projects

2018–2021   Synthesis of output current waveforms of power electronic converters for increasing the hosting capacity of renewable energy sources in the distribution networks

Papers

1. M. N. Iqbal and L. Kütt, "End-user electricity consumption modelling for power quality analysis in residential building," in 2018 19th International Scientific Conference on Electric Power Engineering (EPE), IEEE, May 2018

2. M. N. Iqbal, L. Kütt, and A. Rosin, "Complexities associated with modeling of residential electricity consumption," in 2018 IEEE 59th International Scientific Conference on Power and Electrical Engineering of Riga Technical University (RTUCON), IEEE, Nov 2018

3. M. N. Iqbal, M. Jarkovoi, L. Kütt, and N. Shabbir, "Impact of LED Thermal Stability to Household Lighting Harmonic Load Current Modeling," in 2019 Electric Power Quality and Supply Reliability Conference (PQ) and 2019 Symposium on Electrical Engineering and Mechatronics (SEEM), IEEE, June 2019

4. M. Jarkovoi, M. N. Iqbal, and L. Kütt, "Analysis of harmonic current stability and summation of LED lamps," in 2019 Electric Power Quality and Supply Reliability Conference and Symposium on Electrical Engineering and Mechatronics, PQ and SEEM2019, IEEE, June 2019

5. N. Shabbir, R. Ahmadiahangar, L. Kütt, M. N. Iqbal, A. Rosin, "Forecasting Short Term Wind Energy Generation using Machine Learning," IEEE 60th International Scientific Conference on Power and Electrical Engineering of Riga Technical University (RTUCON). Riga, Latvia, Oct. 2019

6. N. Shabbir, L. Kutt, M. Jawad, R. Amadiahanger, M. N. Iqbal, A. Rosin, "Wind Energy Forecasting Using Recurrent Neural Networks," 2019 Big Data, Knowledge and Control Systems Engineering, BdKCSE, Sofia, Bulgaria, Nov. 2019

7. B. Asad, T. Vaimann, A. Kallaste, A. Rassolkin, A. Belahcen, M. N. Iqbal, "Improving Legibility of Motor Current Spectrum for Broken Rotor Bars Fault Diagnostics," Electrical Control and Communication Engineering, 15 (1), 2020

8. B. Asad, T. Vaimann, A. Kallaste, A. Rassolkin, A. Belahcen, M. N. Iqbal, "Broken rotor bar fault detection of the grid and inverter fed induction motor by effective attenuation of the fundamental component," Electric Power Applications, IET, 13 (12), 2020

9. M. Jarkovoi, L. Kütt, and M. N. Iqbal, "Probabilistic bivariate modeling of harmonic current," in 19th International Conference on Harmonics and Quality of Power (ICHQP), IEEE, July 2020

10. T. E. Anijärv, N. Shabbir, L. Kütt, M. N. Iqbal, "Requirements to Data Acquisition and Signal Analysis for Electrical Grid Condition Monitoring," IEEE 61st International Scientific Conference on Power and Electrical Engineering of Riga Technical University, Riga, Latvia, Nov. 2020

11. B. Asad, T. Vaimann, A. Belahcen, A. Kallaste, A. Rassolkin, M. N. Iqbal, "The Cluster Computation-Based Hybrid FEM–Analytical Model of Induction Motor for Fault Diagnostics," Applied Sciences, 10(21), 7572, 2020

12. T. Vinnal, H. Puusepp, N. Shabbir, L. Kütt, M. N. Iqbal, "Case Study of Non-linear PV Inverter Devices Attached to the LV Distribution Network," Agronomy Research, 18 (4), 2020

13. N. Shabbir, L. Kütt, M. Jawad, M. N. Iqbal, P. S. Ghahfaroki, "Forecasting of energy consumption and production using recurrent neural networks," Advances in Electrical and Electronic Engineering, 18 (3), 190-197, 2020

14. N. Shabbir, L. Kütt, M. Jarkovoi, M. N Iqbal, A. Rassõlkin, K. Daniel, "An Overview of Measurement Standards for Power Quality," Agronomy Research, 19, 2021

15. N. Shabbir, M. Usman, M. Jawad, M. H. Zafar, M. N. Iqbal, L. Kütt, "Economic Analysis and Impact on National Grid by Domestic Photovoltaic System Installations in Pakistan," Renewable Energy, 153, 509-521, 2020

16. B. Asad, T. Vaimann, A. Belahcen, A. Rassõlkin, A. Kallaste, M. N. Iqbal, "Modified Winding Function-based Model of Squirrel Cage Induction Motor for Fault Diagnostics," Electric Power Applications, IET, 14(9), 1722, 2020

17. N. Shabbir, L. Kütt, B. Asad, M. Jawad, M. N. Iqbal, K. Daniel, "Spectrum Analysis for Condition Monitoring and Fault Diagnosis of Ventilation Motor: A Case study," Energies, 14 (7), 1-16, 2021

18. M. N. Iqbal, L. Kütt, B. Asad, N. Shabbir, "Impact of Cable Impedance on the Harmonic Emission of LED Lamps," in 21st International Scientific Conference on Electric Power Engineering (EPE), Oct. 2020

19. M. N. Iqbal, L. Kütt, B. Asad, N. Shabbir, and I. Rasheed, "Time-dependent variations in current harmonic emission by LED lamps in the low-voltage network," Electrical Engineering, 103, 1525–1539, 2021

20. M. N. Iqbal, L. Kütt, B. Asad, T. Vaimann, A. Rassõlkin, and G. L. Demidova, "Time Dependency of Current Harmonics for Switch-Mode Power Supplies," Applied Sciences, 10, 2020

21. M. N. Iqbal, L. Kütt, M. Lehtonen, R. J. Millar, V. Püvi, A. Rassõlkin, and G. L. Demidova, "Travel Activity Based Stochastic Modelling of Load and Charging State of Electric Vehicles," Sustainability, 13, 1550, 2021

22. M. N. Iqbal, L. Kutt, N. Shabbir, and B. Asad, "Comparison of Current Harmonic Emis-sion by Different Lighting Technologies," in 2020 IEEE 61th International Scientific Conference on Power and Electrical Engineering of Riga Technical University (RTU-CON), IEEE, Nov 2020

23. M. N. Iqbal, L. Kütt, K. Daniel, M. Jarkovoi, B. Asad, and N. Shabbir, "Bivariate stochastic model of current harmonic analysis in the low voltage distribution grid," Proceedings of the Estonian Academy of Sciences, 70(2), 190, 2021

24. M.N. Iqbal; L. Kütt; K. Daniel; B. Asad; P. S. Ghahfarokhi, "Estimation of Harmonic Emission of Electric Vehicles and Their Impact on Low Voltage Residential Network," Sustainability, 13, 8551, 2021

Elulookirjeldus

1. Isikuandmed

Nimi	Muhammad Naveed Iqbal
Sünniaeg	01.08.1988
Sünnikoht	Pakistan
Kodakondsus	Pakistani

2. Kontaktandmed

Aadress	Tallinna Tehnikaülikool, Inseneriteaduskond, Elektroenergeetika ja mehhatroonika instituut Ehitajate tee 5, 19086 Tallinn, Estonia
Telefon	+372 56602170
E-post	miqbal@taltech.ee

3. Haridus

2017–…	Tallinna Tehnikaülikool, Eesti, Doktoriõpe
2010–2011	University of New South Wales, Australia, Electrical Engineering, M.Sc
2004–2008	Islamia University of Bahawalpur, Pakistan, Electronics Engineering, B.Sc

4. Keelteoskus

Urdu keel	emakeel
Inglise keel	kõrgtase

5. Teenistuskäik

2017– …	Tallinna Tehnikaülikool, Eesti, Nooremteadur
2012–2017	Government College University Lahore, Pakistan, Lektor

6. Teadustöö põhisuunad

Elektrotehnika, Signaalitöötlus, Vahelduvvoolusuuruste mõõtmine

7. Projektid

2018–2021	PSG 142: Pooljuhtmuundurite väljundvoolukuju süntees taastuvenergiaallikate võrguga liitmisvõimaluse suurendamiseks